Reconciling turnover models of roots and soil organic carbon with radiocarbon measurements

Von der Naturwissenschaftlichen Fakultät der

Gottfried Wilhelm Leibniz Universität Hannover

zur Erlangung des Grades

Doktor der Naturwissenschaften (Dr. rer. nat.)

genehmigte Dissertation

von

Bernhard Ahrens, *M. Sc.*

2021

So muß man leben!
Die kleinen Freuden aufpicken,
bis das große Glück kommt.
Und wenn es nicht kommt,
dann hat man wenigstens
die "kleinen Glücke" gehabt.

Theodor Fontane

Kurzzusammenfassung

Terrestrische Ökosysteme und Böden sind wichtige Akteure im globalen Kohlenstoffkreislauf der Erde und eng mit der Entwicklung der atmosphärischen CO_2-Konzentration und dem Klimawandel verbunden. Allein der Boden speichert ein Vielfaches des Kohlenstoffs in der Atmosphäre, und Bodenkohlenstoff-Prozesse könnten daher erhebliche Auswirkungen auf die atmosphärischen CO_2-Konzentrationen haben. Um die Zeitskalen des Kohlenstoffkreislaufs in terrestrischen Ökosystemen zu verstehen, sind Radiokohlenstoffmessungen ein wichtiges Werkzeug. Dennoch stehen die Ergebnisse von Radiokohlenstoffmessungen oft im Widerspruch zu den Ergebnissen anderer Messtechniken: Für die Untersuchung des Wurzelumsatzes hat Radiokohlenstoff im Vergleich zu anderen Methoden, wie z.B. dem sequenziellen Entkernen oder Wurzelkameras, wesentlich längere Umsatzzeiten ergeben. Für die Untersuchung der organischen Bodensubstanz hat Radiokohlenstoff auf Pools verwiesen, die sich auf einer hundert- bis tausendjährigen Zeitskala befinden. Empirische Erkenntnisse deuten jedoch darauf hin, dass einzelne Verbindungen der organischen Bodensubstanz wesentlich schneller umgesetzt werden. Das übergeordnete Ziel dieser Dissertation ist es, Umsatzmodelle von Wurzeln und organischem Kohlenstoff im Boden mit Radiokohlenstoffdaten in Einklang zu bringen, indem neues Prozessverständnis in diese Modelle integriert wird.

Der erste Teil der Dissertation befasst sich mit der Vereinbarkeit von Radiokohlenstoffgehalten von Feinwurzeln und Minirhizotron-Beobachtungen von Feinwurzellebensspannen. Zur Simulation des Wurzelumsatzes wurde bisher hauptsächlich ein Ein-Pool-Modell verwendet. Dieses Modell geht von einer konstanten Wahrscheinlichkeit für das Absterben einer Wurzel über ihre gesamte Lebensdauer aus. Minirhizotron-Beobachtungen haben jedoch auf eine höhere Wahrscheinlichkeit für das Absterben einer Wurzel zu Beginn ihrer Lebensdauer hingewiesen. In dieser Arbeit wurde eine Methode entwickelt, die es ermöglicht, Minirhizotron- und Radiokohlenstoffdaten zur gemeinsamen Schätzung der Wurzelumsatzzeiten zu verwenden. Zu diesem Zweck wurden Überlebensfunktionen aus dem Feld der Ereigniszeitanalyse verwendet, um die Lebensspanne einzelner Wurzeln zur Bestimmung der mittleren Verweilzeit von Feinwurzeln zu nutzen. Radiokohlenstoff in Feinwurzeln wurde über eine Faltung der Überlebensfunktionen mit der atmosphärischen Radiokohlenstoff-Kurve modelliert. Dieser Ansatz ermöglicht es, eine Kalibrierung von mittleren Verweilzeiten an Radiokohlenstoff- und Minirhizotron-Daten durchzuführen.

Der zweite Teil der Dissertation befasst sich mit der Vereinbarkeit von Tiefengradienten des organischen Kohlenstoffs und Radiokohlenstoffs im Boden mit einem neuen Modell zum Umsatz organischer Bodensubstanz. Das neue Modell berücksichtigt mechanistische Beschreibungen mikrobieller und organo-mineralischer Wechselwirkungen. Ziel war es, den Beitrag der mikrobiellen Limitierung und der organo-mineralischen Wechselwirkungen zu scheinbar tausendjährigen Radiokohlenstoffaltern des organischen Kohlenstoffs im Unterboden zu bestimmen. Hier wird einem Modell, das mit standortspezifischen Sorptionskapazitäten parametrisiert ist, eine allgemeingültigere Parametrisierung der Sorptionskapazität gegenübergestellt. Mit dieser allgemeingültigen Formulierung der Sorptionskapazität, die auf dem Ton- und Schluffgehalt basiert, können Unterschiede der Tiefengradienten von Radiokohlenstoff zwischen Standorten dargestellt werden. Nach der Kalibrierung an Profile von bodenorganischem Kohlenstoff und Radiokohlenstoff wurde mit Hilfe von Modellexperimenten die Bedeutung einzelner Prozesse und deren Zusammenspiel zur Erklärung von Radiokohlenstoff-Tiefengradienten untersucht. Ein besonderer Schwerpunkt wurde darauf gelegt, wie verschiedene Sorptionskapazitäten mit mikrobieller Limitierung zusammenwirken. Dieser Ansatz erlaubte es uns, scheinbar jahrtausendealte Radiokohlenstoffalter mit Mechanismen des mikrobiellen Abbaus und der Sorptionskapazität anstelle von chemischer Rekalzitranz zu erklären.

Der mechanistische Rahmen, der in dieser Arbeit entwickelt wurde, hilft den Umsatz organischer Substanz im Boden, die unterirdischen Teile des globalen Kohlenstoffkreislaufs und schließlich seine Reaktion auf die globale Erwärmung besser zu verstehen.

Abstract

Terrestrial ecosystems and soils are major actors in the Earth's carbon cycle, and tightly linked to the evolution of atmospheric CO_2 concentrations and climate change. Soils alone store several times more carbon than the atmosphere, and carbon cycling in soils could hence have substantial impact on atmospheric CO_2 concentrations. To understand the timescales of carbon cycling in terrestrial ecosystems, radiocarbon measurements are an important tool. Yet, results from radiocarbon measurements have often conflicted with results other measurement techniques: In the study of root turnover, radiocarbon has yielded turnover times that are much longer compared to those attained by other methods, such as sequential coring or minirhizotrons. In the study of soil organic carbon turnover, radiocarbon has pointed to pools that cycle on centennial to millennial timescales. Empirical evidence, however, has suggested that individual compounds turn over more rapidly. This dissertation's overarching goal is to reconcile turnover models of roots and soil organic carbon with radiocarbon data by incorporating new process understanding into these models.

The first part of the dissertation reconciles radiocarbon contents of fine roots with observations of root lifetimes from minirhizotrons. Previously root turnover had mainly been estimated by a one-pool model. This kind of model assumes an equal likelihood for root death throughout the lifetime of a root. Minirhizotron observations, however, have pointed to higher likelihoods of root turnover at the beginning of a root's lifetime. In this thesis, a framework was developed that allows using minirhizotron and radiocarbon data in conjunction to estimate mean fine-root residence times. Survival functions from the field of survival analysis were used to estimate mean fine-root residence times from lifetime data of individual roots. Convoluting fine-root survival functions with the atmospheric radiocarbon bomb curve allowed performing a joint estimation of mean fine-root residence times from radiocarbon and minirhizotron data.

The second part of the dissertation develops a new soil organic carbon profile model that incorporates mechanistic descriptions of microbial and organo-mineral interactions. The aim is to reconcile apparent millennial radiocarbon ages of soil organic carbon in the subsoil with other observations by considering the contribution of microbial decomposition limitation and organo-mineral interactions. A version of the model parametrized with site-specific sorption capacities was contrasted with a more generic parametrization of sorption capacity. With this generic formulation of sorption capacity based on clay and silt content, between-site differences of radiocarbon depth gradients could be represented. After calibration to profiles of soil organic carbon and radiocarbon, model experiments were used to study the importance of individual processes and their interaction for explaining radiocarbon depth gradients. A special focus was put on how different levels of sorption capacity interact with microbial substrate limitation. This approach allowed us to reconcile apparent millennial radiocarbon ages with mechanisms of microbial decomposition and sorption capacity instead of chemical recalcitrance.

The mechanistic framework developed in this thesis can be used to better understand soil organic matter turnover, the belowground parts of the global carbon cycle, and eventually its response to global warming.

Schlagworte

Umsatz von organischer Bodensubstanz

Umsatz von Feinwurzeln

Radiokohlenstoff-Modellierung

Keywords

Soil organic matter turnover

Fine-root turnover

Radiocarbon modelling

Table of contents

List of tables

List of figures

Abbreviations

COMISSION	Soil organic carbon model with a **CO**ntinuous representation of soil organic carbon in the organic layer and the mineral soil with **M**icrobial **I**nteractions and **S**orptive **S**tabilizat**ION**
DOC	dissolved organic carbon
DOM	dissolved organic matter
MAOC	mineral-associated organic carbon
MAOM	mineral-associated organic matter
MCMC	Monte Carlo Markov Chain
OC	organic carbon
OM	organic matter
Pg	petagram
pM	percent Modern ^{14}C content
q_{max}	maximum sorption capacity based on batch sorption experiments
Q_{max}	maximum sorption capacity based on clay and silt (< 20 µm) content
τ_a	mean age
τ_o	turnover time
τ_r	mean residence time
SOC	soil organic carbon
SOM	soil organic matter

1 General Introduction

1.1 Importance of belowground processes for the terrestrial carbon cycle

In 2018, fossil CO_2 emissions passed the mark of 10 Pg C yr^{-1} for the first time in history (1 Pg C = 1 Gigaton carbon = 10^{15} g carbon; Friedlingstein et al., 2019). These emissions have contributed to an increase of carbon in the atmosphere in the form of CO_2 from 589 Pg C in the preindustrial era to 860 Pg C (Ciais et al., 2014; Friedlingstein et al., 2019) and a warming effect of around 1.68 W m^{-2} (Myhre et al., 2014).

Soil organic carbon could have a considerable feedback to climate warming. Soils contain 1500 to 2400 Pg C in the first meter and between 1500 Pg and 2600 Pg C below (Fan et al., 2020). Thus, soils store more than three times the carbon of the atmosphere and more carbon than the Earth's fossil fuel reserves of 1005 to 1940 Pg C (Ciais et al., 2014). The global flux out of the soil as heterotrophic respiration is estimated to be around 51 Pg C yr^{-1} (Hashimoto et al., 2015) and is thereby around five times greater than anthropogenic fossil fuel emissions.

Compared to fossil fuel reserves, which receive basically no contemporaneous inputs, the global soil organic carbon pool receives inputs via dead leaves, roots, and wood that roughly equal its effluxes via heterotrophic respiration. Just a 2% imbalance of global heterotrophic respiration over global litter inputs would equal to about 10% of annual global fossil fuel emissions (Davidson, 2020). Due to the considerable size of the global soil organic carbon pool, an accelerated heterotrophic decomposition due to climate warming has the potential to result in a substantial positive feedback loop and to further exacerbate climate warming (Bradford et al., 2016; Koven et al., 2017).

To better understand the potential of soil organic carbon turnover to accelerate climate warming, it is paramount to improve our mechanistic understanding of inputs to, transformations within, and losses from the soil organic carbon pool.

1.2   Uncertainties of belowground processes in the terrestrial carbon cycle

Processes that affect the largest carbon store in the terrestrial biosphere occur mostly belowground. Belowground processes are 'hidden' from direct observation, such as root production and turnover, and soil organic matter (SOM) formation and turnover. These hidden belowground ecosystem processes are inherently more challenging to study than aboveground ecosystem processes. Methods of observation for belowground processes are generally less direct than for aboveground processes. Yet, given their importance for the terrestrial carbon cycle, it is crucial to better understand belowground processes despite their hidden nature.

The most obvious symptom of the inherent difficulty in studying belowground processes is the high uncertainty in estimates of the global soil organic carbon stocks. Estimates in the first meter of soil alone differ by 900 Pg C (Fan et al., 2020), which is more than the carbon content of the atmosphere (Friedlingstein et al., 2019). Similarly, the amount of carbon stored globally belowground in root biomass is not very well constrained. According to recent estimates, the global vegetation stores around 410 Pg C (Fan et al., 2020). These estimates include both aboveground and belowground biomass. Earlier estimates of biome-level stocks root-biomass amounted to 292 Pg C globally (Jackson et al., 1997). Using shoot-to-root ratios, Robinson (2007) estimated that belowground biomass could amount to 268 Pg C, while Saugier et al. (2001) estimate that belowground biomass stores 160 Pg C. More recent biomass stocks are based on the combined estimation from various satellite remote sensing retrievals (Fan et al., 2020). By the nature of satellite remote sensing, these yield aboveground biomass estimates. Belowground biomass is then derived from allometric relationships with aboveground biomass (Saatchi et al., 2011; Thurner et al., 2014; Fan et al., 2020) and thereby inherently uncertain.

Uncertainties remain not only in the size of belowground carbon stocks, but also in corresponding input and output fluxes of carbon to and from the soil. Inputs to the soil organic carbon pool via plant litter can be as aboveground and belowground litter. In different biome types, between 23% (croplands) and 70% (Mediterranean/montane shrublands) of net primary productivity (NPP) is allocated belowground and eventually enters the soil organic matter pool (Supplementary Table 1 in Luo et al., 2019). Globally, it is estimated that plants allocate around 40% of NPP belowground (Del Grosso et al., 2008; Luo et al., 2019). The quantification of aboveground litter inputs with litter traps is relatively straightforward (Vitousek, 1984). Conversely, belowground inputs are quantified with a

multitude of techniques (Lukac, 2012) that can lead to seemingly contradictory results calling into question how much root litter supplies to the soil organic carbon pool (Trumbore and Gaudinski, 2003). Additionally, the point-of-entry for inputs to the soil organic pool is crucial since vertically distributed belowground litter inputs provide a different sequestration potential depending on where litter inputs occur in relation to their position in the soil micro-environment, e.g., in contact with the mineral matrix or not (Sokol and Bradford, 2019). The development of ^{13}C- and ^{14}C-based measurement techniques to estimate root turnover times have led to speculations that belowground litter inputs to the soil organic pool have been overestimated (Matamala et al., 2003; Trumbore and Gaudinski, 2003).

Similar to root turnover times, ^{14}C measurements of soil organic carbon have presented a puzzle to researchers for a long time in their attempt to understand soil organic matter formation and turnover. ^{14}C has provided evidence on the formation and turnover of soil organic carbon on centennial to millennial time-scales (Trumbore, 2009). While ^{14}C has provided researchers with insights on the time horizon of SOM formation and decomposition, mathematical models were not equipped with enough mechanistic understanding to integrate the ^{14}C data into the model-knowledge integration loop (Bradford et al., 2016). Under the paradigm of chemical recalcitrance as the dominant mechanism for SOC formation and turnover, mathematical models of soil organic carbon turnover could explain apparent millennial ^{14}C ages. However, recent experimental advances have questioned the chemical recalcitrance paradigm (Schmidt et al., 2011).

^{14}C measurements have added new pieces to the puzzle of root turnover, and soil organic matter formation and turnover. In both cases, new findings were irreconcilable under the prevailing paradigms of root turnover and soil organic matter turnover. After a short overview on ^{14}C measurements and the use of ^{14}C in closed and open system (chapter 1.3), chapter 1.4 outlines how ^{14}C has contributed to a paradigm shift in both fields.

1.3 Radiocarbon as a tracer for time scales of carbon turnover

Radiocarbon has been used as a proxy to measure time in various fields. Most commonly known is the use in archeology and related fields where scientists use the radioactive decay of radiocarbon to determine the age of an artifact (Geyh, 2005). In archeology, one generally assumes a closed system – this means that one assumes that after deposition of a sample in an archeological setting, the

sample receives no further external input of carbon, which would change the artifact's apparent age. Archeological dating seems straightforward at first glance. If the studied system is closed, so called conventional radiocarbon ages can be calculated using the approach first introduced by Willard Libby and James Richard Arnold in 1949 (Arnold and Libby, 1949):

$$\text{conventional } {}^{14}\text{C age} = -8033 \cdot \log\left(\frac{A_{SN}}{A_{ON}}\right) \tag{1-1}$$

where 8033 years is the mean lifetime of ${}^{14}\text{C}$ based on the Libby half-life of ${}^{14}\text{C}$ of 5568 years, and A_{SN} describes the activity of the sample normalized for ${}^{13}\text{C}$ fractionation relative to the activity of the standard, A_{ON}. Depending on the activity of the sample, the ${}^{14}\text{C}$ activity can be measured with decay counting or, most commonly for samples with natural abundances with accelerator mass spectrometry.

In addition to the necessary condition of a closed system, calculating conventional ${}^{14}\text{C}$ ages relies on the precondition that over the last 100000 years, the atmospheric ${}^{14}\text{C}$ production rate, the atmosphere's, biosphere's, and hydrosphere's carbon contents, and the exchange rate between these spheres were constant.
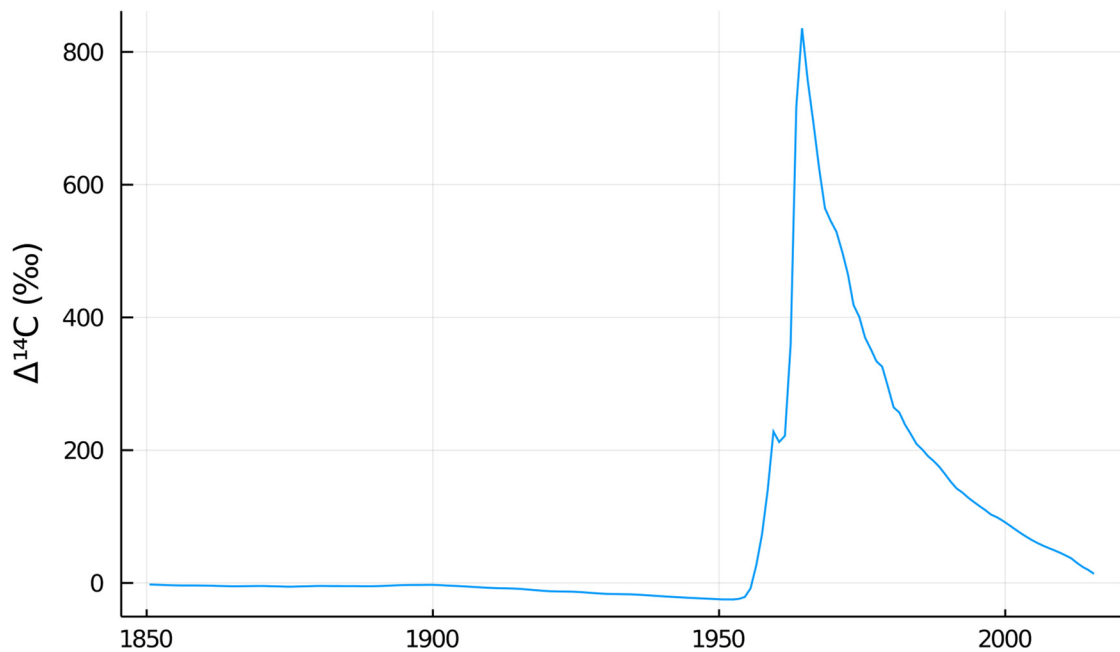
Figure 1-1: Δ^{14}C of atmospheric CO_2 for the Northern Hemisphere (30-90° N) as compiled by Graven et al. (2017).

Since these preconditions generally do not hold and the Libby half-life of 5568 years is used for honorary purposes, conventional ^{14}C ages do not represent the ages of samples even in closed systems. The main cause for deviations from the conventional ^{14}C age are fluctuations in the atmospheric ^{14}C content. These have been acting on various time-scales such as the de Vries effect, which describes changes in the atmospheric ^{14}C content due to changes in the dipole moment of the earth, the sun's activity and magnetism, as well as climate (Trumbore et al., 2016). Fossil fuel emissions have started to influence the Earth's atmospheric ^{14}C content since the 1850s and have diluted the Earth's ^{14}C content. Aboveground nuclear weapons testing in the 1950s has led to a peak in atmospheric ^{14}C due to the creation of large quantities of ^{14}C (Figure 1-1).

As ecosystems are generally open systems, two quantities that describe the absolute amount of ^{14}C in a sample are generally reported (Stuiver and Polach, 1977; Trumbore et al., 2016):

$$\text{percent Modern} = \% \text{ Modern} = \text{ pM} = \frac{A_{SN}}{A_{ABS}} \cdot 100 \text{ \%} \tag{1-2}$$

$$\Delta^{14}C = \left(\frac{A_{SN}}{A_{ABS}} - 1\right) \cdot 1000 \, ‰ \qquad (1\text{-}3)$$

Where percent Modern describes the amount of carbon relative to 100% in the year 1950 (time point for modern), while $\Delta^{14}C$ describes the permille deviation from a sample activity that is equal to the standard in the year 1950. The activity of the standard is absolute (A_{ABS}), i.e., the activity of the standard is decay-corrected to the activity of the standard in 1950. Both quantities, percent Modern and $\Delta^{14}C$ are not influenced by the year of measurement of the sample.

All these changes in the atmospheric ^{14}C content show the importance of using calibrated ^{14}C ages over conventional ^{14}C ages for closed systems. Calibrated ^{14}C ages generally refer to sample ages estimated with the so-called wiggle-matching approach which uses the wiggles of the atmospheric ^{14}C curve to determine ^{14}C ages (Pearson, 1986; Reimer et al., 2013). Wiggle-matching can be performed on samples from before 1950, which were mainly influenced by the de Vries effect (Reimer et al., 2004a), and samples from the bomb-radiocarbon period (Reimer et al., 2004b; Hua et al., 2013).

Conventional and calibrated ^{14}C ages rely on strictly closed systems for dating. For the use in soil organic matter research, open systems are the typical situation. Therefore, conventional and calibrated ^{14}C ages can only be used for illustrative purposes (as when reported in this thesis) or to date individual compounds for which a closed system can be assumed. Instead, using ^{14}C as a 'clock' in open systems such as soils generally relies on process-based modeling of the carbon and radiocarbon dynamics. The radiocarbon dynamics generally are submitted to the same processes as carbon with the addition of radioactive decay and input of ^{14}C from the source reservoir (e.g., plant litter). Thereby, radiocarbon provides a tool to understand processes and time-scales of carbon cycling provided by the radioactive decay of ^{14}C and the 'wiggles' of the atmospheric curve from the de Vries, Suess, and bomb effect.

1.4 Paradigm shifts in root and SOC turnover

The fields of studying root turnover and SOC formation and turnover have witnessed paradigm shifts in the last 20 years that have been driven, in part, by the irreconcilability of ^{14}C measurements with the prevailing paradigm in the field. A paradigm shift is generally characterized by an accumulation of observations that cannot be reconciled with the current paradigm, which leads to a period of revolutionary science and finally to the formulation of a new paradigm. In the study of root turnover and SOC turnover, the field is generally split into rather disparate communities of modelers and experimentalists. Therefore, the transfer of knowledge to modelers from experimentalists is relatively small. The symptoms for irreconcilable differences to the current paradigm may accumulate both in the modelling and the experimental realm. The following two subchapters outline how ^{14}C measurements were one of the symptoms for irreconcilable observations in root and SOC turnover that led to the formulation of new paradigms in both fields.

1.4.1 Irreconcilable differences in root turnover?

Fine-root turnover times were generally studied with production-based techniques in the 1990s. Fine root production can be measured directly with ingrowth cores or by sequential coring of root biomass throughout seasons (Brunner et al., 2013). Using the common definition of turnover time as stock divided by production led to the derivation of root turnover times of 1 to 3 years. The disparity of the experimental and modeling realm in the study of root turnover is characterized by the absence of a notable use of root turnover models before new measurement techniques such as ^{13}C labeling, minirhizotrons (Strand et al., 2008), and using the ^{14}C bomb curve (Riley et al., 2009) appeared on the scene. Only the experimentalists' prevailing sentiment that the different measurement techniques yielded irreconcilable differences due to the techniques' biases led to the development of a dedicated root turnover modeling field. The qualifier dedicated is used here to clarify that root turnover was considered in ecosystem models before. However, turnover times therein were solely reliant on production-based estimates or on back-of-the-envelope calculations. The diagnosis of seemingly irreconcilable differences between different measurement techniques led to considerable modeling efforts for fine-root dynamics (Riley et al., 2009). Formalizing experimentalists' insights into equations was a prerequisite for testing their assertion that the new isotope-based techniques (^{13}C labeling and ^{14}C) generally lead to longer turnover time estimates than the conventional production-based estimates and the minirhizotron technique.

Thereby, two directions emerged: one making a case for longer than previously thought turnover times (^{13}C labeling and ^{14}C) and one making a case for shorter turnover times in the range of the established production-based estimates (minirhizotrons). Biases of production-based and minirhizotron-based turnover times and biases of the isotope-based techniques were commonly highlighted to emphasize the correctness of one approach over the other or to make a case for the irreconcilability of all techniques. One-pool models with first-order turnover rates were used to translate ^{14}C or ^{13}C contents in roots into turnover times. For minirhizotrons, statistical models were used to derive mean turnover times (Pritchard and Strand, 2008). These turnover times were then compared, but no attempt was made to integrate different measurements into one framework.

After initial statements about the irreconcilability of different measurement types, mathematical models were developed to check if the different kinds of observations could be reconciled (Guo et al., 2008; Riley et al., 2009). In the early stages of root turnover modeling, the irreconcilability of the observations had been emphasized, leading to statements like "long turnover times suggest that root production and turnover in forests have been overestimated and that sequestration of anthropogenic atmospheric carbon in forest soils may be lower than currently estimated" (Matamala et al., 2003). Riley et al. (2009) were the first to attempt to reconcile minirhizotron and ^{14}C data. However, their efforts fell short since they simply used the root turnover time of minirhizotrons as determined with statistical methods to parametrize a fast pool's turnover time in a two-pool turnover model. Riley et al. (2009) did not attempt to reconcile both types of observations available to them. Nevertheless, Riley et al. (2009) started to formulate ideas towards a reconciliation of the various techniques by considering that different measurement techniques might reflect different parts of the root lifetime continuum. This idea has been voiced early in the debate on the irreconcilability of different datastreams (Trumbore and Gaudinski, 2003) and helped formulate the new paradigm of root turnover: the probability for a root to die changes through its lifetime. In other words, a one-pool exponential decay model is not able to capture the changing probability for a root to die. The apparent irreconcilability of root turnover observations has sparked a debate whether the probability for a root to die stays the same over its lifetime. The evidence has led to abandoning the previous paradigm of equal survival probability throughout its lifetime, an assumption initially made as a consequence of the previous methods of determining root turnover based on root biomass and root production. The wealth of apparently irreconcilable approaches to root turnover has led to the new paradigm of changing survival probabilities of roots over their lifetime and acceptance of inherent biases of the different techniques. Overall, the new consensus highlights that various

techniques offer constraints for different parts of the survival probability of a root during its lifespan. The acknowledgement of their inherent biases is at the same time crucial for the ability to reconcile data from various techniques. The apparent irreconcilability of the various root turnover time observations is a testament to the changing survival probability of fine-roots as they enter different stages of their life cycle. The consideration of the inherent biases of the various techniques was the prerequisite for being able to reconcile different measurements and to develop the new paradigm of changing survival probabilities of roots throughout their lifetime.

1.4.2 Irreconcilable differences in SOC turnover?

The prevailing paradigm for the long-term persistence of soil organic carbon has been chemical recalcitrance (Schmidt et al., 2011). The chemical recalcitrance paradigm states that the chemical structure of plant inputs and soil organic carbon is the dominant explanatory factor for forming persistent organic carbon pools in soils.

Two schools of thought fall under the umbrella of the chemical recalcitrance paradigm: The chemical recalcitrance via humification school, the chemical recalcitrance via selective preservation school, and a combination of the two. The humification theory assumes that chemically recalcitrant compounds are formed through de novo synthesis in the soil. Followers of this school regarded chemical recalcitrance through humification as the main reason why organic compounds persist in soils. Millennial ^{14}C ages in the subsoil have been cited as the principal witness that these hypothesized humic substances must be so chemically recalcitrant that they persist in soils. The selective preservation school assumed that individual compounds in plant litter such as lignin or lipids are so chemically recalcitrant that they persist in soil: The selectively preserved compounds are left behind in the decomposition process and form the bulk of persistent soil organic carbon. As for fine-root turnover times and humic substances, ^{14}C ages were taken as a principal witness to substantiate this theory. Compound specific ^{14}C ages that indicated up to millennial ages of these individual compounds seemed to corroborate this theory. In the modeling realm, the chemical recalcitrance paradigm crystallized by the invention of stable, passive, or even inert pools that decomposed according to a slow first-order decomposition rate (i.e., a turnover time of several centuries) without or with minimal influence of the biotic and abiotic environment. ^{14}C observations were used to determine the size of these inherently slow pools, but ^{14}C observations were not used as a tool to gain process knowledge or elucidate stabilization pathways in the models (Coleman et al., 1997; Jenkinson and Coleman, 2008). This simplistic de facto reconciliation of millennial ^{14}C

24

observations and SOC stocks to determine the slow pools' size was one of the symptoms of the crisis of the chemical recalcitrance paradigm: the slow pools were 'fudge pools' (Goldsmith, 1997) invented to represent unresolved processes. Due to their role as 'fudge pools', the slow pools' response to environmental changes was at best a transfer of empirical knowledge to these 'fudge pools' but always poorly backed by process knowledge. However, the gravest symptoms that the chemical recalcitrance paradigm is not justifiable came from the experimental realm: The humification theory could not be held up after the hypothesized de novo synthesized macromolecules described with the umbrella term humic substances could not be observed with modern analytical techniques (Kelleher and Simpson, 2006; Lehmann et al., 2008). Similarly, a review by Amelung et al. (2008) showed that in ^{13}C labeling experiments, seemingly chemical recalcitrant compounds such as lignin and lipids have apparent turnover times faster than the bulk of soil organic carbon. Therefore, selective preservation could not be the main reason for long-term persistence of organic matter in soils.

Instead of the humification theory and the selective preservation theory, a concerted effort of scientists acknowledged and possibly announced the paradigm shift in the landmark review and opinion paper of Schmidt et al. (2011). This paper formulated the idea that SOC persistence is an ecosystem property. The chemical recalcitrance paradigm stated that the long-term persistence of SOC is primarily a molecular property but does depend less on the interaction of organic matter with its biotic and abiotic environment. The formulation of the new paradigm as an 'ecosystem property' paradigm is a misnomer since this rather excludes chemical structure as the main factor to SOC persistence than stating which factors are crucial to SOC persistence. Lehmann and Kleber (2015) instead highlighted that microbial and mineral interactions are among the most important interactions with the biotic and abiotic environment that have to be addressed to understand SOC persistence.

Along with these two factors comes the treatment of soil as a three-dimensional medium. The vertical position of where SOC is formed and decomposed is vital in the new paradigm since microbial and mineral interactions change as a function of soil depth. Soil depth is here a proxy for various processes that change as a function of depth such as weathering, which influence soil texture and in turn rooting patterns (Schenk and Jackson, 2002). Rooting patterns influence microbes via the amount of substrate that is supplied to them (Iversen, 2010). The amount of microbial biomass in a certain depth in turn influences SOC formation and decomposition in that depth. Microbes are now

regarded as the primary actors for SOC formation and decomposition (Bradford et al., 2016). The interaction of microbes with their microenvironment, i.e., the position of a microbe with regard to mineral surfaces, their substrate, and the moisture and temperature conditions they experience, primarily controls the decomposition rate of SOC instead of a primary control by the molecular structure of the substrate (Schmidt et al., 2011). In a similar vein, the acquisition of chemical recalcitrance throughout the decomposition process through humification has been abandoned in favor of putting microbes point and center for understanding the long-term persistence of SOC (Schmidt et al., 2011).

^{14}C measurements have always played a major role in justifying both mathematical and conceptual models of SOC formation and decomposition based on the humification and selective preservation theories. ^{14}C measurements have not been fully incorporated into efforts of understanding the long-term persistence of SOC but were rather treated as an afterthought or as direct evidence for either schools of the chemical recalcitrance paradigm. Thereby the scientific community only had limited possibilities to learn from radiocarbon observations. The difficulty in reconciling radiocarbon observations with models led to a standstill in model development and a disconnect between the progress the scientific community made experimentally and how this progress could be translated into models. The paper by Schmidt et al. (2011) constituted an important step to incorporate processes such as association with mineral surfaces and microbial decomposition limitation into models. These processes could potentially explain ^{14}C age-depth gradients in soils.

1.5   The need for modeling in reconciling radiocarbon with other observations

In the study of carbon turnover in ecosystems, ^{14}C has the role of a complementary measurement. ^{14}C measurements are commonly made in addition to other measurements such as inventories of roots or SOC. Compared to its use in archeology where the direct interest lies in dating an object but not understanding which processes lead to persistence of that object in its environment, the use of ^{14}C in the study of carbon turnover in ecosystems always has to be combined with modelling. In the infant stages of ^{14}C as a tracer for turnover in ecosystems, simple pool models were fitted to ^{14}C observations. These fitting exercises often were restricted to ^{14}C without taking into consideration the carbon counterpart or estimates on the inputs to the system or outputs from the system. Hence these were then often not in agreement with the ^{14}C-based turnover time estimate (Gaudinski et al., 2000). Only the integration of ^{14}C with other measurements into process-based models can constrain

the overall turnover of carbon in ecosystems. One-pool models fitted to ^{14}C measurements generally disagree with stock-based turnover time estimates, such as in the study of root turnover, if there is additional information content in these measurements. Both in studies on root turnover and SOC turnover, ^{14}C generally tends to provide information on the long-tail of the residence time distribution (Sierra et al., 2017; Metzler et al., 2018).

Radiocarbon is a unique tracer as, except for its radioactive decay, models do not need to incorporate additional processes. Isotopic discrimination is already accounted for during the reporting of ^{14}C values by additionally also measuring ^{13}C and by employing double the discrimination of ^{13}C. Radiocarbon and carbon in soil organic matter are the results of the same processes. Thereby, we have two constraints that must be reconciled under the umbrella of the same processes. In previous state-of-the-art models, targeted pools were introduced to reproduce ^{14}C depth gradients.

1.6   Motivation and objectives

The overall aim of this dissertation is to reconcile radiocarbon observations of fine-roots and soil organic carbon with the emerging understanding of fine-root and soil organic carbon turnover. As outlined before, the apparent irreconcilability of radiocarbon with the previous understanding of fine-root and soil organic carbon turnover has sparked a shift in conceptual models and the understanding of fine-root and soil organic carbon turnover. In both fields, this shift in conceptual understanding had not been formalized in mathematical models and had not been tested against observations. This thesis therefore aims at using radiocarbon observations for constraining and testing models of fine-root and soil organic carbon turnover that reflect the emerging process understanding.

The attempt to reconcile radiocarbon data from fine-roots with minirhizotron data was motivated by the following main objectives (Obj-Root1 to Obj-Root4):

(Obj-Root1) Unify various root turnover models to a convolution of the atmospheric radiocarbon curve with root survival functions.

(Obj-Root2) Clarify the concepts of turnover time, mean residence time and mean age for the estimation of fine-root turnover with radiocarbon.

(Obj-Root3) Quantify root turnover with radiocarbon and minirhizotron data as joint constraints using different survival functions.

(Obj-Root4) Address systematic biases of radiocarbon and minirhizotron data.

The attempt to reconcile radiocarbon data of SOC profiles with the emerging understanding of SOC turnover was motivated by the following main objectives (Obj-SOC1 to Obj-SOC4):

(Obj-SOC1) Develop a SOC model that simulates the SOC and ^{14}C profile while incorporating new process understanding such as microbial and organo-mineral interactions.

(Obj-SOC2) Explore different concepts to represent a maximum sorption capacity for mineral-associated organic matter.

(Obj-SOC3) Elucidate the importance of microbial and organo-mineral interactions for the formation of the SOC and radiocarbon profile.

(Obj-SOC4) Compare how a generic way to represent sorptive stabilization of OC interacts with other processes such as microbial energy limitation, the point-of-entry of litter inputs, and temperature across various sites.

To address these objectives, the following studies were conducted:

(Study I) Reconciling ^{14}C and minirhizotron-based estimates of fine-root turnover with survival functions. This study aimed at introducing a general framework for analyzing ^{14}C fine-root data that allows to use survival functions that are commonly used for analyzing minirhizotron data.

(Study II) Reconcilable Differences: A Joint Calibration of Fine-Root Turnover Times with Radiocarbon and Minirhizotrons. This study shows that minirhizotron data and ^{14}C fine-root data can be reconciled when the biases of the two techniques are addressed.

(Study III) Contribution of Sorption, DOC Transport and Microbial Interactions to the ^{14}C Age of a Soil Organic Carbon Profile: Insights from a Calibrated Process Model. This study introduces the COMISSION model and uses data from batch sorption experiments to model soil organic carbon and mineral-associated organic carbon profiles and their ^{14}C contents in a Podzol.

(Study IV) Combination of energy limitation and sorption capacity explains ^{14}C depth gradients. This study extends the concept of the COMISSION model to a cross-site setup with a scalable definition of sorption capacity based on the clay and silt (< 20 μm) content. Compared to the previous version of the COMISSION model in study III, the mineral-associated organic carbon is formed also directly from microbial residues and not only dissolved organic carbon. The importance of different factors for explaining between site-differences in ^{14}C is explored.

1.7   References Chapter 1

Amelung, W., Brodowski, S., Sandhage-Hofmann, A., Bol, R., 2008. Combining biomarker with stable isotope analyses for assessing the transformation and turnover of soil organic matter. Advances in agronomy 100, 155-250.

Arnold, J.R., Libby, W.F., 1949. Age Determinations by Radiocarbon Content: Checks with Samples of Known Age. Science 110, 678-680.

Bradford, M.A., Wieder, W.R., Bonan, G.B., Fierer, N., Raymond, P.A., Crowther, T.W., 2016. Managing uncertainty in soil carbon feedbacks to climate change. Nature Clim. Change 6, 751-758.

Brunner, I., Bakker, M.R., Björk, R.G., Hirano, Y., Lukac, M., Aranda, X., Børja, I., Eldhuset, T.D., Helmisaari, H.S., Jourdan, C., Konôpka, B., López, B.C., Miguel Pérez, C., Persson, H., Ostonen, I., 2013. Fine-root turnover rates of European forests revisited: an analysis of data from sequential coring and ingrowth cores. Plant and Soil 362, 357-372.

Ciais, P., Sabine, C., Bala, G., Bopp, L., Brovkin, V., Canadell, J., Chhabra, A., DeFries, R., Galloway, J., Heimann, M., 2014. Carbon and other biogeochemical cycles, Climate change 2013: the physical science basis. Contribution of Working Group I to the Fifth Assessment Report of the Intergovernmental Panel on Climate Change. Cambridge University Press, pp. 465-570.

Coleman, K., Jenkinson, D.S., Crocker, G.J., Grace, P.R., Klír, J., Körschens, M., Poulton, P.R., Richter, D.D., 1997. Simulating trends in soil organic carbon in long-term experiments using RothC-26.3. Geoderma 81, 29-44.

Davidson, E.A., 2020. Carbon dioxide loss from tropical soils increases on warming. Nature 584, 198-199.

Del Grosso, S., Parton, W., Stohlgren, T., Zheng, D., Bachelet, D., Prince, S., Hibbard, K., Olson, R., 2008. Global potential net primary production predicted from vegetation class, precipitation, and temperature. Ecology 89, 2117-2126.

Fan, N., Koirala, S., Reichstein, M., Thurner, M., Avitabile, V., Santoro, M., Ahrens, B., Weber, U., Carvalhais, N., 2020. Apparent ecosystem carbon turnover time: uncertainties and robust features. Earth System Science Data 12, 2517-2536.

Friedlingstein, P., Jones, M.W., O'Sullivan, M., Andrew, R.M., Hauck, J., Peters, G.P., Peters, W., Pongratz, J., Sitch, S., Le Quéré, C., Bakker, D.C.E., Canadell, J.G., Ciais, P., Jackson, R.B., Anthoni, P., Barbero, L., Bastos, A., Bastrikov, V., Becker, M., Bopp, L., Buitenhuis, E., Chandra, N., Chevallier, F., Chini, L.P., Currie, K.I., Feely, R.A., Gehlen, M., Gilfillan, D., Gkritzalis, T., Goll, D.S., Gruber, N., Gutekunst, S., Harris, I., Haverd, V., Houghton, R.A., Hurtt, G., Ilyina, T., Jain, A.K., Joetzjer, E., Kaplan, J.O., Kato, E., Klein Goldewijk, K., Korsbakken, J.I., Landschützer, P., Lauvset, S.K., Lefèvre, N., Lenton, A., Lienert, S., Lombardozzi, D., Marland, G., McGuire, P.C., Melton, J.R., Metzl, N., Munro, D.R., Nabel, J.E.M.S., Nakaoka, S.I., Neill, C., Omar, A.M., Ono, T., Peregon, A., Pierrot, D., Poulter, B., Rehder, G., Resplandy, L., Robertson, E., Rödenbeck, C., Séférian, R., Schwinger, J., Smith, N., Tans,

P.P., Tian, H., Tilbrook, B., Tubiello, F.N., van der Werf, G.R., Wiltshire, A.J., Zaehle, S., 2019. Global Carbon Budget 2019. Earth Syst. Sci. Data 11, 1783-1838.

Gaudinski, J.B., Trumbore, S.E., Davidson, E.A., Zheng, S.H., 2000. Soil carbon cycling in a temperate forest: radiocarbon-based estimates of residence times, sequestration rates and partitioning of fluxes. Biogeochemistry 51, 33-69.

Geyh, M.A., 2005. Handbuch der physikalischen und chemischen Altersbestimmung. Wiss. Buchges.

Goldsmith, D., 1997. Einstein's greatest blunder?: the cosmological constant and other fudge factors in the physics of the universe. Harvard University Press.

Graven, H., Allison, C.E., Etheridge, D.M., Hammer, S., Keeling, R.F., Levin, I., Meijer, H.A., Rubino, M., Tans, P.P., Trudinger, C.M., 2017. Compiled records of carbon isotopes in atmospheric CO2 for historical simulations in CMIP6. Geoscientific Model Development 10, 4405-4417.

Guo, D., Li, H., Mitchell, R.J., Han, W., Hendricks, J.J., Fahey, T.J., Hendrick, R.L., 2008. Fine root heterogeneity by branch order: exploring the discrepancy in root turnover estimates between minirhizotron and carbon isotopic methods. New Phytologist 177, 443-456.

Hashimoto, S., Carvalhais, N., Ito, A., Migliavacca, M., Nishina, K., Reichstein, M., 2015. Global spatiotemporal distribution of soil respiration modeled using a global database. Biogeosciences 12, 4121-4132.

Hua, Q., Barbetti, M., Rakowski, A.Z., 2013. Atmospheric radiocarbon for the period 1950-2010. Radiocarbon 55.

Iversen, C.M., 2010. Digging deeper: fine‐root responses to rising atmospheric CO2 concentration in forested ecosystems. New Phytologist 186, 346-357.

Jackson, R.B., Mooney, H.A., Schulze, E.-D., 1997. A global budget for fine root biomass, surface area, and nutrient contents. Proceedings of the National Academy of Sciences 94, 7362-7366.

Jenkinson, D.S., Coleman, K., 2008. The turnover of organic carbon in subsoils. Part 2. Modelling carbon turnover. European Journal of Soil Science 59, 400-413.

Kelleher, B.P., Simpson, A.J., 2006. Humic Substances in Soils: Are They Really Chemically Distinct? Environmental Science & Technology 40, 4605-4611.

Koven, C.D., Hugelius, G., Lawrence, D.M., Wieder, W.R., 2017. Higher climatological temperature sensitivity of soil carbon in cold than warm climates. Nature Climate Change 7, 817-+.

Lehmann, J., Kleber, M., 2015. The contentious nature of soil organic matter. Nature 528, 60-68.

Lehmann, J., Solomon, D., Kinyangi, J., Dathe, L., Wirick, S., Jacobsen, C., 2008. Spatial complexity of soil organic matter forms at nanometre scales. Nature Geoscience 1, 238-242.

Lukac, M., 2012. Fine Root Turnover, In: Mancuso, S. (Ed.), Measuring Roots. Springer Verlag, Berlin Heidelberg, pp. 363-373.

Luo, Z., Wang, G., Wang, E., 2019. Global subsoil organic carbon turnover times dominantly controlled by soil properties rather than climate. Nature Communications 10.

Matamala, R., Gonzalez-Meler, M.A., Jastrow, J.D., Norby, R.J., Schlesinger, W.H., 2003. Impacts of fine root turnover on forest NPP and soil C sequestration potential. Science 302, 1385-1387.

Metzler, H., Müller, M., Sierra, C.A., 2018. Transit-time and age distributions for nonlinear time-dependent compartmental systems. Proceedings of the National Academy of Sciences 115, 1150-1155.

Myhre, G., Shindell, D., Pongratz, J., 2014. Anthropogenic and natural radiative forcing.

Pearson, G.W., 1986. Precise calendrical dating of known growth-period samples using a curve fitting technique. Radiocarbon 28, 292-299.

Pritchard, S.G., Strand, A.E., 2008. Can you believe what you see? Reconciling minirhizotron and isotopically derived estimates of fine root longevity. New Phytologist 177, 287-291.

Reimer, P.J., Baillie, M.G., Bard, E., Bayliss, A., Beck, J.W., Bertrand, C.J., Blackwell, P.G., Buck, C.E., Burr, G.S., Cutler, K.B., 2004a. IntCal04 terrestrial radiocarbon age calibration, 0–26 cal kyr BP.

Reimer, P.J., Bard, E., Bayliss, A., Beck, J.W., Blackwell, P.G., Ramsey, C.B., Buck, C.E., Cheng, H., Edwards, R.L., Friedrich, M., 2013. IntCal13 and Marine13 radiocarbon age calibration curves 0–50,000 years cal BP. Radiocarbon 55, 1869-1887.

Reimer, P.J., Brown, T.A., Reimer, R.W., 2004b. Discussion: Reporting and calibration of post-bomb ^{14}C data. Radiocarbon 46, 1299-1304.

Riley, W.J., Gaudinski, J.B., Torn, M.S., Joslin, J., Hanson, P.J., 2009. Fine‐root mortality rates in a temperate forest: Estimates using radiocarbon data and numerical modeling. New Phytologist 184, 387-398.

Robinson, D., 2007. Implications of a large global root biomass for carbon sink estimates and for soil carbon dynamics. Proceedings of the Royal Society B: Biological Sciences 274, 2753-2759.

Saatchi, S.S., Harris, N.L., Brown, S., Lefsky, M., Mitchard, E.T., Salas, W., Zutta, B.R., Buermann, W., Lewis, S.L., Hagen, S., 2011. Benchmark map of forest carbon stocks in tropical regions across three continents. Proceedings of the National Academy of Sciences 108, 9899-9904.

Saugier, B., Roy, J., Mooney, H., 2001. Estimations of global terrestrial productivity: Converging toward a single number? Terrestrial Global Productivity, 543-557.

Schenk, H.J., Jackson, R.B., 2002. The global biogeography of roots. Ecological Monographs 72, 311-328.

Schmidt, M.W.I., Torn, M.S., Abiven, S., Dittmar, T., Guggenberger, G., Janssens, I.A., Kleber, M., Kogel-Knabner, I., Lehmann, J., Manning, D.A.C., Nannipieri, P., Rasse, D.P., Weiner, S., Trumbore, S.E., 2011. Persistence of soil organic matter as an ecosystem property. Nature 478, 49-56.

Sierra, C.A., Müller, M., Metzler, H., Manzoni, S., Trumbore, S.E., 2017. The muddle of ages, turnover, transit, and residence times in the carbon cycle. Global Change Biology 23, 1763-1773.

Sokol, N.W., Bradford, M.A., 2019. Microbial formation of stable soil carbon is more efficient from belowground than aboveground input. Nature Geoscience 12, 46-53.

Strand, A.E., Pritchard, S.G., McCormack, M.L., Davis, M.A., Oren, R., 2008. Irreconcilable differences: Fine-root life spans and soil carbon persistence. Science 319, 456-458.

Stuiver, M., Polach, H.A., 1977. Reporting of ^{14}C data – discussion. Radiocarbon 19, 355-363.

Thurner, M., Beer, C., Santoro, M., Carvalhais, N., Wutzler, T., Schepaschenko, D., Shvidenko, A., Kompter, E., Ahrens, B., Levick, S.R., Schmullius, C., 2014. Carbon stock and density of northern boreal and temperate forests. Global Ecology and Biogeography 23, 297-310.

Trumbore, S., 2009. Radiocarbon and soil carbon dynamics. Annual Review of Earth and Planetary Sciences 37, 47-66.

Trumbore, S., Sierra, C., Pries, C.H., 2016. Radiocarbon Nomenclature, Theory, Models, and Interpretation: Measuring Age, Determining Cycling Rates, and Tracing Source Pools, Radiocarbon and Climate Change. Springer, pp. 45-82.

Trumbore, S.E., Gaudinski, J.B., 2003. The secret lives of roots. Science 302, 1344-1345.

Vitousek, P.M., 1984. Litterfall, Nutrient Cycling, and Nutrient Limitation in Tropical Forests. Ecology 65, 285-298.

2 Study I

"Reconciling ^{14}C and minirhizotron-based estimates of fine-root turnover with survival functions"

Contribution: I conceived the idea for the study, conducted the study, visualized the results, and wrote the manuscript with inputs from Markus Reichstein.

Reconciling ^{14}C and minirhizotron-based estimates of fine-root turnover with survival functions

Bernhard Ahrens[1*], Markus Reichstein[1]

[1] Max-Planck-Institute for Biogeochemistry, Hans-Knöll-Str. 10, 07745 Jena, Germany

* Correspondence: B. Ahrens; e-mail: bernhard.ahrens@bgc-jena.mpg.de

Number of text pages: 20

Number of tables: 3

Number of figures: 2

Short running title: Reconciling ^{14}C and minirhizotron-based estimates of fine-root turnover with survival functions

Corresponding author: Bernhard Ahrens, Max-Planck-Institute for Biogeochemistry, Hans-Knöll-Str. 10, 07745 Jena, Germany

e-mail: bernhard.ahrens@bgc-jena.mpg.de

telephone: +49 3641 576295

FAX: +49 3641 577200

2.1 Abstract

The turnover of fine-roots is a crucial component for the input of carbon to the soil. The amount of root litter input is depending on estimates of turnover times from different techniques. Turnover times from fine-root cameras (minirhizotrons) often yield 75% higher root litter input estimates than turnover times estimated with the bomb-radiocarbon signature of fine-roots. We introduce a generic framework for the analysis of fine-root ^{14}C with different survival functions. So far, mostly an exponential function has been used to estimate the turnover time and mean age of fine-roots. In the context of the introduced survival function framework we clarify the terms turnover time, mean residence time, mean longevity and mean age commonly used in studies of root turnover. Using a unique time series of fine-root ^{14}C (Fröberg, 2012), we test if survival functions other than the exponential function are better in accordance with turnover time estimates commonly found with other methods. A survival function that corresponds to a two-pool model was best in agreement with minirhizotron-based estimates (mean residence time of 1.9 years). We argue that using fine-root ^{14}C and minirhizotron time-to-death data together would give the best constraints on fine-root turnover. At the same time this could allow quantifying systematic biases inherent two both techniques.

2.2 Introduction

Fine-root turnover constitutes a substantial component of the global terrestrial carbon cycle (Jackson et al., 1996; Gill and Jackson, 2000). It is, however, challenging to constrain the magnitude of belowground carbon transfer because root turnover is very difficult to quantify in situ compared to aboveground litterfall (Trumbore and Gaudinski, 2003).

Turnover time, mean residence time, mean longevity, mean lifespan, and mean lifetime are often used interchangeably to describe root turnover. Often these notions are used as synonyms, although turnover time is only equal to the other notions if the root system is in steady state (Bolin and Rodhe, 1973; Strand et al., 2008; Gaudinski et al., 2010). In this case root production or root mortality can be calculated as the root biomass divided by one of these notions. Further, studies often report the mean age of roots which is equal to the aforementioned notions if the probability that a root dies follows an exponential function (Rodhe, 1992).

Different experimental methods exist to quantify fine-root turnover. However, the turnover times estimated by different methods largely differ: turnover times from inventory based approaches are commonly between < 1 and 3 years (Trumbore and Gaudinski, 2003), minirhizotrons yield turnover times of e.g. ~ 1.8 years when the roots around the tube have reached steady state (Strand et al., 2008). Turnover times estimated using the measurements of ^{14}C in fine-roots are, however, much longer, e.g. Gaudinski (2001) 3-18 years, Gaul et al. (2008) 7.6 years and Fröberg (2012) ~ 8 years.

The implications of such differences in fine-root turnover times would be of great significance for the global estimation of the belowground carbon budget (Lukac, 2012). Assuming steady state of the root population, root production (allocation of net primary productivity to the root system) and root mortality (root litter input to the soil organic matter pool) would be reduced by 75% for a root turnover time of 8 years compared to a root turnover time of 2 years. Hence, it is necessary to try to reconcile the data gathered with the different methods by using a common model which would allow addressing the possible drawbacks of the different methods.

Fröberg (2012) presented a unique time series of fine-root ^{14}C measured from archived samples of O horizons of Norway spruce (*Picea abies* (L.) H.Karst.) dominated forests in Southern Sweden and used two simple root-turnover models presented in Gaudinski et al. (2001) to estimate a turnover time of 8 years. This time series is unique because it covers the complete length of the "bomb radiocarbon" curve, which describes the prominent peak of the ^{14}C content in the troposphere due to aboveground thermonuclear weapons testing during the late 1950s and early 1960s, and the subsequent quasi-exponential decline of the atmospheric ^{14}C content due to dilution into biosphere and oceans (Hua and Barbetti, 2004; Levin and Kromer, 2004).

There has been some debate if the turnover time estimated with the ^{14}C of fine-roots actually represents the root turnover time *(Gaudinski, 2001; Guo et al., 2008; Sah et al., 2011)*: If also stored carbon and not only recent photosynthate is used to grow new roots (Gaudinski et al., 2001), the fine-root ^{14}C mean residence time would overestimate the fine-root mean residence time by the time the carbon atoms have already spent as stored carbon. Gaudinski et al. (2009), for example, estimated that the carbon used to grow roots in a temperate deciduous oak forest is already 0.4 years old, while Tierney and Fahey (2002) and Gaul et al. (2009) found that newly grown roots in a northern hardwood forest and a Norway spruce stand have the ^{14}C signature of freshly assimilated photosynthate. Sah et al. (2011) found that for very fine roots (with a diameter < 0.5 mm as in

Fröberg (2012)) the age estimated with fine-root ^{14}C is in accordance with the known age of roots, while for roots with a diameter of 1.5-2 mm storage carbon might play a substantial role.

Using the fine-root ^{14}C time series from Fröberg (2012) as a test case, our objectives for this paper are: (i) To present a unifying framework that allows to break down all root turnover models to a convolution of the atmospheric radiocarbon curve with a root survival function

(ii) To clarify the concepts of turnover time, mean residence time and mean age, and the relations between these notions for a root system under steady state with the help of this framework.

(iii) To analyze the performance and characteristics of different root survival functions, and to compare the fitted mean residence times with mean residence times commonly found with inventory based approaches (<1-3 years Trumbore and Gaudinski (2003)) and especially minirhizotron studies (~ 1.8 years, Strand et al. (2008)).

2.3   Material and methods

2.3.1   Atmospheric ^{14}C record

We constructed a time series of tropospheric Δ^{14}C measurements from Vermunt (1959-1976) and Schauinsland (1976-2011) (personal communication by Ingeborg Levin 2011), which are representative for sites influenced by fossil fuel emissions (Levin and Kromer, 2004). From the individual atmospheric flask samples we calculated time-weighted averages for the summer months from May to August which are commonly used for a good representation of the ^{14}C values in the vegetation (Levin and Kromer, 2004). For the years 1955-1958 these time-weighted averages were appended with data from the Northern Hemisphere Zone 1 compilation by Hua and Barbetti (2004). This compilation is representative for the Northern Hemisphere north of 40°N and consists of tree ring data from Kiel (Germany), Hungary and Bear Mountain (New York, USA). Prior to 1955 the UW 14C atmospheric single year data set from 1510 to 1954 was used (Stuiver and Braziunas, 1993; Stuiver et al., 1998).

2.3.2 Survival function framework for root turnover

Fröberg (2012) used his unique fine-root ^{14}C time series to test two simple root-turnover models presented in Gaudinski et al. (2001):

(1) A time-shift model (model 1 in Fröberg (2012)) was not able to give consistent estimates of fine-root ^{14}C for samples before 1985. This model assumes that all fine-roots are grown in the same year and that the root age can be calculated as the necessary time shift τ for the atmospheric ^{14}C time series to match the fine-root ^{14}C value of a certain year t :

$$Root\,^{14}C(t) = Atm\,^{14}C(t - \tau)$$

(2-1)

where $Root\,^{14}C(t)$ and $Atm\,^{14}C(t)$ is the ^{14}C content in roots and in the atmosphere in year t (in pM, *percent Modern* as defined in Stuiver and Polach (1977)).

(2) Model 2 in Fröberg (2012) is a 1-pool model, which assumes that root ^{14}C follows first-order kinetics with turnover rate *k* and that root biomass is in steady-state:

$$\frac{dRoot^{14}C(t)}{dt} = k \cdot Atm^{14}C(t) - (k + \lambda) \cdot Root^{14}C(t)$$

(2-2)

where λ accounts for radioactive decay of ^{14}C and the term $k \cdot Atm\,^{14}C(t)$ describes the production of new fine-root ^{14}C under steady state. Fröberg (2012) uses forward differencing or Euler integration with yearly time-steps to solve Equation (2-2):

$$Root\,^{14}C(t) = k \cdot Atm\,^{14}C(t) + Root\,^{14}C(t-1) \cdot (1 - k - \lambda)$$

(2-3)

This first-order kinetics model was able to reproduce the measurements presented in Fröberg (2012) with a mean residence time of 8 years.

Mean residence time, τ_r, can generally be defined as the mean time that a carbon atom spends in the root system. Table 2-1 gives an overview of commonly used synonyms for mean residence time: the term mean longevity is frequently used when analyzing time-to-death curves of

roots from minirhizotron studies; mean lifespan or mean lifetime are often used as equivalent terms (Strand et al., 2008; Gaul et al., 2009; Riley et al., 2009; Kikuzawa and Lechowicz, 2011).

Table 2-1: Overview of time measures commonly used to describe survival functions and age functions. Some of these measures are common in all ecological fields, while some are used as synonyms when studying root turnover. Most of the distinctions are taken from Bolin and Rodhe (1973) and Rodhe (1992), and refined with notions used in Majdi (2001) and Strand et al. (2008).

Measure	Description
τ_r	mean residence time, mean transit time, mean longevity, mean lifespan, mean lifetime
τ_a	mean age
τ_o	turnover time

Root turnover time, τ_o, is equal to mean residence time, τ_r, if the root system is in steady state. Following the definitions by Rodhe (1992) the root turnover time can generally be defined as

$$\tau_o = \frac{\text{root biomass}}{\text{root mortality}}\text{, and under steady state of the root system as}$$

$$\tau_o = \frac{\text{root biomass}}{\text{root mortality}} = \frac{\text{root biomass}}{\text{root production}}\text{.}$$

Fine-root ^{14}C studies often use the notion *mean root carbon residence time* instead of *mean root residence time* (e.g. Gaudinski et al. (2001) and Fröberg (2012)) to highlight that they cannot rule out the use of storage carbon for growth of new fine-roots. If, however, this is the case, the notion *mean root carbon residence time* is not a very meaningful quantity because it comprises the residence time of carbon in two different reservoirs: storage pools and roots. Instead we follow the strategy proposed by Riley et al. (2009) in the Radix model to account for the age of carbon that is used to build new fine-roots. Instead of assuming that $Atm^{14}C(t)$ constitutes the ^{14}C content of new roots, $Atm^{14}C(t)$ is modified so that it also reflects the time the carbon has already spent in a storage pool.

For the fine-root ^{14}C values presented by Fröberg (2012) we follow the findings by Sah et al. (2011) that the ^{14}C content of very fine roots (0-0.5 mm diameter) reflects their known age. Further, we compared the ^{14}C content of root screens of a Norway spruce dominated forest in central Sweden

(Knottåsen, Table S11 in Gaudinski et al. (2009)) with the individual atmospheric ^{14}C flask samples at Schauinsland (Levin and Kromer, 2004), and could not find evidence for the use of stored carbon for fine-root growth (cf. Gaudinski et al. (2009)). Hence, we assumed a storage residence time of 0 years for this study. Nevertheless, one could use minirhizotron time-to-death data together with the fine-root ^{14}C to estimate the storage residence time. These time-to-death data, however, might also be biased towards longer lifespans because roots are still classified as alive when they are dead, but have not disappeared yet. One could try to account for this bias by introducing a parameter that cuts off time-to-death data earlier.

Based on the framework by Manzoni and Porporato (2009) we can formulate a generic time-shift model for the pM value of roots, $Root\,^{14}C(t)$, if we define survival functions for roots and assume steady state of root dynamics:

$$Root^{14}C(t) = \int\limits_{0}^{\infty} \tau_o^{-1} \cdot Atm^{14}C(t-\tau) \cdot S(\tau) \cdot e^{-\lambda \cdot \tau} d\tau, \qquad (2\text{-}4)$$

where τ_o is the turnover time, $Atm^{14}C(t)$ the atmospheric pM value in year t, $S(\tau)$ describes the fraction of roots surviving **at least** to age τ (cf. Niinemets and Lukjanova (2003), Manzoni et al. (2009), and Manzoni et al. (2012)), and $e^{-\lambda \cdot \tau}$ accounts for the radioactive decay of ^{14}C. When the root population is in steady state, the turnover time τ_o is equal to the mean residence time τ_r (Table 2-1). The mean residence time can be calculated as $\tau_r = \int\limits_{0}^{\infty} S(\tau)d\tau$ (Manzoni et al., 2012). Equation (2-4) essentially describes $Root^{14}C$ in a certain year t as the sum of ^{14}C inputs via root production from previous years τ weighted by the fraction of fine-roots $S(\tau)$ that live at least for τ years. The atmospheric pM values $Atm^{14}C$ are used as a proxy for the ^{14}C content of new roots. Consequently, the term $\tau_o^{-1} \cdot Atm^{14}C(t-\tau)$ describes the ^{14}C input via root production under the assumption that root biomass is in steady state (equivalent to the term $k \cdot Atm^{14}C(t)$ in Equations (2-2) and 3.

Mean age of roots, τ_a, is often reported apart from τ_r and/or τ_o in studies on root dynamics. τ_a can be derived from the age distribution of roots. The age density distribution can be calculated as the amount of roots with age τ over the total root biomass (Manzoni et al., 2009). When root

biomass is in steady state, the age density distribution $a(\tau)$ is directly related to the survival function via $a(\tau) = \dfrac{S(\tau)}{\tau_r}$ (Manzoni et al., 2009). In order to make the age density distribution comparable to the survival function, we calculate the age function as $A(\tau) = \int\limits_{\tau}^{\infty} a(\tau)d\tau$. Hence, $A(\tau)$ describes the fraction of roots that are at least τ years old. The mean age $\tau_a = \int\limits_{0}^{\infty} A(\tau)d\tau$. Please note that the commonly used exponential distribution is the only survival function for which $\tau_a = \tau_r = \tau_o$ (Rodhe (1992); Gaudinski et al. (2010), Table 3).

2.3.3 Calibration of different survival functions

If we translate the description of the first method in Fröberg (2012) and Gaudinski et al. (2001), which was designed to estimate root age and turnover of **single roots**, to a **root population,** the survival function has to follow a unit step function (Table 2-2 and Table 3, "UnitStep"). When we use the "UnitStep" survival curve for a root population in steady state $\tau_a = 0.5 \cdot \tau_r$, and $A(\tau)$ decreases linearly with increasing τ (Table 3).

If we want to force Equation 1 into the generic survival function framework (Equation 4), we have to employ a root survivorship function $S(\tau)$ that has a single spike where τ is equal to the root age (survival curve "Dirac" in Table 2-2 and Table 2-3). This kind of function is commonly referred to as a Dirac delta function (Weisstein, 2013). However, this survival function is actually already mathematically impossible because survival functions $S(\tau)$ are only allowed to be monotonically decreasing (cf. section 2.2). Gaudinski et al. (2001) and Fröberg (2012) also emphasized that the time-shift model only makes sense for single roots, but not for root populations. Hence, the survival curve "UnitStep" represents a translation of how model 1 in Fröberg (2012) is described, while "Dirac" directly employs a shifted $Atm^{14}C(t)$ to estimate $Root^{14}C$.

Nevertheless, Equation 1 (and thus the survival function "Dirac") is sometimes used in soil organic matter (SOM) models (Michalzik et al., 2003; Tipping et al., 2005; Schulze et al., 2009) to quantify the ^{14}C input to the SOM pool because it gives similar fine-root ^{14}C contents as a 1-pool model in the time after 1990 when $\tau_r < 10$ years (Fröberg, 2012). "Dirac" was fitted to all four data

points simultaneously to highlight how wrong the model is when used for root populations and several data points in time.

Model 2 from Fröberg (2012) corresponds to an exponential relationship between root survivorship S and root age τ ("Exponential", Table 2-3):

$$S(\tau) = \exp(-k \cdot \tau), \tag{2-5}$$

where k is equivalent to the first-order decomposition rate from Equations (2-2) and (2-3) and to τ_o^{-1} in Equation (2-4). As another one-parameter survival function we tried a linearly decreasing function ("Linear", Table 2-2 and Table 2-3).

Other survival functions $S(\tau)$ that were tested either stem from simple pool models (here a serial 2-pool model) or are derived from cumulative distributions functions $F(\tau)$ commonly used for modeling lifetime data, so that $S(\tau) = 1 - F(\tau)$ with τ from $[0, \infty)$ (Table 2-2, Table 2-3).

Table 2-2: Overview of used survival functions.

What S(τ) i	Equation of survival function	Number of parameters
UnitStep	$S(\tau) = \begin{cases} 0 & \text{for } \alpha < \tau < 0 \\ 1 & \text{for } 0 \leq \tau \leq \alpha \end{cases}$	1
Dirac ≙ model 1 in Fröberg (2012)	$S(\tau) = \begin{cases} 0 & \text{for } \tau \neq \alpha \\ 1 & \text{for } \tau = \alpha \end{cases}$	1
Exponential ≙ model 2 in Fröberg (2012)	$S(\tau) = \exp(-k \cdot \tau)$	1
Linear	$S(\tau) = \max(1 - \theta \cdot \tau; 0)$	1
Weibull	$S(\tau) = \exp\left(-\left(\dfrac{\tau}{\lambda}\right)^k\right)$	2
Series2Pools[a]	$S(\tau) = \dfrac{\exp(-(k_1 + k_2) \cdot \tau) \cdot (\exp(k_2 \cdot \tau) \cdot (k_1 \cdot r - k_2) - k_1 \cdot (r-1) \cdot \exp(k_1 \cdot \tau))}{k_1 - k_2}$	3
GenEx	$S(\tau) = 1 - (1 - \exp(-\beta \cdot \tau))^\alpha$	2
LogNorm[b]	$S(\tau) = 1 - \left(\dfrac{1}{2}\left(1 + \mathrm{erf}\left(\dfrac{\ln(\tau) - \mu}{\sigma \cdot \sqrt{2}}\right)\right)\right)$	2

[a] The "Series2Pool" survival function is based on the derivation by Manzoni et al. (2009).

[b] erf(x) denotes the Gaussian error function.

The 2-pool model in serial setting ("Series2Pools"), for example, is mathematically equivalent to the Introductory Carbon Balance Model (ICBM) used for soil organic carbon modeling (Andrén and Kätterer, 1997). The "Series2Pools" survival function is based on the assumption that all roots belong at first to a fast-cycling root population while a part of this population can undergo a "work hardening" (Tahmasbi and Rezaei, 2008) to a slowly-cycling root population. This "work-hardening" could for example be interpreted mechanistically as progressive suberization of roots. Please note that the Radix model as presented in Riley et al. (2009) and Gaudinski et al. (2010) is in essence also a 2-pool model, but in contrast uses a parallel setting.

Weibull and log-normal distributions (2 parameters, Table 2-2) are frequently used to analyze root survival times from minirhizotrons (Strand et al., 2008; Gaul et al., 2009). Apart from the well-known Weibull- and log-normal distribution, we also introduced the generalized exponential distribution ("GenEx" in Table 2-2 and Table 2-3, Gupta and Kundu (1999), Mahmoudi and Jafari (2012)) with its two parameters α and β (Table 2-2).

Table 2-2 gives an overview of the different survival functions used in this study. The second-last column in Table 2-3 should be used to get an idea what these functions look like. The parameters of these functions were fitted to the root ^{14}C values reported in Fröberg (2012) with the differential evolution adaptive metropolis algorithm (Vrugt et al., 2009a; Vrugt et al., 2009b; Guillaume and Andrews, 2012). Here, we only used this algorithm to get the best parameter set, but did not use all accepted parameter sets after convergence of the algorithm to quantify parameter uncertainty.

2.3.4 Performance measures

The performance of the different survival functions in Table 2-2 was compared using the sum of squared weighted residuals (SSWR) between the measured live fine-root ^{14}C and the modeled $Root\,^{14}C(t)$, where the analytical uncertainties reported in Fröberg (2012) are used as weight. Further, we used the Akaike information criterion corrected for small sample sizes (AICc, Burnham and Anderson (2004)) and the Bayesian information criterion (BIC, Kass and Raftery (1995)) to evaluate the performance of the different survival functions relative to their number of parameters. We report $AICc_i$ and BIC_i values of the individual survival curves i rescaled to the minimum AICc or BIC value observed across all survival functions i used in Table 2-3: $\Delta AICc_i = AICc_i - AIC_{min}$ and $\Delta BIC_i = BIC_i - BIC_{min}$ (Burnham and Anderson, 2004; Manzoni et al., 2012). This allows for a quick strength-of-evidence comparison (Burnham and Anderson, 2004) across the different survival functions i.

Survival functions with a $\Delta AICc_i$ or $\Delta BIC_i < 2$ show no evidence for a difference in model performance (Kass and Raftery, 1995; Burnham and Anderson, 2004).

Most importantly, we checked if the mean residence time of the fitted survival curve is in accordance with inventory based approaches (<1-3 years Trumbore and Gaudinski (2003)) and especially minirhizotron studies (e.g. ~ 1.8 years estimated from fine-root survival times in the Duke FACE minirhizotron study, cf. Figure 2 in Strand et al. (2008)).

2.4 Results and discussion

2.4.1 Performance and characteristics of different survival curves

The "Series2Pools" survival function shows the best fit to the fine-root ^{14}C data (SSWR, Table 2-3). The survival functions "GenEx", "Weibull", "LogNorm" and "Exponential" still have a reasonably low SSWR (in ascending order), while the survival function "UnitStep", "Dirac" and "Linear" show a considerable worse fit (Table 2-3). The ΔBIC values – also taking the goodness-of-fit relative to the number of parameters into account (Table 2-2) – show the same pattern as the SSWR (Table 2-3): ΔBIC values > 10 for "UnitStep", "Dirac" and "Linear" are a strong evidence against these models, while the evidence against survival functions "GenEx", "Weibull", "LogNorm" and "Exponential" is less strong, but still substantial. The "Series2Pools" survival function has the best BIC value.

The results for the $\Delta AICc$ deviate from the findings for the two aforementioned performance measures: The "Exponential" survival function with the lowest SSWR of all one-parameter-models has the by far best AICc value (Table 2-3). The second best AICc value is achieved by the "Linear" survival function, which has a rather poor SSWR, but also only one parameter to fit. All other survival functions show a rather poor AICc value; the AICc is even always infinity for the "Series2Pools" model due to the relation of the number of data points to the number of parameters.

Using the data from Fröberg (2012) as a test case, these statistical performance measures do not give a conclusive picture in terms of model selection, except that "UnitStep", "Dirac" and maybe also "Linear" may be discarded. Hence, we take a look at further characteristics of the different survival curves such as mean residence time and mean age.

The mean residence time of the "Dirac" model is theoretically always 1 (!) year, because the

integral $\tau_r = \int_0^\infty S(\tau)d\tau$ is not different from 0 over the whole interval of integration [0;∞) except for

$\tau = \alpha$ where $S(\tau) = 1$ (Table 2-3). The fitted parameter α (for this dataset ca. 2 years) is always

equal to the mean age τ_a because $A(\tau)$ is 1 in the interval from 0 to α, and 0 for $\tau > 0$. Hence,

$\tau_a = \int_0^\infty A(\tau)d\tau = 1 \cdot (\alpha - 0)$. This highlights again that the "Dirac" model or time-shift model is

physically impossible. The fitted mean residence time (τ_r = 7 years) of the "UnitStep" survival

function is also considerably longer than what we would expect from minirhizotron studies (Strand et

al., 2008).

Table 2-3: Characteristics and performance of different survival functions i. τ_r gives the mean residence time in years based on the fitted parameters of the respective survival function S(τ); τ_a is the corresponding mean age. SSWR is the best sum of squared weighted residuals of fitted against observed ^{14}C in roots, where the analytical errors are used as weight. ΔAICc$_i$ and ΔBIC$_i$ show the performance of the survival function i in relation to the number of parameters. A value of 0.0 indicates the best performing model with regard to ΔAICc$_i$ and ΔBIC$_i$. The second-last column shows the fitted survival (black solid line) and age functions (gray dashed line) with τ_r visualized as a black square and the mean age τ_a as a gray circle. Please note that the Dirac delta function is denoted as a black arrow. The last column shows the ^{14}C content of roots in pM (modeled and observed) and the atmospheric curve as a comparison.

What S(τ) i	τ_r [yr]	τ_a [yr]	SSWR	ΔAICc_i	ΔBIC_i	A(τ) fraction of roots being at least τ years old, mean age τ_a / S(τ) fraction of roots surviving at least to age τ, mean residence time τ_r	¹⁴C (pM) in the atmosphere (gray lines) and in roots (black line modeled, open circles observed)
UnitStep	7.0	3.5	1147	11.0	19.9		
irac ≙ model 1 in Fröberg (2012)	1.0	2.0	893	10.0	18.9		
Exponential ≙ model 2 in Fröberg (2012)	7.1	7.1	73	0.0	8.9		
Linear	10.1	6.7	378	6.6	15.5		
Weibull	5.0	8.0	19	10.7	4.9		
Series2Pools	1.9	7.7	4	∞	0.0		
GenEx	2.5	7.8	10	8.0	2.3		
LogNorm	6.7	8.7	44	14.0	8.2		

If we take a look at the currently most used survival function for root populations, "Exponential", we see that this is the only survival function for root populations for which $A(\tau)$ follows $S(\tau)$, and τ_r and τ_a are equal. This also means that the risk for a newly grown root to die remains constant throughout the course of its life. The fitted mean residence time τ_r of 7.1 years does not at all agree with mean residence times estimates from minirhizotrons.

The difference in the τ_r fitted in the study by Fröberg (2012) of 8 years and 7.1 years in this study stem from the forward differencing used by Fröberg (2012) (Equation 3) to solve Equation (2-2) and the numerical integration procedure used to solve Equation 4. This procedure gives the same results as a solver for ordinary differential equations (here Equation 2) with extra function evaluations at flexible time steps.

The linearly decreasing survival function $S(\tau)$, "Linear", yields a best τ_r of 10.1 years and is thus also in disagreement with mean residence time estimates from inventory and minirhizotron approaches. "UnitStep" and "Linear" are the only survival functions where the mean residence time τ_r (or mean longevity, Table 2-1) of roots is higher than the mean age τ_a of the root population (Table 2-3). This means that for this kind of survival functions the risk for a root to die a young age is low, but increases with age (Bolin and Rodhe, 1973).

The mean residence time τ_r of "Weibull" is 5 years, and thus 2.1 years lower than the τ_r of the "Exponential" survival curve. Therefore, the Weibull distribution is slightly better in accordance with the expectations from minirhizotron studies.

The fitted τ_r of 1.9 years of "Series2Pools" is very well within the range of what we expect from minirhizotron and inventory based approaches (Trumbore and Gaudinski, 2003; Strand et al., 2008). If we employed a 2-pool model in parallel setting (not shown), the best fit survival function is essentially the same as the best fit survival function for "Series2Pools". Also the mean residence time of both 2-pool models would be the same, while the parameters are obviously different and the mechanistic interpretation would be slightly different: Already at root growth it would be predetermined that a part of roots are short lived, while the rest is long lived. Nevertheless, both 2-pool models essentially show the same behavior of the survival curve.

The mean residence time τ_r of "GenEx" (2.5 years) is very similar to the one of the 2-pool serial model. Finally, a log-normal survival function ("LogNorm") gave a best τ_r of 6.7 years, which is very close to that of the "Exponential" survival function. For the survival functions "Weibull", "Series2Pools", "GenEx" and "LogNorm" the mean age τ_a is always higher than the mean residence time τ_r (Table 2-3) which means that the risk for a newly grown root to die within a short period after establishment is high, but decreases subsequently.

2.4.2   Differences between fine-root mean residence times and mean ages

While the best estimates of mean residence times τ_r are quite different between the different survival functions (Table 2-3), the best estimates of τ_a are quite similar (6.7 years to 8.7 years) for survival functions $S(\tau)$ that are positively skewed or not skewed (the last 6 survival functions in Table 2-3). Apart from using the relation of τ_a to τ_r to characterize the behavior of the survival function at hand, the benefit of reporting mean age estimates is limited because we cannot use τ_a to constrain any flux in belowground carbon cycling. It has to be noted that studies using the "Exponential" survival curve and only reporting the mean age of roots, τ_a, avoid to state the fact that for this survival function $\tau_a = \tau_r = \tau_o$. Hence, by reporting the mean age of roots they implicitly also report the turnover time of roots.

2.4.3   Minirhizotrons versus bomb-^{14}C estimates of mean root residence time

Overall, from our findings the "Series2Pools" and "GenEx" survival functions are best in accordance with estimates of τ_r from minirhizotrons (Trumbore et al., 2006; Strand et al., 2008). The mean residence times of these survival functions are considerably shorter than τ_r estimates from the commonly used "Exponential" survival function. These two functions have in common that the probability that a roots dies is high at a young age, but decreases with age. For the "Exponential" survival function the probability that a root dies stays the same regardless of the root's age.

One has to acknowledge, however, that even with the use of archived roots samples a multitude of models ("Exponential", "Weibull", "Series2Pools", "GenEx", "LogNorm") are able to fit the observations that were used here as a test case sufficiently well (Table 2-3). The fact that the curvature of these models can be quite different, especially during the first few years, highlights the

opportunity that a joint calibration to minirhizotron and fine-root ^{14}C data offers. The two extremes are the "GenEx" model (also the "Series2Pools" model) with very fast turnover in the first year and the "Exponential" model with very slow turnover in the first year.

The fact that the mean ages of the abovementioned survival functions are relatively similar (Table 2-3) shows that the fine-root ^{14}C rather provides a good constraint for that part of roots that is turning over on longer time scales, while it provides a poor constraint for what happens in the first year after root growth. Hence, comparing bomb-^{14}C derived τ_r with minirhizotron-based τ_r estimates gives an indication which models are able to reconcile both types of measurements in general, but might very well give an incomplete picture because fine-root ^{14}C data alone are unable to unequivocally constrain root turnover during the first growth year. Here, one has to mention that reported minirhizotron-based τ_r estimates often are median and not mean residence times which may lead to an underestimation of turnover for positively skewed distributions (Strand et al., 2008).

The depiction of root turnover models with differential equations in a pool setting (e.g. Equation 2 or the "Series2Pools" model in Andrén and Kätterer (1997)) facilitates a mechanistic interpretation. However, it hinders a comparison with time-to-death data from minirhizotrons which are commonly analyzed with survival functions such as the Weibull or log-normal distribution. Up to now the joint evaluation of fine-root ^{14}C and minirhizotron data has been difficult because of different evaluation frameworks.

Survival functions that are derived from cumulative distribution functions seem to be a step away from a mechanistic interpretation, but the curvature of the survival function gives a good impression what the differences between survival curves are (Table 2-3). Furthermore, the position of the age function relative to the survival function gives an indication of root turnover dynamics:

If $S(\tau) > A(\tau)$, roots live for a considerable time before a considerable part of them dies (most extreme example "UnitStep"). If $S(\tau) < A(\tau)$, most of the roots will die relatively soon, while a minority of roots will live relatively long (e.g. "Series2Pool" or "GenEx"). The distance between $S(\tau)$ and $A(\tau)$ allows assessing which of the both cases is prevailing. The "LogNormal" survival curve constitutes an exception because it is changing from $S(\tau) > A(\tau)$ to $S(\tau) < A(\tau)$ with age (Table 2-3).

2.4.4   Strategy to reconcile ^{14}C mean residence times with data from other methods

Generally, we have to take into account that a time series of ^{14}C in fine-roots that covers more than three decades and the most prominent part of the "bomb peak", as the one presented by Fröberg (2012) is definitely quite unique. Moreover, most of the studies will probably have not more than 2 data points of fine-root ^{14}C within a period of 3 years (duration of dissertations!) if archived soil samples are not available.

In this case it might be even harder to justify fitting a 2-parameter survival curve (e.g. "GenEx") or even a 3-paramater survival curve (e.g. "Series2Pools"). Still, one should at least be aware that survival curves other than "Exponential" can give much shorter mean residence times.

Better, however, we should try to use the proposed framework in a multiple constraints approach (Reichstein and Beer, 2008) to estimate τ_r from different methods quantifying root turnover. We should not only use the 1-2 data points from fine-root ^{14}C as observational constraints, but also direct estimates of τ_o from inventory based approaches (e.g. sequential coring, ingrowth cores and ingrowth nets; for a comprehensive overview cf. Lukac (2012) and especially time-to-death data from minirhizotrons as joint observational constraints.

For fine-root [14]C Gaudinski et al. (2001), for example, state that, due to a bias for larger roots when hand-picking roots, the contribution of fast cycling roots is underestimated, while minirhizotrons would be biased towards fast cycling roots. Furthermore, it is well established that mean longevity estimates from minirhizotrons have not reached equilibrium in the first 3 years after installation of the tube and are, in this case, biased towards shorter mean longevity estimates (Strand et al., 2008). Still, the strategy to use minirhizotron data solely to parameterize a fast root pool, and fine-root ^{14}C solely to parameterize a slow pool as in the Radix model (Riley et al., 2009; Gaudinski et al., 2010), introduces a non-existing relation between what we model and what we measure. This problem has already been recognized in soil organic matter (SOM) modeling where an attribution of measured SOM fractions to conceptual SOM model pools requires that the measured fraction is unique and non-composite (Smith et al., 2002). In the case of roots this would mean that roots observed in minirhizotrons would be missed when sampling roots for the analysis of ^{14}C, and vice versa. Instead the survival functions "Series2Pools" and "GenEx" show, for example, that also fine-root ^{14}C data are consistent with fast cycling pools (Table 2-3).

Fitting a survival function to data from methods other than fine-root ^{14}C, also gives the possibility to sort out reported or alleged problems of the different methods in a unifying framework. Hence, we suggest to try to account for possible drawbacks of the different methods (cf. Lukac (2012)) within the proposed unified framework, so that we possibly can quantify trade-offs between methods. This could be done by introducing bias parameters that account for systematic biases inherent to the specific method.

2.5 Conclusion

The apparent contradiction between mean residence times inferred from bomb ^{14}C and mean residence times from direct observation hinges on the assumption of a simple exponential root survival function. For an exponential survival function the probability that a root dies is independent of root age. As soon as the root survival function has a stronger curvature, i.e. a higher death rate at a young age compared to the exponential model, mean residence times are much lower than the mean age, and closer to mean residence times commonly observed in minirhizotron studies. The two-pool "suberization" model is best in accordance with minirhizotron-based estimates of mean residence times and gives at the same time a sound interpretation, however at the expense of being overparameterized, when only compared to bomb-^{14}C data. Hence, we suggest exploring to constrain this model with both fine-root ^{14}C and minirhizotron observations. This would also allow tackling systematic biases of the bomb-^{14}C and the minirhizotron method.

2.6 Supporting Material

R scripts for all analyses performed in this paper are available upon request by email to Bernhard Ahrens (bahrens@bgc-jena.mpg.de).

2.7 Acknowledgements

2.8 Symbols and Abbreviations

Symbol	Description	Units
t	time	yr
$Root^{14}C$	^{14}C content in roots	pM
$Atm^{14}C$	^{14}C content in the atmosphere	pM
k	turnover rate	yr^{-1}
λ	radioactive decay rate of ^{14}C	yr^{-1}
τ	generic age of roots in the system	yr
τ_r	mean residence time	yr
τ_o	turnover time	yr
$S(\tau)$	survival function, fraction of roots surviving at least to age τ	-
τ_a	mean age	yr
$a(\tau)$	age density distribution	-
$A(\tau)$	age function, fraction of roots that are at least τ years old	-
SSWR	sum of squared weighted residuals	-
AICc	Akaike information criterion corrected for small sample sizes	-
BIC	Bayesian information criterion	-
ΔAICc	AICc rescaled to the minimum AICc of all tested survival functions	-
ΔBIC	BIC rescaled to the minimum BIC of all tested survival functions	-

2.9 References

Andrén, O., Kätterer, T., 1997. ICBM: The introductory carbon balance model for exploration of soil carbon balances. Ecological Applications 7, 1226-1236.

Bolin, B., Rodhe, H., 1973. A note on the concepts of age distribution and transit time in natural reservoirs. Tellus 25, 58-62.

Burnham, K.P., Anderson, D.R., 2004. Multimodel Inference: Understanding AIC and BIC in Model Selection. Sociological Methods & Research 33, 261-304.

Fröberg, M., 2012. Residence time of fine-root carbon using radiocarbon measurements of samples collected from a soil archive. Journal of Plant Nutrition and Soil Science 175, 46-48.

Gaudinski, J.B., 2001. Belowground carbon cycling in three temperate forests of the eastern United States. University of California, Irvine.

Gaudinski, J.B., Torn, M.S., Riley, W.J., Dawson, T.E., Joslin, J.D., Majdi, H., 2010. Measuring and modeling the spectrum of fine-root turnover times in three forests using isotopes, minirhizotrons, and the Radix model. Global Biogeochemical Cycles 24, GB3029.

Gaudinski, J.B., Torn, M.S., Riley, W.J., Swanston, C., Trumbore, S.E., Joslin, J.D., Majdi, H., Dawson, T.E., Hanson, P.J., 2009. Use of stored carbon reserves in growth of temperate tree roots and leaf buds: analyses using radiocarbon measurements and modeling. Global Change Biology 15, 992-1014.

Gaudinski, J.B., Trumbore, S.E., Davidson, E.A., Cook, A.C., Markewitz, D., Richter, D.D., 2001. The age of fine-root carbon in three forests of the eastern United States measured by radiocarbon. Oecologia 129, 420-429.

Gaul, D., Hertel, D., Leuschner, C., 2008. Effects of experimental soil frost on the fine-root system of mature Norway spruce. Journal of Plant Nutrition and Soil Science 171, 690-698.

Gaul, D., Hertel, D., Leuschner, C., 2009. Estimating fine root longevity in a temperate Norway spruce forest using three independent methods. Functional Plant Biology 36, 11-19.

Gill, R.A., Jackson, R.B., 2000. Global patterns of root turnover for terrestrial ecosystems. New Phytologist 147, 13-31.

Guillaume, J., Andrews, F., 2012. dream: DiffeRential Evolution Adaptive Metropolis.

Guo, D., Li, H., Mitchell, R.J., Han, W., Hendricks, J.J., Fahey, T.J., Hendrick, R.L., 2008. Fine root heterogeneity by branch order: exploring the discrepancy in root turnover estimates between minirhizotron and carbon isotopic methods. New Phytologist 177, 443-456.

Gupta, R.D., Kundu, D., 1999. Generalized exponential distributions. Australian & New Zealand Journal of Statistics 41, 173-188.

Hua, Q., Barbetti, M., 2004. Review of tropospheric bomb ^{14}C data for carbon cycle modeling and age calibration purposes. Radiocarbon 46, 1273-1298.

Jackson, R.B., Canadell, J., Ehleringer, J.R., Mooney, H.A., Sala, O.E., Schulze, E.D., 1996. A global analysis of root distributions for terrestrial biomes. Oecologia 108, 389-411.

Kass, R., Raftery, A., 1995. Bayes factors. Journal of the American Statistical Association 90, 773-795.

Kikuzawa, K., Lechowicz, M.J., 2011. Ecology of leaf longevity. Springer Verlag, Tokyo.

Levin, I., Kromer, B., 2004. The tropospheric ^{14}CO$_2$ level in mid-latitudes of the Northern Hemisphere (1959-2003). Radiocarbon 46, 1261-1272.

Lukac, M., 2012. Fine Root Turnover, In: Mancuso, S. (Ed.), Measuring Roots. Springer Verlag, Berlin Heidelberg, pp. 363-373.

Mahmoudi, E., Jafari, A.A., 2012. Generalized exponential-power series distributions. Computational Statistics & Data Analysis 56, 4047–4066.

Majdi, H., 2001. Changes in fine root production and longevity in relation to water and nutrient availability in a Norway spruce stand in northern Sweden. Tree Physiology 21, 1057-1061.

Manzoni, S., Katul, G.G., Porporato, A., 2009. Analysis of soil carbon transit times and age distributions using network theories. Journal of Geophysical Research 114, 1-14.

Manzoni, S., Piñeiro, G., Jackson, R.B., Jobbágy, E.G., Kim, J.H., Porporato, A., 2012. Analytical models of soil and litter decomposition: Solutions for mass loss and time-dependent decay rates. Soil Biology and Biochemistry 50, 66-76.

Manzoni, S., Porporato, A., 2009. Soil carbon and nitrogen mineralization: Theory and models across scales. Soil Biology and Biochemistry 41, 1355-1379.

Michalzik, B., Tipping, E., Mulder, J., Lancho, J.F.G., Matzner, E., Bryant, C.L., Clarke, N., Lofts, S., Esteban, M.A.V., 2003. Modelling the production and transport of dissolved organic carbon in forest soils. Biogeochemistry 66, 241-264.

Niinemets, Ü., Lukjanova, A., 2003. Total foliar area and average leaf age may be more strongly associated with branching frequency than with leaf longevity in temperate conifers. New Phytologist 158, 75-89.

Reichstein, M., Beer, C., 2008. Soil respiration across scales: The importance of a model-data integration framework for data interpretation. Journal of Plant Nutrition and Soil Science 171, 344-354.

Riley, W.J., Gaudinski, J.B., Torn, M.S., Joslin, J.D., Hanson, P.J., 2009. Fine-root mortality rates in a temperate forest: estimates using radiocarbon data and numerical modeling. New Phytologist 184, 387-398.

Rodhe, H., 1992. Modeling Biogeochemical Cycles, In: Butcher, S.S., Charlson, R.J., Orians, G.H., Wolfe, G.V. (Eds.), Global Biogeochemical Cycles. Academic Press, San Diego, pp. 55-72.

Sah, S., Jungner, H., Oinonen, M., Kukkola, M., Helmisaari, H.S., 2011. Does the age of fine root carbon indicate the age of fine roots in boreal forests? Biogeochemistry 104, 91-102.

Schulze, K., Borken, W., Muhr, J., Matzner, E., 2009. Stock, turnover time and accumulation of organic matter in bulk and density fractions of a Podzol soil. European Journal of Soil Science 60, 567-577.

Smith, J.U., Smith, P., Monaghan, R., MacDonald, J., 2002. When is a measured soil organic matter fraction equivalent to a model pool? European Journal of Soil Science 53, 405-416.

Strand, A.E., Pritchard, S.G., McCormack, M.L., Davis, M.A., Oren, R., 2008. Irreconcilable differences: Fine-root life spans and soil carbon persistence. Science 319, 456-458.

Stuiver, M., Braziunas, T.F., 1993. Sun, ocean, climate and atmospheric $^{14}CO_2$: an evaluation of causal and spectral relationships. The Holocene 3, 289-305.

Stuiver, M., Polach, H.A., 1977. Reporting of ^{14}C data – discussion. Radiocarbon 19, 355-363.

Stuiver, M., Reimer, P.J., Braziunas, T.F., 1998. High-precision radiocarbon age calibration for terrestrial and marine samples. Radiocarbon 40, 1127-1151.

Tahmasbi, R., Rezaei, S., 2008. A two-parameter lifetime distribution with decreasing failure rate. Computational Statistics and Data Analysis 52, 3889-3901.

Tierney, G.L., Fahey, T.J., 2002. Fine root turnover in a northern hardwood forest: a direct comparison of the radiocarbon and minirhizotron methods. Canadian Journal of Forest Research 32, 1692-1697.

Tipping, E., Froberg, M., Berggren, D., Mulder, J., Bergkvist, B., 2005. DOC leaching from a coniferous forest floor: modeling a manipulation experiment. Journal of Plant Nutrition and Soil Science 168, 316-324.

Trumbore, S., Da Costa, E.S., Nepstad, D.C., De Camargo, P.B., Martinelli, L., Ray, D., Restom, T., Silver, W., 2006. Dynamics of fine root carbon in Amazonian tropical ecosystems and the contribution of roots to soil respiration. Global Change Biology 12, 217-229.

Trumbore, S.E., Gaudinski, J.B., 2003. The secret lives of roots. Science 302, 1344-1345.

Vrugt, J.A., ter Braak, C.J.F., Diks, C.G.H., Robinson, B.A., Hyman, J.M., Higdon, D., 2009a. Accelerating Markov Chain Monte Carlo Simulation by Differential Evolution with Self-Adaptive Randomized Subspace Sampling. International Journal of Nonlinear Sciences and Numerical Simulation 10, 273-290.

Vrugt, J.A., ter Braak, C.J.F., Gupta, H.V., Robinson, B.A., 2009b. Equifinality of formal (DREAM) and informal (GLUE) Bayesian approaches in hydrologic modeling? Stochastic environmental research and risk assessment 23, 1011-1026.

Weisstein, E.W., 2013. Delta function, From MathWorld – A Wolfram Web Resource.

3 Study II

"Reconcilable Differences: A Joint Calibration of Fine-Root Turnover Times with Radiocarbon and Minirhizotrons"

Contribution: I conceived the idea of the study, conducted the study, created all visualisations, and wrote the manuscript with inputs from all co-authors. Karna Hansson provided the minirhizotron data.

Published in New Phytologist, 204, 932-942.

Reconcilable Differences: A Joint Calibration of Fine-Root Turnover Times with Radiocarbon and Minirhizotrons

Bernhard Ahrens[1], Karna Hansson[2], Emily F. Solly[1], Marion Schrumpf[1]

[1]Max Planck Institute for Biogeochemistry, Hans-Knöll-Str. 10, 07445 Jena, Germany

[2]Institut National de la Recherche Agronomique, UR 1138 Biogéochimie des Ecosystèmes Forestiers, 54280 Champenoux, France

Author for correspondence:

Bernhard Ahrens

Tel: +49 3641 576295

Email: bahrens@bgc-jena.mpg.de

3.1 Summary

- We used bomb-radiocarbon and raw minirhizotron lifetimes of fine-roots (<0.5 mm in diameter) in the organic layer of Norway spruce (*Picea abies*) forests in southern Sweden to test if different models are able to reconcile the apparently contradicting turnover time estimates from both techniques.

- We present a framework based on survival functions that is able to jointly model bomb-radiocarbon and minirhizotron data. At the same time we integrate prior knowledge about biases of both techniques – the classification of dead roots in minirhizotrons and the use of carbon reserves to grow new roots.

- *Two-pool* models, either in parallel or in serial setting, were able to reconcile the bomb-radiocarbon and minirhizotron data. These models yielded a mean residence time of 3.80 ± 0.16 years (mean ± SD). On average 60 ± 2 % of fine-roots turned over within 0.75 ± 0.10 years, while the rest was turning over within 8.4 ± 0.2 years. Bomb-radiocarbon and minirhizotron data alone give a biased estimate of fine-root turnover.

- The *two-pool* models allow a mechanistic interpretation for the coexistence of fast- and slow-cycling roots – suberization and branching for the *serial-two-pool* model and branching due to ectomycorrhizal fungi-root interactions for the *parallel-two-pool* model.

Key words: root turnover, radiocarbon, minirhizotron, survival function, two-pool model, root age, bomb-radiocarbon, root longevity

3.2   Introduction

The turnover of fine-roots is a crucial part of the terrestrial carbon cycle. In addition to litterfall from leaves, needles, twigs and fruits, root litter constitutes a major addition of carbon and nutrients to the soil organic matter pool. Contrary to aboveground litterfall, the flux of root litter has eluded quantification, partly because roots, the "hidden half" of the terrestrial biosphere, are more difficult to observe and study. In addition, different techniques used to quantify fine-root turnover – ranging from ^{13}C labeling, tracing the ^{14}C bomb peak, sequential soil coring, and ingrowth cores to root cameras (minirhizotrons) – yielded widely contradictory estimates of root turnover (Trumbore and Gaudinski, 2003; Pritchard and Strand, 2008; Strand et al., 2008; Lukac, 2012).

The largest differences in inferred root turnover times are between isotopic techniques (here we use bomb-radiocarbon) and direct observations of root growth and persistence (minirhizotron methods) (Trumbore and Gaudinski, 2003; Guo et al., 2008). For a given standing stock of fine-roots in a forest stand, the root litter input estimated from common minirhizotron turnover times (~ 2 yr, Strand et al. (2008); Hansson et al. (2013)) is a priori 75% higher than the root litter input based on bomb-radiocarbon derived turnover times (~ 8 yr, Gaudinski et al. (2001); Gaul et al. (2009); Fröberg (2012)).

The *Radix* model (Gaudinski et al., 2009; Riley et al., 2009; Gaudinski et al., 2010) has been a recent attempt to model complete fine-root dynamics with five different pools – a storage pool with carbon reserves that can be used to grow new roots, two live-root pools and two dead-root pools. Gaudinski et al. (2010) made use of both bomb-radiocarbon and minirhizotron data to parameterize the turnover times of the two parallel, independent live-root pools. In their parameterization, however, Gaudinski et al. (2010) solely used the median longevity from minirhizotrons for the turnover time of the short-lived root pool. They then estimated the turnover time of the long-lived root pool using the ^{14}C content of fine-roots given the turnover time of the short-lived root pool. However, the *separate* parameterization of the short-lived and the long-lived root pool does not fully reconcile minirhizotron observations with the ^{14}C in fine-roots because this would relate the minirhizotron observations only to the short-lived pool. Modelled fine-root dynamics, though, should represent the whole spectrum of fine-root dynamics observed with both techniques. Further, the use of a single metric (median longevity) to represent minirhizotron observations throws away the majority of the information content of minirhizotron data. Finally, Strand et al. (2008) noted that

median longevities yields turnover time estimates that are systematically too fast. This, in turn, possibly yields too slow turnover times of the long-lived root pool for the parameterization of the *Radix* model in Gaudinski et al. (2010).

We therefore want to make full use of the information content of minirhizotron data, and aim to quantify root turnover with minirhizotron and bomb-radiocarbon data as true **joint** constraints. To this end we developed a unified evaluation framework (Ahrens and Reichstein, 2014) that makes it possible to compare survival functions against both bomb-radiocarbon and minirhizotron data. We assess the performance of several survival functions that are commonly used to evaluate data from either technique: the *exponential*, *Weibull* and *log-normal* model (Gaudinski et al., 2001; Pritchard and Strand, 2008; Strand et al., 2008; Gaul et al., 2009; Fröberg, 2012). Furthermore we test *two-pool* models, coupled either in parallel (equivalent to the live root-pool structure of *Radix*) or in series (as in Ahrens and Reichstein (2014)).

In Ahrens and Reichstein (2014) we already pointed to the possibility of accounting for biases of the minirhizotron and the bomb-radiocarbon technique. In this paper, we refine the unified evaluation framework by including prior knowledge on possible biases. Firstly, one cannot rule out that carbon reserves are used for the growth of fine-roots. This constitutes a bias for the bomb-radiocarbon technique because we cannot use the atmospheric ^{14}C record as a direct proxy for the ^{14}C content of newly grown roots, but must employ an (unknown) storage residence time. Thus, ^{14}C fine-root turnover times that do not include storage residence times yield estimates of root turnover that are too slow.

Second, it is hard to identify roots as dead or still alive in minirhizotron studies. Hence, the time-to-disappearance of a root segment is sometimes used instead of the time-to-death as a measure of fine-root longevity (e.g. Withington et al. (2006), Gaul et al. (2009)). This overestimates root longevity by the time it takes for a root to be decomposed.

Our objectives in this study are: (1) to quantify root turnover with radiocarbon and minirhizotron data as **joint** constraints using different survival functions; (2) to assess the performance of these survival functions; (3) to address systematic biases of radiocarbon and minirhizotron data in the joint calibration framework.

Using Bayesian parameter estimation we calibrate the survival functions from our joint calibration framework with published ^{14}C contents in fine-roots (Fröberg, 2012) and minirhizotron data (Hansson et al., 2013) from the organic layer of Norway spruce forests in southern Sweden.

3.3 Materials and Methods

3.3.1 Fine-root ^{14}C data

Fröberg (2012) measured the radiocarbon content of fine-roots from archived O-horizons of middle aged to mature stands dominated by Norway spruce (*Picea abies* (L.) Karst.) in southern Sweden. Well preserved roots (diameter 0-0.5 mm) were selected to represent predominately live fine-roots (Fröberg, 2012). We used the ^{14}C (% Modern) contents reported by Fröberg (2012) of fine-roots from 1964, 1972, 1985 and 1998 and their analytical uncertainties as observational constraints for a comparison against the tested survival functions (Table 3-1).

3.3.2 Minirhizotron data

Hansson et al. (2013) studied fine-root turnover with minirhizotrons in eight different forest stands in southern Sweden. Here, we use fine-root minirhizotron data with the same diameter as for the ^{14}C data (0-0.5 mm) of the three mature Norway spruce stands in the Tönnersjöheden Experimental Forest. We use data from 14 tubes, five of which are solely located in the O-horizons, while nine other also include the upper 10 cm of the mineral soil. One of these nine tubes was from understory spruce in a pine stand. Starting 1 year after tube installation, roots were monitored throughout four growing seasons (2007-2010) and 14 photo sessions. Roots were monitored from growth to disappearance, so that root longevity is possibly overestimated by the timespan a dead root needs to be decomposed. Hansson et al. (2013) assume that this systematic bias is in the range of 1-4 months.

3.3.3 Analysis of minirhizotron data with survival functions

Ideally, minirhizotron tubes allow monitoring of fine-root segments from their formation to death. Unfortunately, it is difficult to actually classify fine-roots as dead or alive, so fine-root segments are monitored from their first appearance until their disappearance (Table 3-1, Case C0). Four different cases are distinguishable (Table 3-1):

In the most common case C1, the lifetime data is interval-censored, where both the appearance and the disappearance of a root segment occur in the time between two photo sessions. Consequently, we can define a minimum (τ_{min}) and maximum lifetime (τ_{max}) for these root segments (Table 3-1, C1).

All other cases can be classified as right-censored because we know that the true lifetime, τ_L, of a root segment is longer than a certain minimum lifetime, τ_{min}. If a root segment did not disappear until the last photo session, we can define two possible minimum lifetimes, $\tau_{min,1}$ and $\tau_{min,2}$ (schematic drawing in Table 3-1, C2). Similarly, if a root-segment has already been present before the first photo session, but died before the last photo session, we also can define two possible minimum lifetimes, $\tau_{min,1}$ and $\tau_{min,2}$ (schematic drawing in Table 3-1, C3). Finally, if a root segment has been present throughout the study period (from first to last photo session), we get an absolute minimum lifetime, τ_{min} (right-censoring, *sensu strictu* Kleinbaum and Klein (2005)).

Approaches to derive fine-root turnover estimates include non-parametric and parametric approaches. Common to both approaches is the definition of so-called survival functions which – in the case of roots – describe the fraction of roots that are surviving until age τ. The non-parametric Kaplan-Meier survival function is basically a cumulative frequency function of the observed fine-root lifetimes. The Kaplan-Meier approach has been used in numerous studies to estimate median longevities of fine-root segments although Pritchard and Strand (2008) rightly argue that median longevity is underestimating mean longevity and thereby the fine-root turnover time.

Parametric survival functions should be preferred over non-parametric ones, because the mean longevity and thereby the fine-root turnover time is here well defined. Parametric survival functions, $S(\tau)$, are commonly derived from cumulative distribution functions $F(\tau)$:

$$S(\tau) = 1 - F(\tau)$$

Throughout the study we used five different survival functions (Table 3-2). *Exponential* survival functions have been commonly used to determine fine-root turnover from the ^{14}C in fine-roots (Gaudinski et al., 2001; Gaul et al., 2009; Fröberg, 2012), while *Weibull* and *log-normal* survival functions have been used to determine mean longevity from minirhizotron data (Strand et al., 2008; Gaul et al., 2009; Hansson et al., 2013). Additionally, we tested two *two-pool* models – one in serial setting as in Ahrens and Reichstein (2014), and one in parallel setting which is equivalent to the pool structure of live fine-roots of the *Radix* model (Riley et al., 2009). The survival functions corresponding to the *serial-two-pool* and *parallel-two-pool* model are also given in Table 3-2.

The formulation of the likelihood for cases C1 and C4 (Table 3-1) can be directly taken from textbooks on survival analysis (Kleinbaum and Klein, 2005). For cases C2 and C3 we also applied the

likelihood function for the right-censored case C4, but assumed that the overall likelihood is the mean of the individual likelihoods of both possible minimum lifetimes, $\tau_{min,1}$ and $\tau_{min,2}$ (Table 3-1). This definition accounts for the probability of a shorter minimum lifetime $\tau_{min,1}$ in comparison to the probability of longer minimum lifetime $\tau_{min,2}$. This formal definition of likelihood functions is able to deal with apparently shortened root lifetimes due to transparent root material (Tierney and Fahey, 2001) or due to the disappearance of root segments because of causes other than death (Hansson et al., 2013). The likelihood functions only rely on the minimum observed time that root segments are actually present (Table 3-1). Table 3-1 also gives an overview about the frequency of cases C1 to C4 at the Tönnersjöheden Experimental Forest.

The parameters of the different survival functions can be summarized with metrics like mean residence time, τ_r, or mean age, τ_a (Ahrens and Reichstein, 2014). For the quantification of root turnover, mean residence time is the most important metric and is used interchangeably with notions like mean longevity, mean lifespan or mean lifetime (Strand et al., 2008; Gaul et al., 2009; Riley et al., 2009; Kikuzawa and Lechowicz, 2011). In steady state, the mean residence time can be calculated as

$$\tau_r = \int_0^\infty S(\tau)d\tau \qquad \text{Eqn 3-1}$$

(Manzoni et al., 2012).

Throughout this study we assume that the root system is in steady state; therefore the root turnover time, τ_0, is equal to the mean residence time, τ_r (Rodhe, 1992). The root turnover time, τ_0, is defined as the ratio of the root biomass over the root litter input. Consequently, one can calculate the root litter input to the soil organic carbon pool from root biomass measurements and estimates of τ_r.

Although the mean age of roots, τ_a, cannot be used to constrain any component of the belowground carbon cycle, we also report the mean age of the root population. Mean ages were calculated as described in Ahrens and Reichstein (2014).

3.3.4 Convolution of the atmospheric bomb-radiocarbon curve with survival functions

Due to aboveground testing of thermonuclear weapons during the 1950s and 1960s the tropospheric ^{14}C content nearly doubled. After the Partial Test Ban Treaty in 1963, the atmospheric ^{14}C content declined quasi-exponentially due to the uptake of ^{14}C in the vegetation and oceans, but also due to fossil fuel emissions which practically contain no [14]C. The atmospheric bomb-radiocarbon record has proven to be a powerful tracer to shed light on carbon dynamics on annual to decadal timescales (Trumbore and Gaudinski, 2003; Trumbore, 2009). In ecological studies where bomb-radiocarbon is used as a tracer, ^{14}C contents are commonly reported in *percent Modern*, pM, or [14]C (% Modern). A [14]C (% Modern) value over 100 is typically indicative for the presence of bomb-radiocarbon and processes on yearly to decadal time-scales, while a [14]C (% Modern) value below 100 may indicate carbon cycling on centennial or millennial time-scales.

We showed that the same survival functions (Table 3-2) can be used, to analyze both, fine-root ^{14}C using the atmospheric radiocarbon curve as a tracer, and minirhizotron lifetime data (Ahrens and Reichstein, 2014). We formulated a generic time-shift model for the [14]C (% Modern) content of fine-roots, $Root^{14}C(t)$, based on a framework proposed by Manzoni et al. (2009):

$$Root^{14}C(t) = \int_0^\infty \frac{1}{\tau_0} \cdot Atm^{14}C(t - \tau) \cdot S(\tau) \cdot e^{-\lambda \cdot \tau} d\tau,$$

Eqn 3-2

where τ_0 is the turnover time, $Atm^{14}C(t)$ the atmospheric [14]C (% Modern) value in year t, $S(\tau)$ is the survival function describing the fraction of roots surviving **at least** to age τ (cf. Niinemets and Lukjanova (2003), Manzoni et al. (2009), and Manzoni et al. (2012)), and $e^{-\lambda \cdot \tau}$ accounts for the radioactive decay of [14]C. When the root population is in steady state, the turnover time τ_0 is equal to the mean residence time τ_r.

Eqn 3-2 essentially describes $Root^{14}C(t)$ in a certain year t as the sum of ^{14}C inputs via root production from previous years τ weighted by the fraction of fine-roots $S(\tau)$ that live at least for τ years. The atmospheric [14]C (% Modern) values, $Atm^{14}C$, can be used as a proxy for the ^{14}C content of new roots. Consequently, the term $\frac{1}{\tau_0} \cdot Atm^{14}C(t - \tau)$ describes the ^{14}C input via root production under the assumption that root biomass is in steady state.

3.3.5 Accounting for methodological biases

If neither of the methods had a systematic bias, we could directly compare $Root^{14}C(t)$ and the corresponding $S(\tau)$ with the measured fine-root ^{14}C and time-to-disappearance data, respectively. If, however, we cannot rule out that the above mentioned systematic biases of the two methods are relevant, we need to modify the described framework.

In Eqn 3-2 we have to replace the atmospheric $Atm^{14}C(t - \tau)$ curve with a curve that actually represents the ^{14}C input to the root system and accounts for the possibility that stored carbon has been used to build new roots. This could be achieved by calculating a ^{14}C curve under the assumption that carbon to grow new roots ($NewGrowth^{14}C(t)$) is on average x years old. This can, for example, be modelled by a survival function that follows an exponential function with a storage turnover time, T_S:

$$NewGrowth^{14}C(t) = \int_0^\infty \frac{1}{T_S} \cdot Atm^{14}C(t - \tau) \cdot e^{-\frac{\tau}{T_S}} \cdot e^{-\lambda \cdot \tau} d\tau \qquad \text{Eqn 3-3}$$

The ^{14}C in fine-roots is then calculated as (compare to Eqn 3-2):

$$Root^{14}C(t) = \int_0^\infty \frac{1}{\tau_0} \cdot NewGrowth^{14}C(t - \tau) \cdot S(\tau) \cdot e^{-\lambda \cdot \tau} d\tau \qquad \text{Eqn 3-4}$$

Minirhizotron data are biased because they often represent time-to-disappearance instead of time-to-death. This means that one should additionally account for the time-to-decomposition:

$$\text{time-to-disappearance} = \text{time-to-death} + \text{time-to-decomposition} \qquad \text{Eqn 3-5}$$

$$\tau_{dis} = \tau + \tau_{dec}$$

This corresponds to a transfer from a live-root pool to a dead-root pool. In the survival function framework we have to convolute the survival function $S(\tau)$ that accounts for the death of roots with an exponential function with a dead root turnover time, T_D:

$$S_{\text{time-to-disappearance}}(\tau_{dis}) = \int\limits_{0}^{\infty} S(\tau_{dis} - \tau_{dec}) \cdot \frac{1}{T_D} \cdot e^{-\frac{\tau_{dec}}{T_D}} \, d\tau_{dec}$$
Eqn 3-6

This gives a survival curve $S_{\text{time-to-disappearance}}(\tau_{dis})$ which describes the fraction of roots that are present (live or dead) at least for a time τ_{dis}. The term $\frac{1}{T_D} \cdot e^{-\frac{\tau_{dec}}{T_D}}$ in Eqn 3-6 is the decomposition function for dead roots which weights the relative contribution of fine-roots $S(\tau)$ that have lived for a time $\tau = \tau_{dis} - \tau_{dec}$ to fine-roots that have not disappeared until time τ_{dis}. This curve should be directly compared with the minirhizotron data. In the calibration we use prior knowledge for the two parameters, T_S and T_D, describing the systematic biases of both techniques (see next section).

3.3.6   Parameter estimation with minirhizotron and bomb-radiocarbon data

We optimized the parameters $\boldsymbol{\theta}$ of the different survival functions, $S(\tau)$, (Table 3-2) and the two additional bias parameters, T_S and T_D, by maximizing the logarithm of the posterior of the joint evaluation framework with the DiffeRential Evolution Adaptive Metropolis algorithm (Guillaume and Andrews, 2012). The posterior distribution of parameters expresses the uncertainty of the parameters after accounting for the prior knowledge we have about the parameters, and the likelihood to reproduce the minirhizotron and fine-root ^{14}C data with the model using these parameters. Because we aim to reconcile minirhizotron fine-root lifetimes and the ^{14}C content of fine-roots, we define a joint likelihood function for both techniques. For mathematical convenience we use the logarithm of the joint likelihood, which is the sum of the log-likelihood of the minirhizotron data, $\ell_{Mini}(\boldsymbol{\theta})$, and the log-likelihood of the fine-root ^{14}C data, $\ell_{14C}(\boldsymbol{\theta})$.

The log-likelihood for the minirhizotron data can be formulated as:

$$\ell_{Mini}(\boldsymbol{\theta}) = \sum_{i=1}^{case} \boldsymbol{n}_i \cdot \log\left(L_i\left(\boldsymbol{\theta}|\boldsymbol{D}_{Mini,i}\right)\right),$$
Eqn 3-7

where L_i is the likelihood function for one of the cases i (cases C1-C4, Table 3-1), with $\boldsymbol{n}$ the respective number of roots with the same time-to-disappearance $\boldsymbol{D}_{Mini,i}$.

The log-likelihood for the fine-root ^{14}C data can be formulated as:

$$\ell_{14C}(\boldsymbol{\theta}) = -0.5 \cdot \left(\sum_{t=1964}^{\text{meas. yrs.}} \left(\frac{\boldsymbol{D}_{14C}(t) - M(t,\boldsymbol{\theta})}{\sigma(t)} \right)^2 + \sum_{t=1964}^{\text{meas. yrs.}} \log(2 \cdot \pi \cdot \sigma(t)^2) \right),$$

Eqn 3-8

where $\boldsymbol{D}_{14C}(t)$ is the fine-root ^{14}C data, $M(t, \boldsymbol{\theta})$ are the model results of a certain survival function for the proposed set of parameters. t denotes here the points in time when fine-root ^{14}C measurements are available, and $\sigma(t)$ the respective measurement uncertainty.

We only defined priors for the two bias parameters, T_D and T_S. Based on considerations by Hansson et al. (2013), we chose a log-normal prior for T_D with its mode at 2 months and its 90th percentile at 7 months (Figure 3-1 (a)). We chose the 0.4 years of mean storage time found by Gaudinski et al. (2009) as the mode for a log-normal prior for T_S. The 90th percentile for this log-normal prior was set to 2 years (Figure 3-1 (b)). Both log-normal priors were truncated – at 1 year for T_D and at 5 years for T_S – to avoid the possibility that the observations would solely be explained by the two bias parameters.

3.4 Results

3.4.1 Performance of different survival functions in explaining bomb-radiocarbon and minirhizotron observations of fine-roots

The two *two-pool* models (Table 3-2) were best able to capture both, the minirhizotron time-to-disappearance data, and the bomb-radiocarbon in fine-roots (Table 3-3). Although the *two-pool* models have the largest number of parameters (three + two bias parameters), they have by far the best likelihoods of all survival functions relative to the number of parameters as indicated by the Bayesian information criterion (BIC, Kass and Raftery (1995), Table 3-3). The BIC would favor survival functions with a lower complexity (fewer parameters) if they achieve a similar maximum likelihood. The *serial-two-pool* survival function and the *parallel-two-pool* survival function perform equally well in terms of the BIC (Table 3-3).

The differences in BIC (ΔBIC in Table 3-3) are considerable between the *two-pool* survival functions and the *log-normal*, *Weibull* and *exponential* survival function. The *exponential* (*one-pool*) survival function performs particularly poorly and is neither able to capture the dynamics of long-lived roots in minirhizotrons (Table 3-3, blue dashed line vs orange step function) nor the time-series of fine-root ^{14}C (Table 3-3). Both the *Weibull* and *log-normal* survival functions perform much better than the *exponential* survival function. The *Weibull* survival function is better able to capture fine-root ^{14}C compared to the *log-normal* survival function, while the *log-normal* survival function is better at capturing the minirhizotron time-to-disappearance data (Table 3-3, blue dashed line vs orange step function). However, the *serial-two-pool* and the *parallel-two-pool* survival function outperform the *Weibull* and *log-normal* survival function both in explaining the minirhizotron data and the ^{14}C of fine-roots.

3.4.2 Minirhizotron bias – T_D

The bad performance of the *exponential* survival function is also reflected in the posterior distribution of the bias parameter for minirhizotron observations, the dead root turnover time, T_D. The posterior distribution is the combination of the prior knowledge we had about this parameter and the information contained in the data to further constrain this parameter. The posterior distribution of T_D (Figure 3-2, blue line) for the *exponential* survival function is hitting the edge of the truncated log-normal distribution that describes our prior knowledge about T_D (Figure 3-2, gray

area). This indicates that our optimization algorithm strives for longer dead root turnover times in order to be able to explain the quite long-lived roots observed with the minirhizotrons (Table 3-3, orange step function).

For the other survival functions we do not see any edge hitting for T_D, although the posterior mean of T_D is located in the 90th percentile of the prior distribution for the *two-pool* and *Weibull* survival functions (Figure 3-2). The posterior uncertainty of T_D is best constrained compared to our prior knowledge for the *log-normal* survival function with a dead root turnover time of 0.23 ± 0.04 years (posterior mean ± SD). For the *two-pool* survival functions we obtain the same posterior T_D of 0.60 ± 0.08 years (mean ± SD).

3.4.3   Bomb-radiocarbon bias – T_S

Similar to the findings for the minirhizotron bias parameter, T_D, we also observe edge-hitting of the storage turnover time, T_S, for the *exponential* survival function. For the *exponential* model the posterior distribution of T_S (Figure 3-2, blue line), which accounts for the use of stored carbon to grow new roots, is concentrated at the upper edge of the truncated log-normal prior knowledge (Figure 3-2, gray area). This again indicates that the *exponential* model is not remotely able to fit the minirhizotron and bomb-radiocarbon data jointly without attributing too much of the observed variation to the bias parameters.

The posterior distribution of the *log-normal* model follows again most closely our prior knowledge, while the posterior means of T_S of the *two-pool* models and the *Weibull* survival functions are located in the 10th percentile of the prior distribution (Figure 3-2). The uncertainty of T_S is best constrained compared to our prior knowledge (Figure 3-2) for the *two-pool* survival functions with a storage turnover time of 0.08 ± 0.04 years (posterior mean ± SD).

3.4.4   Mean residence times and mean ages

The mean residence time estimate, τ_r, for the *exponential* survival function is seriously biased because the model error is considerable. The model error of the *exponential* model can be illustrated by its inability to reproduce short **and** long lifetimes observed in the minirhizotrons (Table 3-3, column 1) and by its inability to fit all ^{14}C measurements of fine-roots reasonably well (Table 3-3, column 2). The τ_r estimates for the other survival functions can be reliably interpreted because the

model error is not dominating in these cases. τ_r ranges from 3.53 ± 0.16 years for the *Weibull* survival function to 3.80 ± 0.16 years for the two *two-pool* survival functions (Table 3-3).

Apart from the mean residence times, the individual parameters that describe the shape of the survival curves can give interesting insights on the timescales that fine-roots are turning over. For the one-parameter *exponential* survival function the inverse of the decomposition rate k constitutes already the mean residence time $-\frac{1}{k} = \tau_r = T$ (Figure 3-2).

Also the parameters of the *two-pool* survival functions can be readily interpreted. In the *parallel-two-pool* model 60 ± 2 % of fine-roots belong to a fast-cycling pool with a turnover time T_1 of 0.75 ± 0.10 years (mean ± SD), while the remainder belongs to a slow-cycling pool with a turnover time T_2 of 8.4 ± 0.2 years (mean ± SD) (Figure 3-2). The parameters of the *log-normal* and *Weibull* model elude such a straightforward interpretation because the shape and scale parameters cannot directly be translated into how many roots are turning over on a certain timescale.

The turnover times of the *serial-two-pool* survival function are in accord with the turnover times of the *parallel-two-pool* model – the turnover time of the fast-cycling root pool, T_Y, is also 0.75 ± 0.10 years (mean ± SD), and the turnover time of the slow-cycling pool is also 8.4 ± 0.2 years (mean ± SD). 36 ± 2 % (mean ± SD) of the roots that turn over in the fast-cycling pool, R_Y, (Table 3-2) are entering the slow-cycling pool, R_O, via the transfer coefficient h (Table 3-2, Figure 3-2).

This shows that the *serial-two-pool* model and the *parallel-two-model* are generally able to reproduce the same shape of the survival curve with same turnover times of the respective fast- and slow-cycling pools (T_{Fast}, T_{Slow}). The relation between the parameters h and α is given by $h = (1 - \alpha) \frac{T_{Fast} - T_{Slow}}{T_{Slow}}$ (derived from equations for $S(\tau)$ in Table 3-2).

Although the mean age, τ_a, of a root population is not a really useful quantity for constraining belowground carbon cycling, the distance of τ_a to the mean residence time, τ_r, at least gives a quick indication how the survival probability of a root changes with increasing age τ (Table 3-3). For the *exponential* survival function the mean age is equal to the mean residence time (Table 3-3). This means that the probability for a root to die does not change with increasing root age τ. For all the other survival functions the mean age τ_a is longer than the mean residence time τ_r (Table 3-3). This indicates that most fine-roots will die relatively soon after they grew, while a minority of

roots survives for a relatively long time. The *log-normal* survival function shows the longest mean age of 9.3 ± 0.4 years of fine-roots (mean ± SD), while the mean age for the *two-pool* models is shortest with 7.5 ± 0.2 years (mean ± SD). The *Weibull* model has a mean age of 7.9 ± 0.3 years (mean ± SD). Apart from the *exponential* model, the distance between τ_a and τ_r is shortest for the *two-pool* survival functions, indicating that the probability for a root to die is not decreasing as strongly with increasing age as for the *Weibull* and *log-normal* survival function.

3.5   Discussion

3.5.1   Mechanistic interpretation of the *two-pool* models

We showed that we are able to obtain the same shape of the survival curve for the *serial-two-pool* model and the *parallel-two-pool* model using the same turnover times of the respective fast- and slow-cycling pools. Although the *two-pool* survival functions are obviously equivalent, these two models are open to different potential mechanistic interpretations.

Serial-two-pool model: After growth all roots at first belong to a relatively fast-cycling pool where the majority of roots die after a relatively short period, while the remainder of fine-roots are getting suberized and are thereby able to increase their survival probability. Evidence from Pregitzer et al. (2002) for *Picea glauca* (we studied *Picea abies*) also suggests that in the <0.5 mm size class at least the first three orders of roots are present. Branching of roots can generally be associated with enhanced transport, but also with the development of protective features such as suberin deposits or lignified cells (Eissenstat and Yanai, 1997; Hishi, 2007). Hence, branching is a process that should be taken into consideration when interpreting the transfer from the fast-cycling pool R_Y to the slow-cycling pool R_O.

Parallel-two-pool model: In this survival function structural differences between fine-roots existing already at their establishment would predetermine their longevity. Similar to the *serial-two-pool* model, branching could play a major role in explaining the coexistence of a fast- and slow-cycling pool. However, the interpretation for the *parallel-two-pool* model has to be different because the two pools would describe roots whose function and structure would be predetermined at root establishment. The structural differences could stem from the interaction between root growth and ectomycorrhizal fungi which leads to a typical lateral root branching pattern with short lateral ectomycorrhizal roots and long supportive roots. This type of branching is commonly called heterorhizy (Brundrett et al., 1996). Taylor et al. (2000) found that in a SW Sweden spruce forest more than 99% of root tips are colonized by ectomycorrhiza. While the ectomycorrhizal infection of the slow-growing short lateral roots may prevent the deposition of suberin in cortical cells (Hishi, 2007), the longer roots may undergo more rapid secondary growth (Brundrett et al., 1996), which is accompanied by suberization. Hence, the interactions of ectomycorrhizal fungi and plants could be interpreted as a predetermination of new roots to develop into short ectomycorrhizal roots (short-lived, T_1) or long suberized roots (long-lived, T_2).

Overall, the attribution of processes to either the *serial-two-pool* or the *parallel-two-pool* model is a rather philosophical exercise, which essentially reduces to a dichotomous decision between root development that could also depend on changing conditions in the micro-environment of the root (*serial-two-pool*), and the predetermination of root function at establishment regardless of changing micro-environmental conditions (*parallel-two-pool*). Nevertheless, given that both *two-pool* models are able to produce the same shape of the survival curve, our results do not allow for favoring one of the two possible approaches.

3.5.2 Constraints on systematic biases

Overall, the estimates of the bias parameters for the bomb-radiocarbon and the minirhizotron technique did not converge across the different survival functions. As already mentioned, the *exponential* survival function could not reconcile both techniques, but both bias parameters, the dead root turnover time T_D and the storage turnover time T_S, were hitting the edge of the truncated log-normal prior distributions. Hence, the bias parameters would explain the major part of the apparent irreconcilability of both datasets for the *exponential* model.

The posterior distribution of the bias parameters, T_D and T_S, (Figure 3-2, blue line) closely follows the prior knowledge (Figure 3-2, gray area) for the *log-normal* survival function, which may indicate that its particular shape is actually helpful for explaining fine-root dynamics. For the *log-normal* survival function the risk for a root to die increases at first for rather short root ages τ, but declines after a certain age τ. For the other survival functions the risk for a root to die is either independent of its age (*exponential* model) or is monotonically decreasing with longer ages τ. The bias parameters, T_D and T_S, only influence the model output of the corresponding datastreams, as indicated by the weak correlations (r^2 between 0.008 and 0.09) between the posteriors of T_D and T_S (see Fig S1 for correlation matrices of the parameters).

Although we have identified the storage turnover time and the dead root turnover time as the most important biases of the ^{14}C and the minirhizotron technique, one cannot rule out that additional biases also influence the posterior estimates of our parameters. Adams and Eissenstat (2014) found evidence that not only stored carbon might be used for the growth of new roots, but also recent photosynthate is incorporated into structural root tissue after root formation. This process would lead to a shorter storage turnover time T_S in our modelling framework. For the *Weibull* and both *two-pool* models, the fact that the posterior estimate of T_S is located in the 10th

percentile of the prior knowledge (Figure 3-2), could also be explained by a tradeoff between the use of stored carbon to grow new roots and the continuous incorporation of recent photosynthate into roots (Adams and Eissenstat, 2014).

Similarly, Fröberg (2012) selected the archived roots to represent predominately live roots, but he could not rule out the possibility that recently dead roots might have been included. This possible bias would lead to a longer estimate of T_S; this however does not seem to be relevant here, given that the posterior estimate of T_S is not located at the upper end of the prior knowledge (Figure 3-2). This possible bias is also different from the dead root turnover time that we proposed to account for the time-to-decomposition in minirhizotrons because we would still sample a mixture of live and dead roots for the ^{14}C analysis, while in minirhizotrons root segments are most likely dead when they disappear.

3.5.3 Trade-off to single calibrations with minirhizotron or bomb-radiocarbon data

Trumbore and Gaudinski (2003) stated that both techniques – minirhizotrons and bomb-radiocarbon – would "gather information about different ends of the root lifetime continuum". The validity of this statement relies on sampling and evaluation details of the two different techniques. The statement that minirhizotrons sample only at the younger end of the lifetime continuum is largely dependent on the length of the study period. Obviously, one strives to capture also the tails of the fine-root lifetimes monitored with minirhizotrons (Table 3-3), which is decisive for the extrapolation of root lifetimes outside of the observed (also censored) lifetimes. The commonly reported *median* longevity estimates from *Kaplan-Meier point estimates* from minirhizotrons depend even stronger on the length of the study period than *parametric estimates* of *mean* longevity. Nevertheless, also in parametric approaches, which are used to determine *mean* longevities/*mean* residence times (Table 3-1), the length of the study period determines how much information is contained in the minirhizotron data not only for the fast-cycling pool, but also for the slow-cycling pool.

Up to now, the evaluation of minirhizotron data has been inadequate for the nature of the data: parametric survival functions have commonly been fit to Kaplan-Meier point estimates (Strand et al., 2008; Gaul et al., 2009; Hansson et al., 2013). First, the fit to Kaplan-Meier point estimates throws away a lot of information – in a least-square fitting approach longer survival times receive less weight because of the smaller numbers (fraction of roots surviving). Second, the information about censoring in the Kaplan-Meier survival curve is lost to a large part when a parametric survival

curve is fit to the point estimates. The Kaplan-Meier approach is especially not able to account for the complex cases of censoring occurring in minirhizotron studies (Table 3-1, cases C2 and C3). In this study we employed a formal likelihood approach also for the minirhizotron data, which ensures a proper accounting for the different cases of censoring and a proper weighting also of long-living roots.

The information content of fine-root ^{14}C alone does not constrain the total fine-root turnover (fast- **and** slow-cycling roots) because survival functions with more than one parameter generally have enough flexibility to fit the same ^{14}C content in fine-roots almost equally well with quite different mean residence times τ_r. However, the ^{14}C content of fine-roots determines the mean age of fine-roots τ_a to a large extent (Table 3-3, Ahrens and Reichstein (2014)), which is dominated by the slow-cycling pool. Overall, we conclude that minirhizotron data are the ideal complement to the ^{14}C measurements in fine-roots, especially for studies without archived fine-root ^{14}C samples or a shorter minirhizotron sampling period: With minirhizotron data we are able to constrain the survival curve for short longevities τ, while the ^{14}C of fine-roots alone would allow too much flexibility for short τ. Survival functions just fit to fine-root ^{14}C data had quite different mean residence times τ_r (1.9-7.1 years, Ahrens and Reichstein (2014)), while the mean ages τ_a were already quite similar (7.1-8.7 years, Ahrens and Reichstein (2014)).

The mean residence times found in this study with the joint calibration to ^{14}C in fine-roots **and** minirhizotron data (Table 3-3) showed that the joint calibration not only leads to a convergence of mean ages, but also to a convergence of mean residence times estimates (3.53-3.81 years) between the different survival functions. Here, the exception is the *exponential* survival function which is generally unable to explain both datasets with its constant survival probability.

3.5.4   Implications, future research directions

Generally, one should probably take a step back and ask oneself "Why are we interested in estimating fine-root turnover times?" – the most general answer being "We want to quantify the input of root litter to the soil organic carbon pool".

This also means that the mean residence time τ_r *per se* is not of primary interest, but the root litter input which is defined as $\frac{\text{root biomass}}{\tau_r}$ under the assumption that root biomass is in equilibrium. We argue for an overall more integrative approach for determining the root litter input to soils.

Richardson et al. (2010) showed in a model-data fusion exercise with joint constraints (NEE, soil respiration, aboveground litterfall) that they were not able to constrain the turnover rate of fine-roots. This indicates that the integration of minirhizotron data or fine-root ^{14}C into calibration exercises with whole ecosystem models might be beneficial to constrain the central parameter that determines the carbon input levels to the soil organic carbon pool.

Contrary to statistical survival functions (e.g. *log-normal* and *Weibull*), modelling the root turnover with *two-pool* models has the advantage of fitting seamlessly into ecosystem models. The survival functions for *two-pool* models essentially correspond to a system of ordinary differential equations. One would model the decrease of the fraction of roots still being alive without further new root growth. This curve can be used for comparison with the raw minirhizotron time-to-disappearance data. This would make it possible to use minirhizotron data along with the ^{14}C content of fine-roots for calibrating parameters of ecosystem models in multiple constraints approaches. In addition, accounting for systematic biases of the minirhizotron and the bomb-radiocarbon technique, is easier achieved in a traditional pool setting, while the convolution of two functions is quite uncommon for ecosystem models.

Overall, our results show that fine-roots of trees are indeed cycling on quite different time-scales. A *one-pool*, *exponential* model assumes a constant mortality risk of fine-roots regardless of their age – it is impossible to reconcile minirhizotron data and bomb-radiocarbon data using this assumption. Other survival functions, however, that exhibit a decreasing mortality risk with increasing age are able to reconcile the apparently contradictory datastreams. *Two-pool* survival functions, nonetheless, perform better than survival functions derived from statistical cumulative distribution functions, such as the *Weibull* and *log-normal* survival function. Moreover, the *two-pool* models can be better integrated into ecosystem models and are more open to a mechanistic interpretation. Therefore, the *two-pool* survival functions are best suited to represent fine-root turnover in models and to reconcile bomb-radiocarbon and minirhizotron data. The combination of both datasets is essential to reasonably constrain the proportion of short- to long-lived fine-roots.

Our and other studies (Tierney and Fahey, 2002; Matamala et al., 2003; Trumbore et al., 2006; Gaudinski et al., 2010) showed that fine-roots in rather well-drained forest ecosystems do not belong to just one homogenous pool. If also fine-roots in non-forested ecosystems show this decreasing mortality risk with increasing age is questionable. Solly et al. (2013) found that fine-root ^{14}C in grasslands was generally much closer to the atmospheric ^{14}C curve than fine-root ^{14}C in forests,

so the issue of reconciling minirhizotron observations with ^{14}C observations is probably less pressing for fine-roots in grasslands. Nevertheless, Solly et al. (2013) found that the presence of perennial species in grasslands, yields longer apparent ^{14}C fine-root turnover times. Also fine-roots of grasslands could be modelled with our proposed framework, although the storage turnover time bias will be of minor importance in grasslands. The use of the radiocarbon technique could be useful to study fine-roots in grasslands with considerable amounts of perennial species, although using the minirhizotron technique might suffice. In poorly-drained or even wetland soils the decomposition of dead roots might be impeded considerably (Iversen et al., 2012). Therefore, it would be important to account for this substantial bias that would affect observations of fine-root turnover with minirhizotrons and bomb-radiocarbon.

3.6 Acknowledgements

3.7 Tables

Table 3-1: Likelihood functions (L) for minirhizotron observations are depending on the timing of image collection. The schematics show how well the fine-root lifetime (τ_L) can be constrained for typical cases. n is the number of respective cases for the Norway spruce minirhizotron data (0-0.5 mm) in Hansson et al. (2013).

Schematics of hypothetical lifetimes of root segments in minirhizotrons

$\tau_{max} :=$ max. lifetime
$\tau_{min} :=$ min. lifetime
$:=$ photo at time i

Schematic	Lifetime (τ_L)	Likelihood (L)	case	n
τ_L — Appearance / Disappearance	τ_L	$f(\tau_L)$	C0	0
τ_{max}, τ_{min}	$\tau_{min} < \tau_L < \tau_{max}$	$S(\tau_{min}) - S(\tau_{max})$	C1	1435
$\tau_{min,2}$, $\tau_{min,1}$	$\tau_L > \tau_{min,1}$ or $\tau_L > \tau_{min,2}$	$\dfrac{S(\tau_{min,1}) + S(\tau_{min,2})}{2}$	C2	1088
$\tau_{min,2}$, $\tau_{min,1}$	$\tau_L > \tau_{min,1}$ or $\tau_L > \tau_{min,2}$	$\dfrac{S(\tau_{min,1}) + S(\tau_{min,2})}{2}$	C3	54

Table 3-2: Overview of tested survival functions; τ denotes the age of a root, $\#\theta$ is the number of parameters of a survival function.

Survival function	Equation	Model structure	$\#\theta$
Exponential[a]	$S(\tau) = \mathrm{e}^{-k\tau}$		1
Weibull[b]	$S(\tau) = \mathrm{e}^{-\left(\frac{\tau}{\gamma}\right)^{\beta}}$		2
Log-normal[c]	$S(\tau) = 0.5\left[\mathrm{erf}\left(\frac{\ln(\tau) - \mu}{\sigma\sqrt{2}}\right)\right]$		2
Serial-two-pool[d]	$S(\tau) = \dfrac{\mathrm{e}^{-(k_Y + k_O)\tau}[(k_Y(1-h) - k_O)\mathrm{e}^{k_O \cdot \tau} + h \cdot k_Y \mathrm{e}^{k_Y \cdot \tau}]}{k_Y - k_O}$		3
Parallel-two-pool[e]	$S(\tau) = \alpha \mathrm{e}^{-k_1\tau} + (1-\alpha)\mathrm{e}^{-k_2\tau}$		3

[a] The only parameter for the *exponential* survival function is the turnover rate k.

[b] The *Weibull* survival function can be described by the scale parameter γ and the shape parameter β.

[c] The *log-normal* model can be described by the location parameter μ and the shape parameter σ. erf(x) denotes the Gaussian error function

[d] In the *serial-two-pool* model new roots belong at first to a fast-cycling root pool, R_Y. These roots are turning over with rate k_Y. A fraction h of the turnover from the fast-cycling pool R_Y is transferred to the slow-cycling pool R_O which is turning over with rate k_O. This survival function is based on the derivation by Manzoni et al. (2009).

[e] In the *parallel-two-pool* model roots either belong to the fast-cycling pool R_1 or the slow-cycling pool R_2. The pools are turning over with the respective rates k_1 and k_2. α describes the fraction of roots belonging to pool R_1. This survival function is based on the derivation by Manzoni et al. (2009).

Table 3-3: Modelled and observed time-to-disappearance of Norway spruce fine-roots in minirhizotrons; modelled and observed ^{14}C in Norway spruce fine-roots; performance of different survival functions as indicated by the difference of Bayesian information criterions (ΔBIC) between the respective survival function and the survival functions with the best performance (*serial-two-pool* and *parallel-two-pool*). τ_r is the mean residence time (mean ± SD), τ_a is the mean age of the root population. Minirhizotron data from Hansson et al. (2013) and radiocarbon data from Fröberg (2012).

Minirhizotrons	Radiocarbon	ΔBIC	τ_r (yr); mean (SD)
		0	3.80 (0.16)
		0	3.81 (0.16)
		75	3.65 (0.12)
		103	3.53 (0.16)
		615	1.12 (0.04)

[A] The observed time-to-disappearance data (orange step function) provides just an approximate visual depiction of the frequency of different times-to-disappearance, but does not account for the different cases of censoring (C2-C4 in Table 3-1). Here, we assumed that the time-to-disappearance is $\frac{1}{2}(\tau_{max} + \tau_{min})$ for case C1, $\frac{1}{2}(\tau_{min,1} + \tau_{min,2})$ for cases C2 and C3, and τ_{min} for case C4 in Table 3-1.

3.8 Figures
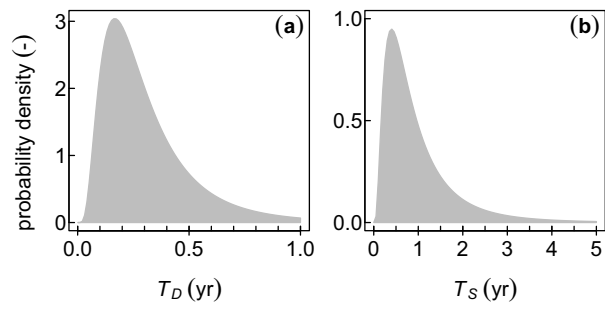
Figure 3-1: Priors for the bias parameters T_D (a) and T_S (b). T_D describes the time it takes for a fine-root segment to disappear from a minirhizotron photo after its death. T_S accounts for the time carbon has potentially spent in storage pools after its photosynthetic fixation before it it used to grow new roots.
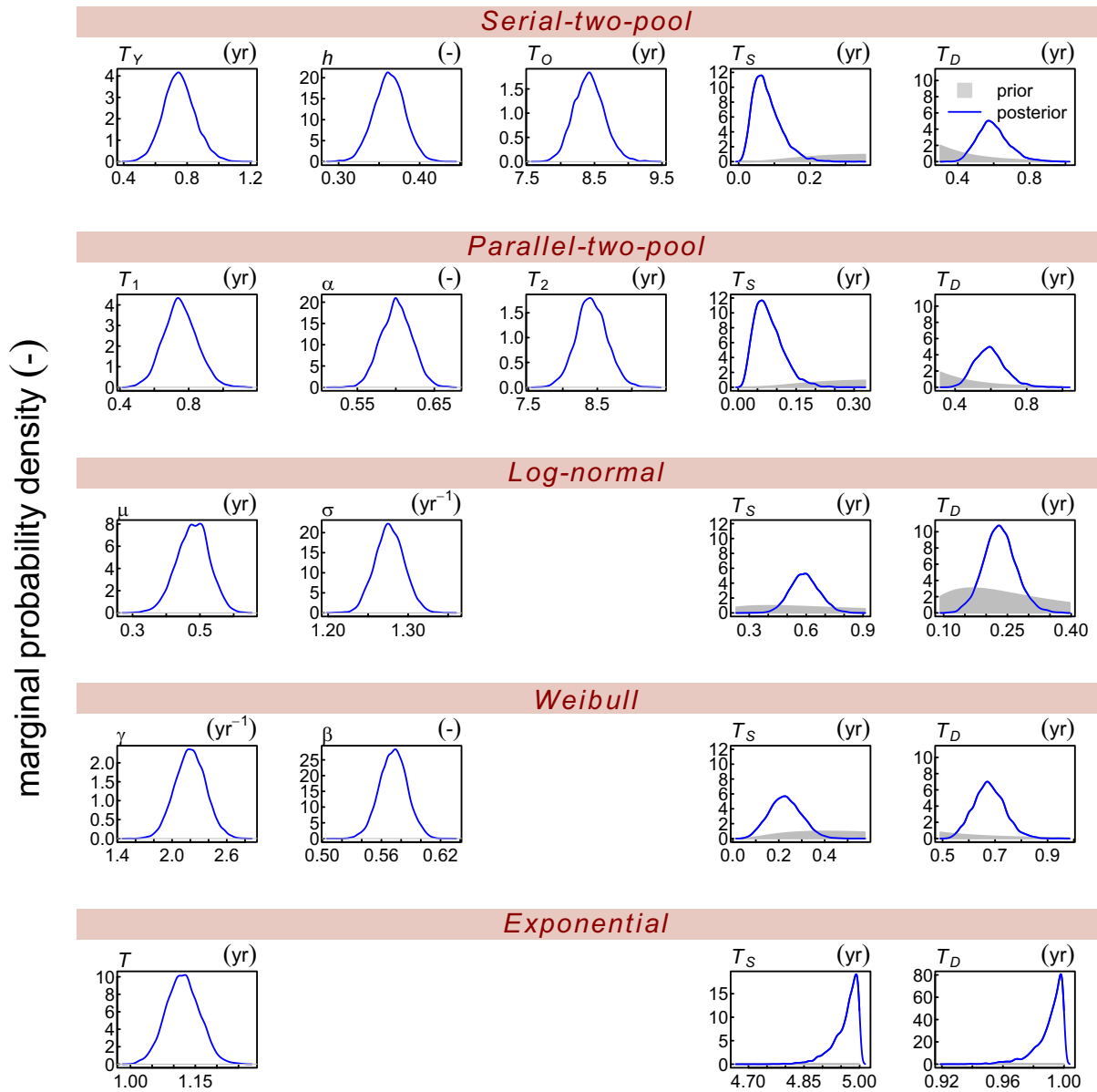
Figure 3-2: Comparison of parameter probability distributions for different survival functions. The maximum density of the marginal posterior distribution (blue line) is an indicator for how well a parameter is constrained by the data. For the storage turnover time, T_S, and the dead root turnover time, T_D, the marginal posterior distribution (blue line) shows how much information is contained in the data compared to prior knowledge about these two parameters (gray area). *Serial-two-pool*: T_Y, turnover time of the young root pool R_Y; h, transfer coefficient from young to old root pool; T_O, turnover time of the old root pool R_O. *Parallel-two-pool*: T_1, turnover time of root pool R_1; T_2, turnover time of root pool R_2; α, fraction roots belonging to R_1. μ, location parameter and σ, shape parameter of the *log-normal* survival function. γ, scale parameter and β, shape parameter of the *Weibull* survival function. T, turnover time of the *exponential* model.

3.9   Supporting Information

(a) Serial-two-pool

(b) Log-normal

(c) Parallel-two-pool
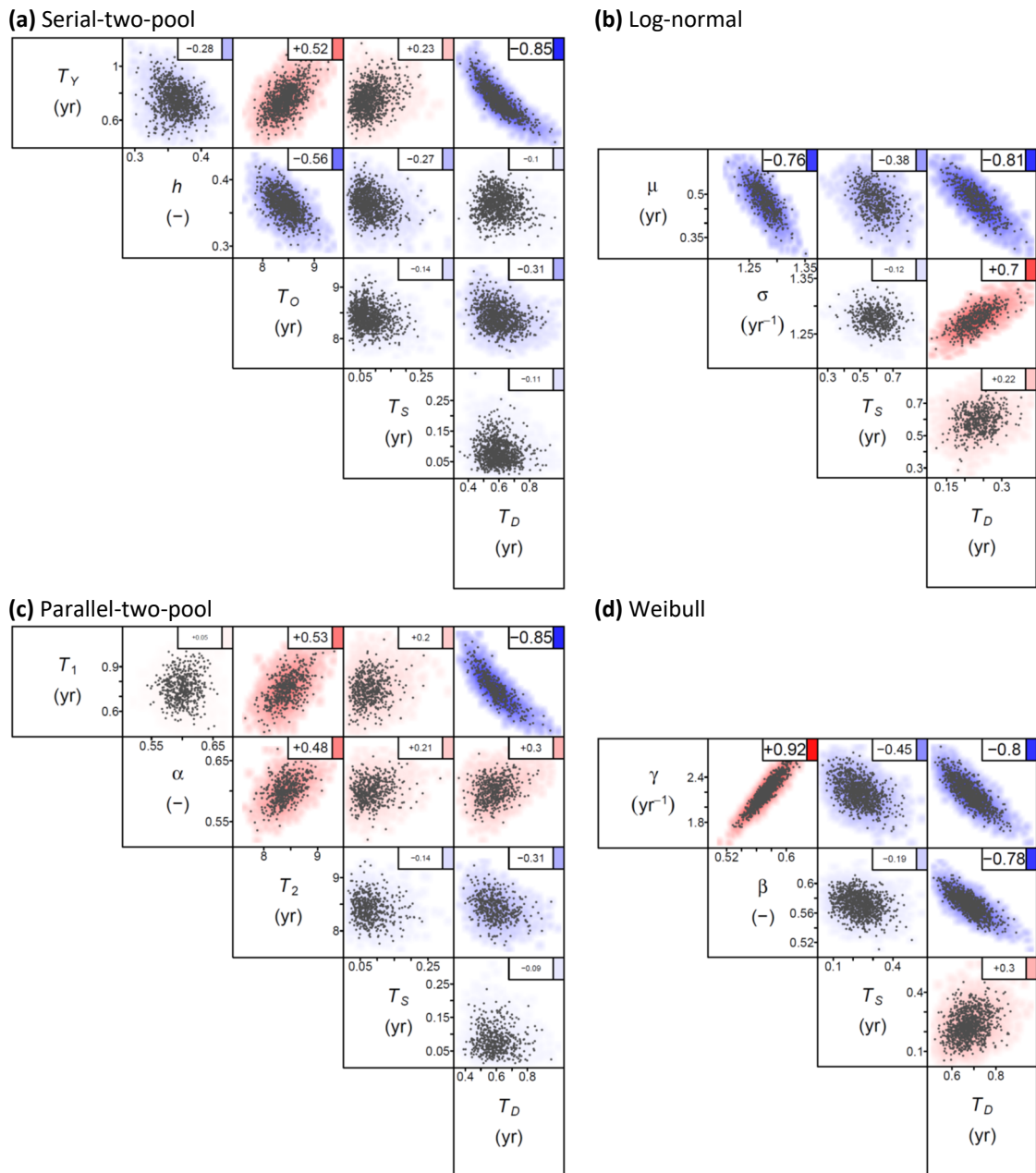
(d) Weibull

Fig S1. Correlations between the posterior parameters of (a) the *serial-two-pool*, (b) the *log-normal*, (c) the *parallel-two-pool*, and (d) the *Weibull* survival function. , T_S, storage turnover time, and T_D, dead root turnover time. *Serial-two-pool*: T_Y, turnover time of the young root pool R_Y; h, transfer coefficient from young to old root pool; T_O, turnover time of the old root pool R_O. *Parallel-two-pool*: T_1, turnover time of root pool R_1; T_2 turnover time of root pool R_2; α, fraction roots belonging to R_1. μ, location parameter and σ, shape parameter of the *log-normal* survival function. γ, scale parameter and β, shape parameter of the *Weibull* survival function. T, turnover time of the *exponential* model.

3.10 References

Adams, T.S., Eissenstat, D.M., 2014. The Continuous Incorporation of Carbon into Existing Sassafras albidum Fine Roots and Its Implications for Estimating Root Turnover. Plos One 9, e95321.

Ahrens, B., Reichstein, M., 2014. Reconciling ^{14}C and minirhizotron-based estimates of fine-root turnover with survival functions. Journal of Plant Nutrition and Soil Science 177, 287-296.

Brundrett, M., Bougher, N., Dell, B., Grove, T., Malajczuk, N., 1996. Working with mycorrhizas in forestry and agriculture, ACIAR monograph 32. Australian Centre for International Agricultural Research, Canberra, Australia.

Eissenstat, D., Yanai, R., 1997. The ecology of root lifespan. Advances in ecological research 27, 1-60.

Fröberg, M., 2012. Residence time of fine-root carbon using radiocarbon measurements of samples collected from a soil archive. Journal of Plant Nutrition and Soil Science 175, 46-48.

Gaudinski, J.B., Torn, M.S., Riley, W.J., Dawson, T.E., Joslin, J.D., Majdi, H., 2010. Measuring and modeling the spectrum of fine-root turnover times in three forests using isotopes, minirhizotrons, and the Radix model. Global Biogeochemical Cycles 24, GB3029.

Gaudinski, J.B., Torn, M.S., Riley, W.J., Swanston, C., Trumbore, S.E., Joslin, J.D., Majdi, H., Dawson, T.E., Hanson, P.J., 2009. Use of stored carbon reserves in growth of temperate tree roots and leaf buds: analyses using radiocarbon measurements and modeling. Global Change Biology 15, 992-1014.

Gaudinski, J.B., Trumbore, S.E., Davidson, E.A., Cook, A.C., Markewitz, D., Richter, D.D., 2001. The age of fine-root carbon in three forests of the eastern United States measured by radiocarbon. Oecologia 129, 420-429.

Gaul, D., Hertel, D., Leuschner, C., 2009. Estimating fine root longevity in a temperate Norway spruce forest using three independent methods. Functional Plant Biology 36, 11-19.

Guillaume, J., Andrews, F., 2012. dream: DiffeRential Evolution Adaptive Metropolis.

Guo, D., Li, H., Mitchell, R.J., Han, W., Hendricks, J.J., Fahey, T.J., Hendrick, R.L., 2008. Fine root heterogeneity by branch order: exploring the discrepancy in root turnover estimates between minirhizotron and carbon isotopic methods. New Phytologist 177, 443-456.

Hansson, K., Helmisaari, H.-S., Sah, S.P., Lange, H., 2013. Fine root production and turnover of tree and understorey vegetation in Scots pine, silver birch and Norway spruce stands in SW Sweden. Forest Ecology and Management 309, 58-65.

Hishi, T., 2007. Heterogeneity of individual roots within the fine root architecture: causal links between physiological and ecosystem functions. Journal of Forest Research 12, 126-133.

Iversen, C.M., Murphy, M.T., Allen, M.F., Childs, J., Eissenstat, D.M., Lilleskov, E.A., Sarjala, T.M., Sloan, V.L., Sullivan, P.F., 2012. Advancing the use of minirhizotrons in wetlands. Plant and Soil 352, 23-39.

Kass, R., Raftery, A., 1995. Bayes factors. Journal of the American Statistical Association 90, 773-795.

Kikuzawa, K., Lechowicz, M.J., 2011. Ecology of leaf longevity. Springer Verlag, Tokyo.

Kleinbaum, D., Klein, M., 2005. Survival Analysis: A Self-Learning Text. New York, Springer-Verlag.

Lukac, M., 2012. Fine Root Turnover, In: Mancuso, S. (Ed.), Measuring Roots. Springer Verlag, Berlin Heidelberg, pp. 363-373.

Manzoni, S., Katul, G.G., Porporato, A., 2009. Analysis of soil carbon transit times and age distributions using network theories. Journal of Geophysical Research 114, 1-14.

Manzoni, S., Piñeiro, G., Jackson, R.B., Jobbágy, E.G., Kim, J.H., Porporato, A., 2012. Analytical models of soil and litter decomposition: Solutions for mass loss and time-dependent decay rates. Soil Biology and Biochemistry 50, 66-76.

Matamala, R., Gonzalez-Meler, M.A., Jastrow, J.D., Norby, R.J., Schlesinger, W.H., 2003. Impacts of fine root turnover on forest NPP and soil C sequestration potential. Science 302, 1385-1387.

Niinemets, Ü., Lukjanova, A., 2003. Total foliar area and average leaf age may be more strongly associated with branching frequency than with leaf longevity in temperate conifers. New Phytologist 158, 75-89.

Pregitzer, K.S., DeForest, J.L., Burton, A.J., Allen, M.F., Ruess, R.W., Hendrick, R.L., 2002. Fine root architecture of nine North American trees. Ecological Monographs 72, 293-309.

Pritchard, S.G., Strand, A.E., 2008. Can you believe what you see? Reconciling minirhizotron and isotopically derived estimates of fine root longevity. New Phytologist 177, 287-291.

Richardson, A., Williams, M., Hollinger, D., Moore, D., Dail, D., Davidson, E., Scott, N., Evans, R., Hughes, H., Lee, J., Rodrigues, C., Savage, K., 2010. Estimating parameters of a forest ecosystem C model with measurements of stocks and fluxes as joint constraints. Oecologia 164, 25-40.

Riley, W.J., Gaudinski, J.B., Torn, M.S., Joslin, J., Hanson, P.J., 2009. Fine‐root mortality rates in a temperate forest: Estimates using radiocarbon data and numerical modeling. New Phytologist 184, 387-398.

Rodhe, H., 1992. Modeling Biogeochemical Cycles, In: Butcher, S.S., Charlson, R.J., Orians, G.H., Wolfe, G.V. (Eds.), Global Biogeochemical Cycles. Academic Press, San Diego, pp. 55-72.

Solly, E., Schoning, I., Boch, S., Muller, J., Socher, S.A., Trumbore, S.E., Schrumpf, M., 2013. Mean age of carbon in fine roots from temperate forests and grasslands with different management. Biogeosciences 10, 4833-4843.

Strand, A.E., Pritchard, S.G., McCormack, M.L., Davis, M.A., Oren, R., 2008. Irreconcilable differences: Fine-root life spans and soil carbon persistence. Science 319, 456-458.

Taylor, A., Martin, F., Read, D., 2000. Fungal diversity in ectomycorrhizal communities of Norway spruce [Picea abies (L.) Karst.] and beech (Fagus sylvatica L.) along north-south transects in Europe, Carbon and nitrogen cycling in European forest ecosystems. Springer, pp. 343-365.

Tierney, G.L., Fahey, T.J., 2001. Evaluating minirhizotron estimates of fine root longevity and production in the forest floor of a temperate broadleaf forest. Plant and Soil 229, 167-176.

Tierney, G.L., Fahey, T.J., 2002. Fine root turnover in a northern hardwood forest: a direct comparison of the radiocarbon and minirhizotron methods. Canadian Journal of Forest Research 32, 1692-1697.

Trumbore, S., 2009. Radiocarbon and soil carbon dynamics. Annual Review of Earth and Planetary Sciences 37, 47-66.

Trumbore, S., Da Costa, E.S., Nepstad, D.C., De Camargo, P.B., Martinelli, L., Ray, D., Restom, T., Silver, W., 2006. Dynamics of fine root carbon in Amazonian tropical ecosystems and the contribution of roots to soil respiration. Global Change Biology 12, 217-229.

Trumbore, S.E., Gaudinski, J.B., 2003. The secret lives of roots. Science 302, 1344-1345.

Withington, J.M., Reich, P.B., Oleksyn, J., Eissenstat, D.M., 2006. Comparisons of structure and life span in roots and leaves among temperate trees. Ecological Monographs 76, 381-397.

4 Study III

"Contribution of Sorption, DOC Transport and Microbial Interactions to the 14C Age of a Soil Organic Carbon Profile: Insights from a Calibrated Process Model"

Contribution: I conceived the main ideas for the COMISSION model with inputs from Markus Reichstein and Marion Schrumpf. Maarten Braakhekke and I developed the ideas for continuous profile representation collaboratively. I conducted the analysis, created all visualisations, and wrote the manuscript with inputs from all co-authors.

Published in Soil Biology and Biochemistry, 88, 390-402.

Contribution of Sorption, DOC Transport and Microbial Interactions to the [14]C Age of a Soil Organic Carbon Profile: Insights from a Calibrated Process Model

[a]Bernhard Ahrens, Maarten C. Braakhekke[a,b,c], Georg Guggenberger[d],

Marion Schrumpf[a], Markus Reichstein[a]

_____

[a]Max-Planck-Institute for Biogeochemistry, Hans-Knöll-Str. 10, 07445 Jena, Germany

[b]Copernicus Institute of Sustainable Development, Faculty of Geosciences, Utrecht University, Netherlands

[c]Wageningen University, Earth System Science Group, Wageningen, Netherlands

[d]Institute of Soil Science, Leibniz Universität Hannover, Hannover, Germany

4.1 Key words

stabilization mechanisms, sorptive stabilization, microbial interaction, transport model, radiocarbon profile, soil organic carbon

4.2 Highlights

- A SOC profile model was developed and calibrated to explain ^{14}C ages > 1000 years of subsoil OC
- Factorial model-experiments revealed processes explaining the persistence of SOC:
- ^{14}C ages could be explained without introducing a SOC pool with a millennial turnover time
- Sorptive stabilization is the dominant process for modeled topsoil ^{14}C ages
- Energy limitation, microbial recycling and sorption govern modeled subsoil ^{14}C ages

4.3 Graphical abstract
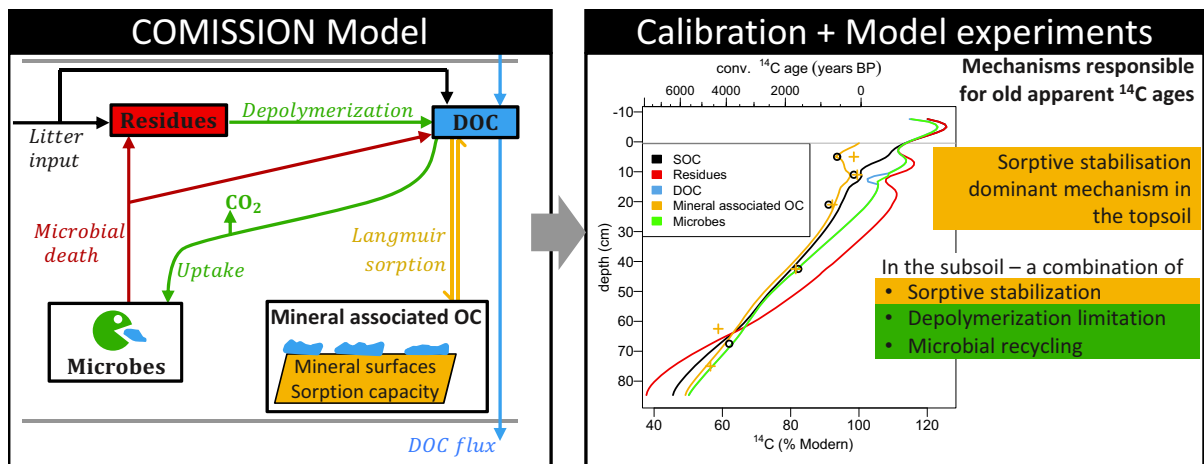
Corresponding author:

Bernhard Ahrens

Max Planck Institute for Biogeochemistry

Hans-Knöll-Str. 10

07745 Jena

Germany

bahrens@bgc-jena.mpg.de

4.4   Abstract

Profiles of soil organic carbon (SOC) are often characterized by a steep increase of ^{14}C age with depth, often leading to subsoil ^{14}C ages of more than 1000 years. These observations have generally been reproduced in SOC models by introducing a SOC pool that decomposes on the time-scale of millennia. The overemphasis of chemical recalcitrance as the major factor for the persistence of SOC was able to provide a mechanistic justification for these very low decomposition rates. The emerging view on SOC persistence, however, stresses that apart from molecular structure a multitude of mechanisms can lead to the long-term persistence of organic carbon in soils. These mechanisms, however, have not been incorporated into most models. Consequently, we developed the SOC profile model COMISSION which simulates vertically resolved SOC concentrations based on representations of microbial interactions, sorption to minerals, and vertical transport. We calibrated COMISSION using published concentrations of SOC, microbial biomass and mineral-associated OC (MOC), and in addition, ^{14}C contents of SOC and MOC of a Haplic Podzol profile in North-Eastern Bavaria, Germany. In order to elucidate the contribution of the implemented processes to the ^{14}C age in different parts of the profile, we performed model-experiments in which we switched off the limitation of SOC decomposition by microbes, sorptive stabilization on soil minerals, and dissolved OC (DOC) transport. By splitting all model pools into directly litter-derived carbon and microbe-derived organic carbon, we investigated the contribution of repeated microbial recycling to ^{14}C ages throughout the profile. The model-experiments for this site lead to the following implications: Without rejuvenation by DOC transport, SOC in the subsoil would be on average 1700 ^{14}C years older. Across the profile, SOC from microbial recycling is on average 1400 ^{14}C years older than litter-derived SOC. Without microbial limitation of depolymerization, SOC in the subsoil would be on average 610 ^{14}C years younger. Sorptive stabilization is responsible for relatively high ^{14}C ages in the topsoil. The model-experiments further indicate that the high SOC concentrations in the Bh horizon are caused by the interplay between sorptive stabilization and microbial dynamics. Overall, the model-experiments demonstrate that the high ^{14}C ages are not solely caused by slow turnover of a single pool, but that the increase of ^{14}C ages along a soil profile up to ages > 1000 years is the result of different mechanisms contributing to the overall persistence of SOC. The dominant reasons for the persistence of SOC are stabilization processes, followed by repeated microbial processing of SOC.

4.5   Introduction

Investigating soil profiles, i.e. studying the sequence of horizons, and the change of biological, chemical and physical properties with soil depth, is one of the cornerstones of soil science (Hartemink, 2009). The vertical distribution of soil organic carbon (SOC) has long been an interest of soil scientists from plot to global scale (Jobbágy and Jackson, 2000). The size of global SOC stocks as the largest active terrestrial pool in the global carbon cycle is considered increasingly important due concerns about the potential feedback of SOC to climate change. Global SOC stocks are usually estimated down to 1 m depth (around 1500 Pg C) although there is 1.5-2 times more SOC if one considers a soil depth down to 3 m (Scharlemann et al., 2014).

Most SOC models, especially in Earth system models, are modeling SOC stocks without considering their vertical distribution. For most Earth system models it is unclear if they simulate SOC stocks throughout the full soil depth, the top 100 cm or top 30 cm (Todd-Brown et al., 2013; Carvalhais et al., 2014). This complicates the comparison of the modeled SOC stock with observations.

Models describing the complete SOC profile have been published since the late 1970s (Kaneyuki and Kichiro, 1978; Dörr and Münnich, 1989; Elzein and Balesdent, 1995), and recent years have witnessed a renewed interest (Baisden et al., 2002; Freier et al., 2010; Braakhekke et al., 2011; Guenet et al., 2013; Koven et al., 2013; Riley et al., 2014). These models are generally very well able to reproduce the SOC profile using representations of DOC transport, bioturbation, vertically distributed root litter input and microbial decomposition. In addition to the vertical distribution of SOC, its ^{14}C profile provides important information about the time-scale at which soil organic carbon is turning over.

The ^{14}C age of SOC generally increases strongly with soil depth up to ages of 1000 – 10000 years (Rumpel et al., 2012). Vertical SOC profile models were generally successful at reproducing these millennial ^{14}C ages by introducing a SOC pool that decomposes according to first-order kinetics at the time-scale of millennia (e.g. Elzein and Balesdent, 1995; Baisden et al., 2002; Braakhekke et al., 2014) or by assuming a substantial slow-down of first-order decomposition rates with depth (e.g. Jenkinson and Coleman, 2008; Koven et al., 2013). This might have been well justified within what Schmidt et al. (2011) call the historical view on SOC cycling, namely that the molecular structure (chemical recalcitrance) was mainly responsible for the long-term persistence of organic carbon in

soils. Schmidt et al. (2011), however, posed that, in addition to molecular structure, multiple processes are responsible for the long-term persistence of SOC. These can be distinguished between *stabilization processes* such as sorption of organic matter to mineral surfaces, energy limitation of the microbial decomposition, and mere *persistence processes* such as the repeated recycling of SOC through the microbial biomass (Gleixner, 2013) and the slow downward transport of soil organic matter, where sorption is a retardation factor (Braakhekke et al., 2011). For modeling the SOC profile, this implies that these different processes contribute to varying degrees to the apparent stability of soil organic carbon within the profile. In vertical profile models, however, these processes have rarely been explicitly incorporated. The models developed by Guenet et al. (2013) and Riley et al. (2014) are a recent effort to represent these mechanisms more explicitly.

Our objective for this study was to quantify the contribution of these different stabilization and persistence processes to the distribution of ^{14}C ages across an exemplary Haplic Podzol profile under a Norway spruce forest, using a mechanistic model. To this end we applied several well-established approaches such as the representation of transport from traditional SOC profile models, namely the SOMPROF model and its bioturbation and advection formulation (Braakhekke et al., 2011), the Schimel and Weintraub (2003) link between microbial dynamics and SOC decomposition, and a Langmuir representation of sorptive SOC stabilization (Kaiser and Guggenberger, 2003; Mayes et al., 2012). We combined these different approaches to the COMISSION model. The acronym **COMISSION** highlights that this SOC model includes a **CO**ntinuous representation of SOC in the organic layer and the mineral soil, **M**icrobial **I**nteractions and **S**orptive **S**tabilizat**ION**. By performing model-experiments with the calibrated COMISSION model we want to answer the following questions:

(1) What is the relative importance of DOC advection for the formation of the SOC and radiocarbon profile?

(2) How much can microbes limit the depolymerization of SOC and what is their effect on the formation of the SOC and radiocarbon profile?

(3) How important is sorptive stabilization of DOC on soil minerals for the formation of the SOC and radiocarbon profile?

(4) How important are microbial products for the formation of the SOC and radiocarbon profile compared to plant-derived SOC?

4.6   Material and methods

4.6.1   The COMISSION model

The COMISSION model has all the typical elements of SOC profile models. The profile is discretized in several layers, in the current implementation 100, and the different layers receive organic carbon either as aboveground litter input on top, vertically distributed root litter input, or transport from other layers via advection with the water flux or bioturbation (Figure 4-1). In order to represent the SOC profile continuously in the organic layer and the mineral soil, an additional advective term accounts for the upward shift of the soil surface during the buildup of an organic layer. Figure 4-1 shows a conceptual overview of the COMISSION model, while all constitutive equations of the COMISSION model are listed with annotated terms in Table 4-1.

Two different model pools receive aboveground litter input and the vertically distributed root litter input. The readily leachable and soluble fraction of litter input enters a dissolved OC (DOC) pool (C_{DOC}), while the rest enters a residue pool (C_R) which represents polymeric, non-soluble SOC (Figure 4-1, Table 4-1 – Eqs. (4-4), (4-5)). The residue pool is depolymerized by extracellular enzymes produced by a microbial pool (C_B) to enter the C_{DOC} pool which represents SOC potentially available for assimilation by microbes. We assume that levels of extracellular enzymes scale with microbial biomass C_B, so that we do not model enzymes explicitly (Figure 4-1, Table 4-1). Interactions of microbes with the C_R and C_{DOC} pool are modeled with traditional and reverse Michaelis-Menten kinetics (Eqs. (5-3) and (4-2)). This makes it possible to represent the priming effect, i.e. that SOC decomposition is accelerated by the amendment of substrate (Schmidt et al., 2011; Wutzler and Reichstein, 2013). In the COMISSION model an additional input to the C_{DOC} pool can increase the microbial biomass (Eqn (4-7)) and thereby enhance the depolymerization of the C_R pool (Eqn (4-4)). By analogy, this approach is also able to represent the retardation of decomposition via energy limitation of microbes in the deep soil where substrate might be scarce. Here, the growth of microbial biomass can be limited due to lower inputs to the C_{DOC} pool (Eqn (4-7)) or a higher sorption of C_{DOC} on soil minerals. In turn, this slows down the depolymerization of the C_R pool (Eqn (4-4)).Overall, the representation of microbial decomposition is similar to the approaches of Schimel and Weintraub (2003) and Allison et al. (2010).

The adsorption and desorption of DOC to and from mineral surfaces controls the availability of carbon in the C_{DOC} pool for assimilatory uptake by microbes. The adsorption and desorption of

DOC is modeled dynamically using Langmuir equations (Figure 4-1, Eqn (4-3)). The C_{DOC} pool not only constitutes the substrate for the microbial pool, but is also transported via advection (Eqn (4-5)), and, after sorption, DOC forms the mineral-associated, stabilized C_q pool (Eqn (4-6)).

Soil organic carbon in COMISSION is recycled within the soil profile through microbial processing – dead microbes (Figure 4-1, Eqn (4-7)) either enter the C_{DOC} pool (e.g. the cytosol, Eqn (4-5)) or the C_R pool (e.g. cell envelopes, Eqn (4-4)), and might thereby also contribute to longer residence times with soil depth.

In the following three subsections we cover in-depth the three processes that form the acronym of the **COMISSION** model – a **CO**ntinuous SOC profile model with **M**icrobial **I**nteractions and **S**orptive **S**tabilizat**ION**.
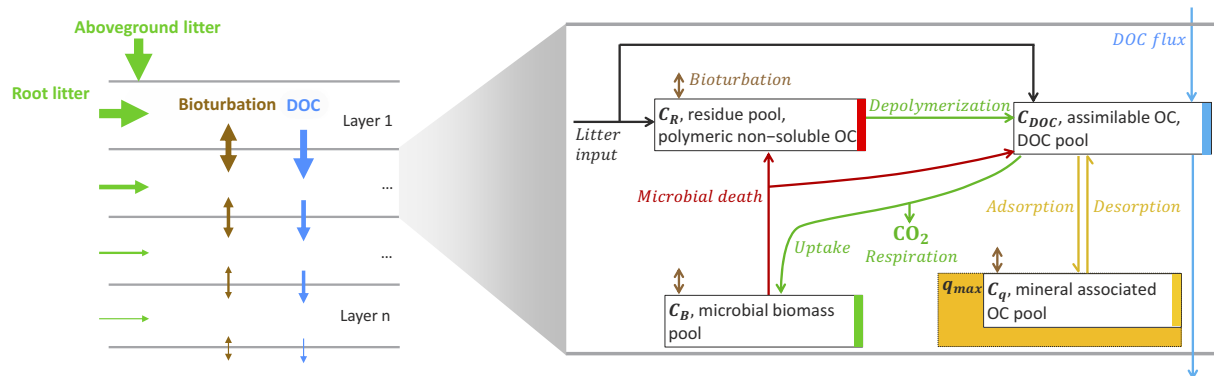
Figure 4-1: Schematic representation of the COMISSION model. Left: The soil profile is split in different soil layers (n = 100), aboveground litterfall is added on top of the profile; root litter input enters the different soil layers according to the root biomass profile. Bioturbation and DOC transport translocate carbon between the soil layers. Right: In each layer the non-leachable part of the litter input enters the C_R pool (polymeric non-soluble SOC, residue pool), while the leachable part of litter input directly enters the C_{DOC} pool (OC assimilable by microbes, DOC). The C_R pool is decomposed (depolymerization) with extracellular enzymes produced by the C_B pool (microbial biomass). Extracellular enzymes levels are assumed to be directly related to microbial biomass levels. Due to the depolymerization the carbon is now potentially available for assimilation as C_{DOC}. C_{DOC} can be either taken up microbes, transported with the water flux through the profile, or sorbed to soil minerals until the sorption capacity q_{max} filled. The sorbed OC in the C_q pool can also be desorbed again. All respiratory losses of the system are represented with a lumped parameter $1 - CUE$, where CUE describes the carbon use efficiency of microbes. Microbes die with the first-order rate π. A part p of the dying microbes enters the C_{DOC} pool. The insoluble part of dying microbes $1 - p$ (e.g. cell walls) enters the residue pool C_R. All pools except the C_{DOC} pool are transported via bioturbation and particle advection. Please note that this model structure resembles the models presented by Schimel and Weintraub (2003), Allison et al. (2010) and Todd-Brown et al. (2012) in terms of pool arrangement.

4.6.2 Microbial Interactions

The spatial separation between microbes and SOC can potentially limit the decomposition of SOC (Schmidt et al., 2011). In the COMISSION model we assume that this spatial separation limits two processes mediated by microbes. First, to overcome the spatial separation from the C_R pool microbes produce extracellular enzymes that diffuse through the soil matrix and depolymerize the C_R pool upon contact. Second, the produced substrate, C_{DOC}, has to diffuse back to the microbes. Similar to other studies (Vetter et al., 1998; Schimel and Weintraub, 2003; Rothman and Forney, 2007) we propose that the diffusing substance that overcomes the spatial separation limits the rate of the respective process.

Maximum depolymerization rates of C_R are attained at high microbial biomass levels, while low microbial biomass levels limit the depolymerization, assuming that extracellular enzyme levels scale with the microbial biomass C_B (Todd-Brown et al., 2012):

$$Depolymerization = \underbrace{V_{max,D} \cdot C_R}_{\substack{\text{maximum} \\ \text{depolymerization}}} \cdot \underbrace{\frac{C_B}{K_{m,B} + C_B}}_{\substack{\text{rate limitation} \\ \text{by microbes}}}, \tag{4-1}$$

where $V_{max,D}$ is the maximum specific depolymerization rate for C_R by extracellular enzymes excreted by C_B, and $K_{m,B}$ is the half-saturation constant for the depolymerization of C_R. This type of microbial interactions is commonly called "reverse Michaelis-Menten" kinetics (Schimel and Weintraub, 2003) or biomass-saturated approach (Moorhead and Sinsabaugh, 2006).

Microbial uptake and growth is limited by the availability of the substrate (DOC), while at high DOC concentrations the ability of microbes to assimilate C_{DOC} is limiting microbial uptake of DOC:

$$Uptake = \underbrace{V_{max,U} \cdot C_B}_{\substack{\text{maximum} \\ \text{DOC uptake}}} \cdot \underbrace{\frac{C_{DOC}}{K_{m,U} + C_{DOC}}}_{\substack{\text{rate limitation} \\ \text{by DOC}}}, \tag{4-2}$$

where $V_{max,U}$ is the maximum specific assimilation rate of C_B by uptake of C_{DOC}, and $K_{m,U}$ is the half-saturation constant for the assimilation of C_{DOC} by C_B. We refer to this type of microbial interactions as "traditional Michaelis-Menten" kinetics or substrate-saturated approach (Moorhead and Sinsabaugh, 2006).

While both the traditional and reverse Michaelis-Menten kinetics have been used separately to represent microbial dynamics in different SOC decomposition models (Wutzler and Reichstein, 2008), we argue for a combination of both approaches in the COMISSION model because the spatial separation of microbes and the C_R pool controls on the one hand the depolymerization of C_R by the availability of extracellular enzymes and on the other hand the microbial assimilation by the availability of DOC.

4.6.3 Sorptive stabilization

Using a dynamic Langmuir approach for representing mineral stabilization of SOC has the advantage that sorptive strength is dependent on the availability of sorption sites. Thereby more SOC is getting sorbed in horizons where most sorption sites are unoccupied compared to horizons where sorption sites are almost saturated:

$$Adsorption = \underbrace{k_{ads} \cdot C_{DOC}}_{\substack{\text{maximum} \\ \text{adsorption}}} \cdot \underbrace{\left(q_{max} - C_q\right)}_{\substack{\text{rate limitation by} \\ \text{availability of} \\ \text{sorption sites}}}$$

$$\hspace{8cm} (4\text{-}3)$$

$$Desorption = k_{des} \cdot C_q,$$

where C_q is the mineral-associated OC pool, k_{ads} is the maximum adsorption rate, when the surface is not occupied at all, q_{max} is the maximum sorption capacity, and k_{des} is the desorption rate.

The Langmuir sorption approach also has the advantage that we can relate the total sorption capacity q_{max} to soil properties, such as clay and silt content, or iron and aluminum oxides (Kothawala et al., 2009; Mayes et al., 2012) across different soils, but also within a soil profile.

Most SOC profile models have adopted a linear, equilibrium isotherm sorption approach. This simplification is likely unjustified under field conditions because the assumption of an

instantaneous local equilibrium between adsorption and desorption is only reasonable if all the other processes (e.g. microbial uptake, depolymerization, microbial death, advective transport, diffusion) are several orders of magnitude slower. In batch sorption experiments, however, this is a valid assumption if microbial growth is suppressed through the addition of low quantities of $HgCl_2$ (Mikutta et al., 2007).

4.6.4 Continuous profile

Most SOC profile models do not account for the additional downward advective flux that stems from the accumulation of an organic layer on the soil surface due to litterfall and the counteracting upward advective flux that stems from the loss of organic matter due to decomposition. One might regard this phenomenon as only relevant for modeling forest soils which are generally characterized by the presence of an organic layer. However, the absence or presence of an organic layer could be treated as an integral part of modeling when we explicitly account for this additional advective flow (Braakhekke and Ahrens, in prep.)

In marine ecology the problem of an additional advective flow due to sedimentation, when modeling reactive transport in sediments, has been extensively studied (Boudreau and Imboden, 1987; Mulsow et al., 1998; Meysman et al., 2005). In soils a similar approach has been adopted for modeling the effect of soil erosion on the soil carbon balance (Van Oost et al., 2005; Yoo et al., 2005). In both settings the deposition of sediments on top of the surface is accounted for with an additional advective term which moves soil or sediment layers downwards according to the sedimentation velocity.

In the COMISSION model we are able to simulate the SOC profile as a continuum by introducing the particle velocity ω that is driving an additional advective flux for all model pools (particle fluxes in Table 4-1). The particle velocity ω comprises two terms: an additional downward velocity due to aboveground and belowground litter inputs, and a counteracting upward advection velocity due to the loss of soil volume during litter decomposition, which effectively moves the reference frame for the soil profile upwards. More details on the continuous representation of the organic layer and the mineral soil can be found in the Supplementary Information.

The continuous profile approach also makes it possible to consistently model the advective transport of the DOC pool with an average pore water velocity, v, (Table 4-1, Eqn (4-5)) and

bioturbation as a diffusive flux (Table 4-1, Eqn (4-4) - (4-7)) throughout the soil profile. Compared to the SOMPROF approach towards bioturbation (Braakhekke et al., 2011), we do not have to resort to an extra parameter that translates the bioturbation rate in the organic layer into a diffusion coefficient in the mineral soil.

Table 4-1: Governing equations of the COMISSION model. All state variables are expressed in mass of C per volume bulk soil (kg C m^{-3}).

Description	Differential equation
C_R, polymeric non-soluble OC, residue pool	$\frac{\partial}{\partial t} C_R = \underbrace{(1-L) \cdot i}_{\substack{\text{non-leachable} \\ \text{litter input}}} + \underbrace{(1-p) \cdot \pi \cdot C_B}_{\substack{\text{non-soluble} \\ \text{microbial remains}}} - \underbrace{V_{max,D} \cdot C_R \cdot \frac{C_B}{K_{m,B} + C_B}}_{\text{Depolymerization}} + \underbrace{\frac{\partial}{\partial z}\left(D_b \frac{\partial C_R}{\partial z}\right)}_{\substack{\text{Diffusion via} \\ \text{Bioturbation}}}$ $\qquad$ (4-4) $- \underbrace{\frac{\partial(\omega \cdot C_R)}{\partial z}}_{\substack{\text{particle} \\ \text{flux}}}$
C_{DOC}, assimilable OC, DOC pool	$\frac{\partial}{\partial t} C_{DOC} = \underbrace{L \cdot i}_{\substack{\text{DOC input} \\ \text{from litter}}} + \underbrace{p \cdot \pi \cdot C_B}_{\substack{\text{soluble} \\ \text{microbial remains}}} + \underbrace{V_{max,D} \cdot C_R \cdot \frac{C_B}{K_{m,B} + C_B}}_{\text{Depolymerization}}$ $\qquad$ (4-5) $- \underbrace{V_{max,U} \cdot C_B \cdot \frac{C_{DOC}}{K_{m,U} + C_{DOC}}}_{\substack{\text{uptake of DOC} \\ \text{by microbes}}} - \underbrace{k_{ads} \cdot C_{DOC} \cdot (q_{max} - C_q)}_{\text{adsorption}}$ $+ \underbrace{k_{des} \cdot C_q}_{\text{desorption}} - \underbrace{\frac{\partial(v \cdot C_{DOC})}{\partial z}}_{\substack{\text{DOC transport} \\ \text{with water flux}}} - \underbrace{\frac{\partial(\omega \cdot C_{DOC})}{\partial z}}_{\substack{\text{particle} \\ \text{flux}}}$
C_q, mineral-associated OC pool	$\frac{\partial}{\partial t} C_q = \underbrace{k_{ads} \cdot C_{DOC} \cdot (q_{max} - C_q)}_{\text{adsorption}} - \underbrace{k_{des} \cdot C_q}_{\text{desorption}} + \underbrace{\frac{\partial}{\partial z}\left(D_b \frac{\partial C_q}{\partial z}\right)}_{\substack{\text{Diffusion via} \\ \text{Bioturbation}}} - \underbrace{\frac{\partial(\omega \cdot C_q)}{\partial z}}_{\substack{\text{particle} \\ \text{flux}}}$ $\qquad$ (4-6)
C_B, microbial biomass pool	$\frac{\partial}{\partial t} C_B = \underbrace{CUE \cdot V_{max,U} \cdot C_B \cdot \frac{C_{DOC}}{K_{m,U} + C_{DOC}}}_{\substack{\text{uptake of DOC} \\ \text{by microbes used for growth}}} - \underbrace{\pi \cdot C_B}_{\substack{\text{microbial} \\ \text{death}}} + \underbrace{\frac{\partial}{\partial z}\left(D_b \frac{\partial C_B}{\partial z}\right)}_{\substack{\text{Diffusion via} \\ \text{Bioturbation}}} - \underbrace{\frac{\partial(\omega \cdot C_B)}{\partial z}}_{\substack{\text{particle} \\ \text{flux}}}$ $\qquad$ (4-7)

where:

t	time (yr)
z	depth (m)
L	leachable fraction of litter input (-)
i	change in concentration due to litter input from roots or aboveground in depth z (kg C m^{-3} yr^{-1})
p	soluble fraction of dead microbes (-)
π	mortality rate of C_B, first-order kinetics (yr^{-1})
$V_{max,D}$	maximum specific depolymerization rate for C_R by extracellular enzymes excreted by C_B (yr^{-1})
$K_{m,B}$	half-saturation constant for the depolymerization of C_R (kg C m^{-3})
D_b	bioturbation/biodiffusion coefficient (m^2 yr^{-1})
ω	particle advection velocity due to particle displacement from litter input and SOM decomposition (m^3 m^{-2} yr^{-1})
$V_{max,U}$	maximum specific assimilation rate of C_B by uptake of C_{DOC} (yr^{-1})

$K_{m,U}$ half-saturation constant for the assimilation of C_{DOC} by C_B (kg C m^{-3})

k_{ads} adsorption rate (m^3 (kg C)$^{-1}$ yr^{-1})

q_{max} maximum sorption capacity (kg C m^{-3})

k_{des} desorption rate (yr^{-1})

v average pore water velocity (m^3 m^{-2} yr^{-1})

CUE carbon use efficiency of microbes C_B (-)

4.6.5   Site description

The Coulissenhieb I site is a Norway spruce forest located in the Waldstein hillsides in the Fichtelgebirge Mountains in NE Bavaria (Germany). The site has been intensively studied and is referred to as Waldstein or Coulissenhieb (I) in the literature. The Waldstein hillsides have a continental temperate climate (Köppen classification), with high annual precipitation of 1163 mm and a mean annual temperature of 5.3°C (Foken, 2003).

The soil was classified as a Haplic Podzol (FAO, 1998) with a sandy loam to loam texture and is overlain by a mor-like organic layer of 8.5 cm approximate thickness (Gerstberger et al., 2004). The soil developed on granitic bedrock and is characterized by low pH values throughout the soil profile.

The C/N ratio of the organic layer is rather low for a mor type (21-25) due to high levels of atmospheric nitrogen deposition. The soil receives a mean annual aboveground litterfall of 0.103 kg C m^{-2} yr^{-1} (Berg and Gerstberger, 2004). Belowground litter input from dead fine roots was estimated to be 0.21 kg C m^{-2} yr^{-1} using an estimate of fine-root turnover in the organic layer from sequential coring (Gaul et al., 2008a; Gaul et al., 2008b) which was extrapolated down to 80 cm of the mineral soil using fine-root biomass stocks. The B horizons of the Haplic Podzol of the Coulissenhieb I site are characterized by high amounts of pedogenic oxides (Gerstberger et al., 2004).

4.6.6   Data and calibration

For the calibration of COMISSION we selected data from different studies conducted at the Coulissenhieb I site. The COMISSION model was driven by the aforementioned above- and belowground litter inputs. Belowground litter input was distributed in the different layers according to the observed cumulative root biomass distribution using an exponential cumulative distribution function (Persson, 2000, e-folding depth 7.5 cm). Vertical profiles of five different variables were used together as constraints to estimate the parameters of COMISSION:

(1) Volumetric SOC concentrations (kg m^{-3}) of the three organic layer horizons and six mineral soil horizons, calculated from measurements reported by Rumpel et al. (2002), were compared to the sum of the 4 different model pools ($C_R + C_{DOC} + C_q + C_B$).

(2) The ^{14}C content of SOC (in *percent Modern*, pM, according to Stuiver and Polach (1977)) in 5 mineral soil horizons (Rumpel et al., 2002) was compared with the combined ^{14}C content of the 4 different model pools. The ^{14}C module of COMISSION was driven by atmospheric ^{14}C

contents as described in Ahrens et al. (2014). Radioactive decay of ^{14}C was accounted for by an additional first-order decomposition rate $\lambda = \frac{1}{8267}$ yr[-1] that affects all pools of the ^{14}C module of COMISSION.

(3) The C_q pool, representing mineral-associated organic carbon, was compared to the organic carbon content of the >1.6 g cm^{-3} density fraction as reported by Kaiser et al. (2002) for 6 mineral soil horizons. The >1.6 g cm^{-3} density fraction is thought to represent mineral-associated carbon, and is commonly referred to as the heavy fraction (HF) (Kögel-Knabner et al., 2008) or mineral-associated organic carbon (MOC) (Trumbore and Zheng, 1996). Throughout this study we will use the acronym MOC to refer to the >1.6 g cm^{-3} density fraction. The maximum sorption capacity q_{max} was prescribed based on findings by Guggenberger and Kaiser (2003). They performed DOC sorption experiments to estimate the available sorption capacity for 6 mineral horizons of the Haplic Podzol profile at Coulissenhieb. The available sorption capacity signifies organic carbon that can be sorbed in addition to what is already stabilized on minerals. Thus, following the considerations by Guggenberger and Kaiser (2003), we prescribe q_{max} (Fig. S2) as the sum of the available sorption capacity from the sorption experiments and the mineral-associated organic carbon fraction.

(4) The ^{14}C content of MOC (in *percent Modern*) of 6 mineral horizons as reported by Kögel-Knabner et al. (2008) was compared against the ^{14}C content of the C_q pool of the COMISSION model.

(5) Hamer and Marschner (2005) estimated microbial biomass C contents for the Oa, EA and Bs horizon of the Coulissenhieb I profile with a fumigation-extraction method. We compared the measurements against the C_B pool of the COMISSION model.

In total eleven model parameters (Table S1) were calibrated with the Differential Evolution algorithm for global optimization (Price et al., 2006; Ardia et al., 2013) by minimizing the total sum of squared residuals of all five observed variables (see Eqn S5 for the definition of the multi-constraint cost function). The COMISSION model was started from close to zero SOC and microbial biomass concentrations and run from 13500 years BCE until present day, assuming a constant average pore water velocity, v, and constant litter inputs. As water flux we used the mean of modeled yearly water fluxes at Coulissenhieb I reported in Matzner et al. (2004a) and Matzner et al. (2004b). We further assumed that water fluxes decreased linearly with soil depth from throughfall at the soil surface to the modeled seepage flux in 90 cm soil depth.

4.6.7 Contribution of processes to SOC concentration and ^{14}C age

To study how much the different processes in the COMISSION model contribute to observed organic carbon and ^{14}C profiles, we ran COMISSION forward using the parameter set retrieved by the calibration and the same settings as in the calibration, while switching off processes that we want to study. This approach gives an indication of the relevance of a certain process in COMISSION given the parameterization for the Haplic Podzol profile at Coulissenhieb I. Table 4-2 gives an overview on the different model-experiments.

Furthermore, to quantify the importance of microbial recycling along the soil profile, we split the different carbon pools in directly litter-derived and microbe-derived carbon. For this purpose we set up a second set of the differential equations in Table 4-1. Contrary to the previous model-experiments we did not have to switch off any process to quantify the contribution of litter-derived against microbe-derived organic carbon along the SOC profile. Instead, the second set of pools just receives input in the form of microbial remains. The first set of pools on the other hand only receives litter input, but no organic carbon from microbial recycling. To assure that overall the same dynamics are achieved, the different rate-limiting terms (Eqn (4-1), (4-2), (4-3)) are based on the sum of the respective litter- and microbe-derived carbon pools C_B, C_{DOC} and C_q.

In order to summarize and discuss the results of COMISSION in different parts of the soil profile, we adopt the notation of topsoil and subsoil as used in the Harmonized World Soil Database (Nachtergaele et al., 2008). We refer to the top 30 cm of the mineral soil as topsoil. For the mineral soil below the top 30 cm we use the notation subsoil.

Table 4-2: Model-experiments to elucidate the effect of different mechanisms on ^{14}C age profiles

Model-experiment	Description
No Advection	$v \stackrel{\text{def}}{=} 0$ in Eq. (4-5)
No depolymerization limitation by microbes	$Depolymerization = \underbrace{V_{max,D} \cdot C_R}_{\substack{\text{maximum} \\ \text{depolymerization}}} \cdot \underbrace{\frac{C_B}{K_{m,B}+C_B}}_{\substack{\text{rate limitation} \\ \text{by microbes}}} \stackrel{\text{def}}{=} \underbrace{V_{max,D} \cdot C_R}_{\substack{\text{maximum} \\ \text{depolymerization}}}$ in Eqs. (4-4) and (4-5)
No sorptive stabilization	$k_{ads} \stackrel{\text{def}}{=} 0$ and $k_{des} \stackrel{\text{def}}{=} 0$ in Eqs. (4-5) and (4-6)
Litter- vs microbe-derived OC	Recycling of microbial remains in separate pools

4.7   Results

4.7.1   Full COMISSION model for a Haplic Podzol, $COMISSION_{Full}$

After calibration the COMISSION model is well able to represent the observations of the Haplic Podzol profile at the Coulissenhieb I site (Figure 4-2A and C). The thickness of the organic layer is correctly represented, and it consists mainly of the C_R pool. The secondary maximum of OC concentrations in the Bh horizon is captured with the maximum of the C_q pool and a secondary peak of the C_R pool (Figure 4-2A).

Also the modeled ^{14}C profiles represent the observed profiles well (Figure 4-2C). From the organic layer down to the Bh horizon the ^{14}C profiles of the C_R, C_{DOC}, and C_B pool are characterized by the presence of modern "bomb-radiocarbon", i.e. a ^{14}C value (% Modern) >100. From the Bw horizon downward the ^{14}C signatures of the C_{DOC} and the C_B pool approach the ^{14}C signature of the C_q pool more and more. Of all model pools the C_R pool shows the steepest increase in apparent ^{14}C age with soil depth.

This calibration of the COMISSION model with all processes included ($COMISSION_{Full}$) serves as the reference point for the following model-experiments targeted at elucidating the importance of different processes for the formation of the SOC, MOC and microbial biomass profiles, and the ^{14}C age profiles of SOC and MOC. The parameters retrieved in the calibration can be found in the Supplementary Information in Table S1.
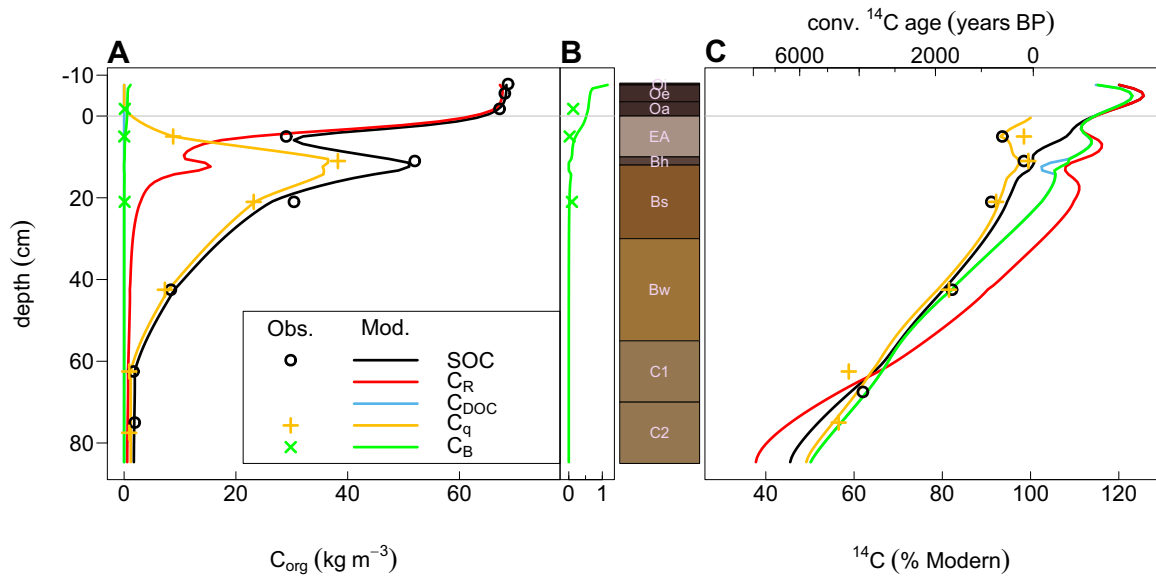
Figure 4-2: Fit of the full COMISSION model pools to different organic carbon fractions (A) and their respective 14C profiles (C). Panel (B) shows the vertical distribution of the C_B pool in more detail. Lines show the model results, while circles, crosses and x's denote the measurements.

4.7.2   Interaction between DOC transport, sorptive stabilization and microbes

Advection

Switching off DOC transport (Table 4-2, "No Advection") influences the formation of the secondary OC maximum in the Bh horizon twofold: First, the Bh horizon receives less DOC input from upper soil layers and thereby is not able to fill the available sorption capacity (Figure 4-3A). Second, the microbial pool C_B and the free sorption sites compete for DOC, and the overall lower DOC levels also lead to a smaller microbe density in the Bh horizon due to substrate scarcity (Figure 4-3B). This slows down the depolymerization of the C_R pool in the Bh horizon, which is mediated by the microbial biomass C_B. Consequently, the secondary peak of the C_R pool is more pronounced compared to the $COMISSION_{Full}$ setup. Concurrently, the overall apparent ^{14}C ages in the Bh horizon would be slightly older with DOC transport switched off (Figure 4-3D). Without DOC transport the apparent ^{14}C ages of SOC in the subsoil would be up to 4240 ^{14}C years higher (Figure 4-3D). For the deep subsoil horizons, C1 and C2, DOC transport is also important for SOC stocks. Without the input of OC via advection into the subsoil horizons the overall SOC stocks would be up to 20% lower in these horizons (Figure 4-3B).
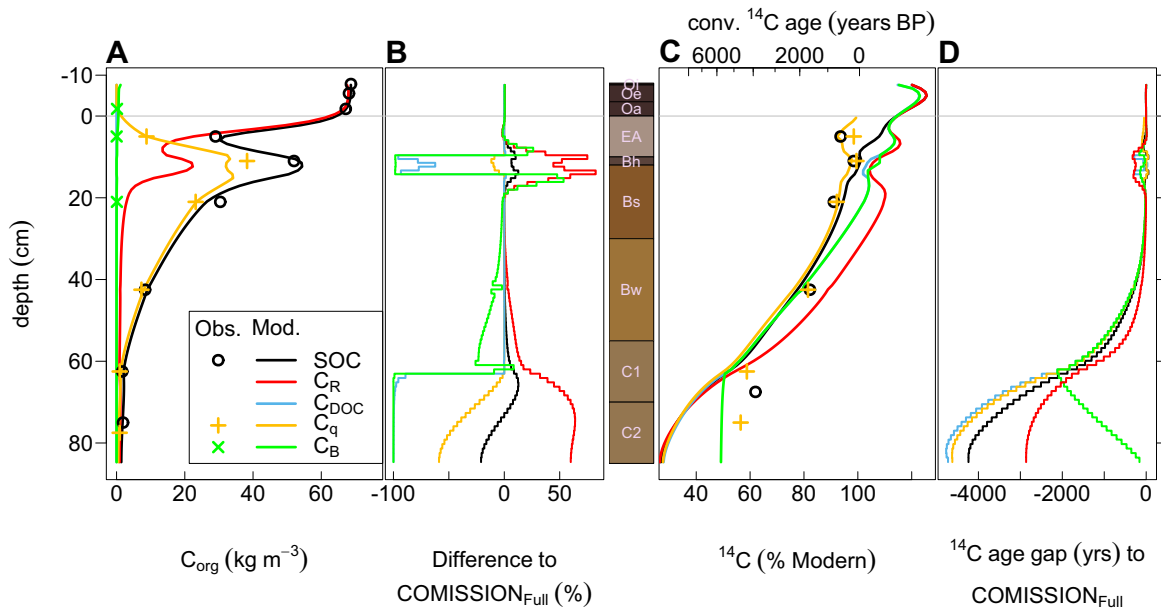
Figure 4-3: Results of a COMISSION simulation in which DOC advection is switched off – panel (A) shows organic carbon pools/fractions and panel (C) the respective ^{14}C signatures. Panel (B) shows the difference of COMISSION without DOC advection to the full COMISSION model in percent. Panel (D) compares the conventional ^{14}C ages of COMISSION without advection to the full model.

Microbial depolymerization limitation

The most obvious change when switching off the rate limiting term for the depolymerization of the C_R pool (Table 4-2, "No depolymerization limitation by microbes") is the disappearance of the secondary peak of the C_R pool in the Bh horizon (Figure 4-4A). While the overall OC levels would still be well captured along the profile, the mismatch in the Bh horizon would be considerable (Figure 4-4B). Nevertheless, switching off the rate limiting term for the depolymerization flux considerably affects OC dynamics throughout the soil profile (Figure 4-4B). Especially, in the subsoil horizons the C_R pool would be so rapidly depolymerized that it is virtually absent (Figure 4-4B). In the Bh horizon the lift of the depolymerization limitation leads to ample available DOC, alleviating the competition between microbes and soil minerals for DOC, and thereby to a disproportionate growth of the microbial biomass (Figure 4-4B). In $COMISSION_{Full}$ the microbial biomass levels were very low because the competition for DOC with soil minerals via q_{max} was important.

Lifting the depolymerization limitation also has pronounced consequences for the apparent ^{14}C age profiles (Figure 4-4C and D). Without depolymerization limitation the apparent ^{14}C age of SOC would be on average 610 years younger in subsoil horizons (Figure 4-4D). The ^{14}C signature of the C_R

112

pool would even reach modern levels down to the Bw horizon because the turnover of C_R would be so rapid that the root litter input essentially determines the ^{14}C signature (Figure 4-4C). Depolymerization limitation is especially relevant in the C2 horizon where the C_R turnover is so fast – compared to the input to the layer – that C_R is almost absent (Figure 4-4B). Overall, the depolymerization limitation contributes considerably to the apparent ^{14}C ages especially in subsoil horizons (Figure 4-4D).
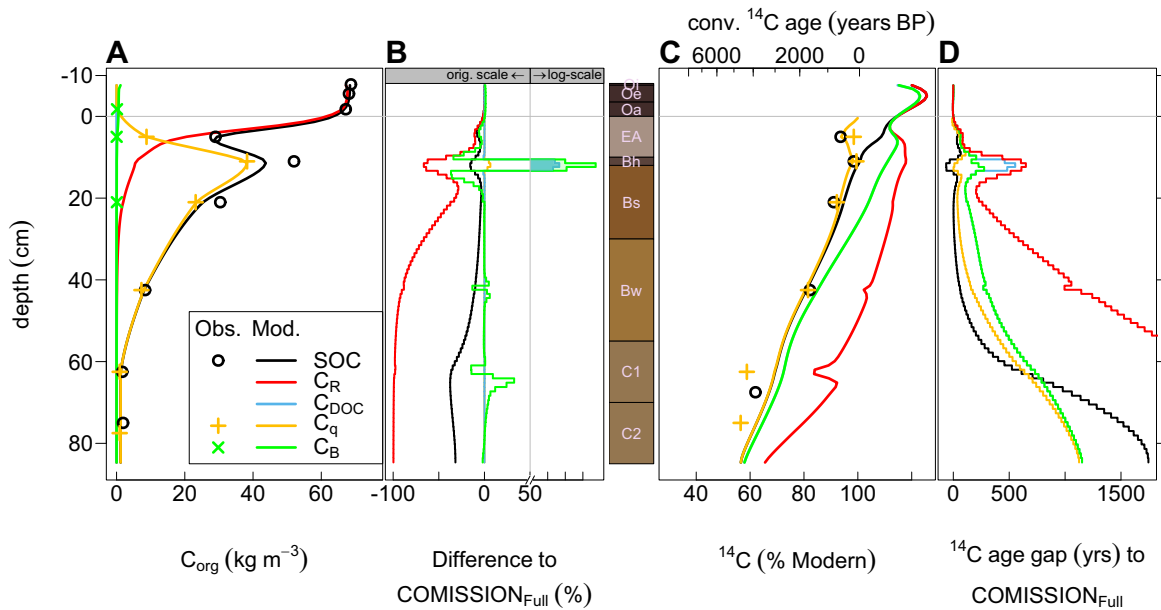
Figure 4-4: Results of a COMISSION simulation in which the limitation of depolymerization by microbial biomass is switched off – panel (A) shows organic carbon pools/fractions and panel (C) the respective ^{14}C signatures. Panel (B) shows the difference of COMISSION without depolymerization limitation to the full COMISSION model in percent. Panel (D) compares the conventional ^{14}C ages of COMISSION without depolymerization limitation to the full model. The shading in panel (B) is intended to highlight the change to log-scale.

Sorptive stabilization

Switching off the sorptive stabilization of DOC on soil minerals (Table 4-2, "No sorptive stabilization") obviously leads to the disappearance of the C_q pool (Figure 4-5A). While the organic layer is not affected by the omission of sorption, the topsoil and subsoil mineral horizons show considerable differences to $COMISSION_{Full}$. First, the secondary peak of the C_R pool disappears due to the missing interactions between q_{max} and microbes. Apparently, the overall high sorption capacity of the Bh horizon was responsible for the development of a secondary peak of the C_R pool (together with the depolymerization limitation). Apart from the decrease of the C_R pool in the Bh horizon,

without sorption the C_R pool becomes more prominent in deeper parts of the soil profile compared to $COMISSION_{Full}$ (Figure 4-5B). This is because without sorption more DOC is translocated or leaving the soil in the subsoil horizons; thereby less substrate is available for microbial growth and ultimately depolymerization of the C_R pool (Figure 4-5B). This means that sorption has a dual role: It can suppress microbes by removing substrate, but also may stimulate them by retaining substrates (preventing loss by advection) and gradually releasing them.

In the $COMISSION_{Full}$ model run sorptive stabilization is responsible for ^{14}C ages of around 600 years in the topsoil horizons (Figure 4-2C). Without sorption the apparent ^{14}C ages would be much younger in the topsoil (Figure 4-5C and D). In the subsoil horizons the ^{14}C signature of the C_R pool diverges from that of the C_{DOC} and C_B pools. Without adsorption and desorption DOC is transported without retardation to deeper soil layers and is dominated by the ^{14}C signature of litter inputs (Figure 4-5C). Due to the strong coupling of microbes and DOC, microbes follow the ^{14}C signature of DOC throughout the soil profile (Figure 4-5C). With faster decomposition and lower SOC stocks in the absence of sorptive stabilization, the C_R pool and the overall SOC stocks show modern ^{14}C signatures down to the Bw horizon (Figure 4-5C). Below the Bw horizon the C_R pool consists mainly of microbial remains (cf. Figure 4-7B), which is reflected in the high apparent ^{14}C ages in deeper subsoil horizons for the COMISSION model without sorption.
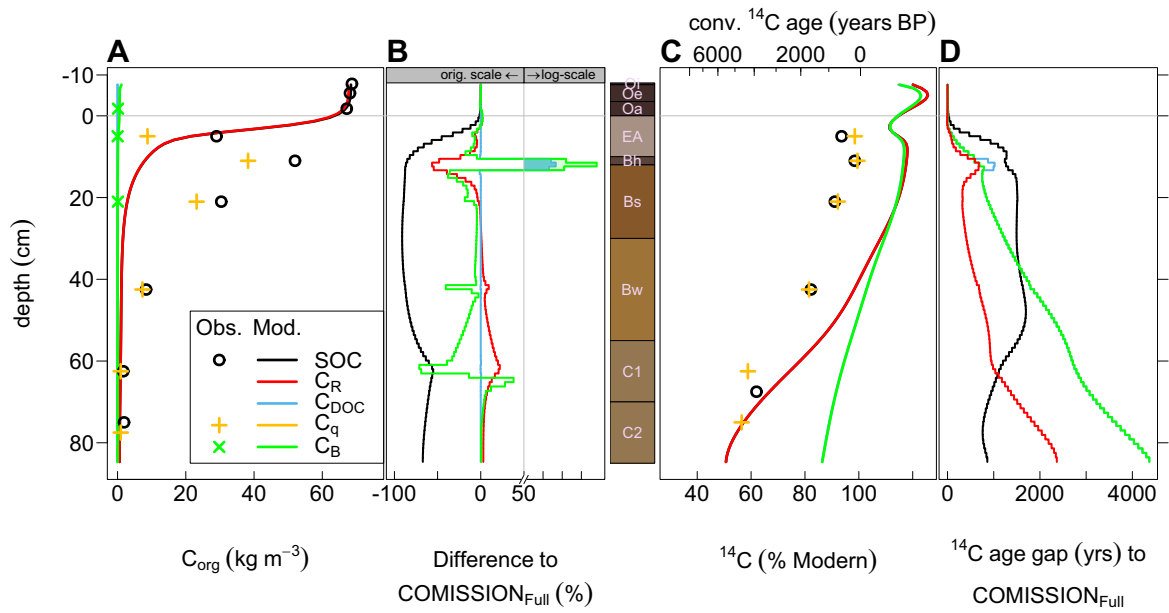
Figure 4-5: Results of a COMISSION simulation in which sorption is switched off – panel (A) shows organic carbon pools/fractions and panel (C) the respective ^{14}C signatures. Panel (B) shows the difference of COMISSION without sorption to the full COMISSION model in percent. Panel (D) compares the conventional ^{14}C ages of COMISSION without sorption to the full model. The shading in panel (B) is intended to highlight the change to log-scale.

4.7.3   Contribution of litter-derived *vs* microbe-derived organic carbon

In order to quantify the contribution of litter and microbe-derived organic carbon we split the model pools into a set that only receives input in form of microbial remains and a set that only receives input from litter (cf. section 2.3, Table 4-2, "Litter- vs microbe-derived OC"). In the Oi horizon litter-derived OC makes up more than 70% of the total SOC stocks (Figure 4-6B). In the organic layer the contribution of litter-derived carbon is, however, already decreasing to about 50% at the boundary between the organic layer and the mineral soil. This is in line with the concept that the Oa horizon of the organic layer represents more "humified" material (i.e. processed by the soil food web) (Figure 4-7A,B). With the transition to the mineral soil sorptive stabilization comes into play and the depolymerization of root litter input is impeded because of lower microbial growth due to the competition of sorption capacity and microbes for DOC. Overall, this leads to a higher depolymerization limitation in the topsoil horizons than in the organic layer. This is reflected in a higher contribution of litter-derived carbon in the first mineral horizon (EA horizon) compared to the last organic horizon (Oa horizon) (Figure 4-6B). The split in litter-derived and microbe-derived organic carbon also reveals that the secondary peak of the C_R pool in the Bh horizon is derived from root litter input and not microbial recycling (Figure 4-6A,B and Figure 4-7A,B).

Starting from the Bw horizon the importance of microbe-derived OC is increasing up to contributions of around 60% in the C1 and C2 horizons (Figure 4-7B). This is partially explained by the fact that root litter is not the dominant form of carbon input there (Figure 4-6B), but also because continued microbial recycling is getting more important with soil depth.

The importance of continued microbial recycling is even more evident from the ^{14}C age difference between litter-derived carbon and microbe-derived carbon along the soil profile (Figure 4-6D, Figure 4-7D). The apparent ^{14}C age of the litter-derived SOC is on average more than 1400 years younger than the ^{14}C age of microbe-derived SOC. More importantly, the ^{14}C age gap between litter-derived and microbe-derived carbon is increasing with depth due to the continued recycling of SOC through microbes (Figure 4-6D, Figure 4-7D). The ^{14}C age difference of the litter-derived C_R pool to the microbe-derived C_R pool is even more positive (Figure 4-6D) because, "modern" root litter input is dominating the litter-derived C_R and because microbe-derived C_R is getting older while being processed again and again. The ^{14}C signature of the litter-derived C_R, however, would not be "modern" throughout the soil profile (Figure 4-6D). Due to the small amount of root litter input in the subsoil and the interaction of stabilization mechanisms (depolymerization limitation and

sorption), the ^{14}C signature of litter-derived C_R would still show apparent ^{14}C ages of more than 2000 years in the deep subsoil.
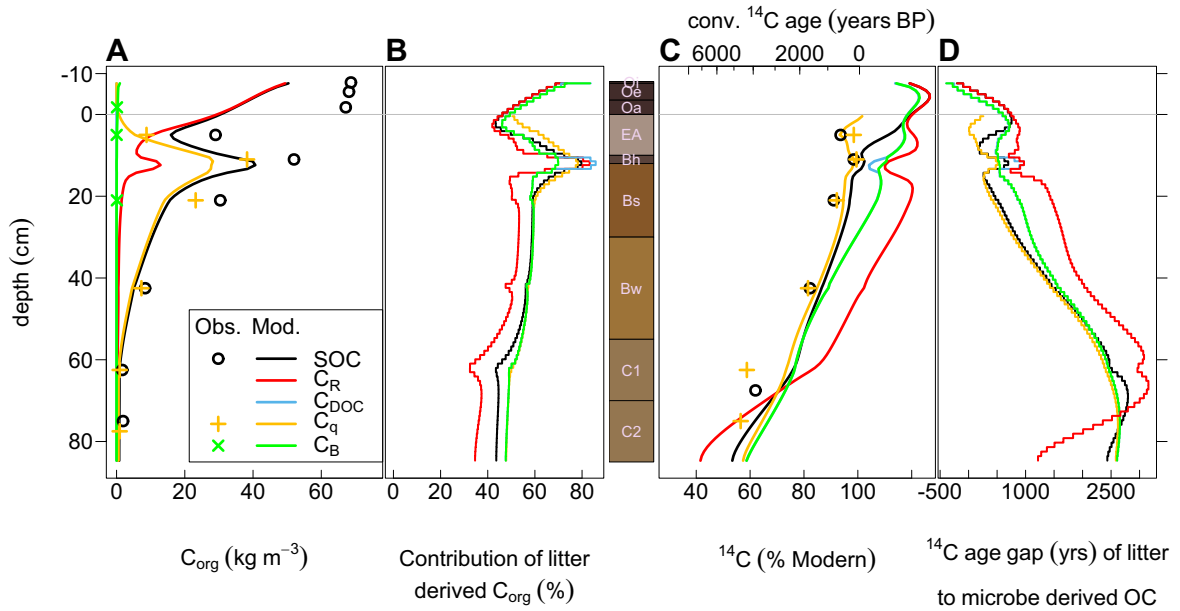
Figure 4-6: Contribution of plant litter along the SOC profile. COMISSION model forward run showing only litter-derived organic carbon – panel (A) shows organic carbon pools/fractions and panel (C) the respective ^{14}C signatures. Panel (B) shows the contribution of plant-litter-derived OC to overall OC of COMISSION in percent. Panel (D) compares the conventional ^{14}C ages of litter-derived carbon to microbially recycled OC.
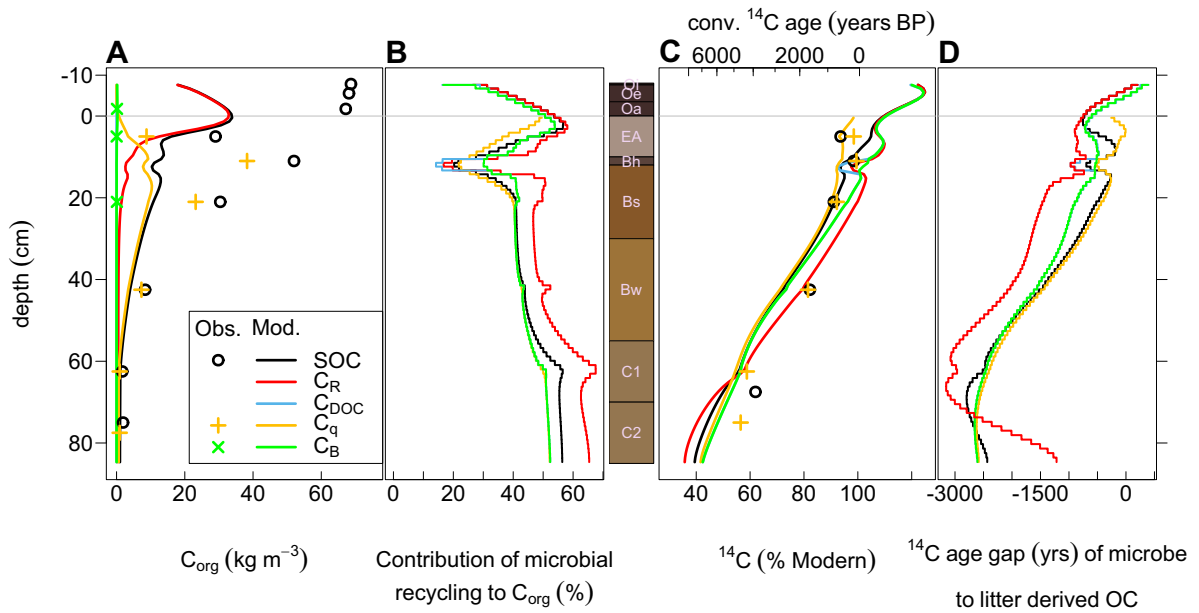
Figure 4-7: Contribution of microbial recycling along the SOC profile. COMISSION model forward run showing only microbially recycled organic carbon – panel (A) shows organic carbon pools/fractions and panel (C) the respective ^{14}C signatures. Panel (B) shows the contribution of microbially recycled OC to overall OC of COMISSION in percent. Panel (D) compares the conventional ^{14}C ages of microbially recycled carbon to litter-derived OC.

4.8   Discussion

4.8.1   Contribution of different model processes to the observed SOC and ^{14}C profiles

The goal of our study is to explain observed ^{14}C ages of more than 1000 years using a more mechanistic representation of soil carbon cycling than the models typically applied. Riley et al. (2014) showed recently that the formerly used decomposition rates on millennial time scales for "stable" pools are not necessary to explain observed ^{14}C age trends with depth. The insights gained with the calibration of the COMISSION model and the model-experiments support and extend these findings.

In particular with the factorial model-experiment in which processes were switched off, we were able to shed light on the relative importance of the different processes implemented in COMISSION. Based on their conceptual model of dissolved organic matter cycling along the soil profile, Kaiser and Kalbitz (2012) suggested that the transport of microbially recycled DOC is responsible for millennial ^{14}C ages in the subsoil. Due to an increasing energy limitation of microbes, especially in the C1 and C2 horizons, which are dependent on DOC transport for SOC input, our

model-experiment suggests that without DOC transport ^{14}C ages in the subsoil would be much older (Figure 4-3D). Nevertheless, as microbe-derived DOC makes up around 50-60% of DOC in the subsoil (Figure 4-7B), microbially recycled DOC contributes considerably to ^{14}C ages in the subsoil.

Switching off depolymerization limitation and sorption showed how different stabilization mechanisms act in different parts of the soil profile. In the topsoil the ^{14}C age is quite high, mainly due to stabilization on mineral surfaces. In the subsoil both the depolymerization limitation of microbes (Figure 4-4D) and sorptive stabilization explain (Figure 4-5D) a large portion of the observed ^{14}C ages (1280 and 610 ^{14}C years on average in subsoil SOC) according to our model-experiments. Depolymerization limitation can be regarded as one of the processes that were "unresolved" in other modeling studies (Jenkinson and Coleman, 2008; Koven et al., 2013) and inspired the use of an "arbitrary" depth-dependence of decomposition rates (Riley et al., 2014). Although other first-order SOC profile models did not use this depth-dependence of decomposition (Elzein and Balesdent, 1995; Baisden et al., 2002; Braakhekke et al., 2014), in these models a pool with a millennial turnover time was needed to explain observed ^{14}C profiles. In these studies this "stable" or "slow" pool is present throughout the soil profile, but it is unclear if this pool is meant to represent SOC that is chemically recalcitrant or stabilized on minerals.

Overall, this means that the value of the information contained in ^{14}C data has been overestimated with SOC profile models that lacked a mechanistic description of processes that could lead to the long-term persistence of SOC. By attempting to explain the ^{14}C profile with these models, one had to either introduce a depth-dependence of decomposition rates (Jenkinson and Coleman, 2008) or include a pool with a millennial turnover time (Braakhekke et al., 2014). At the same time these models underutilized the ^{14}C data because the steep increase of ^{14}C ages with depth has in essence not been used to constrain any of the mechanisms that could lead to a long-term persistence of SOC.

Riley et al. (2014) showed with their BAMS1 model that relatively fast decomposition rates can be reconciled with the observed ^{14}C age profile if stabilization mechanisms, similar to those implemented in COMISSION, are explicitly considered. In addition, we highlight the importance of continued microbial recycling (Gleixner, 2013) for the ^{14}C age profile (Figure 4-7D). It is noteworthy that this process cannot be necessarily subsumed under the term "stabilization process", but is merely a process that leads to long-term persistence of plant litter inputs in the soil profile. This persistence is so pronounced that radioactive decay is relevant for the radiocarbon signal of this part

of SOC. Especially the increasing contribution of microbe-derived OC along soil profiles (Figure 4-7B) contributes substantially to the observed apparent ^{14}C age trends (Figure 4-7C). Therefore, it is crucial that SOC profile models not only consider explicit stabilization processes such as depolymerization limitation or sorptive stabilization, but also processes such as continued microbial recycling that just lead to a long-term persistence of SOC in the soil.

4.8.2 Key features of COMISSION

DOC links microbial interactions and sorptive stabilization

From our model-experiments it is evident that the C_{DOC} pool is a crucial component for models that include both microbial interactions and sorptive stabilization. In the COMISSION model soil minerals and the microbial biomass essentially compete for DOC throughout the profile in the mineral soil. The representation of sorption using the Langmuir equations made it possible to fit the secondary peak of the C_R pool in the Bh horizon which is mainly made up of root litter-derived OC (Figure 4-6B). In the Bh horizon, where the sorption capacity, q_{max}, is at its maximum, the adsorption strength is strongest and reduces the microbial uptake of DOC in the Bh horizon. As we assumed traditional Michaelis-Menten kinetics for the microbial uptake of DOC (Eq (4-2)), DOC concentrations limit the rate of microbial uptake and growth (Figure 4-4B).

Although the COMISSION model is not designed to represent the process of podsolization, our link between microbial interactions and sorption in COMISSION is able to amend theories of podzolization. Buurman and Jongmans (2005) noted that traditional theories of podzolization cannot explain the dominance of silt- and sand-sized pellets of particulate organic matter in Podzol-B horizons. Although our Bh horizon is not dominated by this material, we still observe a secondary peak of the light fraction/C_R pool in the Bh horizon. The competition between soil minerals and microbial biomass offers a mechanistic explanation as to why root residues might be more abundant in Podzol-B horizons.

SOC decomposition models with explicit microbial interactions and explicit DOC pools often overlook the effect of "competition" for DOC by processes other than microbial uptake (e.g. Schimel and Weintraub, 2003; Allison et al., 2010; Moorhead et al., 2012) because these models are neither accounting for the sorptive stabilization of DOC, nor for DOC leaching into deeper soil layers. If this seeming competition for DOC is not taken explicitly taken into account, soil mineralogy would have

no direct influence on the ability of soil microbes to take up substrate and thereby to decompose SOM. Other SOC models with explicit representations of microbial biomass and DOC have started to take sinks for DOC other than microbial uptake into account (Wang et al., 2013; Riley et al., 2014), while Sulman et al. (2014) have already addressed possible effects of interactions between microbial decomposition and protection on soil minerals with the CORPSE model. This model, however, does not have an explicit DOC pool.

In order to be able to model the response of SOC to increased ecosystem productivity under elevated CO_2, it is essential to consider interactions between microbial decomposition and protection on soil minerals (Sulman et al., 2014). Plants could allocate more carbon to root exudates to enhance nutrient uptake or the mineralization of SOM in order to meet their increased nutrient demands under CO_2 fertilization (Norby et al., 2010). The input of root exudates may lift a potential depolymerization limitation of microbes and hence prime the decomposition of SOM or the elevated litter inputs. The modeling results of Sulman et al. (2014) with the CORPSE model at two FACE sites indicated that stabilization on soil minerals can attenuate the priming effect induced by increased root exudates. In the COMISSION model the carbon loss via priming may also be reduced if the available sorption sites are competing with microbes for the root exudates. With the COMISSION model we are able to address the question of whether increased carbon allocation to the subsoil is leading to an increase or decrease of subsoil SOC stocks due to sorptive stabilization and increased litter inputs or exudate priming. Compared to the model of Sulman et al. (2014), in which sorptive stabilization is represented with linear sorption kinetics, the response to increased root exudates may vary depending on soil depth if an upper limit of SOC storage on soil minerals is defined via the q_{max} parameter. q_{max} might be saturated in the topsoil and would thereby not be able to alleviate the priming effect induced by root exudates, while in the subsoil root exudates can still be stabilized on minerals, depriving the microbial pool of a potential energy source.

Combination of traditional and reverse Michaelis-Menten kinetics

A novel feature in the structure of the decomposition equations of COMISSION is the combination of traditional and reverse Michaelis-Menten kinetics. Wutzler and Reichstein (2008) and later Wang et al. (2014) showed that the traditional Michaelis-Menten kinetics have the undesired effect that the steady-state of the main SOC pools is completely independent of litter inputs. For reverse Michaelis-Menten kinetics on the other hand the main SOC pools scale with litter inputs (Wutzler and Reichstein, 2008). For COMISSION we mechanistically argued that the decomposition of litter inputs

and microbial remains in the C_R pool would be limited by the diffusion of extracellular enzymes and thereby by the amount of microbes C_B, while the microbial uptake of DOC would be limited by the diffusion of the substrate (DOC) to the microbes and thereby by the amount of DOC available. This combination of reverse (for C_R) and traditional Michaelis-Menten kinetics (for C_{DOC}) leads to the desired feature that the steady state of the main carbon pool (C_R) scales with litter inputs (Eq. S6). However, without sorption the steady state of the C_{DOC} pool would be independent of litter inputs (Eq. S7). We believe that this more mechanistically justified use of either the reverse or traditional Michaelis-Menten equation warrants further investigation, especially whether the Michaelis-Menten uptake of DOC has desired properties for a DOC pool.

Langmuir sorption – making the heavy fraction modelable

Representing mineral stabilization with Langmuir sorption has been of interest in several modeling studies. Riley et al. (2014) noted that they aim to represent sorption as Langmuir sorption in future versions of their model. Wang et al. (2013) included Langmuir sorption in their MEND model. Overall, these and our approaches can be seen as a scheme to represent mineral stabilization more mechanistically in models. Representing mineral sorption as Langmuir adsorption has the advantage of being able to represent an upper limit of mineral-associated OC storage in soils (q_{max}) which is widely assumed to exist (Wiesmeier et al., 2014). Hassink (1997) and Hassink and Whitmore (1997) were the first to define such a maximum mineral sorption capacity both for field studies and model applications. While the empirical approach of Hassink (1997) has found widespread use in experimental studies (Feng et al., 2013; Beare et al., 2014; Wiesmeier et al., 2014), the use of the empirical q_{max} in its modeling counterpart – the Langmuir equation – is limited.

Our approach with the COMISSION model showed that Langmuir sorptive stabilization is very helpful to be able to model what is perceived as the "mineral-associated fraction" obtained from various physical SOM fractionation methods (von Lützow et al., 2007). The concept of mineral-associated SOC implies that the size of this pool is limited by the amount of mineral surfaces available (Hassink et al., 1997). Also if one adopts the view of a zonal model of organo-mineral interactions as by Kleber et al. (2007) with intermediate and outer zones based on organo-organo interactions, the amount of OC in these zones would still depend on the amount of mineral surfaces being in immediate contact with the first layer of organic molecules. There is ample evidence from different studies that organo-mineral associations do not form monolayer equivalents that cover the complete mineral surface area (e.g. Ransom et al., 1997; Mayer, 1999; Kaiser and Guggenberger,

2003), but that OC attaches preferentially on the rough surfaces of minerals (Vogel et al., 2014). Nevertheless the amount of these rough surfaces should also scale with the amount of total mineral surfaces available, regardless whether they are suited for organo-mineral interactions or not.

4.8.3   Model limitations and future directions

Stabilization by aggregation

The stabilization of SOM by occlusion within aggregates (Six et al., 2004; Conant et al., 2011) is not explicitly modeled in COMISSION. In principle one could model the effect of aggregation similar to the q_{max} approach with dynamic Langmuir equations, where q_{max} would here be the capacity of a soil horizon to occlude SOM within aggregates. To a certain extent this capacity would also be dependent on the clay and oxide content of a soil horizon (Six et al., 2004). Compared to the q_{max} for sorptive stabilization, however, the capacity to occlude SOM within aggregates would be much more dynamic as the formation and turnover of aggregates also depend on soil physical conditions such as freezing and thawing, and drying and rewetting (Six et al., 2004). Furthermore, the capacity to occlude SOM within aggregates would depend on the size and turnover time of the microbial pool as aggregate formation is enhanced by microbial extracellular polysaccharides (Wagai et al., 2009).

Multi-profile calibration and application to global scale models

In order to apply and calibrate COMISSION within an ecosystem model it is necessary to represent the temperature and moisture sensitivity of the different processes. In this study we purposefully did not do this as within COMISSION soil temperature and moisture are not modeled. This is especially important for disentangling the contributions of the root biomass profile, soil texture changes, and soil temperature and moisture profiles to between-site differences in depth trends of ^{14}C ages.

The depolymerization of the C_R pool and the microbial uptake of C_{DOC} are assumed to be limited by diffusion of enzymes and DOC. Based on the considerations of Davidson et al. (2012) for their DAMM model, the concentrations of enzymes and DOC at the respective reaction sites (C_R and C_B) could constitute the respective rate-limiting resource in Eqs. (5-3) and (4-2). These concentrations at the reaction site are dependent on how well enzymes and DOC can diffuse through the soil water film. Davidson et al. (2012) argue that diffusion is higher in thick soil water films. Geometrical considerations imply that the thickness of the soil water film is related to the cube of the volumetric soil water content. Similarly, to account for oxygen limitation in wet soils one can

introduce another Michaelis-Menten term where oxygen constitutes the rate-limiting resource (Davidson et al., 2012). The oxygen concentration can then be calculated as a function of volumetric soil moisture and porosity (Davidson et al., 2012; Sulman et al., 2014). Here, one could include a dependence on soil aggregation as also aggregates limit oxygen diffusion (Six et al., 2004).

Little is known about the temperature sensitivities of the half-saturation constants and adsorption and desorption rates. However, several authors have already provided useful descriptions and parameterizations for the temperature sensitivity of the maximum depolymerization and uptake rate, $V_{max,D}$ and $V_{max,U}$ (Allison et al., 2010; Todd-Brown et al., 2012; Wang et al., 2012). Regarding the sensitivity of CUE to temperature several scenarios and strategies have been proposed (Allison et al., 2010; Manzoni et al., 2012; Todd-Brown et al., 2012), but the uncertainty is high (Wieder et al., 2013).

The application of COMISSION in an Earth system model requires a global map of q_{max}. Using the Harmonized World Soil Database, q_{max} could be derived globally from quantile regressions of MOC data against the clay + silt content (Feng et al., 2013; Beare et al., 2014), or hydrological properties that can be related to the surface area of soil minerals. This would lead to quite similar q_{max} estimates in the top- and subsoil, while based on our current definition of q_{max}, the MOC profile closely follows the prescribed q_{max} because the available sorption capacity from the batch sorption experiments is relatively low in subsoil horizons. In future work we aim to study the effect of different q_{max} definitions, especially if other stabilization mechanisms apart from DOC sorption might be relevant for these alternative definitions.

4.9   Conclusions

We showed with the COMISSION model that an explicit consideration of stabilization and persistence processes renders millennial turnover times unnecessary. Our model results suggest that in the topsoil sorptive stabilization is responsible for relatively high apparent ^{14}C ages, while in the subsoil the combination of depolymerization limitation and sorption is responsible for a large part of the observed ^{14}C ages. However, apart from processes that can be clearly characterized as stabilization processes, observed ^{14}C age trends along a soil profile could be traced back with the COMISSION model to the continued microbial recycling of SOM. Together with microbial interactions the

transport of DOC along the profile leads to lower ^{14}C ages in the subsoil compared to a hypothetical situation without advection.

Overall, our results lead us to conclude that a more detailed description of stabilization and persistence processes give a more realistic explanation of apparent ^{14}C ages in soil profiles of more than 1000 years. Apart from explaining ^{14}C age trends, the explicit representation of SOC profiles in Earth system models is essential to assess the feedbacks between climate change, changing atmospheric deposition and SOC, and to make the SOC module of Earth system models comparable with observations. The interaction of microbial processes and sorptive stabilization is especially relevant for studying the response of SOC to potentially higher belowground C allocation under elevated CO_2 concentrations. Sorption may reduce potential SOC losses due to priming by root exudates, especially in the subsoil where the sorption capacity may be far from saturation. This once again highlights the importance of a vertically explicit representation of different stabilization processes in SOC models.

4.10 Acknowledgments

4.11 References

Ahrens, B., Reichstein, M., Borken, W., Muhr, J., Trumbore, S.E., Wutzler, T., 2014. Bayesian calibration of a soil organic carbon model using Δ14C measurements of soil organic carbon and heterotrophic respiration as joint constraints. Biogeosciences 11, 2147-2168.

Allison, S.D., Wallenstein, M.D., Bradford, M.A., 2010. Soil-carbon response to warming dependent on microbial physiology. Nature Geosci 3, 336-340.

Ardia, D., Mullen, K., Peterson, B., Ulrich, J., Boudt, C.K., Mullen, M.K., 2013. 'DEoptim': Differential Evolution in 'R'.

Baisden, W.T., Amundson, R., Brenner, D.L., Cook, A.C., Kendall, C., Harden, J.W., 2002. A multiisotope C and N modeling analysis of soil organic matter turnover and transport as a function of soil depth in a California annual grassland soil chronosequence. Global Biogeochemical Cycles 16.

Beare, M.H., McNeill, S.J., Curtin, D., Parfitt, R.L., Jones, H.S., Dodd, M.B., Sharp, J., 2014. Estimating the organic carbon stabilisation capacity and saturation deficit of soils: a New Zealand case study. Biogeochemistry, 1-17.

Berg, B., Gerstberger, P., 2004. Element Fluxes with litterfall in mature stands of Norway Spruce and European Beech in Bavaria, South Germany, In: Matzner, E. (Ed.), Biogeochemistry of forested catchments in a changing environment: a German case study. Springer-Verlag, Berlin, Heidelberg, pp. 271-277.

Boudreau, B.P., Imboden, D.M., 1987. Mathematics of tracer mixing in sediments: III. The theory of nonlocal mixing within sediments. American Journal of Science 287, 693-719.

Braakhekke, M.C., Ahrens, B., in prep. A new mathematical description of vertically resolved organic matter dynamics in organic and mineral soil layers.

Braakhekke, M.C., Beer, C., Hoosbeek, M.R., Reichstein, M., Kruijt, B., Schrumpf, M., Kabat, P., 2011. SOMPROF: A vertically explicit soil organic matter model. Ecological Modelling 222, 1712-1730.

Braakhekke, M.C., Beer, C., Schrumpf, M., Ekici, A., Ahrens, B., Hoosbeek, M.R., Kruijt, B., Kabat, P., Reichstein, M., 2014. The use of radiocarbon to constrain current and future soil organic matter turnover and transport in a temperate forest. Journal of Geophysical Research: Biogeosciences, 2013JG002420.

Buurman, P., Jongmans, A.G., 2005. Podzolisation and soil organic matter dynamics. Geoderma 125, 71-83.

Carvalhais, N., Forkel, M., Khomik, M., Bellarby, J., Jung, M., Migliavacca, M., Mu, M., Saatchi, S., Santoro, M., Thurner, M., Weber, U., Ahrens, B., Beer, C., Cescatti, A., Randerson, J.T., Reichstein, M., 2014. Global covariation of carbon turnover times with climate in terrestrial ecosystems. Nature 514, 213-217.

Conant, R.T., Ryan, M.G., Ågren, G.I., Birge, H.E., Davidson, E.A., Eliasson, P.E., Evans, S.E., Frey, S.D., Giardina, C.P., Hopkins, F.M., Hyvönen, R., Kirschbaum, M.U.F., Lavallee, J.M., Leifeld, J., Parton, W.J., Megan Steinweg, J., Wallenstein, M.D., Martin Wetterstedt, J.Å., Bradford, M.A., 2011. Temperature and soil organic matter decomposition rates – synthesis of current knowledge and a way forward. Global Change Biology 17, 3392-3404.

Davidson, E.A., Samanta, S., Caramori, S.S., Savage, K., 2012. The Dual Arrhenius and Michaelis–Menten kinetics model for decomposition of soil organic matter at hourly to seasonal time scales. Global Change Biology 18, 371-384.

Dörr, H., Münnich, K.O., 1989. Downward movement of soil organic-matter and its influence on trace-element transport (Pb-210, Cs-137) in the soil. Radiocarbon 31, 655-663.

Elzein, A., Balesdent, J., 1995. Mechanistic simulation of vertical-distribution of carbon concentrations and residence times in soils. Soil Science Society of America Journal 59, 1328-1335.

FAO, I., 1998. World reference base for soil resources. World soil resources reports 84, 21-22.

Feng, W., Plante, A.F., Six, J., 2013. Improving estimates of maximal organic carbon stabilization by fine soil particles. Biogeochemistry 112, 81-93.

Foken, T., 2003. Lufthygienisch-bioklimatische Kennzeichnung des oberen Egertales. Bayreuther Forum Ökologie 100, 1-118.

Freier, K.P., Glaser, B., Zech, W., 2010. Mathematical modeling of soil carbon turnover in natural *Podocarpus* forest and *Eucalyptus* plantation in Ethiopia using compound specific δ^{13}C analysis. Global Change Biology 16, 1487-1502.

Gaul, D., Hertel, D., Borken, W., Matzner, E., Leuschner, C., 2008a. Effects of experimental drought on the fine root system of mature Norway spruce. Forest Ecology and Management 256, 1151-1159.

Gaul, D., Hertel, D., Leuschner, C., 2008b. Effects of experimental soil frost on the fine-root system of mature Norway spruce. Journal of Plant Nutrition and Soil Science 171, 690-698.

Gerstberger, P., Foken, T., Kalbitz, K., 2004. The Lehstenbach and Steinkreuz catchments in NE Bavaria, Germany, Biogeochemistry of forested catchments in a changing environment: a German case study. Springer-Verlag, Berlin, Heidelberg, pp. 15-41.

Gleixner, G., 2013. Soil organic matter dynamics: a biological perspective derived from the use of compound-specific isotopes studies. Ecological Research 28, 683-695.

Guenet, B., Eglin, T., Vasilyeva, N., Peylin, P., Ciais, P., Chenu, C., 2013. The relative importance of decomposition and transport mechanisms in accounting for soil organic carbon profiles. Biogeosciences 10, 2379-2392.

Guggenberger, G., Kaiser, K., 2003. Dissolved organic matter in soil: challenging the paradigm of sorptive preservation. Geoderma 113, 293-310.

Hamer, U., Marschner, B., 2005. Priming effects in different soil types induced by fructose, alanine, oxalic acid and catechol additions. Soil Biology and Biochemistry 37, 445-454.

Hartemink, A.E., 2009. The depiction of soil profiles since the late 1700s. CATENA 79, 113-127.

Hassink, J., 1997. The capacity of soils to preserve organic C and N by their association with clay and silt particles. Plant and Soil 191, 77-87.

Hassink, J., Whitmore, A.P., 1997. A model of the physical protection of organic matter in soils. Soil Science Society of America Journal 61, 131-139.

Hassink, J., Whitmore, A.P., Kubát, J., 1997. Size and density fractionation of soil organic matter and the physical capacity of soils to protect organic matter. European Journal of Agronomy 7, 189-199.

Jenkinson, D.S., Coleman, K., 2008. The turnover of organic carbon in subsoils. Part 2. Modelling carbon turnover. European Journal of Soil Science 59, 400-413.

Jobbágy, E.G., Jackson, R.B., 2000. The vertical distribution of soil organic carbon and its relation to climate and vegetation. Ecological Applications 10, 423-436.

Kaiser, K., Eusterhues, K., Rumpel, C., Guggenberger, G., Kögel-Knabner, I., 2002. Stabilization of organic matter by soil minerals — investigations of density and particle-size fractions from two acid forest soils. Journal of Plant Nutrition and Soil Science 165, 451-459.

Kaiser, K., Guggenberger, G., 2003. Mineral surfaces and soil organic matter. European Journal of Soil Science 54, 219-236.

Kaiser, K., Kalbitz, K., 2012. Cycling downwards – dissolved organic matter in soils. Soil Biology and Biochemistry 52, 29-32.

Kaneyuki, N., Kichiro, S., 1978. A mathematical model of the behavior and vertical distribution of organic carbon in forest soils. Japanese Journal of Ecology 28, 111-122.

Kleber, M., Sollins, P., Sutton, R., 2007. A Conceptual Model of Organo-Mineral Interactions in Soils: Self-Assembly of Organic Molecular Fragments into Zonal Structures on Mineral Surfaces. Biogeochemistry 85, 9-24.

Kögel-Knabner, I., Guggenberger, G., Kleber, M., Kandeler, E., Kalbitz, K., Scheu, S., Eusterhues, K., Leinweber, P., 2008. Organo-mineral associations in temperate soils: Integrating biology, mineralogy, and organic matter chemistry. Journal of Plant Nutrition and Soil Science 171, 61-82.

Kothawala, D., Moore, T., Hendershot, W., 2009. Soil properties controlling the adsorption of dissolved organic carbon to mineral soils. Soil Science Society of America Journal 73, 1831-1842.

Koven, C.D., Riley, W.J., Subin, Z.M., Tang, J.Y., Torn, M.S., Collins, W.D., Bonan, G.B., Lawrence, D.M., Swenson, S.C., 2013. The effect of vertically resolved soil biogeochemistry and alternate soil C and N models on C dynamics of CLM4. Biogeosciences 10, 7109-7131.

Manzoni, S., Taylor, P., Richter, A., Porporato, A., Ågren, G.I., 2012. Environmental and stoichiometric controls on microbial carbon-use efficiency in soils. New Phytologist, no-no.

Matzner, E., Zuber, T., Alewell, C., Lischeid, G., Moritz, K., 2004a. Trends in Deposition and Canopy Leaching of Mineral Elements as Indicated by Bulk Deposition and Throughfall Measurements, In: Matzner, E. (Ed.), Biogeochemistry of Forested Catchments in a Changing Environment. Springer Berlin Heidelberg, pp. 233-250.

Matzner, E., Zuber, T., Lischeid, G., 2004b. Response of Soil Solution Chemistry and Solute Fluxes to Changing Deposition Rates, In: Matzner, E. (Ed.), Biogeochemistry of Forested Catchments in a Changing Environment. Springer Berlin Heidelberg, pp. 339-360.

Mayer, L., 1999. Extent of coverage of mineral surfaces by organic matter in marine sediments. Geochimica et Cosmochimica Acta 63, 207-215.

Mayes, M.A., Heal, K.R., Brandt, C.C., Phillips, J.R., Jardine, P.M., 2012. Relation between Soil Order and Sorption of Dissolved Organic Carbon in Temperate Subsoils. Soil Science Society of America Journal 76, 1027-1037.

Meysman, F.J.R., Boudreau, B.P., Middelburg, J.J., 2005. Modeling reactive transport in sediments subject to bioturbation and compaction. Geochimica et Cosmochimica Acta 69, 3601-3617.

Mikutta, R., Mikutta, C., Kalbitz, K., Scheel, T., Kaiser, K., Jahn, R., 2007. Biodegradation of forest floor organic matter bound to minerals via different binding mechanisms. Geochimica et Cosmochimica Acta 71, 2569-2590.

Moorhead, D.L., Lashermes, G., Sinsabaugh, R.L., 2012. A theoretical model of C- and N-acquiring exoenzyme activities, which balances microbial demands during decomposition. Soil Biology and Biochemistry 53, 133-141.

Moorhead, D.L., Sinsabaugh, R.L., 2006. A theoretical model of litter decay and microbial interaction. Ecological Monographs 76, 151-174.

Mulsow, S., Boudreau, B.P., Smith, J.N., 1998. Bioturbation and Porosity Gradients. Limnology and Oceanography 43, 1-9.

Nachtergaele, F., Van Velthuizen, H., Verelst, L., Batjes, N., Dijkshoorn, K., Van Engelen, V., Fischer, G., Jones, A., Montanarella, L., Petri, M., 2008. Harmonized world soil database. Food and Agriculture Organization of the United Nations.

Norby, R.J., Warren, J.M., Iversen, C.M., Medlyn, B.E., McMurtrie, R.E., 2010. CO2 enhancement of forest productivity constrained by limited nitrogen availability. Proceedings of the National Academy of Sciences 107, 19368-19373.

Persson, H., 2000. Root biomass and root nutrient data. CD-ROM-Data base., In: Schulze, E.-D. (Ed.), Carbon and Nitrogen Cycling in European Forest Ecosystems. Springer Berlin Heidelberg.

Price, K., Storn, R.M., Lampinen, J.A., 2006. Differential evolution: a practical approach to global optimization. Springer.

Ransom, B., Bennett, R., Baerwald, R., Shea, K., 1997. TEM study of in situ organic matter on continental margins: occurrence and the "monolayer" hypothesis. Marine Geology 138, 1-9.

Riley, W.J., Maggi, F., Kleber, M., Torn, M.S., Tang, J.Y., Dwivedi, D., Guerry, N., 2014. Long residence times of rapidly decomposable soil organic matter: application of a multi-phase, multi-component, and vertically resolved model (BAMS1) to soil carbon dynamics. Geosci. Model Dev. 7, 1335-1355.

Rothman, D.H., Forney, D.C., 2007. Physical model for the decay and preservation of marine organic carbon. Science 316, 1325.

Rumpel, C., Chabbi, A., Marschner, B., 2012. Carbon Storage and Sequestration in Subsoil Horizons: Knowledge, Gaps and Potentials, In: Lal, R., Lorenz, K., Hüttl, R.F., Schneider, B.U., von Braun, J. (Eds.), Recarbonization of the Biosphere. Springer Netherlands, pp. 445-464.

Rumpel, C., Kögel-Knabner, I., Bruhn, F., 2002. Vertical distribution, age, and chemical composition of organic carbon in two forest soils of different pedogenesis. Organic Geochemistry 33, 1131-1142.

Scharlemann, J.P., Tanner, E.V., Hiederer, R., Kapos, V., 2014. Global soil carbon: understanding and managing the largest terrestrial carbon pool. Carbon Management 5, 81-91.

Schimel, J.P., Weintraub, M.N., 2003. The implications of exoenzyme activity on microbial carbon and nitrogen limitation in soil: a theoretical model. Soil Biology and Biochemistry 35, 549-563.

Schmidt, M.W.I., Torn, M.S., Abiven, S., Dittmar, T., Guggenberger, G., Janssens, I.A., Kleber, M., Kogel-Knabner, I., Lehmann, J., Manning, D.A.C., Nannipieri, P., Rasse, D.P., Weiner, S., Trumbore, S.E., 2011. Persistence of soil organic matter as an ecosystem property. Nature 478, 49-56.

Six, J., Bossuyt, H., Degryze, S., Denef, K., 2004. A history of research on the link between (micro) aggregates, soil biota, and soil organic matter dynamics. Soil and Tillage Research 79, 7-31.

Stuiver, M., Polach, H.A., 1977. Reporting of ^{14}C data – discussion. Radiocarbon 19, 355-363.

Sulman, B.N., Phillips, R.P., Oishi, A.C., Shevliakova, E., Pacala, S.W., 2014. Microbe-driven turnover offsets mineral-mediated storage of soil carbon under elevated CO2. Nature Clim. Change 4, 1099-1102.

Todd-Brown, K.E.O., Hopkins, F.M., Kivlin, S.N., Talbot, J.M., Allison, S.D., 2012. A framework for representing microbial decomposition in coupled climate models. Biogeochemistry 109, 19-33.

Todd-Brown, K.E.O., Randerson, J.T., Post, W.M., Hoffman, F.M., Tarnocai, C., Schuur, E.A.G., Allison, S.D., 2013. Causes of variation in soil carbon simulations from CMIP5 Earth system models and comparison with observations. Biogeosciences 10, 1717-1736.

Trumbore, S.E., Zheng, S.H., 1996. Comparison of fractionation methods for soil organic matter ^{14}C analysis. Radiocarbon 38, 219-229.

Van Oost, K., Govers, G., Quine, T.A., Heckrath, G., Olesen, J.E., De Gryze, S., Merckx, R., 2005. Landscape-scale modeling of carbon cycling under the impact of soil redistribution: The role of tillage erosion. Global Biogeochemical Cycles 19, GB4014.

Vetter, Y.A., Deming, J.W., Jumars, P.A., Krieger-Brockett, B.B., 1998. A Predictive Model of Bacterial Foraging by Means of Freely Released Extracellular Enzymes. Microbial Ecology 36, 75-92.

Vogel, C., Mueller, C.W., Höschen, C., Buegger, F., Heister, K., Schulz, S., Schloter, M., Kögel-Knabner, I., 2014. Submicron structures provide preferential spots for carbon and nitrogen sequestration in soils. Nat Commun 5.

von Lützow, M., Kögel-Knabner, I., Ekschmitt, K., Flessa, H., Guggenberger, G., Matzner, E., Marschner, B., 2007. SOM fractionation methods: Relevance to functional pools and to stabilization mechanisms. Soil Biology and Biochemistry 39, 2183-2207.

Wagai, R., Mayer, L.M., Kitayama, K., 2009. Nature of the "occluded" low-density fraction in soil organic matter studies: A critical review. Soil Science & Plant Nutrition 55, 13-25.

Wang, G., Post, W.M., Mayes, M.A., 2013. Development of microbial-enzyme-mediated decomposition model parameters through steady-state and dynamic analyses. Ecological Applications 23, 255-272.

Wang, G., Post, W.M., Mayes, M.A., Frerichs, J.T., Sindhu, J., 2012. Parameter estimation for models of ligninolytic and cellulolytic enzyme kinetics. Soil Biology and Biochemistry 48, 28-38.

Wang, Y.P., Chen, B.C., Wieder, W.R., Leite, M., Medlyn, B.E., Rasmussen, M., Smith, M.J., Agusto, F.B., Hoffman, F., Luo, Y.Q., 2014. Oscillatory behavior of two nonlinear microbial models of soil carbon decomposition. Biogeosciences 11, 1817-1831.

Wieder, W.R., Bonan, G.B., Allison, S.D., 2013. Global soil carbon projections are improved by modelling microbial processes. Nature Climate Change.

Wiesmeier, M., Hübner, R., Spörlein, P., Geuß, U., Hangen, E., Reischl, A., Schilling, B., Lützow, M., Kögel‐Knabner, I., 2014. Carbon sequestration potential of soils in southeast Germany derived from stable soil organic carbon saturation. Global Change Biology 20, 653-665.

Wutzler, T., Reichstein, M., 2008. Colimitation of decomposition by substrate and decomposers – a comparison of model formulations. Biogeosciences 5, 749-759.

Wutzler, T., Reichstein, M., 2013. Priming and substrate quality interactions in soil organic matter models. Biogeosciences 10, 2089-2103.

Yoo, K., Amundson, R., Heimsath, A.M., Dietrich, W.E., 2005. Erosion of upland hillslope soil organic carbon: Coupling field measurements with a sediment transport model. Global Biogeochemical Cycles 19, n/a-n/a.

4.12 Appendix A. Supplementary information

4.12.1 The continuous profile approach
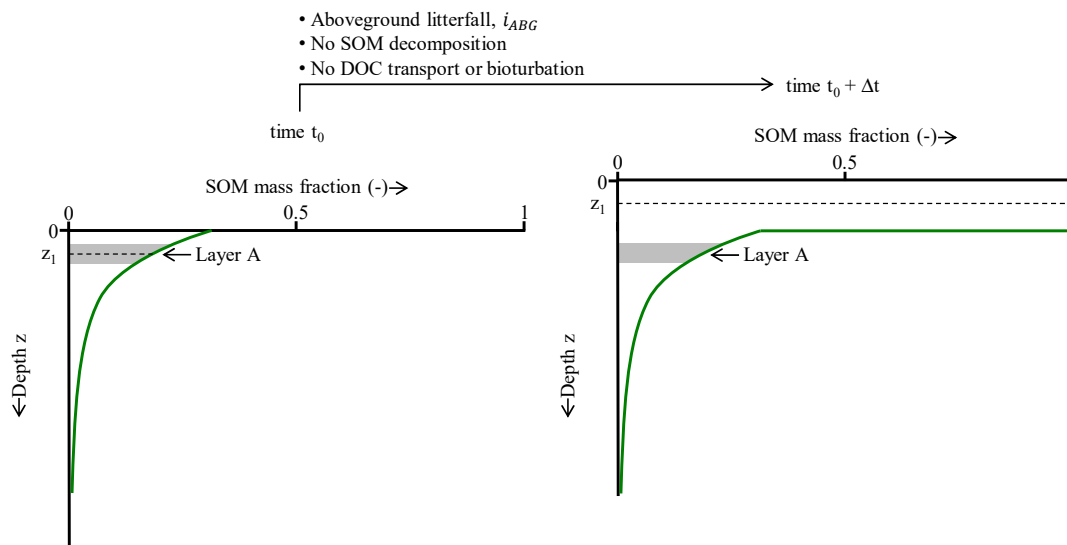
Fig. S1 Schematic for a theoretical situation of no SOM decomposition, no DOC transport, and no bioturbation. Upon burial by aboveground litterfall, the SOM content changes (green line) for a fixed depth, z_1 (dashed line; or equivalently z=0), but does not change for a given layer A (gray box). Figure and caption only slightly adapted from Berner (1980).

In the COMISSION model we introduce an additional advection velocity (Braakhekke and Ahrens, in prep.) that is moving all layers downwards due to litterfall (Fig. S1, Berner (1980)). The commonly measured litterfall flux (kg/m^2/yr) can be converted to an advection velocity (m/yr) if we view this advection velocity as the volume of litter (m^3) added to each unit of soil surface area (m^2) per unit time (yr).

Thus the burial velocity $\omega_{ABG}(z)$ due to aboveground litterfall can be calculated from the aboveground litter input i_{ABG} (kg m^{-2} yr^{-1}) and the bulk density of soil organic matter *sensu* Federer et al. (1993), ρ_{bO} (145 kg m^{-3} at Coulissenhieb I):

$$\omega_{ABG}(z) = \frac{i_{ABG}}{\rho_{bO}} \tag{S1}$$

For SOC profiles (compared to marine organic matter) one also has to consider lateral input of carbon from roots. This constitutes an additional advection velocity due to belowground litter input, ω_{BLG}:

$$\omega_{BLG}(z) = \frac{1}{\rho_{bO}} \int_0^z \Delta i_{BLG}(z)dz, \tag{S2}$$

where $\Delta i_{BLG}(z)$ is the change in concentration with depth z due to root litter input; the integral calculates the cumulative change of carbon concentrations due to root litter input up to depth z.

Further, one has to consider the loss of soil volume due to decomposition. This additional advection velocity reduces the burial velocity from above- and belowground litterfall $\omega_{ABG} + \omega_{BLG}$ by ω_{DEC}

$$\omega_{DEC}(z) = \frac{1}{\rho_{bO}} \int_0^z -k \cdot C^V(z)dz, \tag{S3}$$

where k is a generic decomposition rate and C^V is the volumetric carbon concentration; the integral calculates the cumulative loss of SOC over the soil profile due to decomposition.

The total burial velocity in soils is then:

$$\omega(z) = \omega_{ABG}(z) + \omega_{BLG}(z) + \omega_{DEC}(z) \qquad \text{(S4)}$$

The traditionally used reference frame in soil science is the top of the mineral soil, while here the soil surface is used as the reference frame in order to be able to model the SOC profile as a continuum.

4.12.2 Fixed parameters

Parameter	Symbol	Value
e-folding depth for root litter input	L	7.5 cm
bulk density of soil organic matter *sensu* Federer et al. (1993)	ρ_{bO}	145 kg m^{-3}
bulk density of the mineral matrix *sensu* Federer et al. (1993)	ρ_{bM}	1713 kg m^{-3}
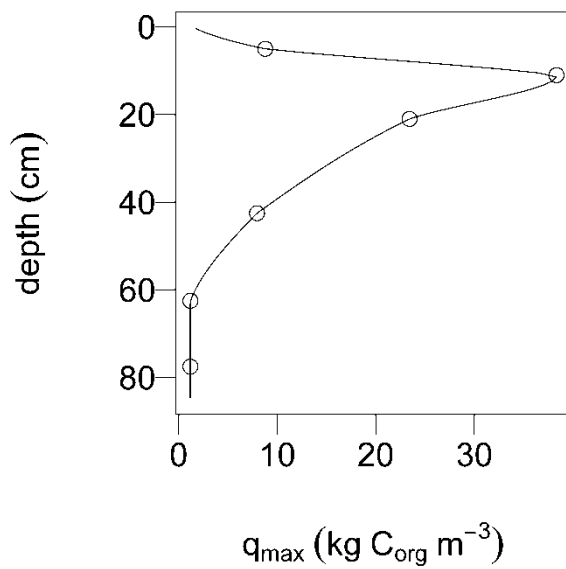
q_{max}

Fig. S2 Profile of prescribed maximum sorption capacity q_{max}. We define q_{max} as the sum of the available sorption capacity from sorption experiments and the mineral-associated organic carbon fraction based on the data reported in Guggenberger and Kaiser (2003)

4.12.3 Multi-constraint cost function

In the following equation $\text{COMISSION}_Y(\theta, z_i)$ signifies the model output of the COMISSION model given the parameter set θ in depth z_i where the respective measurements Obs_Y were taken. Y signifies the different observed variables and their model counterpart:

Observed variable	Model counterpart	Units
SOC	$C_R + C_{DOC} + C_q + C_B$	kg C m^{-3}
pM(SOC)	$pM(C_R + C_{DOC} + C_q + C_B)$	pM, percent Modern
MOC	C_q	kg C m^{-3}
pM(MOC)	$pM(C_q)$	pM, percent Modern
microbial biomass	C_B	kg C m^{-3}

$$SS(\theta) = \sum_Y \sum_i \text{COMISSION}_Y(\theta, z_i) - Obs_Y(z_i) \tag{S5}$$

4.12.4 Steady states of the C_R and C_{DOC} pools

Eq S6, Steady state for the C_R pool without transport and sorption

$C_{R,\text{Steady State,w/o Transport and Sorption}}$

$$= \frac{-(1 + (CUE - 1) \cdot L - CUE \cdot p) \cdot (CUE \cdot i - (CUE - 1) \cdot K_{m,B} \cdot \pi)}{(CUE - 1) \cdot CUE \cdot V_{max,D}}$$

Eq S7, Steady state for the C_{DOC} pool without transport and sorption

$$C_{DOC,\text{Steady State,w/o Transport and Sorption}} = \frac{K_{m,U} \cdot \pi}{-\pi + CUE \cdot V_{max,U}}$$

Please note that when also considering sorption also the steady state of C_{DOC} becomes dependent on litter input i.

4.12.5 Fitted parameter values

Table S1 Fitted parameter values used for the model-experiments

Parameter	Value	Units
L	0.645	-
p	0.172	-
π	7.48×10^{-8}	s^{-1}
$V_{max,D}$	1.33×10^{-9}	s^{-1}
$K_{m,B}$	0.0101	$kg\ C\ m^{-3}$
D_b	3.24×10^{-10}	$m^2\ s^{-1}$
$V_{max,U}$	1.01×10^{-2}	s^{-1}
$K_{m,U}$	3.181	$kg\ C\ m^{-3}$
k_{ads}	1.08×10^{-3}	$m^3\ (kg\ C)^{-1}\ s^{-1}$
k_{des}	1.19×10^{-10}	s^{-1}
CUE	0.392	-

4.12.6 SI References

Berner, R.A., 1980. Early diagenesis: A theoretical approach. Princeton University Press.

Braakhekke, M.C., Ahrens, B., in prep. A new mathematical description of vertically resolved organic matter dynamics in organic and mineral soil layers.

Federer, C.A., Turcotte, D.E., Smith, C.T., 1993. The organic fraction–bulk density relationship and the expression of nutrient content in forest soils. Canadian Journal of Forest Research 23, 1026-1032.

Guggenberger, G., Kaiser, K., 2003. Dissolved organic matter in soil: challenging the paradigm of sorptive preservation. Geoderma 113, 293-310.

5 Study IV

"Combination of energy limitation and sorption capacity explains ^{14}C depth gradients"

Contribution: The idea for the study was the outcome of discussions within the SUBSOM consortium. Data from the 5 sites stems from various PhD projects within the SUBSOM project. Data from the CarboEurope sites stem from work supervised by Marion Schrumpf. I further developed the COMISSION model with inputs from Markus Reichstein, Marion Schrumpf and Georg Guggenberger. I conducted the study, created all visualisations, and wrote the manuscript with inputs from the co-authors.

Combination of energy limitation and sorption capacity explains ^{14}C depth gradients

Bernhard Ahrens[a], Georg Guggenberger[b], Janet Rethemeyer[c], Stephan John[c*], Bernd Marschner[d], Stefanie Heinze[d], Gerrit Angst[e], Carsten W. Mueller[f, g], Ingrid Kögel-Knabner[f, h], Christoph Leuschner[i], Dietrich Hertel[i], Jörg Bachmann[b], Markus Reichstein[a,j], Marion Schrumpf[a,k]

[a] Max Planck Institute for Biogeochemistry, Department Biogeochemical Integration, Hans-Knöll-Straße 10, 07745 Jena, Germany

[b] Institute of Soil Science, Leibniz Universität Hannover, Herrenhäuser Str. 2, 30419 Hannover, Germany

[c] Institute of Geology and Mineralogy, University of Cologne, Zülpicher Straße 49a, D-50674 Cologne, Germany

[d] Department of Geography, Chair for Soil Science and Soil Ecology, Ruhr-Universität Bochum, Universitätsstr. 150, 44801 Bochum, Germany

[e] Biology Centre of the Czech Academy of Sciences, Institute of Soil Biology & SoWa Research Infrastructure, Na Sádkách 7, 37005 České Budějovice, Czech Republic

[f] Chair of Soil Science, Technical University of Munich, Emil-Ramann-Str. 2, 85354 Freising, Germany

[g] Section for Geography, Department of Geosciences and Natural Resource Management, University of Copenhagen, Øster Voldgade 10, DK-1350 Copenhagen K, Denmark.

[h] Institute for Advanced Study, Technical University of Munich, Lichtenbergstraße 2a, D-85748 Garching, Germany

[i] Albrecht von Haller Institute for Plant Sciences, Georg-August-Universität Göttingen, Untere Karspüle 2, 37073 Göttingen, Germany

[j] Michael-Stifel-Center Jena for Data-driven and Simulation Science, Ernst-Abbe-Platz 2, 07743 Jena, Germany

[k] Max Planck Institute for Biogeochemistry, Department Biogeochemical Processes, Hans-Knöll-Straße 10, 07745 Jena, Germany

* Now at TÜV Rheinland

Author for correspondence:

Bernhard Ahrens

Tel: +49 3641 576295

Email: bernhard.ahrens@bgc-jena.mpg.de

5.1 Abstract

During the last decade, a paradigmatic shift regarding which processes determine the persistence of soil organic matter (SOM) took place. The interaction between microbial decomposition and association of organic matter with the soil mineral matrix has been identified as a focal point for understanding the formation of stable SOM. Using an improved version of the vertically resolved SOM model COMISSION (Ahrens et al., 2015), this paper investigates the effect of a maximum sorption capacity (Q_{max}) for mineral-associated organic matter (MAOM) formation and its interaction with microbial processes, such as microbial decomposition and microbial necromass production.

We define and estimate the maximum sorption capacity Q_{max} with quantile regressions between mineral-associated organic carbon (MAOC) and the clay plus silt (< 20 µm) content. In the COMISSION v2.0 model, plant- and microbial-derived dissolved organic matter (DOM) and dead microbial cell walls can sorb to mineral surfaces up to Q_{max}. MAOC can only be decomposed by microorganisms after desorption.

We calibrated the COMISSION v2.0 model with data from ten different sites with widely varying textures and Q_{max} values. COMISSION v2.0 was able to fit the MAOC and SOC depth profiles, as well as the respective ^{14}C gradients with soil depth across these sites. Using the generic set of parameters retrieved in the multi-site calibration, we conducted model experiments to isolate the effects of varying Q_{max}, point-of-entry of litter inputs, and soil temperature. Across the ten sites, the combination of depolymerization limitation of microorganisms due to substrate scarcity in the subsoil and the size of Q_{max} explain ^{14}C depth gradients in OC.

5.2 Keywords

Vertical SOC model;

^{14}C;

Mineral-associated organic carbon;

Microbial model;

Sorption capacity;

Organo-mineral interactions

5.3 Introduction

Soil organic carbon (SOC) models have undergone major changes in recent years. Modelers are attempting to represent the experimental evidence that the persistence of soil organic matter (SOM) is not primarily a function of its molecular structure but an ecosystem property (Schmidt et al., 2011). The stability of SOC depends on physicochemical and biological interactions with the soil environment rather than on the organic compound itself.

Classical first-order decomposition models explain the long-term persistence of organic matter by so-called slow, passive, or inert pools (Davidson and Janssens, 2006). With these models, intrinsic first-order decomposition rates represent the stability of SOC, while interactions with the biotic and abiotic environment are of no or minor importance.

First-order kinetic models do not represent the observation that most organic compounds can turn over on short time-scales that are sometimes magnitudes faster than intrinsic decomposition rates used in models (Parton et al., 1987; Coleman and Jenkinson, 1999; Amelung et al., 2008). The decomposition rates in first-order kinetic models are generally not explicitly mediated by microbial activity. Likewise, organo-mineral interactions are generally not explicitly simulated in these models, but rather clay content or soil texture is used to modify the transfer of SOC to slower pools (RothC and CENTURY) or the decomposition rate of faster pools (CENTURY).

Microorganisms have long been identified as the principal actors in litter and SOM decomposition, e.g., Waksman and Skinner (1926); Waksman and Iyer (1933). However, only starting with the model of Schimel and Weintraub (2003), microorganisms and their function have been more and more incorporated into modeling efforts. The role of microorganisms in stabilizing SOM has been neglected in early microbial models. Bradford et al. (2016) have stated that microorganisms are "now also recognized, somewhat paradoxically, as dominant agents of soil C formation". Microorganisms and mineral surfaces compete for substrate in the form of dissolved organic carbon (DOC; Tang and Riley, 2013; Ahrens et al., 2015), and decomposition can thereby be slowed down. Microbial necromass, however, also contributes to the formation of mineral-associated organic carbon (MAOC, Miltner et al., 2012; Liang et al., 2017; Kopittke et al., 2018; Sokol et al., 2019; Kopittke et al., 2020). Whether microbe-derived MAOC if formed through direct sorption of microbial necromass or the adhesion and turnover of microbial biomass on mineral surfaces (in vivo microbial turnover pathway; Liang et al., 2017; Sokol et al., 2019), is the subject of current studies (Creamer et al., 2019;

Sokol and Bradford, 2019). So far, only the BAMS model (Riley et al., 2014; Dwivedi et al., 2017) has incorporated direct sorption of microbial necromass into a mineral-microbial model.

In the new class of microbial-mineral models (Riley et al., 2014; Ahrens et al., 2015; Dwivedi et al., 2017; Woolf and Lehmann, 2019), substrate limitation of microorganisms and sorption of organic matter on mineral surfaces control soil organic matter stability. Both mechanisms have been invoked to explain high apparent radiocarbon ages of soil organic matter that generally increase with soil depth (Davidson and Janssens, 2006; Conant et al., 2011; Bradford et al., 2016; Gentsch et al., 2018). The relative importance of these two mechanisms to explain ^{14}C age gradients across sites has, however, not been fully elucidated yet.

In this paper, we show how organo-mineral interactions can be implemented in vertically resolved models, such as the COMISSION model (**Co**ntinuous Soil Organic Carbon Profile Model with **M**icrobial **I**nteractions and **S**orptive **S**tabilizat**ion**, Ahrens *et al.*, 2015). We introduce a maximum sorption capacity for mineral-associated organic matter, Q_{max}, that can be easily parameterized with soil texture. In a multi-site calibration across ten sites of contrasting soil texture and mineralogy with consequently widely varying Q_{max}, we test if the COMISSION v2.0 model can reproduce depth profiles of MAOC and SOC and their ^{14}C signature. With model experiments, we investigate the importance of Q_{max} for ^{14}C and soil organic carbon (SOC) profiles and how Q_{max} interacts with microbial energy limitation, the point-of-entry of litter inputs, and temperature.

5.4   Material and Methods

We extended the COMISSION v1.0 model (Ahrens et al., 2015) to make it scalable across sites by introducing a texture-based definition of the organic matter sorption capacity on soil minerals. We calibrated the COMISSION v2.0 model across ten European sites, where detailed measurements of SOC, ^{14}C, and their association with mineral surfaces were available (Schrumpf et al., 2013; Angst et al., 2016a; Angst et al., 2018; Heinze et al., 2018; Kirfel et al., 2019). Seven sites are European beech forests, two sites are coniferous forests, and one site is a grassland soil on volcanic parent material. We conducted model experiments to investigate the effect of a limited organic matter sorption capacity on the persistence of leaf and root litter inputs. The following paragraphs provide a more detailed description of the model, the calibration procedure, and model experiments.

5.4.1 Model description

Previously, we introduced the COMISSION model to investigate stabilization processes in a Haplic Podzol profile (Ahrens et al., 2015). In this earlier work, we used measured maximum sorption capacities from batch sorption experiments ($q_{max, batch}$) along the soil profile to model the sorption of dissolved organic matter (DOM) on mineral surfaces. We now acknowledge, however, that also microbial residues can form associations with mineral surfaces (Miltner et al., 2012; Dwivedi et al., 2017; Kopittke et al., 2018). Measurements of $q_{max, batch}$ are rarely available and are mainly targeted at determining the maximum sorption capacity for DOM but not for microbial residues. Therefore, we now introduced a new approach for parameterizing the maximum sorption capacity based on the clay and silt (< 20 μm) content. Throughout the paper, we refer to the maximum sorption capacity from batch sorption experiments as $q_{max, batch}$, while the texture-based maximum sorption capacity for DOM and microbial residues is termed Q_{max}, facilitating comparisons of SOC storage and turnover across sites and with soil depth. Figure 5-1 gives a conceptual overview of the enhanced model structure, while a full description of the model can be found in the supplementary material.

In COMISSION v2.0, microorganisms depolymerize lignified litter and the microbial residue pool according to reverse Michaelis-Menten kinetics as a function of their biomass. Compared to Ahrens et al. (2015), a soluble litter pool was introduced in addition to the lignified litter pool to improve the representation of DOM generation by leaching from litter on decomposition (Campbell et al., 2016). The soluble litter pool ensures that upon litterfall, the soluble fraction of litter is only gradually released to the DOM pool and thereby made available as substrate to microorganisms. The uptake of DOM by microorganisms is limited by DOC concentrations and simulated with forward Michaelis-Menten kinetics. In both Michaelis-Menten terms, reaction rates are limited by the compound that must diffuse to the respective reaction sites. Tang and Riley (2019) recently found that the extracellular enzymatic depolymerization of larger substrate particles can be approximated by reverse Michaelis-Menten kinetics, and microbial uptake by forward Michaelis-Menten kinetics. Extracellular enzymes diffuse to lignified litter and the microbial residue pool to cleave the polymeric substances into DOM. For model parsimoniousness, we assume that extracellular enzyme concentrations scale with microbial biomass. In the second Michaelis-Menten term, DOM diffuses to microorganisms to be transported into the cell envelope via transporter enzymes. Instead of modelling the diffusion of enzymes and DOM to the respective reaction sites explicitly, we use a macroscopic formulation of these processes with the use of forward and reverse Michaelis-Menten

terms. Advective DOM transport to other soil layers with the water flux between layers is, however, explicitly represented. Both microbial residues and DOM can bind to mineral surfaces to form mineral-associated organic matter according to Langmuir kinetics and saturate Q_{max}. Of the microbial uptake of DOM, microorganisms use a fraction for biomass production (carbon use efficiency, CUE), while the fraction that is not used for biomass production $(1 - CUE)$ is lost from the system as CO_2. For now, we simulate the decomposition of coarse woody debris (CWD, stems, branches, twigs, coarse roots) using a first-order decomposition rate since the decomposition of deadwood is mediated by other agents than the decomposition of litter (Cornwell et al., 2009). Further developments of COMISSION might focus on modeling deadwood decomposition more mechanistically, but this is beyond the scope of the current study. The complete set of equations that make up the COMISSION v2.0 model can be found in section 5.10.1 of the supplementary material.
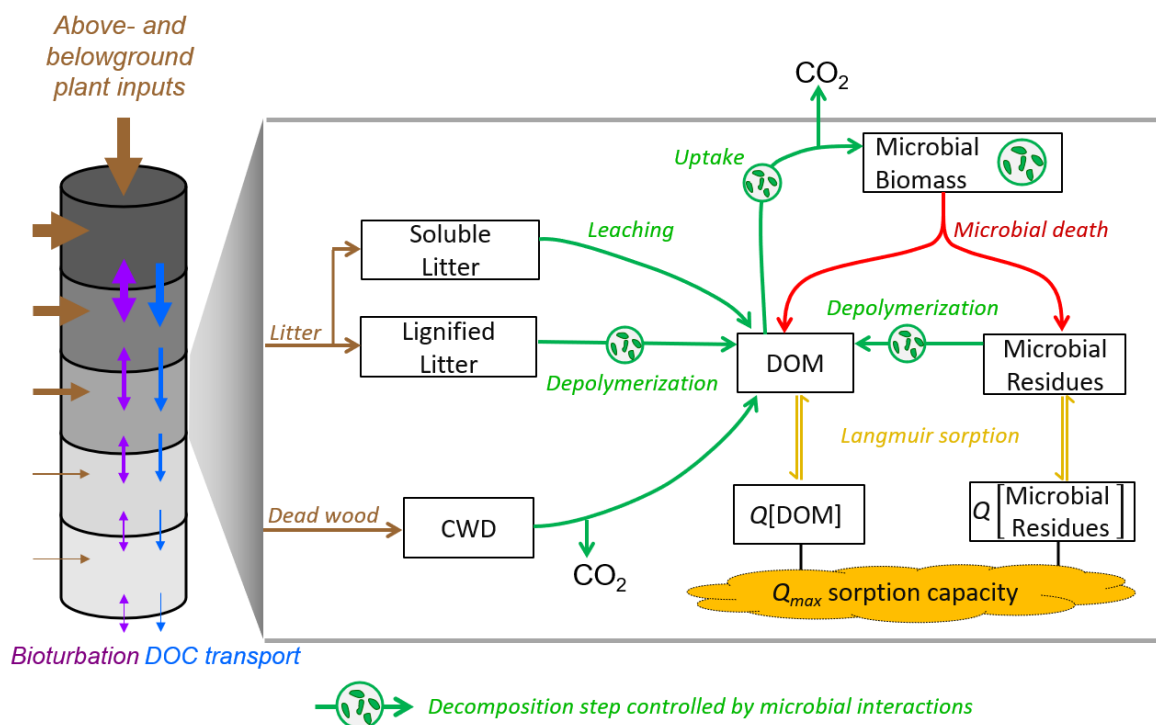
Figure 5-1: Schematic overview of COMISSION v2.0. Microbial biomass depolymerizes lignified litter and microbial residues to DOM. The coarse woody debris (CWD) pool receives input via dead woody litter input and is decomposed according to first-order kinetics. A fraction of the decomposition flux from the CWD pool enters the DOM pool. DOM can be transported to other soil layers with the water flux, taken up by microbial biomass for growth and maintenance, and sorbed to mineral surfaces up to the maximum sorption capacity Q_{max} either directly or after katabolic processing as microbial residues.

5.4.2 Temperature and moisture sensitivity of microbial processes and mineral stabilization

We used Arrhenius kinetics to describe the temperature sensitivity of microbial depolymerization, microbial uptake, microbial biomass death, adsorption, and desorption in COMISSION v2.0:

$$f(T) = \exp\left(-\frac{E_a}{R} \cdot \left(\frac{1}{T} - \frac{1}{T_{ref}}\right)\right)$$

(5-1)

where T is the soil temperature (K), E_a the activation energy specific to a certain process (kJ mol^{-1}), R the universal gas constant (kJ K^{-1} mol^{-1}), and T_{ref} the reference temperature of 283.15 K at which $f(T) = 1$.

Following three literature reviews (Conant et al., 2011; Wang et al., 2013; Bradford et al., 2016), we use activation energies, E_a, for microbial processes (equivalent to Q$_{10}$ values between 1.98 and 2.16) that are substantially higher than the activation energies for adsorption and desorption (equivalent to Q$_{10}$ values between 1.08 and 1.34, Table 5-1).

Table 5-1: Activation energies and Q$_{10}$ values for temperature-sensitive processes in the COMISSION v2.0 model.

Process	E_a, activation energy (kJ mol^{-1})	Equivalent Q$_{10}$ at 20°C	Reference
Depolymerization	53	2.16	Wang et al. (2012)
Microbial uptake	47	1.98	Allison et al. (2010)
Microbial biomass death	47	1.98	Allison et al. (2010), Hagerty et al. (2014)
Adsorption	5	1.08	Wang et al. (2013)
Desorption	20	1.34	Wang et al. (2013)

For microbial assimilation, we implemented a flexible soil moisture rate-modifier. The functional form is similar to the one presented in Yan et al. (2018) with an optimum moisture content at which microorganisms operate at their physiological maximum:

$$f(\theta) = \begin{cases} \left(\dfrac{\theta}{\theta_{opt}}\right)^a, & \theta < \theta_{opt} \\ \left(\dfrac{\phi - \theta}{\phi - \theta_{opt}}\right)^b, & \theta \geq \theta_{opt} \end{cases} \tag{5-2}$$

where θ is the volumetric water content (m^3 m^{-3}), ϕ is the soil porosity (m^3 m^{-3}), θ_{opt} is the optimum moisture content (m^3 m^{-3}, parameterized as $0.65 \cdot \phi$ as in Yan et al. (2018)), and a and b are two parameters (-) that were fitted during the multi-site calibration (see section 5.4.5). The function is intended to represent the limitation of microbial activity through diffusion of DOM at soil moistures smaller than θ_{opt} and oxygen limitation at soil moistures larger than θ_{opt}.

5.4.3 Definition of Q$_{max}$

Compared to our approach in Ahrens et al. (2015), we are using a definition of the maximum sorption capacity, Q_{max}, which is scalable across sites. Thereby, it can also be used in global terrestrial biosphere models. The maximum sorption capacity, $q_{max, batch}$, in Ahrens et al. (2015) was based on batch sorption experiments (Guggenberger and Kaiser, 2003), which relate to the direct sorption of DOM on mineral surfaces but does not cover the *in vivo* turnover of microorganisms attached to mineral surfaces (*sensu* Sokol et al. (2019)). Here, we use empirical estimates of a maximum sorption capacity as derived by Feng et al. (2013) and Beare et al. (2014). This maximum sorption capacity of organic matter on mineral surfaces is based on quantile regressions of the mineral-associated fraction with the clay plus < 20 µm silt content. The findings of Six et al. (2002), Feng et al. (2013), and Beare et al. (2014) indicate that the concept of a maximum sorption capacity is adequate.

We reanalyzed the data presented in Feng et al. (2013) using the 90th percentile regression approach as used by Beare et al. (2014). This analysis yields the following relationship between the fine mineral fraction (clay + < 20 µm silt fraction) and mineral-associated organic matter:

$$Q_{max}^m = m \cdot f_{\text{clay} + < 20 \, \mu m \, \text{silt fraction}}$$ (5-3)

where Q_{max}^m is the maximum sorption capacity (g OC (g mineral soil)$^{-1}$), m is the slope retrieved from the 90th percentile regression (g OC (g fine particles)$^{-1}$), and $f_{\text{clay} + < 20 \, \mu m \, \text{silt fraction}}$ (g fine particles (g mineral soil)$^{-1}$) is the clay and silt (< 20 μm) fraction. m is 0.153 for allophanic soils (Beare et al., 2014), 0.079 for soils dominated by 2:1 minerals, and 0.044 for soils dominated by 1:1 minerals. For this study, we used nine sites dominated by 2:1 minerals and one site with allophanic properties. The mean Q_{max}^m values over the complete profiles are given in Table 5-2. For the sites TSA_A, LOE_A, BUN_A, and BAS_A (Table 5-2), only measurements according to the German definition of silt (2 - 63 μm, Blume et al. (2015)) were available. We used a log-linear transformation of soil texture data as implemented by Moeys (2018) to approximate the 2 – 20 μm size class, which is required by the empirical definition of maximum sorption capacity by Feng et al. (2013) and Beare et al. (2014).

5.4.4 Development of the organic layer, Q_{max}, and bulk density

To account for changes in bulk density due to the accumulation of SOM, we used the semi-mechanistic description of bulk density by Adams (1973) and its refinement by Federer et al. (1993). They proposed that organic matter (OM) and mineral soil occupy additive soil volumes V_O and V_M, which both make up the total soil volume V_T. Masses of OM and mineral soil are also additive, so that OM and mineral soil both have theoretical bulk densities of ρ_{bO} and ρ_{bM}. Hence, we start the simulation with a soil bulk density that is equal to ρ_{bM}. For ρ_{bO} we used a universal value of 150 kg m^{-3} for all sites, while we calculated the theoretical ρ_{bM} as a function of sand content per site and midpoint depth (Tranter et al., 2007):

$$\rho_{bM}(z) = 1.35 + 0.0045 \cdot p_{sand}(z) + 6 \cdot 10^{-5} \cdot \left(44.7 - p_{Sand}(z)\right)^2 + 0.06 \cdot \log(z)$$

(5-4)

where p_{Sand} is the sand content (%) at the midpoint depth of the layer (z in cm).

The volumetric maximum sorption capacity, Q_{max}^V, in each layer at the beginning of the simulations is the product of ρ_{bM} and the mass- and texture-based maximum sorption capacity Q_{max}^m in depth z.

We model the accumulation of SOM in the organic layer localized on top of the mineral soil and within the profile through root litter input via an advective transport term. The build-up of an organic layer leads to a bulk density equal to ρ_{bO}. This advective transport term is built on the concept of Adams (1973) and Federer et al. (1993), i.e., changes in SOC concentrations induce a change in volume V_O. This change in SOM volume, V_O, can be translated into an advection velocity $\omega(z)$ that varies with depth z. $\omega(z)$ is defined as the change of V_O in depth z due to the accumulation of OM from aboveground and belowground litter inputs i_{ABG} and i_{BLG} minus losses from SOM decomposition. The losses from decomposition are displayed here with a generic decomposition rate k and volumetric SOM concentrations SOM^V.

$$\omega(z) = \frac{i_{ABG} + \int_0^z \Delta i_{BLG}(z)\,dz + \int_0^z -k \cdot SOM^V\,dz}{\rho_{bO}} \tag{5-5}$$

All model pools are transported by $\omega(z)$. Likewise, the initial Q_{max}^V is transported with the advection velocity $\omega(z)$ to represent the buildup of an organic layer in which mineral surfaces are absent. Q_{max}^V is introduced as a state variable to represent the available sorption sites throughout the time course of the simulation and is shifted downwards or upwards depending on changes in SOM (see supplementary material 5.10.1).

5.4.5 Multi-site calibration

In a multi-site calibration, we calibrated the parameters of the COMISSION v2.0 model against ten intensively measured SOC profiles from the SUBSOM project (Angst et al., 2016b; Angst et al., 2018; Heinze et al., 2018; Kirfel et al., 2019) and the CarboEurope project (Schrumpf et al. (2013), Table 5-2). We started all simulations from pure mineral soil at 12 000 years BP without considering soil weathering processes, i.e. constant soil texture and fixed physico-chemical soil parameters throughout the simulation.

Table 5-2: Overview of the sites used in the multi-site calibration. Q_{max}^m is a function of the clay plus silt (< 20 µm) content (see equation 3). Soil types are given according to the World Reference Base for Soil Resources WRB (IUSS Working Group WRB, 2015).

Site ID	Site name	Location		Land use	Soil type	Mean Q_{max}^m (% OC)	Parent material	MAT (°C)	MAP (mm)
DE-Gri	Grinderwald, Germany	52° 34' 22.115"N	9° 18' 49.762"E	Deciduous forest	Dystric Cambisol	1.2	Pleistocene sand	8.7	718
BUN_A	Ebergötzen, Germany	51° 34' 45.89"N	10° 03' 59.52"E	Deciduous forest	Dystric Cambisol	3.5	Triassic sandstone	7.7	772
LOE_A	Rüdershausen, Germany	51° 34' 51.52" N	10° 14' 43.03" E	Deciduous forest	Semi-eutric Cambisol	5.4	Quaternary loess	8.1	709
BAS_A	Dransfeld, Germany	51° 28' 35.60" N	09° 45' 32.46" E	Deciduous forest	Eutric Cambisol	5.3	Tertiary basalt	7.1	902
TSA_A	Hannoversch-Münden, Germany	51° 26' 25.64" N	09° 41' 24.25" E	Deciduous forest	Dystric Cambisol	2.2	Tertiary sand	8.1	761
DE-Hai	Hainich, Germany	51°04' N	10°27' E	Deciduous forest	Eutric Cambisol	6.6	Pleistocene loess layer over triassic limestone	8.3	800
DK-Sor	Soroe, Denmark	55°29' N	11°38' E	Deciduous forest	Gleyic Cambisol	3.5	Calcareous lodgement till	8.2	660
SE-Nor	Norunda, Sweden	60°5' N	17°29' E	Coniferous forest	Haplic Podzol	3.1	Glacial till	5.45	527
DE-Wet	Wetzstein, Germany	50°27' N	11°27' E	Coniferous forest	Cambic Podzol	5.1	Quartzite	5.74	840
FR-Lq2	Laqueuille, France	45°38' N	02°44' E	Grassland	Umbric Andosol	10.0	Basaltic bedrock	8	1313

In total, we used profiles of volumetric SOC concentrations, volumetric MAOC concentrations, and the respective ^{14}C contents in these fractions. The first five sites in Table 5-2 are part of the DFG funded SUBSOM Research Unit (http://www.subsom.de), which is dedicated to the investigation of the role of subsoils in SOM decomposition and formation. All the SUBSOM sites are mature European beech forests (*Fagus sylvatica* L.). Of the five CarboEurope sites (last five sites in Table 5-2), two are deciduous forests, two are coniferous forests, and one is a grassland site on an Andosol. Of the coniferous sites, SE-Nor is dominated by Scots pine (65%, *Pinus sylvestris* L.) and Norway spruce (33%, *Picea abies* L.), while DE-Wet is a Norway spruce (*Picea abies* L.) plantation (Feigenwinter et al., 2008). Forcing data for each site, such as vertically resolved soil temperature and water fluxes, and leaf and root litter inputs were generated with site-level runs of the JSBACH model (Knauer et al., 2015). For the 5 CarboEurope sites, we evaluated the JSBACH model simulations against eddy covariance measurements of evapotranspiration, gross primary productivity, and sensible heat flux (Table Supp 1-3). At all sites measurements of aboveground litter inputs were available. Modelled aboveground litter inputs were scaled to match observed aboveground litter inputs. The same factor

was applied for scaling belowground litter inputs. We fitted the logistic-dose response function that was proposed by Schenk and Jackson (2002) to the observed root biomass profiles at the ten sites to represent the vertical distribution of root litter (Supplementary figure 1). The ^{14}C contents of litter inputs were generated by convoluting the simulated litter inputs with the Northern Hemisphere atmospheric ^{14}C data reported in Reimer et al. (2013) appended with the RCP8.5 simulation for after 2013 of Graven (2015).

To calibrate the parameters of the model (see supplementary section 0), we minimized the normalized sum of squares $(nSS$, Hengenius et al. (2014)) between modeled and observed variables using the genoud algorithm (Mebane Jr and Sekhon, 2011):

$$nSS = \sum_{i \in Var} \sum_{j \in Sites} \sum_{k=1}^{nObs_{i,j}} \left(\frac{Mod_{i,j,k} - Obs_{i,j,k}}{weight_i} \right)^2,$$

where Var are the four 'data streams' we used in the optimization, i.e., SOC, SO^{14}C, MAOC, and MAO^{14}C, $Sites$ are the ten sites, and $nObs_{i,j}$ are the number of observations for a certain variable and site. $weight_i$ is the range of all observations k for a variable i across all sites j. We ran the genoud algorithm with 35 generations and a population size of 10000 individual parameter sets per generation and used the parameter set with the lowest nSS (see supplementary section 0). The genoud algorithm created an initial population of 10000 parameter sets based on random sampling from the prescribed parameter ranges (Supplementary Table 1), the next 34 generations of 10000 parameter sets were then created by reproducing parameter sets with a low nSS, randomly changing parameters of the best parameter sets, or exchanging parameters between parameter sets. The calibrated parameter set has to be regarded as conditional on the forcing datasets created with the JSBACH model since a complete evaluation of the boundary conditions was not possible (Supplementary Table 1).

We used a flexible time stepping method as integration routine to ensure that we can combine processes such as adsorption and microbial growth that act on the time-scale of hours with processes that act on the time-scale of years and decades. More specifically, we used the DLSODES solver for ordinary differential equations (Hindmarsh, 1983) together with the Yale sparse matrix solver (Eisenstat et al., 1977; Eisenstat et al., 1982) to solve the partial differential equations that constitute the COMISSION v2.0 model (see supplementary material 5.10.1). We employed the finite-difference

method to solve the spatial dimension of the partial differential equations of COMISSION v2.0. We used 15 grid cells per site while adapting the grid cell thickness to account for the varying soil depths between the sites. We used thinner grid cells in the topsoil compared to the subsoil. To ensure efficient parameter estimation, however, we did not run COMISSION with daily forcing data from the JSBACH model for the whole simulation period from 12 000 years BP but employed a spin-up with yearly aggregated forcing data. The spin-up is vital for modeling ^{14}C contents throughout the soil profile. As the model run approached present day, we changed the resolution of the forcing data to monthly using an averaged year of simulations. To account for non-linearities in the temperature and moisture rate modifiers (equations 1 and 2), we supplied the daily forcing data to the respective function and then aggregated the function value to the required resolution.

5.4.6   Model experiments

To evaluate the overall importance of Q_{max}^m to explain differences between sites in the multi-site calibration, we ran two simulations at all sites, where we replaced the site-specific Q_{max}^m with the minimum and maximum Q_{max}^m observed across all sites and horizons: 5 g (kg mineral soil)$^{-1}$ at DE-Gri and 108 g (kg mineral soil)$^{-1}$ at FR-Lq2.

To elucidate the combined effect of the maximum sorption capacity and microbial energy limitation, we conducted model experiments (Table 5-3) using the universal parameter set retrieved in the multi-site calibration. We used a sequence of Q_{max}^m that included the minimum and maximum observed Q_{max}^m, while using the root litter distributions, and forcing, such as soil temperature and litter input from the TSA_A site. To investigate the effect of energy limitation on depth gradients of SOC and ^{14}C, we switched off the microbial limitation of depolymerization by setting the respective half-saturation constant, $K_{m,\ Lignified\ Litter}$, to 0. This process is of special relevance in the subsoil where the substrate for microorganisms is getting scarcer. Hence, the first model experiment combines the variation of Q_{max} with two model-setups: one where microbial limitation of depolymerization is switched on and one where it is switched off.

In a second model experiment, we varied the percentage of overall litter inputs that is allocated belowground as root litter between 38% (coniferous forests, Bloom et al. (2016)) and 80% (grassland in FR-Lq2), to analyze the effect of Q_{max} and the point-of-entry of litter inputs (Sokol et al., 2019), while using the root litter distributions (but different allocation) and forcing from the TSA_A site.

In a third model experiment, we aimed at elucidating the interaction between sorption capacity and different point-of-entries of root litter, specifically different root distributions. We tested the effect of the root litter distributions from the ten different calibration sites (Supplementary figure 1) in a model experiment with a low sorption capacity Q_{max}^m of 5 g (kg mineral soil)$^{-1}$ and a model experiment with a high sorption capacity Q_{max}^m of 108 g (kg mineral soil)$^{-1}$. This model experiment was intended to quantify the input or dilution effect of litter inputs (direct input of modern ^{14}C) compared to the matrix protection effect of Q_{max}^m.

To elucidate the role of energy limitation and root distributions on ^{14}C profiles, in a fourth model experiment, we used the root distributions from all sites (Supplementary figure 1) to run the simulations at the TSA_A site with and without microbial limitation of depolymerization of lignified litter and microbial residues.

To elucidate the combined effect of Q_{max}^m and temperature, in a last model experiment, we used the same variation of Q_{max}^m as before but used the minimum and maximum observed mean annual temperature from the ten sites (Table 5-2), 5.45 °C and 8.70 °C, to replace the mean soil temperatures in the 15 layers, while using the root litter distributions and forcing (except temperature) from the TSA_A site.

Table 5-3: Model experiments to elucidate the interactive effect of Q_{max}^m and microbial depolymerization limitation, point-of-entry of litter inputs, and temperature.

Name of the model experiment	Description
Microbial-Limitation–Q_{max} interaction	Microbial depolymerization on and off while varying Q_{max}^m from 5 to 108 g (kg mineral soil)$^{-1}$
Aboveground-V-Belowground–Q_{max} interaction	Two litter input experiments. 38% and 80% of litter enters aboveground, the rest belowground, while varying Q_{max}^m from 5 to 108 g (kg mineral soil)$^{-1}$
Root-Distribution–Q_{max} interaction	Root distributions from the ten calibration sites with a low Q_{max}^m 5 g (kg mineral soil)$^{-1}$ and a high Q_{max}^m 108 g (kg mineral soil)$^{-1}$ simulation
Root-Distribution–Microbial-Limitation interaction	Root distributions from the ten calibration sites with Q_{max}^m from TSA_A, but with and without microbial depolymerization limitation
MAAT–Q_{max} interaction	MAAT at 5.45 and 8.70 °C while varying Q_{max}^m from 5 to 108 g (kg mineral soil)$^{-1}$

5.5 Results

5.5.1 Multi-site calibration

We calibrated the parameters of the COMISSION v2.0 model across ten sites to retrieve a general parameter set that is applicable across scales and sites. Both the volumetric SOC and MAOC concentrations (Figure 5-2A) and their respective ^{14}C contents (Figure 5-2B) in the ten profiles were well captured. By investigating the range of model parameters after optimization compared to the initially prescribed range of model parameters (Supplementary Table 1), we could describe how well the parameters are constrained by the model-data integration. Following Forkel et al. (2019), we use the proposed parameter sets with the top 5% of nSS (model cost) to define final ranges of accepted parameters. During the calibration, most of the parameter values could be well constrained by the data, except for the parameter a, which describes the functional relationship between water content and decomposition below the optimal water content θ_{opt} (Equation 3, Figure 5-3). The a parameter could not be constrained by the available data as indicated by the lack of reduction in the relative uncertainty of the parameter compared to the prescribed parameter bounds (Figure 5-3A). All the other parameters showed substantial reductions in uncertainty compared to the initial parameter

bounds. Apart from the a parameter, also $V_{max,DOM}$ and $k_{des,DOM}$ were not below the boundary of 20%, which Forkel et al. (2019) used to qualify parameters as well constrained. These two parameters describe the uptake of DOM by microorganisms and the desorption rate of DOM from mineral surfaces. Rate coefficients, however, do not represent the timescales the respective processes are acting on well. Instead, the inverse of the rate coefficients represents better how well the timescale of the process is constrained. This can easily be exemplified by the range of accepted $k_{des,DOM}$ rates. The slowest accepted $k_{des,DOM}$ corresponds to a desorption time of 9 hours, while the fastest accepted $k_{des,DOM}$ corresponds to a desorption time of 2.5 hours. We use the term desorption time to describe the inverse of the desorption rate ($k_{des,DOM}^{-1}$). By contrast, the initial bounds of $k_{des,DOM}$ correspond to desorption times from 52560 hours to 1 hour. Expressed as desorption rates, these ranges, however, appear much less constrained. The rate coefficient of $k_{des,DOM}$ on its original scale was allowed to vary between 0.167 yr^{-1} to 8760 yr^{-1} (lower and upper bound), but were only constrained between 965 yr^{-1} to 3449 yr^{-1} after the calibration. Expressed as desorption times, however, the accepted range is well constrained at 6.5 hours. Expressed as characteristic times, the inverse rate coefficients all showed substantial reductions in uncertainty compared to the prescribed parameter bounds (Figure 5-3B). The timescales of decomposition, sorption, and desorption can, therefore, be considered as well constrained by the model-data integration.
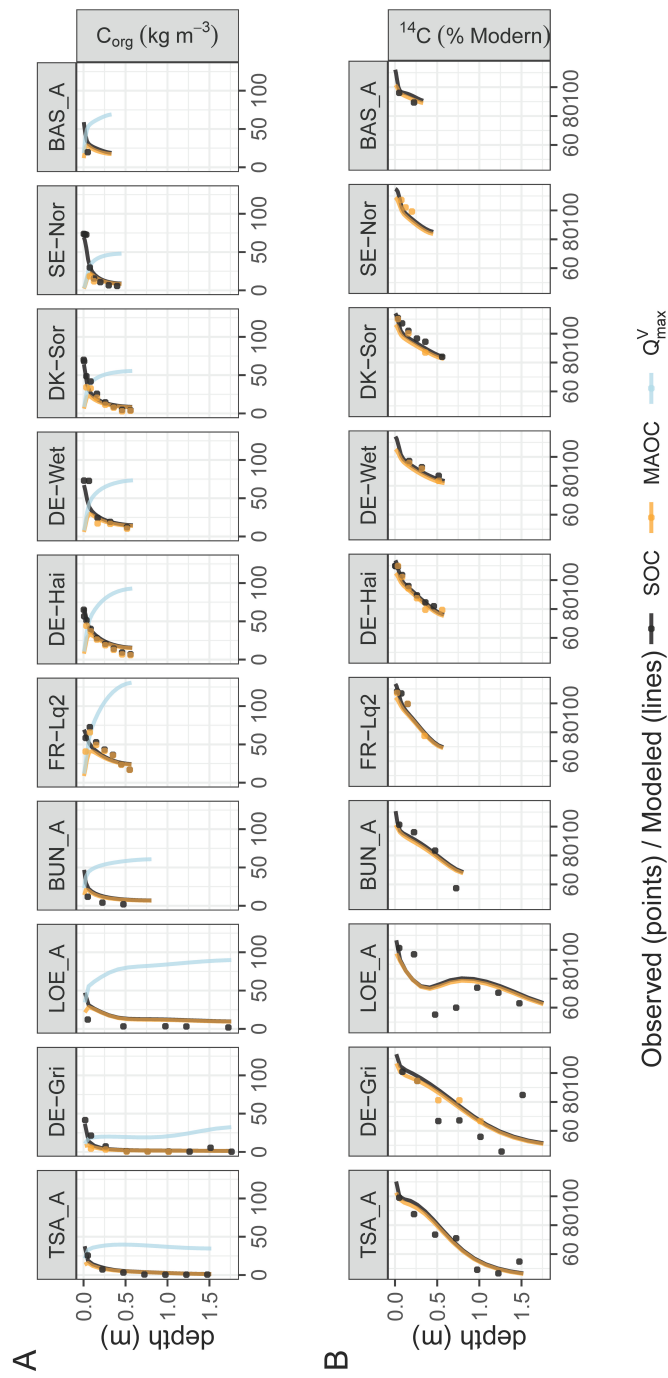
Figure 5-2: Soil organic carbon (SOC) and mineral-associated organic carbon (MAOC) stocks (kg m^{-3}) (A), along with calibrated and observed radiocarbon contents (^{14}C % Modern) (B) in SOC and MAOC at ten calibration sites. The light blue line depicts the volumetric maximum sorption capacity, Q_{max}^{V} (kg m^{-3}).

A

B
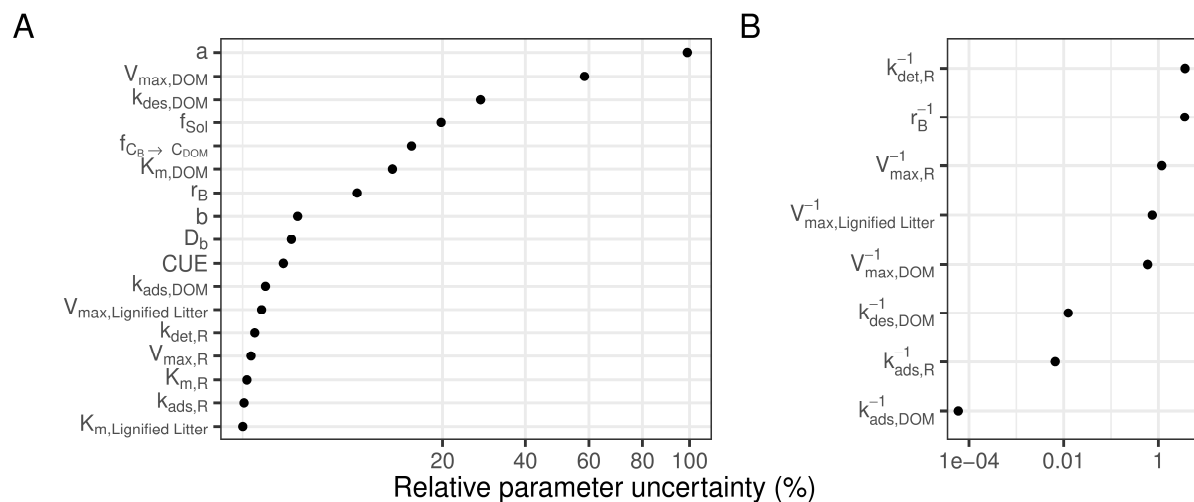
Figure 5-3: Relative uncertainty in parameter values after optimization. Shown is the percentage reduction between final ranges of parameters (top 5% of parameter sets from 350000 proposed parameter sets) and the prescribed initial parameter range. Panel A shows the relative parameter uncertainty on the original parameter scale. Panel B shows the relative parameter uncertainty of characteristic times. Characteristic times are the inverse of rate coefficients and are more indicative of the time scales the process acts on. Parameters and their initial ranges are described in Supplementary Table 1.

Scatterplots of observed and modeled SOC and MAOC concentrations (Figure 5-4A, r^2 of 0.90 and 0.76) and ^{14}C of SOC and MAOC (Figure 5-4B, r^2 of 0.78 and 0.92) confirm that COMISSION v2.0 captured the variation across the ten sites relatively well. In Supplementary figure 2 we show scatterplots of modelled and observed SOC and MOC and their respective ^{14}C values per site. Across all sites, slopes of observations vs. predictions reveal that the SOC concentrations had a smaller model bias (slope = 1.12) than MAOC concentrations (slope = 1.42, Figure 5-4A). This bias can be attributed to the representation of MAOC formation in the topsoil. Since the volumetric maximum sorption capacity is dependent on the accumulation of an organic layer and the size of Q_{max}, differences between modeled and observed MAOC also reflect the ability of COMISSION v2.0 and the maximum sorption capacity approach to reproduce site conditions. In the allophanic soil FR-Lq2, for example, COMISSION v2.0 was not able to match the second data point of MAOC since Q_{max}^{V} is already lower than the observed volumetric MAOC concentrations.

Given the fact that we use one universal parameter set for all ten sites, some pedogenic particularities are not covered by the parametrization and the implemented processes of COMISSION v2.0 adequately (Supplementary figure 2). One example is DE-Gri, where the ^{14}C of bulk SOC is more depleted than the ^{14}C of MAOC. Angst et al. (2016a) pointed out that this could indicate the presence

of geogenic OC at DE-Gri. The COMISSION v2.0 model cannot model this observation without introducing an additional pool that is very depleted in ^{14}C and not sorbed to mineral surfaces (not shown).
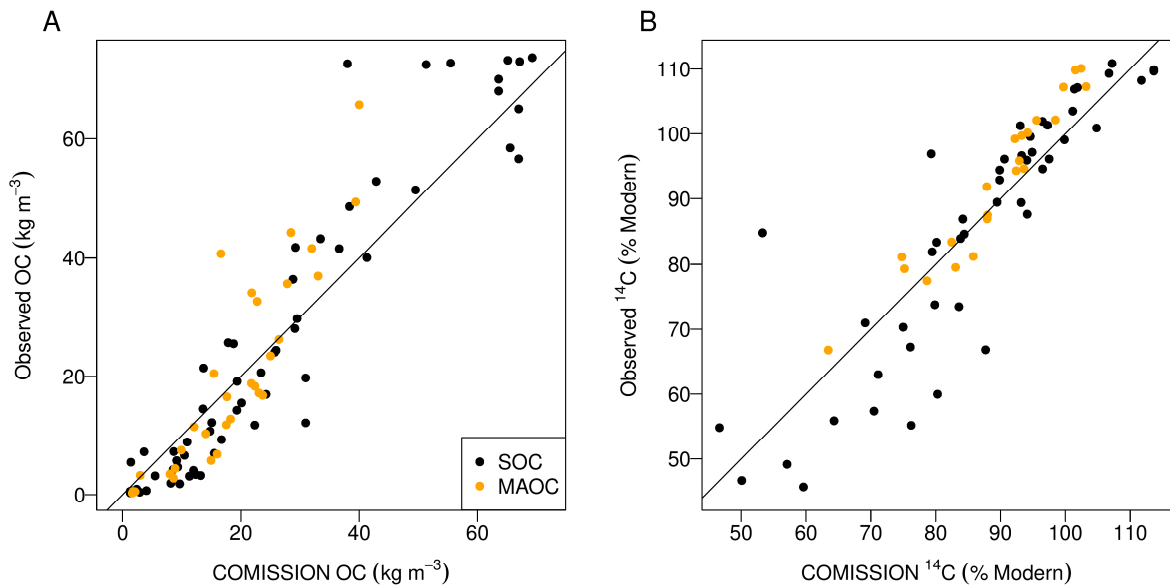
Figure 5-4: Scatterplots of observed vs. modeled volumetric SOC and MAOC concentrations (A) and ^{14}C of SOC and MAOC (B).

5.5.2 Model experiments

The results from the multi-site calibration (Figure 5-4), especially together with tests of replacing the site-specific Q_{max}^m with the minimum and maximum observed Q_{max}^m (Supplementary figure 3B, Supplementary figure 4B), suggest that Q_{max}^m is very important in explaining the characteristic depth-declines of ^{14}C contents at the different sites.

The variation of Q_{max}^m across the observed range at the ten sites corresponds to a shift from a sandy soil to an allophanic soil that is dominated by clay and silt. The model experiments described in Table 5-2 were designed to study the combined effect of sorption capacity and other factors, such as microbial energy limitation, point-of-entry of litter, and temperature.

Microbial-Limitation–Q_{max} interaction

In the Microbial-Limitation–Q_{max} interaction experiment (Figure 5-5), varying the size of Q_{max}^m alone can change the MAOC ^{14}C contents in COMISSION v2.0 from being influenced by "bomb radiocarbon" with a Q_{max}^m of 5 g (kg mineral soil)[-1] in the topsoil to being dominated by radioactive decay with a Q_{max}^m of 108 g (kg mineral soil)[-1] throughout the profile (Figure 5-5A). These radiocarbon contents correspond to apparent conventional ^{14}C ages of more than 6000 years. The matrix protection effect on ^{14}C contents weakens as Q_{max}^m increases (Figure 5-5A). The same holds true for free OC, although the spread in ^{14}C ages is overall much narrower except for very low Q_{max}^m (Figure 5-5A). The effect of increasing Q_{max}^m is also reflected in considerably higher SOC stocks (Figure 5-5B, microbial limitation). For free OC, the size of Q_{max}^m is generally of less importance, especially for free OC stocks (Figure 5-5B). Here, microbial limitation is of larger importance.

In the deeper subsoil (below 0.5 m), both the microbial limitation of depolymerization and high sorption capacities Q_{max}^m are needed to produce apparent ^{14}C ages older than 3000 years (Figure 5-5A, no microbial limitation).
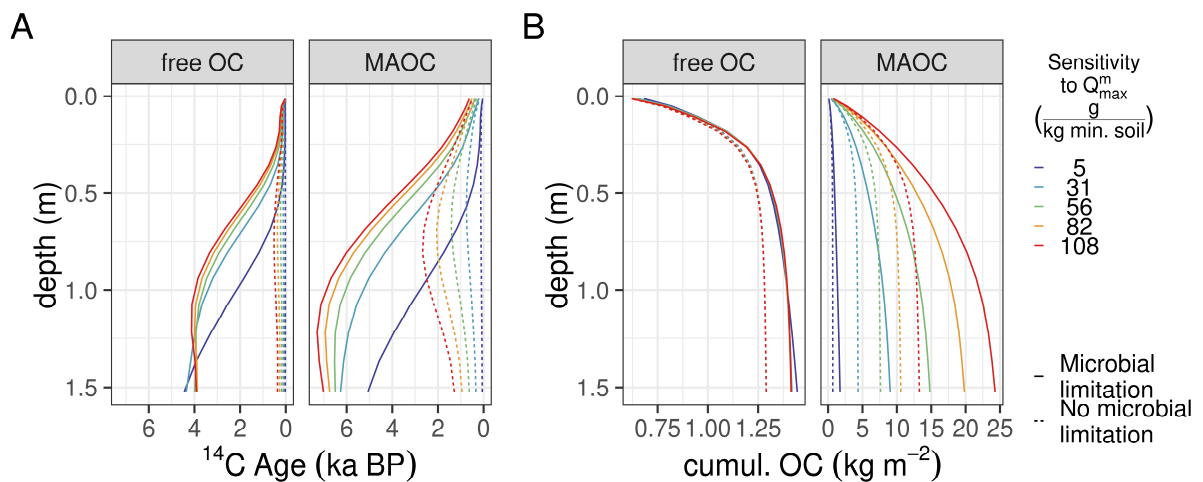
Figure 5-5: Model experiment Microbial-Limitation–Q_{max} interaction: Combined effect of sorption capacity (Q_{max}^m) and microbial activity (energy limitation and substrate scarcity) on apparent ^{14}C ages (A) and cumulative stocks (B) of free organic carbon (free OC) and mineral-associated organic carbon (MAOC). Colored lines represent simulations with varying Q_{max}^m. Root litter distribution and forcing as for TSA_A.

Aboveground-V-Belowground–Q_max interaction

The strong effect of Q_{max}^m on cumulative OC stocks suggests that it matters whether litter inputs are aboveground or belowground, i.e., not in immediate contact with the mineral soil matrix or in direct contact with the mineral soil matrix. The Aboveground-V-Belowground–Q_{max} interaction model experiment (Figure 5-6) shows that, integrated over the profile, belowground litter input persists longer compared to aboveground litter input. If 80% of litter inputs are below ground, as for the grassland site, carbon stocks are up to 2.3 kg C m^{-2} higher compared to an experiment in which only 38% of litter inputs are below ground, as for the coniferous sites (Figure 5-6B). Consequently, the apparent ^{14}C ages are generally younger (up to 1.2 ka BP) in the mineral soil when more litter input is deposited belowground (Figure 5-6A). In the deep subsoil (below 1.25 m) at the two highest Q_{max}^m values, however, apparent ^{14}C ages can be up to 0.2 ka BP older when more litter is deposited belowground. This is dependent on the relative importance of sorption to mineral surfaces compared to microbial limitation. At lower Q_{max}^m values the differences in ^{14}C ages between 38% litter belowground and 80% litter belowground are generally more pronounced than at higher Q_{max}^m values (Figure 5-6A).
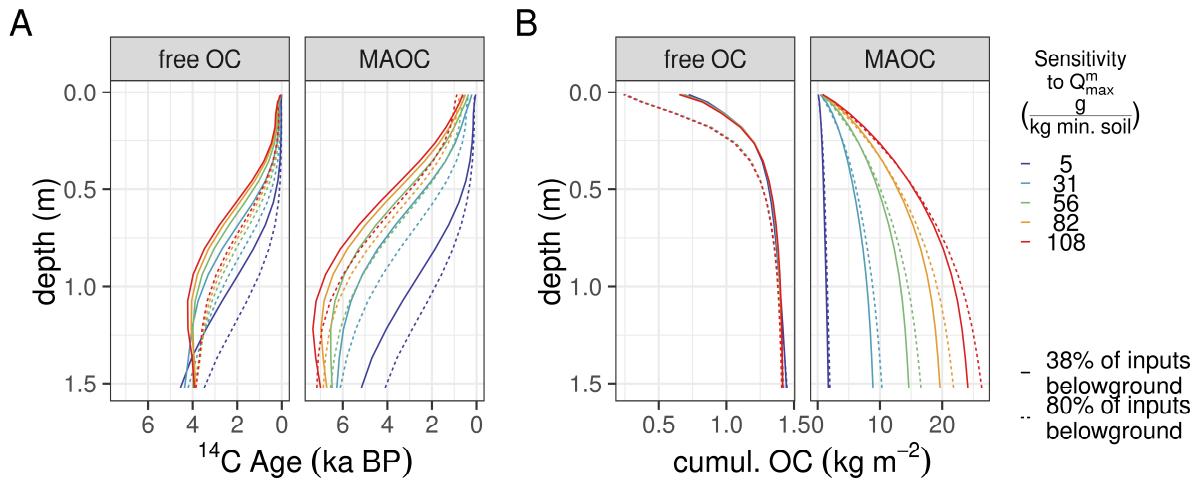
Figure 5-6: Model experiment Aboveground-V-Belowground–Q_{max} interaction: Combined effect of sorption capacity (Q_{max}^m) and point-of-entry (38% and 80% of all inputs belowground, the remainder aboveground) on apparent ^{14}C ages (A) and cumulative stocks (B) of free organic carbon (free OC) and mineral-associated organic carbon (MAOC). Colored lines represent simulations with varying Q_{max}^m. Root litter distribution and forcing as for TSA_A.

Root-Distribution–Q_{max} interaction

To further evaluate the importance of the point-of-entry of root litter with regard to available sorption sites, we took the most extreme sorption capacities of the ten calibration sites and conducted model experiments by forcing the model at the TSA_A site with the different root distributions (Supplementary figure 1) from all ten sites. Figure 5-7A shows that with a high sorption capacity the effect of different root litter distributions results in a much tighter range of ^{14}C ages in the subsoil than for a low sorption capacity. At a low sorption capacity, the root litter distributions result in a much larger range of ^{14}C ages in the subsoil. Excluding the LOE_A root distribution, which has a rather particular shape (Supplementary figure 1) with a lot of deep roots and a small amount of shallow roots, ^{14}C ages have a spread of 1000 years between the different root litter distributions at a Q_{max}^{m} of 108 g (kg min. soil)$^{-1}$, while the spread is 3500 years for a Q_{max}^{m} of 5 g (kg min. soil)$^{-1}$. For MAOC stocks, however, the root litter distribution is more important at high sorption capacities (Figure 5-7B). Overall differences in SOC stocks between root litter distributions from the various sites are, however, not very pronounced except for the root litter distribution from the LOE_A site (Figure 5-7B).
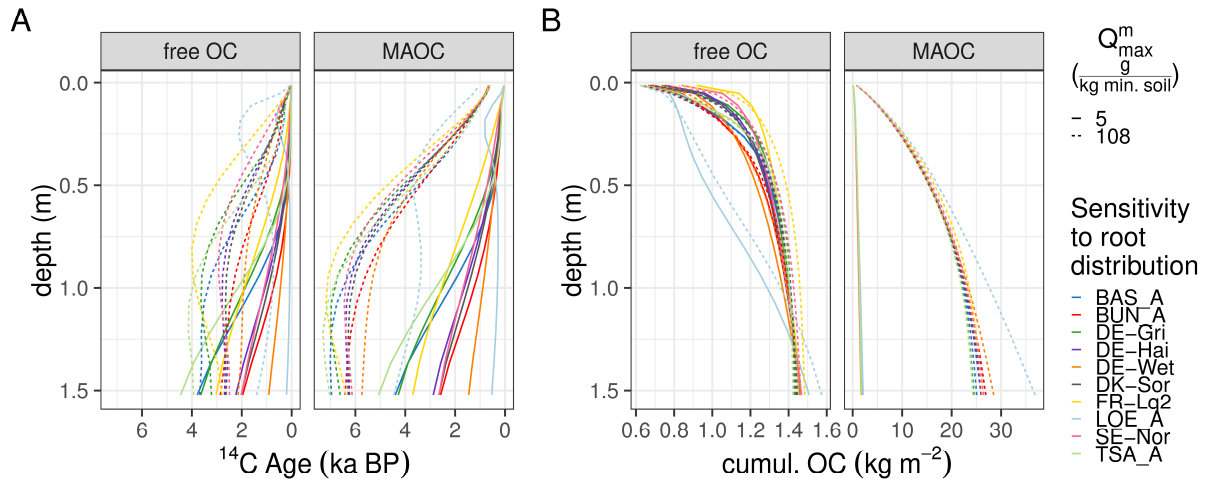
Figure 5-7: Model experiment Root-distribution–Q_{max} interaction: Combined effect of sorption capacity (Q_{max}^{m}) and root litter distributions on apparent ^{14}C ages (A) and cumulative stocks (B) of free organic carbon (free OC) and mineral-associated organic carbon (MAOC). Colored lines represent the root litter distributions at the ten different sites. All other site conditions as for TSA_A.

Root-Distribution–Microbial-Limitation interaction

The point-of-entry of root litter is also relevant for the microbial limitation of decomposition as it directly affects substrate supply and energy limitation of microorganisms. Similar to the previous model experiment, we use the root distributions from the ten different sites (Supplementary figure 1) at the TSA_A site, here with the Q_{max}^m of the TSA_A site but studying the effect of microbial limitation. If there was no microbial limitation of decomposition, the differences in substrate supply would barely cause any differentiation in ^{14}C ages in the subsoil (Figure 5-8A). The interaction of microbial limitation and the point-of-entry of root litter within a profile causes a differentiation of ^{14}C ages of 2000 years both for free OC and MAOC (excluding again the root profile from LOE_A). For free OC and MAOC stocks there is little influence on the overall stocks. The deep reaching root distribution from LOE_A shows the largest effect on MAOC stocks for COMISSION v2.0 with microbial limitation. Without microbial limitation of depolymerization, even the root distribution of LOE_A does not result in a substantial difference in MAOC stocks compared to the other root distributions.
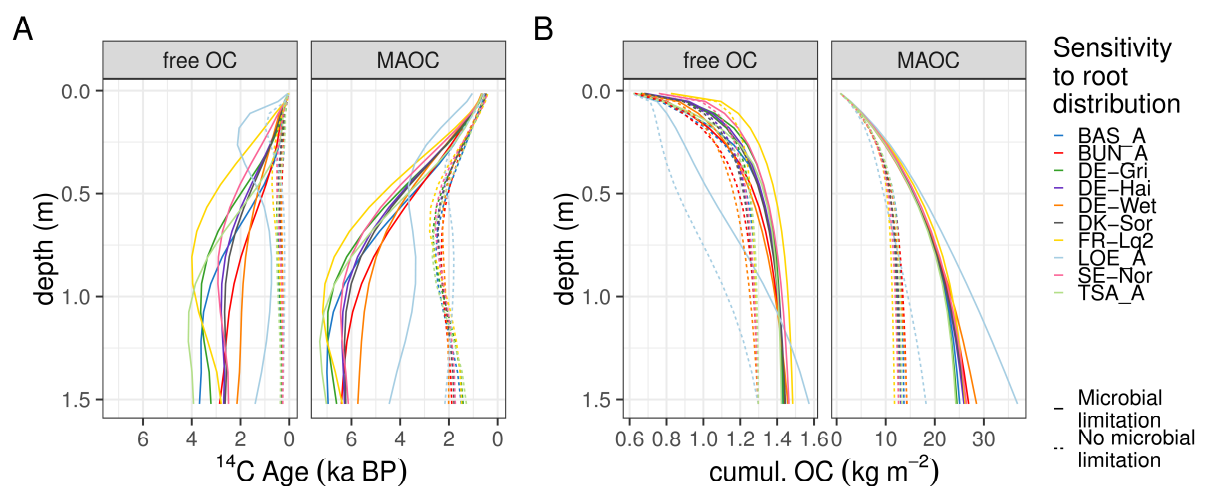
Figure 5-8: Model experiment Root-Distribution–Microbial-Limitation interaction: Combined effect of microbial limitation and root litter input distributions on apparent ^{14}C ages (A) and cumulative stocks (B) of free organic carbon (free OC) and mineral-associated organic carbon (MAOC). Colored lines represent the root litter distributions at the ten different sites. All other site conditions as for TSA_A.

MAAT–Q_{max} interaction

In the MAAT–Q_{max} interaction experiment, the effect of changing the mean annual soil temperature from 5.45 °C to 8.70 °C is responsible for an up to 15% decrease in the MAOC concentrations (Figure

5-9B). The change in temperature makes the largest difference in apparent ^{14}C ages at higher Q_{max}^m values in the deeper subsoil (1 – 1.5 m, Figure 5-9A). Here, apparent ^{14}C ages are up to 300 years older in the 5.45 °C model experiment than in the 8.70 °C model experiment. For free OC the temperature effect on ^{14}C ages can be more variable. In the top meter, apparent ^{14}C ages are generally older for the 5.45 °C model experiment compared to the 8.70 °C model experiment for free OC. The model experiments with a higher Q_{max}^m generally show higher differences in ^{14}C ages between the two temperatures for MAOC. These differences are the result of the interplay of the lower temperature sensitivity for adsorption and desorption with the temperature sensitivity of microbial biomass death which provides microbial residues for adsorption (Table 5-1).
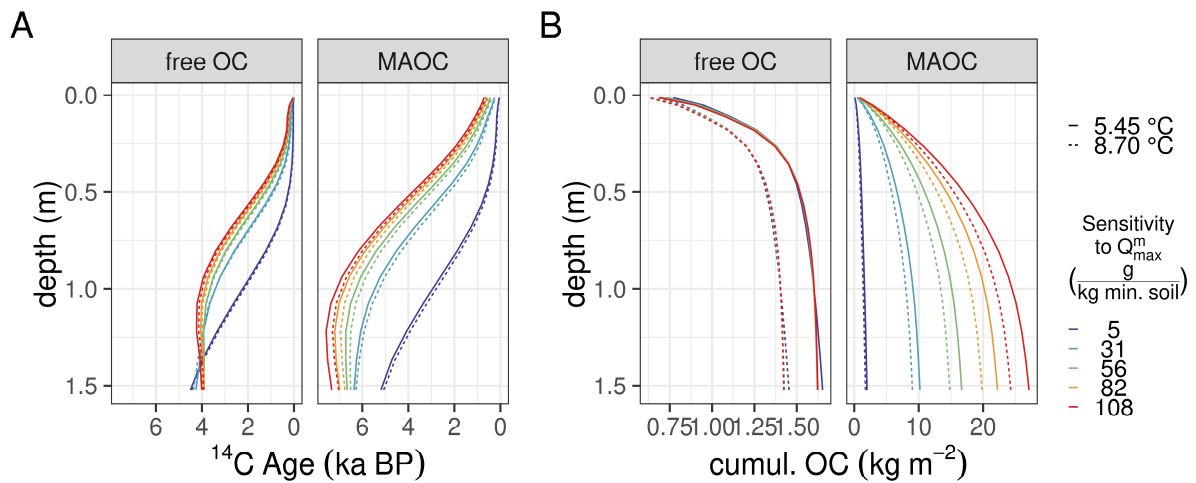
Figure 5-9: Model experiment MAAT–Q_{max} interaction: Combined effect of sorption capacity (Q_{max}^m) and changes in mean annual temperature (5.45 and 8.70 °C) on apparent ^{14}C ages (A) and cumulative stocks (B) of free organic carbon (free OC) and mineral-associated organic carbon (MAOC). Colored lines represent simulations with varying Q_{max}^m. Except for temperature and Q_{max}^m, simulations were performed using the forcing and parameters of TSA_A.

The lower temperature sensitivity of adsorption and desorption also becomes evident when calculating apparent Q_{10} values based on the differences in SOC concentrations between the 8.70 °C and 5.45 °C mean annual temperature model experiment (Figure 5-10, Table 5-1). The apparent Q_{10} values were calculated as $Q_{10} = \left(\frac{SOC_{5.45\,°C}}{SOC_{8.70\,°C}} \right)^{\frac{10}{8.70-5.45}}$ (Todd-Brown et al., 2018), where $SOC_{5.45\,°C}$ and $SOC_{8.70\,°C}$ are the overall SOC concentrations at the respective temperatures. Overall, apparent Q_{10} values are lower at higher Q_{max}^m values when integrated over the whole profile up to depth z (Figure

5-10B). In the organic layer, apparent Q_{10} values are generally low but increase to a maximum in the topsoil (Figure 5-10A). The maximum of apparent Q_{10} values (Figure 5-10A) throughout the profile is deeper when Q_{max}^m values are higher. In the subsoil, apparent Q_{10} values decrease again with a general tendency for stronger decreases when Q_{max}^m is lower (Figure 5-10A, except for Q_{max}^m of 5 g (kg min. soil)$^{-1}$).
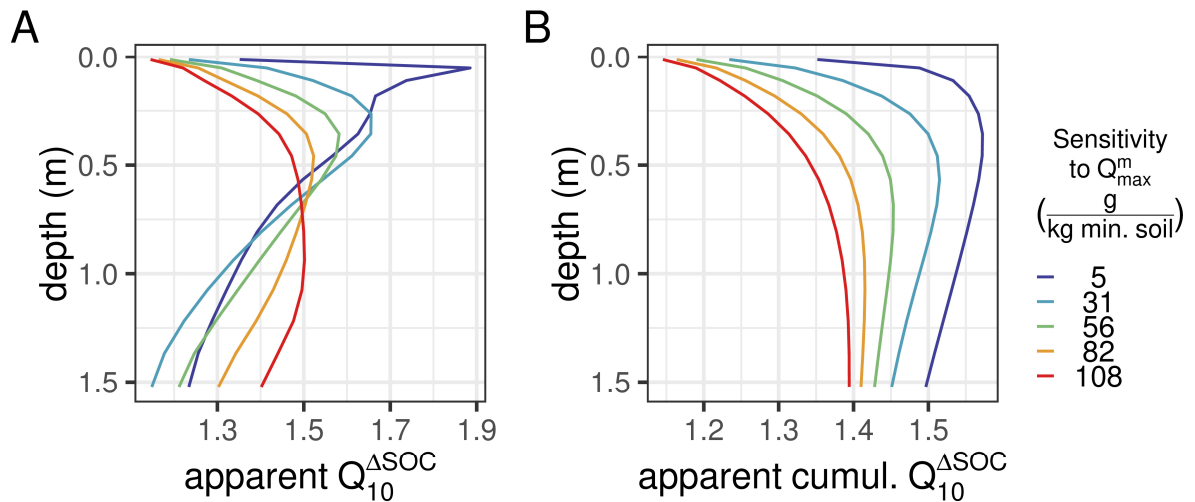
Figure 5-10: Model experiment MAAT–Q_{max} interaction: Effect of sorption capacity (Q_{max}^m) on apparent Q_{10} values in depth z (A) and cumulatively up to depth z (B). Apparent Q_{10} values were calculated from SOC concentration differences between the 5.45 °C and 8.70 °C model experiment. Except for temperature and Q_{max}^m, simulations were performed using the forcing and parameters of TSA_A.

5.6 Discussion

5.6.1 Maximum sorption capacity for mineral-associated organic matter

We tested the concept of a maximum sorption capacity across multiple sites with different parent materials and, thus, textures and soil mineral compositions. Q_{max}^V generally increases with soil depth since bulk density tends to increase with soil depth (Figure 5-11A, Figure 5-2A). SOM models have mainly adopted a mass-based approach for applying Q_{max} as in the papers by Hassink et al. (1997) and Hassink and Whitmore (1997). Feng et al. (2013) and Beare et al. (2014) refined the concept of a maximum sorption capacity of organic matter on clay and silt particles, but the concept has still not been applied to a soil profile or in a volume-based approach. A notable exception is the work of Robertson et al. (2018), however without building a vertically explicit model. Arguably, the

representation of Q_{max}^m as a function of clay plus < 20 µm silt content is empirical, yet plausible since the specific surface area scales with clay content. Changes of Q_{max}^m with depth should generally be based on observed changes of variables with depth, such as changes in texture (Feng et al., 2013), pH, or pedogenic oxide-hydroxides (Rasmussen et al., 2018). Changes in soil texture directly relate to differences in specific surface area of the bulk soil. The amount and composition of pedogenic oxide-hydroxides directly relates to the density of hydroxyl-groups that are the prerequisite for forming mineral associations via ligand exchange, while changes in pH affect the protonation of hydroxyl-groups and thereby their propensity for ligand exchange (Kleber et al., 2015). Empirical relationships to derive a maximum sorption capacity from pH and pedogenic oxide-hydroxide do not exist yet, although first strides into that direction have been made (Rasmussen et al., 2018).

While most models of the new class of mineral-microbial models (also our previous version of COMISSION v1.0 in Ahrens et al. (2015)) assume that only DOM is forming mineral-associations, it is evident that microbial necromass can form mineral associations as well (Miltner et al., 2012; Cotrufo et al., 2015; Bradford et al., 2016; Kopittke et al., 2018). The other SOC profile model that employs a Langmuir-like approach of a maximum sorption capacity and sorption of microbial necromass, the BAMS1 model by Dwivedi et al. (2017), calibrated site-specific depth-declines of specific surface area. Dwivedi et al. (2017) use specific surface area as a proxy for maximum sorption capacity. Maximum sorption capacities that are fitted per site as in Dwivedi et al. (2017) could provide an alternative strategy for making models scalable. For this purpose, general relationships of fitted specific surface areas and depth-declines of sorption capacities with environmental covariates need to be derived.

For COMISSION v2.0, we tested the effect of the characteristic exponential depth-declines that Dwivedi et al. (2017) calibrated (Figure 5-12A). The exponential decrease is described with an exponential function of the form $\exp(-\gamma \cdot z)$. γ is the depth-decline rate. Here, we use the texture-based Q_{max}^m and its changes with depth from the TSA_A site. For the scenario without a depth decline, i.e., $\gamma = 0$, the decrease in Q_{max}^V in the subsoil is the result of the texture profile at this site (Figure 5-12B). For $\gamma \in \{0.5, 0.75, 2.25\}$ the 50% decline depths (the depth at which Q_{max}^m declines to 50%) are 1.39 m, 0.92 m, and 0.31 m. Only the most extreme γ corresponding to a 50% decline depth of 0.31 m has a substantial effect on apparent ^{14}C ages (Figure 5-12C). The effect on overall MAOC stocks, however, is pronounced for all $\gamma > 0$ as it directly decreases the amount of potential MAOC stocks in the respective layers (Figure 5-12D). From this experiment, we conclude that depth-declines of maximum sorption capacity may be relevant to correct for site-conditions that would lead

to lower Q_{max}^m values than predicted by texture changes with depth. At the LOE_A site, this could alleviate problems of overestimated MAOC stocks (Figure 5-2A, Supplementary figure 2). Nevertheless, we propose to strive for generality and try to avoid site-specific and/or depth-dependent scaling parameters.

We have outlined different ideas on how to prescribe sorption capacities throughout soil profiles based on soil texture, Q_{max} (this study), batch sorption experiments, $q_{max, batch}$ (Ahrens et al., 2015), and site-specific fitting of specific surface area (Dwivedi et al., 2017). The definition of Q_{max} is scalable, i.e., it can be employed in global scale modeling efforts. The depth distribution of Q_{max} (Figure 5-11A), however, contradicts the depth distribution of $q_{max, batch}$ from batch sorption experiments (Figure 5-11B) and the depth declines of sorption capacity calibrated by Dwivedi et al. (2017) (Figure 5-12A,B).

The ability of the COMISSION v2.0 model to reproduce both SOC and ^{14}C profiles reasonably well with one universal parameter set shows that the model structure and the representation of a maximum sorption capacity is a promising step towards explaining the long-term persistence of SOM as demonstrated in Figure 5-5. The benefit of a model that does not resort to parameters that are fitted per site lies in the possibility of confronting the model with new datasets and go to larger scales.
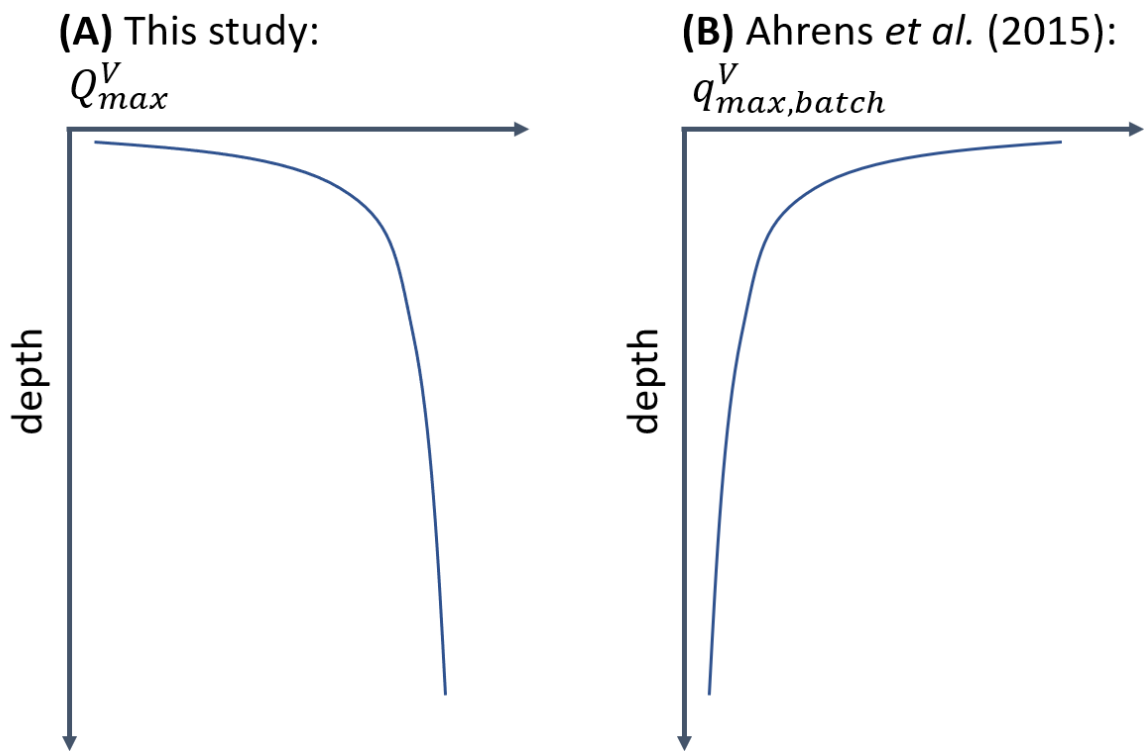
Figure 5-11: Conceptual differences in representing a maximum sorption capacity in current soil profile models. (A) shows the approach used in this study. The maximum sorption capacity is a function of the clay plus silt (< 20 µm) content. Q_{max}^V thereby increases with soil depth. (B) The maximum sorption capacity decreases with soil depth based on measurements from batch sorption, $q_{max,batch}^V$ experiments as in Ahrens et al. (2015).
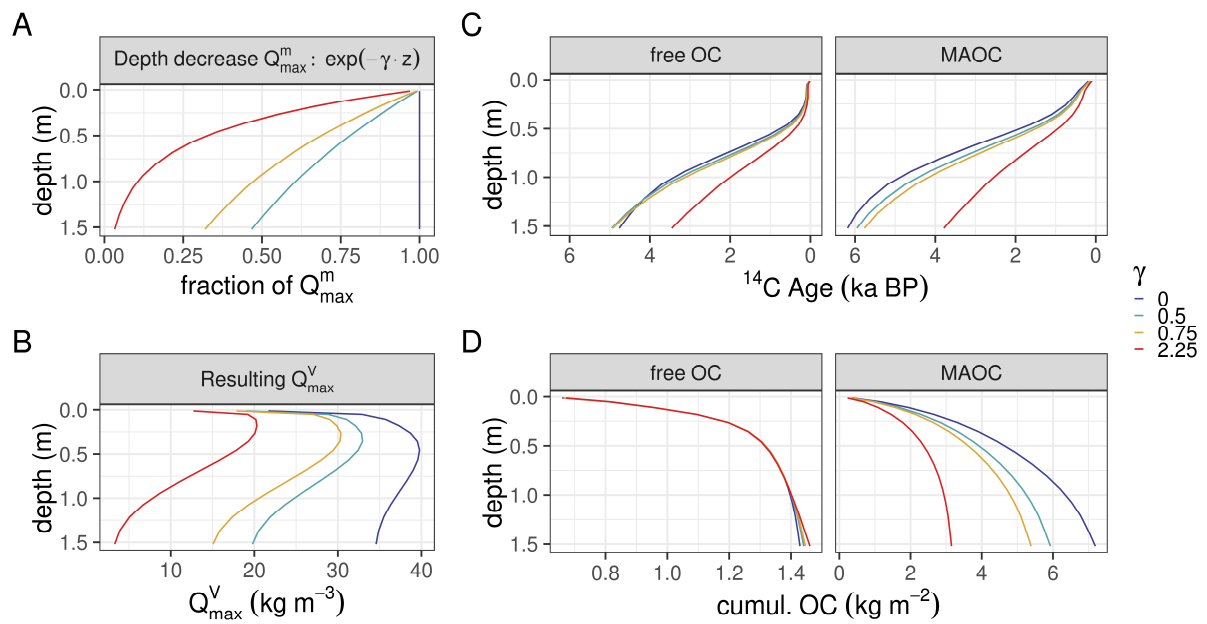
Figure 5-12: Effect of postulated decreases of sorption capacity with depth by Dwivedi et al. (2017) simulated for the TSA_A site. For $\gamma = 0$ the depth distribution of Q_{max}^m is purely dependent on the changes in texture with depth at the TSA_A site. $\gamma > 0$ describes an additional decrease in sorption capacity with soil depth.

5.6.2 Desorption times in COMISSION v2.0

In the previous version of COMISSION (v1.0, Ahrens et al., 2015), we used batch sorption experiments to parameterize $q_{max, batch}$, and only DOC was assumed to form organo-mineral associations. In that version, we calibrated desorption rates that equate to desorption times of 265 years to be able to reproduce the ^{14}C depth-profile of a Haplic Podzol. We define desorption time as the inverse of the desorption rate. While this is fast compared to the slow and passive pools in conventional SOC decomposition models, for COMISSION v2.0, we chose informative initial bounds of maximum desorption times of 6 years. These bounds are based on the maximum desorption times of 3 years found in the batch sorption experiments by Van de Weerd et al. (2002). We employed a safety/uncertainty factor of 100% to allow an upper bound of 6 years. The multi-site calibration of the COMISSION v2.0 model yielded desorption times of 5.4 hours for DOC and 61 days for microbial necromass. Here, one must keep in mind that the definition of DOC in COMISSION is not the same as in measurements in the field with a filtration through a <0.45 µm filter (Borken et al., 2011). DOC in COMISSION rather represents monomers or dimers that are smaller than the 600 Dalton boundary of assimilable organic carbon (Lehmann and Kleber, 2015). Smaller molecules have a much higher probability of getting desorbed because of the smaller number of binding sites with mineral surfaces

(Kaiser et al., 1997). The larger molecular size would also explain the much slower desorption rates for microbial residues. These possess a multitude of binding sites that would need to detach simultaneously for the molecule to desorb. Van de Weerd et al. (2002) reports desorption times of 3-4 hours for molecules with molecular weights of 1500 Da, desorption times between 22 and 69 days for molecules with a molecular weight of 50 kDa, and desorption times between 703 and 996 days for molecules with a molecular weight of 500 kDa. This tendency agrees with the longer calibrated desorption times of microbial residues compared to DOC.

5.6.3 Combined effect of sorption and microbial activity

The model experiments (Figure 5-5 - Figure 5-9) have shown the importance of Q_{max} for SOC stocks and radiocarbon contents. Varying Q_{max} from a sandy to a clayey-silty soil increases SOC stocks by orders of magnitude and increases ^{14}C ages by more than 4000 years in the subsoil (0.5 m) and more than 5000 years in the deep subsoil (1.5 m) when keeping all other site conditions equal (Supplementary figure 6). This model experiment demonstrates that changes in Q_{max} can have large impacts on SOC stocks and ^{14}C ages. The model experiments have also demonstrated that the combination of sorption on mineral surfaces and microbial depolymerization limitation is responsible for the continued increase in ^{14}C ages from 0.2 m to 1.5 m (Supplementary figure 5). Microbial depolymerization limitation alone, i.e., at a low availability of sorption sites as with $Q_{max}^{m} = 5$ g (kg mineral soil)$^{-1}$, does not explain differences in ^{14}C age gradients between sites in COMISSION v2.0. On the other hand, without microbial depolymerization limitation and only considering the sorption effect would lead to constant or decreasing ^{14}C age-depth gradients from 0.5 m onwards (Figure 5-5A, no microbial limitation).

The changes in Q_{max} that we used in the model experiments show that local differences in soil properties can induce substantial differences in apparent ^{14}C ages. In a mechanistic model, such as COMISSION, this model experiment can highlight the importance of pedogenic factors for explaining ^{14}C age depth-gradients compared to climate (Figure 5-9). This result generally agrees with the findings of Mathieu et al. (2015) who analyzed a global database of radiocarbon profiles and found that the ^{14}C content in the deep soil has a strong dependence on pedogenic traits, such as clay content and mineralogy. Compared to the statistical approach of Mathieu et al. (2015), our approach has the advantage that our mechanistic model does not include depth as an explanatory variable, but that the ^{14}C age-depth profile emerges from the interacting mechanisms (transport, ad-/desorption, microbial turnover) implemented in COMISSION.

The depth-integrated apparent Q_{10} emerges from the interactions of different temperature sensitivities prescribed for COMISSION v2.0 (Table 5-1) and the relevant processes throughout the profile (Figure 5-10). The apparent Q_{10} values (Figure 5-10) were calculated from long-term SOC differences under different mean annual temperatures and are the result of the interplay of sorptive and microbial processes. The procedure of calculating apparent Q_{10} values from SOC differences is different from incubation experiments such as Gentsch et al. (2018) which typically extend from weeks to several months and calculate apparent Q_{10} values based on CO_2 respiration. It has to be noted that calculating the apparent Q_{10} based on SOC differences is the result of a model experiment and cannot necessarily be compared to Q_{10} values derived in incubation studies. Only temperature and Q^m_{max} are changing in the model experiment but not the litter inputs which would lead to a different emergent Q_{10} value. In COMISSION v2.0, the long-term apparent Q_{10} values reflect the temperature sensitivities of processes that lead to the formation of MAOC (Q_{10} of 1.34 for desorption and Q_{10} of 1.08 for adsorption) but not necessarily the Q_{10} values of more short-term microbial processes (Q_{10} values of 1.98 to 2.16) that dominate in incubation studies (Table 5-1). In the organic layer and upper mineral soil, volumetric SOC concentrations are close to their physical maximum, so that apparent Q_{10} values for the temperature difference (3.25 K) of this model experiment are close to 1 (Figure 5-10). Apparent Q_{10} values from incubations of SOC from the organic layer or upper topsoil based on CO_2 evolution (Gentsch et al., 2018), would rather reflect the temperature sensitivity of microbial processes (Table 5-1). The depth of the apparent Q_{10} maximum (Figure 5-10A) is related to when desorption processes dominate over adsorption processes (Supplementary figure 7), i.e., the Q_{10} value of 1.34 for desorption (Table 5-1) is responsible for the maximum of the apparent Q_{10} values. Since Q^V_{max} is close to saturation in the upper mineral soil, the temperature sensitivity of desorption emerges as the overall long-term Q_{10} value of SOC formation. In the subsoil, Q^V_{max} is far from saturation, so that the temperature sensitivity of adsorption emerges as the dominant factor for the long-term Q_{10} value of SOC formation (Table 5-1, Q_{10} value of 1.08, Figure 5-10A). The interplay of sorptive and microbial processes is evident from the higher apparent depth-integrated Q_{10} values when Q^m_{max} is lower (Figure 5-10B), i.e., the contribution of free OC to SOC is higher and thereby the overall apparent temperature sensitivity is more influenced by the higher Q_{10} values of the microbial processes (Table 5-1, Q_{10} values of 1.98 to 2.16).

Sorption on mineral surfaces is responsible for a more effective storage of belowground litter inputs compared to aboveground litter inputs in COMISSION v2.0 (Figure 5-6). This model experiment is in line with recent experimental findings by Sokol et al. (2019) that belowground carbon inputs are

stored 190% more efficiently than aboveground carbon inputs. In our model experiments with COMISSION v2.0, however, only between 13.9% (at $Q_{max}^m = 31$ g/kg) and 8.6% (at $Q_{max}^m = 108$ g/kg) more SOC is stored throughout the profile when 80% litter inputs are belowground compared to 38% of litter inputs belowground. In the situation of a low sorption capacity (at $Q_{max}^m = 5$ g/kg), there would still be 8.1% more organic carbon throughout the profile in a model experiment with 80% litter inputs belowground compared to a model experiment with only 38% inputs belowground.

The model experiments with root distributions from the ten different sites show that it is less important how shallow or deep root distributions are, when the capacity for mineral-associations is stronger (Figure 5-7). The matrix protection effect exceeds the direct input or dilution effect of root litter with increasing sorption capacity Q_{max}. This dominance of the matrix protection effect does not exclude the possibility that particular root distributions can have an overwhelming effect on ^{14}C ages, e.g., the root distribution from the LOE_A site. Similarly, the direct input or dilution effect of root distributions is of minor importance compared to the indirect input effect of root distributions which results from substrate limitation of microbial decomposition (Figure 5-8A).

By employing Michaelis-Menten kinetics for describing the dependence of depolymerization on microbial dynamics, we inherently prescribe a depth effect in the model due to the change of root density with soil depth, which is commonly interpreted as an energy limitation or substrate limitation of microbial decomposition. Using Michaelis-Menten kinetics to describe energy limitation, however, might already be a lumped description of microbial hotspots and 'dead' soil as summarized by Kuzyakov and Blagodatskaya (2015). Our finding that energy limitation is responsible for the continued increase in apparent ^{14}C ages with soil depth (Figure 5-5A) is in line with results from Fontaine et al. (2007) and Wild et al. (2014), which suggest that substrate or energy scarcity limit SOC turnover in mineral subsoil horizons, but are of lesser importance in topsoil horizons (Figure 5-5). For the DE-Gri site Heitkötter and Marschner (2018) found that outside of microbial hotspots, SOC turnover in subsoils is limited by substrate availability, while most SOC turnover in the subsoil is concentrated in just <1 to 10% of the soil. Sokol et al. (2019) argued that it matters whether litter inputs occur in microbial hotspots with high microbial density or 'dead' soil, where DOC sorption will prevail over microbial processing and subsequent sorption of microbial necromass. The COMISSION model does not explicitly distinguish between microbial hotspots, which receive frequent input by root litter or DOC transport, and the bulk soil, in which the activity of microorganisms is limited

because of the lack of frequent input of fresh substrate. This distinction, however, may be of importance as indicated by modelling and experimental results of Sulman et al. (2014), Heitkötter and Marschner (2018), and Sokol and Bradford (2019).

5.6.4   Caveats and outlook

In the COMISSION model, we do not distinguish between fungal and bacterial functional groups neither regarding their function in SOM decomposition nor regarding their function in SOM formation due to the sorption behavior of their residues. This distinction could be especially important because of the mycelial nature of resource acquisition of fungi. Their mycelia do not require the diffusive passing of space between enzymatic cleavage of litter and SOM into assimilable molecular sizes and transport to the bacterial transporter enzymes (Harms et al., 2011). In the current version of COMISSION, microorganisms are assumed to be sessile and acquire substrate through extra-cellular enzyme diffusion. Especially for modelling the response of decomposition to drought, the distinction into fungal and bacterial groups will be highly relevant. However, as shown by this model-data integration, the moisture response of decomposition could not be well constrained with the data at hand. The modelling of high-resolution heterotrophic respiration measurements might be able to constrain these parameters and provide insights whether this level of detail is required for COMISSION. Apart from the differences in resource acquisition strategies between bacterial and fungal groups, consequences for speed of decomposition (Wieder et al., 2015) and pH effects on bacterial and fungal growth (Rousk et al., 2009), carbon use efficiencies and C/N ratios of residues of fungal and bacterial groups are different. These differences would result in different relative amounts of microbial residues available for sorption to mineral surfaces along the soil profile.

Using the definition of Feng et al. (2013), Q_{max}^m should not be affected much by aggregation and mineral surfaces properties. The 20 µm boundary excludes larger microaggregates (defined as $53-250$ µm aggregates by Six et al. (2002)). Feng et al. (2013) note that the 20 µm boundary additionally alleviates problems with potential large-silt size aggregates ($20-50$ µm). Q_{max}^m could be improved by including mineral surface properties, but currently, approaches do not exist that would allow for an independent derivation of a Q_{max}^m that would account for that.

In future versions of COMISSION, we plan to also represent occlusion in microaggregates (< 250 µm). We envision an approach similar to the MILLENNIAL model of Abramoff et al. (2018), who devised an

'maximum capacity of C in soil aggregates', A_{max}. Ideally, general relationships for a 'maximum capacity of C in soil aggregates' for different soils can be established in a similar fashion as in Feng et al. (2013) for Q_{max}^m. Castellano et al. (2015) proposed that both mineral-associated organic matter (as done in COMISSION v2.0) and microaggregate-occluded organic matter (not yet considered in COMISSION v2.0) could show a saturation behavior.

5.7   Conclusions

In this study, we have shown that using the relationship between the clay plus silt (< 20 μm) content and the maximum amount of MAOC provides a way forward to implement the effects of sorptive stabilization in models that is applicable across sites of contrasting climate, soil texture, and mineralogy. It is paramount to translate the mass-based maximum sorption capacity Q_{max}^m into a volumetric maximum sorption capacity Q_{max}^V to ensure a mechanistic basis for sorptive processes in SOC profile models.

Model experiments have shown that varying Q_{max} can induce large changes in apparent ^{14}C ages and SOC stocks. It is, however, the combination of energy or substrate limitation of microorganisms in the subsoil and Q_{max} that is responsible for the formation of ^{14}C age-depth gradients from the topsoil to the subsoil. Belowground inputs are stored more efficiently than aboveground inputs due to the formation of mineral-associations. Higher belowground inputs, on the other hand, lead to a rejuvenation of ^{14}C ages. Root distributions lead to differences in ^{14}C ages mainly due to microbial substrate limitation rather than through the input or dilution effect with modern [14]C. Lower mean annual temperatures lead to older ^{14}C ages, but the temperature range across the ten sites of 3.25 K could only lead to differences in apparent ^{14}C ages of, at most, 300 years over the whole profile in conjunction with a low sorption capacity. The differences in Q_{max}^m across the sites alone would lead to differences of up to 2000 years over the whole profile. The differences in Q_{max}^m across sites in combination with energy limitation would even lead to differences in apparent ^{14}C ages of 4000 years over the whole profile.

Overall, it must be emphasized that the implementation of sorptive processes in vertical SOC models is still in an exploratory phase that represents the large uncertainty in understanding these processes. Empiricists and modelers must work hand in hand to refine the representation and parameterization of sorptive processes in models.

5.8 Acknowledgments

5.9 References

Abramoff, R., Xu, X.F., Hartman, M., O'Brien, S., Feng, W.T., Davidson, E., Finzi, A.C., Moorhead, D., Schimel, J., Torn, M., Mayes, M.A., 2018. The Millennial model: in search of measurable pools and transformations for modeling soil carbon in the new century. Biogeochemistry 137, 51-71.

Adams, W., 1973. The effect of organic matter on the bulk and true densities of some uncultivated podzolic soils. Journal of Soil Science 24, 10-17.

Ahrens, B., Braakhekke, M.C., Guggenberger, G., Schrumpf, M., Reichstein, M., 2015. Contribution of sorption, DOC transport and microbial interactions to the 14C age of a soil organic carbon profile: Insights from a calibrated process model. Soil Biology and Biochemistry 88, 390-402.

Allison, S.D., Wallenstein, M.D., Bradford, M.A., 2010. Soil-carbon response to warming dependent on microbial physiology. Nature Geosci 3, 336-340.

Amelung, W., Brodowski, S., Sandhage-Hofmann, A., Bol, R., 2008. Combining biomarker with stable isotope analyses for assessing the transformation and turnover of soil organic matter. Advances in agronomy 100, 155-250.

Angst, G., John, S., Mueller, C.W., Kögel-Knabner, I., Rethemeyer, J., 2016a. Tracing the sources and spatial distribution of organic carbon in subsoils using a multi-biomarker approach. Scientific Reports 6, 29478.

Angst, G., Kögel-Knabner, I., Kirfel, K., Hertel, D., Mueller, C.W., 2016b. Spatial distribution and chemical composition of soil organic matter fractions in rhizosphere and non-rhizosphere soil under European beech (Fagus sylvatica L.). Geoderma 264, 179–187.

Angst, G., Messinger, J., Greiner, M., Häusler, W., Hertel, D., Kirfel, K., Kögel-Knabner, I., Leuschner, C., Rethemeyer, J., Mueller, C.W., 2018. Soil organic carbon stocks in topsoil and subsoil controlled by parent material, carbon input in the rhizosphere, and microbial-derived compounds. Soil Biology and Biochemistry 122, 19–30.

Beare, M.H., McNeill, S.J., Curtin, D., Parfitt, R.L., Jones, H.S., Dodd, M.B., Sharp, J., 2014. Estimating the organic carbon stabilisation capacity and saturation deficit of soils: a New Zealand case study. Biogeochemistry, 1-17.

Bloom, A.A., Exbrayat, J.-F., van der Velde, I.R., Feng, L., Williams, M., 2016. The decadal state of the terrestrial carbon cycle: Global retrievals of terrestrial carbon allocation, pools, and residence times. Proceedings of the National Academy of Sciences 113, 1285-1290.

Blume, H.-P., Brümmer, G.W., Fleige, H., Horn, R., Kandeler, E., Kögel-Knabner, I., Kretzschmar, R., Stahr, K., Wilke, B.-M., 2015. Scheffer/Schachtschabel Soil Science. Springer.

Borken, W., Ahrens, B., Schulz, C., Zimmermann, L., 2011. Site-to-site variability and temporal trends of DOC concentrations and fluxes in temperate forest soils. Global Change Biology 17, 2428-2443.

Bradford, M.A., Wieder, W.R., Bonan, G.B., Fierer, N., Raymond, P.A., Crowther, T.W., 2016. Managing uncertainty in soil carbon feedbacks to climate change. Nature Clim. Change 6, 751-758.

Campbell, E.E., Parton, W.J., Soong, J.L., Paustian, K., Hobbs, N.T., Cotrufo, M.F., 2016. Using litter chemistry controls on microbial processes to partition litter carbon fluxes with the Litter Decomposition and Leaching (LIDEL) model. Soil Biology and Biochemistry 100, 160-174.

Castellano, M.J., Mueller, K.E., Olk, D.C., Sawyer, J.E., Six, J., 2015. Integrating plant litter quality, soil organic matter stabilization, and the carbon saturation concept. Glob Chang Biol 21, 3200-3209.

Coleman, K., Jenkinson, D., 1999. ROTHC-26.3. A model for the turnover of carbon in soils. Herts, Rothamsted Research, Harpenden, Hertfordshire, UK.

Conant, R.T., Ryan, M.G., Ågren, G.I., Birge, H.E., Davidson, E.A., Eliasson, P.E., Evans, S.E., Frey, S.D., Giardina, C.P., Hopkins, F.M., Hyvönen, R., Kirschbaum, M.U.F., Lavallee, J.M., Leifeld, J., Parton, W.J., Megan Steinweg, J., Wallenstein, M.D., Martin Wetterstedt, J.Å., Bradford, M.A., 2011. Temperature and soil organic matter decomposition rates – synthesis of current knowledge and a way forward. Global Change Biology 17, 3392-3404.

Cornwell, W.K., Cornelissen, J.H.C., Allison, S.D., Bauhus, J., Eggleton, P., Preston, C.M., Scarff, F., Weedon, J.T., Wirth, C., Zanne, A.E., 2009. Plant traits and wood fates across the globe: rotted, burned, or consumed? 15, 2431-2449.

Cotrufo, M.F., Soong, J.L., Horton, A.J., Campbell, E.E., Haddix, M.L., Wall, D.H., Parton, W.J., 2015. Formation of soil organic matter via biochemical and physical pathways of litter mass loss. Nature Geoscience.

Creamer, C.A., Foster, A.L., Lawrence, C., McFarland, J., Schulz, M., Waldrop, M.P., 2019. Mineralogy dictates the initial mechanism of microbial necromass association. Geochimica et Cosmochimica Acta 260, 161-176.

Davidson, E.A., Janssens, I.A., 2006. Temperature sensitivity of soil carbon decomposition and feedbacks to climate change. Nature 440, 165-173.

Dwivedi, D., Riley, W.J., Torn, M.S., Spycher, N., Maggi, F., Tang, J.Y., 2017. Mineral properties, microbes, transport, and plant-input profiles control vertical distribution and age of soil carbon stocks. Soil Biology and Biochemistry 107, 244-259.

Eisenstat, S., Gursky, M., Schultz, M., Sherman, A., 1977. Yale sparse matrix package. II. The nonsymmetric codes. DTIC Document.

Eisenstat, S.C., Gursky, M., Schultz, M.H., Sherman, A.H., 1982. Yale sparse matrix package I: The symmetric codes. International Journal for Numerical Methods in Engineering 18, 1145-1151.

Federer, C.A., Turcotte, D.E., Smith, C.T., 1993. The organic fraction–bulk density relationship and the expression of nutrient content in forest soils. Canadian Journal of Forest Research 23, 1026-1032.

Feigenwinter, C., Bernhofer, C., Eichelmann, U., Heinesch, B., Hertel, M., Janous, D., Kolle, O., Lagergren, F., Lindroth, A., Minerbi, S., Moderow, U., Mölder, M., Montagnani, L., Queck, R., Rebmann, C., Vestin, P., Yernaux, M., Zeri, M., Ziegler, W., Aubinet, M., 2008. Comparison of horizontal and vertical advective CO_2 fluxes at three forest sites. 148, 12-24.

Feng, W., Plante, A.F., Six, J., 2013. Improving estimates of maximal organic carbon stabilization by fine soil particles. Biogeochemistry 112, 81-93.

Fontaine, S., Barot, S., Barre, P., Bdioui, N., Mary, B., Rumpel, C., 2007. Stability of organic carbon in deep soil layers controlled by fresh carbon supply. Nature 450, 277-280.

Forkel, M., Drüke, M., Thurner, M., Dorigo, W., Schaphoff, S., Thonicke, K., Von Bloh, W., Carvalhais, N., 2019. Constraining modelled global vegetation dynamics and carbon turnover using multiple satellite observations. Scientific Reports 9.

Gentsch, N., Wild, B., Mikutta, R., Capek, P., Diakova, K., Schrumpf, M., Turner, S., Minnich, C., Schaarschmidt, F., Shibistova, O., Schnecker, J., Urich, T., Gittel, A., Santruckova, H., Barta, J., Lashchinskiy, N., Fuss, R., Richter, A., Guggenberger, G., 2018. Temperature response of permafrost soil carbon is attenuated by mineral protection. Glob Chang Biol 24, 3401-3415.

Graven, H.D., 2015. Impact of fossil fuel emissions on atmospheric radiocarbon and various applications of radiocarbon over this century. Proceedings of the National Academy of Sciences 112, 9542-9545.

Guggenberger, G., Kaiser, K., 2003. Dissolved organic matter in soil: challenging the paradigm of sorptive preservation. Geoderma 113, 293-310.

Hagerty, S.B., van Groenigen, K.J., Allison, S.D., Hungate, B.A., Schwartz, E., Koch, G.W., Kolka, R.K., Dijkstra, P., 2014. Accelerated microbial turnover but constant growth efficiency with warming in soil. Nature Climate Change 4, 903-906.

Harms, H., Schlosser, D., Wick, L.Y., 2011. Untapped potential: exploiting fungi in bioremediation of hazardous chemicals. Nature Reviews Microbiology 9, 177-192.

Hassink, J., Whitmore, A.P., 1997. A model of the physical protection of organic matter in soils. Soil Science Society of America Journal 61, 131-139.

Hassink, J., Whitmore, A.P., Kubát, J., 1997. Size and density fractionation of soil organic matter and the physical capacity of soils to protect organic matter. European Journal of Agronomy 7, 189-199.

Heinze, S., Ludwig, B., Piepho, H.-P., Mikutta, R., Don, A., Wordell-Dietrich, P., Helfrich, M., Hertel, D., Leuschner, C., Kirfel, K., Kandeler, E., Preusser, S., Guggenberger, G., Leinemann, T., Marschner, B., 2018. Factors controlling the variability of organic matter in the top- and subsoil of a sandy Dystric Cambisol under beech forest. Geoderma 311, 37–44.

Heitkötter, J., Marschner, B., 2018. Is There Anybody Out There?: Substrate Availability Controls Microbial Activity outside of Hotspots in Subsoils. Soil Systems 2, 35.

Hengenius, J.B., Gribskov, M., Rundell, A.E., Umulis, D.M., 2014. Making models match measurements: Model optimization for morphogen patterning networks. 35, 109-123.

Hindmarsh, A.C., 1983. ODEPACK, A Systematized Collection of ODE Solvers, RS Stepleman et al.(eds.), North-Holland, Amsterdam,(vol. 1 of), pp. 55-64. IMACS Transactions on Scientific Computation 1, 55-64.

IUSS Working Group WRB, 2015. World reference base for soil resources 2014, update 2015: International soil classification system for naming soils and creating legends for soil maps. World Soil Resources Reports No. 106, FAO Rome, p. 192.

Kaiser, K., Guggenberger, G., Haumaier, L., Zech, W., 1997. Dissolved organic matter sorption on sub soils and minerals studied by 13C-NMR and DRIFT spectroscopy. 48, 301-310.

Kirfel, K., Heinze, S., Hertel, D., Leuschner, C., 2019. Effects of bedrock type and soil chemistry on the fine roots of European beech - A study on the belowground plasticity of trees. Forest Ecology and Management 444, 256-268.

Kleber, M., Eusterhues, K., Keiluweit, M., Mikutta, C., Mikutta, R., Nico, P.S., 2015. Mineral–organic associations: Formation, properties, and relevance in soil environments. Adv. Agron 130, 1-140.

Knauer, J., Werner, C., Zaehle, S., 2015. Evaluating stomatal models and their atmospheric drought response in a land surface scheme: A multibiome analysis. Journal of Geophysical Research: Biogeosciences 120, 1-18.

Kopittke, P.M., Dalal, R.C., Hoeschen, C., Li, C., Menzies, N.W., Mueller, C.W., 2020. Soil organic matter is stabilized by organo-mineral associations through two key processes: The role of the carbon to nitrogen ratio. Geoderma 357, 113974.

Kopittke, P.M., Hernandez-Soriano, M.C., Dalal, R.C., Finn, D., Menzies, N.W., Hoeschen, C., Mueller, C.W., 2018. Nitrogen-rich microbial products provide new organo-mineral associations for the stabilization of soil organic matter. Glob Chang Biol 24, 1762-1770.

Kuzyakov, Y., Blagodatskaya, E., 2015. Microbial hotspots and hot moments in soil: Concept & review. Soil Biology and Biochemistry 83, 184-199.

Lehmann, J., Kleber, M., 2015. The contentious nature of soil organic matter. Nature 528, 60-68.

Liang, C., Schimel, J., Jastrow, J., 2017. The importance of anabolism in microbial control over soil carbon storage. Nature Microbiology 2, 17105.

Mathieu, J.A., Hatte, C., Balesdent, J., Parent, E., 2015. Deep soil carbon dynamics are driven more by soil type than by climate: a worldwide meta-analysis of radiocarbon profiles. Glob Chang Biol 21, 4278-4292.

Mebane Jr, W.R., Sekhon, J.S., 2011. Genetic optimization using derivatives: the rgenoud package for R. Journal of Statistical Software 42, 1-26.

Miltner, A., Bombach, P., Schmidt-Brücken, B., Kästner, M., 2012. SOM genesis: microbial biomass as a significant source. Biogeochemistry 111, 41-55.

Moeys, J., 2018. The soil texture wizard: R functions for plotting, classifying, transforming and exploring soil texture data.

Parton, W.J., Schimel, D.S., Cole, C.V., Ojima, D.S., 1987. Analysis of factors controlling soil organic-matter levels in great-plains grasslands. Soil Science Society of America Journal 51, 1173-1179.

Rasmussen, C., Heckman, K., Wieder, W.R., Keiluweit, M., Lawrence, C.R., Berhe, A.A., Blankinship, J.C., Crow, S.E., Druhan, J.L., Hicks Pries, C.E., Marin-Spiotta, E., Plante, A.F., Schädel, C., Schimel, J.P., Sierra, C.A., Thompson, A., Wagai, R., 2018. Beyond clay: towards an improved set of variables for predicting soil organic matter content. Biogeochemistry 137, 297-306.

Reimer, P.J., Bard, E., Bayliss, A., Beck, J.W., Blackwell, P.G., Ramsey, C.B., Buck, C.E., Cheng, H., Edwards, R.L., Friedrich, M., 2013. IntCal13 and Marine13 radiocarbon age calibration curves 0–50,000 years cal BP. Radiocarbon 55, 1869-1887.

Riley, W.J., Maggi, F., Kleber, M., Torn, M.S., Tang, J.Y., Dwivedi, D., Guerry, N., 2014. Long residence times of rapidly decomposable soil organic matter: application of a multi-phase, multi-component, and vertically resolved model (BAMS1) to soil carbon dynamics. Geosci. Model Dev. 7, 1335-1355.

Robertson, A.D., Paustian, K., Ogle, S., Wallenstein, M.D., Lugato, E., Cotrufo, M.F., 2018. Unifying soil organic matter formation and persistence frameworks: the MEMS model. Biogeosciences Discussions, 1-36.

Rousk, J., Brookes, P.C., Bååth, E., 2009. Contrasting soil pH effects on fungal and bacterial growth suggest functional redundancy in carbon mineralization. Applied and Environmental Microbiology 75, 1589-1596.

Schenk, H.J., Jackson, R.B., 2002. The global biogeography of roots. Ecological Monographs 72, 311-328.

Schimel, J.P., Weintraub, M.N., 2003. The implications of exoenzyme activity on microbial carbon and nitrogen limitation in soil: a theoretical model. Soil Biology and Biochemistry 35, 549-563.

Schmidt, M.W.I., Torn, M.S., Abiven, S., Dittmar, T., Guggenberger, G., Janssens, I.A., Kleber, M., Kogel-Knabner, I., Lehmann, J., Manning, D.A.C., Nannipieri, P., Rasse, D.P., Weiner, S., Trumbore, S.E., 2011. Persistence of soil organic matter as an ecosystem property. Nature 478, 49-56.

Schrumpf, M., Kaiser, K., Guggenberger, G., Persson, T., Kögel-Knabner, I., Schulze, E.D., 2013. Storage and stability of organic carbon in soils as related to depth, occlusion within aggregates, and attachment to minerals. Biogeosciences 10, 1675-1691.

Six, J., Conant, R.T., Paul, E.A., Paustian, K., 2002. Stabilization mechanisms of soil organic matter: Implications for C-saturation of soils. Plant and Soil 241, 155-176.

Sokol, N.W., Bradford, M.A., 2019. Microbial formation of stable soil carbon is more efficient from belowground than aboveground input. Nature Geoscience 12, 46-53.

Sokol, N.W., Sanderman, J., Bradford, M.A., 2019. Pathways of mineral-associated soil organic matter formation: Integrating the role of plant carbon source, chemistry, and point of entry. Glob Chang Biol 25, 12-24.

Sulman, B.N., Phillips, R.P., Oishi, A.C., Shevliakova, E., Pacala, S.W., 2014. Microbe-driven turnover offsets mineral-mediated storage of soil carbon under elevated CO_2. Nature Clim. Change 4, 1099-1102.

Tang, J., Riley, W.J., 2019. Competitor and substrate sizes and diffusion together define enzymatic depolymerization and microbial substrate uptake rates. Soil Biology and Biochemistry 139.

Tang, J.Y., Riley, W.J., 2013. A total quasi-steady-state formulation of substrate uptake kinetics in complex networks and an example application to microbial litter decomposition. Biogeosciences 10, 8329-8351.

Todd-Brown, K., Zheng, B., Crowther, T.W., 2018. Field-warmed soil carbon changes imply high 21st-century modeling uncertainty. Biogeosciences 15, 3659-3671.

Tranter, G., Minasny, B., McBratney, A.B., Murphy, B., McKenzie, N.J., Grundy, M., Brough, D., 2007. Building and testing conceptual and empirical models for predicting soil bulk density. Soil Use and Management 23, 437-443.

Van de Weerd, H., Van Riemsdijk, W., Leijnse, A., 2002. Modeling transport of a mixture of natural organic molecules: Effects of dynamic competitive sorption from particle to aquifer scale. Water Resources Research 38, 1158.

Waksman, S.A., Iyer, K., 1933. Contribution to our knowledge of the chemical nature and origin of humus: IV. Fixation of proteins by lignins and formation of complexes resistant to microbial decomposition. Soil Science 36, 69-82.

Waksman, S.A., Skinner, C.E., 1926. Microörganisms concerned in the decomposition of celluloses in the soil. Journal of bacteriology 12, 57.

Wang, G., Post, W.M., Mayes, M.A., 2013. Development of microbial-enzyme-mediated decomposition model parameters through steady-state and dynamic analyses. Ecological Applications 23, 255-272.

Wang, G., Post, W.M., Mayes, M.A., Frerichs, J.T., Sindhu, J., 2012. Parameter estimation for models of ligninolytic and cellulolytic enzyme kinetics. Soil Biology and Biochemistry 48, 28-38.

Wieder, W.R., Grandy, A.S., Kallenbach, C.M., Taylor, P.G., Bonan, G.B., 2015. Representing life in the Earth system with soil microbial functional traits in the MIMICS model. Geosci. Model Dev. 8, 1789-1808.

Wild, B., Schnecker, J., Alves, R.J.E., Barsukov, P., Bárta, J., Čapek, P., Gentsch, N., Gittel, A., Guggenberger, G., Lashchinskiy, N., Mikutta, R., Rusalimova, O., Šantrůčková, H., Shibistova, O., Urich, T., Watzka, M., Zrazhevskaya, G., Richter, A., 2014. Input of easily available organic C and N stimulates microbial decomposition of soil organic matter in arctic permafrost soil. Soil Biology and Biochemistry 75, 143-151.

Woolf, D., Lehmann, J., 2019. Microbial models with minimal mineral protection can explain long-term soil organic carbon persistence. Sci Rep 9, 6522.

Yan, Z., Bond-Lamberty, B., Todd-Brown, K.E., Bailey, V.L., Li, S., Liu, C., Liu, C., 2018. A moisture function of soil heterotrophic respiration that incorporates microscale processes. Nature Communications 9, 2562.

5.10 Supplement

5.10.1 Model description

The governing equations of the COMISSION v2.0 model are displayed in the following boxes. The terms of the equations are color-coded according to the type of process that is represented. Litter inputs are brown, microbial decomposition losses or transformations are green, transport terms are blue, and sorption is orange. We explain the essential symbols directly under the equation and in section 5.10.3:

C_{CWD}, coarse woody debris

$\dfrac{\partial}{\partial t} C_{CWD} =$	$i_{CWD}(z)$	Litter input	
	$-k_{CWD} \cdot C_{CWD}$	Decomposition loss	
	$-\dfrac{\partial}{\partial z}\left(D_b(z)\dfrac{\partial C_{CWD}}{\partial z}\right) - \dfrac{\partial(\omega(z) \cdot C_{CWD})}{\partial z}$	Transport	

i_{CWD} is the input of coarse woody debris litter in depth z and k_{CWD} is decomposition rate of coarse woody debris (C_{CWD}). $D_b(z)$ is the depth-dependent diffusion coefficient describing bioturbation according to Equation (10) in Jarvis et al. (2010) as $D_b(z) = \dfrac{B}{8 \cdot \rho_B}$. B is further defined in section 5.10.3. ρ_B, the bulk density, varies with depth. $\omega(z)$ is the advection velocity that accounts for the accumulation and decomposition of SOM on top and within the soil profile (see main Material and Methods in the main paper).

$C_{Soluble \atop Litter}$, soluble litter

$\dfrac{\partial}{\partial t} C_{Soluble \atop Litter} =$	$f_{Sol} \cdot i_{Litter}(z)$	Litter input
	$-k_{leach} \cdot C_{Soluble \atop Litter}$	Decomposition loss
	$-\dfrac{\partial}{\partial z}\left(D_b(z) \dfrac{\partial C_{Soluble \atop Litter}}{\partial z} \right) - \dfrac{\partial \left(\omega(z) \cdot C_{Soluble \atop Litter} \right)}{\partial z}$	Transport

f_{Sol} is the fraction of soluble litter of the overall root and leaf litter inputs $i_{Litter}(z)$. k_{leach} is the leaching rate for soluble litter ($C_{Soluble \atop Litter}$).

$C_{Lignified \atop Litter}$, lignified litter

$\dfrac{\partial}{\partial t} C_{Lignified \atop Litter} =$	$(1 - f_{Sol}) \cdot i_{Litter}(z)$	Litter input
	$-V_{max, Lignified \atop Litter} \cdot C_{Lignified \atop Litter} \cdot \dfrac{C_B}{K_{m, Lignified \atop Litter} + C_B}$	Decomposition loss
	$-\dfrac{\partial}{\partial z}\left(D_b(z) \dfrac{\partial C_{Lignified \atop Litter}}{\partial z} \right) - \dfrac{\partial \left(\omega(z) \cdot C_{Lignified \atop Litter} \right)}{\partial z}$	Transport

f_{Sol} is the fraction of soluble litter of the overall root and leaf litter inputs $i_{Litter}(z)$. $V_{max, Lignified \atop Litter}$ is the maximum depolymerization rate of lignified litter $C_{Lignified \atop Litter}$ which is limited by the concentration microorganisms C_B and their half-saturation constant for the depolymerization of lignified litter $K_{m, Lignified \atop Litter}$.

C_{DOM}, dissolved organic matter

$\dfrac{\partial}{\partial t} C_{DOM} =$	$+f_{CWD \to DOM} \cdot k_{CWD} \cdot C_{CWD}$ $+ k_{leach} \cdot C_{Soluble \atop Litter}$ $+ V_{max, Lignified \atop Litter} \cdot C_{Lignified \atop Litter} \dfrac{C_B}{K_{m,Lignified \atop Litter} + C_B}$ $+ V_{max,R} \cdot C_R \cdot \dfrac{C_B}{K_{m,R} + C_B}$ $+ f_{C_B \to C_{DOM}} \cdot r_B \cdot C_B$	Microbial transformation
	$- V_{max,DOM} \cdot C_B \cdot \dfrac{C_{DOM}}{K_{m,DOM} + C_{DOM}}$	Decomposition loss
	$- k_{ads,DOM} \cdot C_{DOM} \cdot \left(Q_{max}^V - \left(C_{Q[DOM]} + C_{Q[R]} \right) \right)$	Adsorption
	$+ k_{des,DOM} \cdot C_{Q[DOM]}$	Desorption
	$- \dfrac{\partial(v(z) \cdot C_{DOM})}{\partial z} - \dfrac{\partial}{\partial z}\left(D_b(z) \dfrac{\partial C_{DOM}}{\partial z} \right) - \dfrac{\partial(\omega(z) \cdot C_{DOM})}{\partial z}$	Transport

$f_{CWD \to DOM}$ is the fraction of coarse woody debris decomposition that enters the DOM pool. $f_{C_B \to C_{DOM}}$ is the soluble fraction of dead microorganisms that enter the DOM pool. r_B is the mortality rate of microorganisms. $V_{max,R}$ is maximum depolymerization rate of microbial residues C_R that are decomposed according to reverse Michaelis-Menten kinetics with a half-saturation constant $K_{m,R}$. $V_{max,DOM}$ is the maximum uptake rate of DOM by microorganisms that is limited by supply of DOM through a Michaelis-Menten term with half-saturation constant $K_{m,R}$. $k_{ads,DOM}$ is the adsorption rate of DOM on mineral surfaces. The amount of mineral surfaces that are available for sorption are described by the difference between the volumetric amount of mineral surfaces in a certain layer, Q_{max}^V and the amount of microbial residues $C_{Q[R]}$ and DOM ($C_{Q[DOM]}$) that is sorbed to mineral surfaces already. $k_{des,DOM}$ is the desorption rates of DOM. $v(z)$ is the advection velocity from the water flux.

C_B, microbial biomass

$\frac{\partial}{\partial t} C_B =$	$+V_{max,DOM} \cdot CUE \cdot C_B \cdot \frac{C_{DOM}}{K_{m,DOM} + C_{DOM}}$	Microbial transformation
	$-r_B \cdot C_B$	Decomposition loss
	$-\frac{\partial}{\partial z}\left(D_b(z)\frac{\partial C_B}{\partial z}\right) - \frac{\partial(\omega(z) \cdot C_B)}{\partial z}$	Transport

CUE is the carbon use efficiency of microbial uptake of DOC.

C_R, microbial residues

$\frac{\partial}{\partial t} C_R =$	$+\left(1 - f_{C_B \rightarrow C_{DOM}}\right) \cdot r_B \cdot C_B$	Microbial transformation
	$-V_{max,R} \cdot C_R \cdot \frac{C_B}{K_{m,R} + C_B}$	Decomposition loss
	$-k_{ads,R} \cdot C_R \cdot \left(Q_{max}^V - \left(C_{Q[DOM]} + C_{Q[R]}\right)\right)$	Adsorption
	$+k_{des,R} \cdot C_{Q[R]}$	Desorption
	$-\frac{\partial}{\partial z}\left(D_b(z)\frac{\partial C_R}{\partial z}\right) - \frac{\partial(\omega(z) \cdot C_R)}{\partial z}$	Transport

$k_{ads,R}$ is the adsorption rates of microbial residues. $k_{des,R}$ is the desorption rate for sorbed microbial residues.

$C_{Q[R]}$, microbial residues sorbed to mineral surfaces Q_{max}^V

$\frac{\partial}{\partial t} C_{Q[R]} =$	$+k_{ads,R} \cdot C_R \cdot \left(Q_{max}^V - \left(C_{Q[DOM]} + C_{Q[R]} \right) \right)$	Adsorption	
	$-k_{des,R} \cdot C_{Q[R]}$	Desorption	
	$-\frac{\partial}{\partial z}\left(D_b(z) \frac{\partial C_{Q[R]}}{\partial z} \right) - \frac{\partial \left(\omega(z) \cdot C_{Q[R]} \right)}{\partial z}$	Transport	

$C_{Q[DOM]}$, DOM sorbed to mineral surfaces Q_{max}^V

$\frac{\partial}{\partial t} C_{Q[DOM]} =$	$+k_{ads,DOM} \cdot C_{DOM} \cdot \left(Q_{max}^V - \left(C_{Q[DOM]} + C_{Q[R]} \right) \right)$	Adsorption	
	$-k_{des,DOM} \cdot C_{Q[DOM]}$	Desorption	
	$-\frac{\partial}{\partial z}\left(D_b(z) \frac{\partial C_{Q[DOM]}}{\partial z} \right) - \frac{\partial \left(\omega(z) \cdot C_{Q[DOM]} \right)}{\partial z}$	Transport	

Q_{max}^V, volumetric maximum sorption capacity

$\frac{\partial}{\partial t} Q_{max}^V =$	$-\frac{\partial}{\partial z}\left(D_b(z) \frac{\partial Q_{max}^V}{\partial z} \right) - \frac{\partial (\omega(z) \cdot Q_{max}^V)}{\partial z}$	Transport	

5.10.2 Temperature and moisture dependent rates

$$V_{max,\genfrac{}{}{0pt}{}{Lignified}{Litter}} = V_{max,\genfrac{}{}{0pt}{}{Lignified}{Litter},T_{ref}} \cdot f(T)$$

$$V_{max,R} = V_{max,R,T_{ref}} \cdot f(T)$$

$$V_{max,DOM} = V_{max,DOM,T_{ref},\theta_{opt}} \cdot f(T) \cdot f(\theta)$$

$$V_{max,\genfrac{}{}{0pt}{}{Lignified}{Litter}} = V_{max,\genfrac{}{}{0pt}{}{Lignified}{Litter},T_{ref}} \cdot f(T)$$

$$V_{max,\genfrac{}{}{0pt}{}{Lignified}{Litter}} = V_{max,\genfrac{}{}{0pt}{}{Lignified}{Litter},T_{ref}} \cdot f(T)$$

$$r_B = r_{B,T_{ref}} \cdot f(T)$$

$$k_{ads,R} = k_{ads,R,T_{ref}} \cdot f(T)$$

$$k_{ads,DOM} = k_{ads,DOM,T_{ref}} \cdot f(T)$$

$$k_{des,DOM} = k_{des,DOM,T_{ref}} \cdot f(T)$$

$$k_{des,DOM} = k_{des,DOM,T_{ref}} \cdot f(T)$$

where $V_{max,Pool,T_{ref}}$ is the maximum depolymerization rate of a pool as modified by soil temperature. $f(T) = \exp\left(-\frac{E_a}{R} \cdot \left(\frac{1}{T} - \frac{1}{T_{ref}}\right)\right)$, where T is the soil temperature (K), E_a the activation energy specific to a certain process, R the universal gas constant, and T_{ref} the reference temperature 283.15 K at which $f(T) = 1$. $E_{a,Pool}$ and $V_{max,Pool,T_{ref}}$ of the respective pools are given in section 5.10.2. $V_{max,DOM}$ is the maximum microbial uptake rate at reference temperature and

optimal moisture content θ_{opt} with $f(\theta) = \begin{cases} \left(\frac{\theta}{\theta_{opt}}\right)^a, & \theta < \theta_{opt} \\ \left(\frac{\phi-\theta}{\phi-\theta_{opt}}\right)^b, & \theta \geq \theta_{opt} \end{cases}$. ϕ is the soil porosity, a and b are

parameters given section 5.10.3. $r_{B,T_{ref}}$ is the reference microbial mortality at T_{ref}; its activation energy is the same as for microbial uptake. $k_{ads,R,T_{ref}}$, $k_{ads,DOM,T_{ref}}$, $k_{des,DOM,T_{ref}}$ and $k_{des,DOM,T_{ref}}$ are the adsorption and desorption rates as modified by temperature and availability of Q_{max} in the case of adsorption. The activation energies and adsorption and desorption rates at reference temperature are given in section 5.10.3.

5.10.3 Parameters

Supplementary Table 1: In column *Parametrization* C stands for calibrated, Ref1 for Wang et al. (2012), Ref2 for Allison et al. (2010), Ref3 for Hagerty et al. (2014), Ref4 for Parton et al. (1993), Ref5 for Wieder et al. (2015), and Ref6 for Wang et al. (2013), Ref7 for Yan et al. (2018).

| Parameter	Description	Value	Lower Bound	Upper Bound	Unit	Parameterization
k_{CWD}	Decomposition rate of coarse woody debris	1.11e-02			yr^{-1}	Prescribed
$f_{CWD \to DOC}$	Fraction of coarse woody debris decomposition that enters DOC pool	1.00e-01			-	Prescribed
$V_{max, \substack{Lignified \\ Litter}}$	Maximum depolymerization rate of lignified litter	2.37e-01	2.00e-02	1.20e+01	yr^{-1}	C
$K_{m, \substack{Lignified \\ Litter}}$	Half-saturation constant for the depolymerization of lignified litter	5.98e-08	1.00e-20	1.00e+00	$kg\,C\,m^{-3}$	C
$E_{a,Lignified\ Litter}$	Activation energy for depolymerization of lignified litter	5.30e+04			$J\,mol^{-1}$	Ref1
f_{Sol}	Fraction of soluble litter	1.02e-01	5.00e-02	4.00e-01	-	C
$V_{max,R}$	Maximum depolymerization rate of microbial residues	8.49e-02	2.00e-02	1.20e+01	yr^{-1}	C
$V_{max,DOM}$	Maximum uptake rate of DOM by microorganisms	5.50e+03	3.65e+01	8.76e+03	yr^{-1}	C
$K_{m,DOM}$	Half-saturation constant for uptake of DOM by microorganisms	8.56e-02	1.00e-20	1.00e+00	$kg\,C\,m^{-3}$	C
CUE	Carbon use efficiency	5.37e-02	1.00e-20	6.00e-01	-	C
r_B	Mortality rate of microorganisms	1.04e+01	4.10e+00	1.46e+01	yr^{-1}	C
$f_{C_B \to C_{DOM}}$	Soluble fraction of dead microorganisms	3.04e-01	5.00e-02	4.00e-01	-	C
$E_{a,Uptake}$	Activation energy for DOM uptake by microorganisms	4.70e+04			$J\,mol^{-1}$	Ref2
$E_{a,MicrobialMortality}$	Activation energy for microbial mortality	4.70e+04			$J\,mol^{-1}$	Ref2, Ref3
$K_{m,R}$	Half-saturation constant for depolymerization of microbial residues	1.14e-03	1.00e-20	1.00e+00	$kg\,C\,m^{-3}$	C
$E_{a,R}$	Activation energy for depolymerization of microbial residues	5.30e+04			$J\,mol^{-1}$	Ref1
a	Parameter for scaling moisture function	3.29e+00	1.00e-20	1.00e+01	-	C
b	Parameter for scaling moisture function	3.83e-02	1.00e-20	1.00e+01	-	C
θ_{opt}	Optimal water content	$0.65 \cdot \phi$				Ref7
k_{leach}	Leaching rate for soluble litter	3.03e+01			yr^{-1}	Ref5
$k_{ads,DOM}$	Adsorption rate DOM	7.07e+02	2.86e-04	6.62e+05	$m^3\,(kg\,C)^{-1}\,yr^{-1}$	C
$k_{des,DOM}$	Desorption rate DOM	1.63e+03	1.67e-01	8.76e+03	yr^{-1}	C
$k_{ads,R}$	Adsorption rate microbial residues	5.62e+00	2.86e-04	6.62e+05	$m^3\,(kg\,C)^{-1}\,yr^{-1}$	C
$k_{des,R}$	Desorption rate microbial residues	5.97e+00	1.67e-01	8.76e+03	yr^{-1}	C
$E_{a,ads}$	Activation energy for DOM and microbial residue adsorption	5.00e+03			$J\,mol^{-1}$	Ref6
$E_{a,des}$	Activation energy for DOM and microbial residue desorption	2.00e+04			$J\,mol^{-1}$	Ref6
B	Ingestion rate ($kg\,m^{-3}\,yr^{-1}$) · earthworm body length squared (m^2)	1.01e-01	1.00e-20	1.00e+00	$m^2\,(kg\,m^{-3})\,yr^{-1}$	C

5.10.4 Supplementary figures
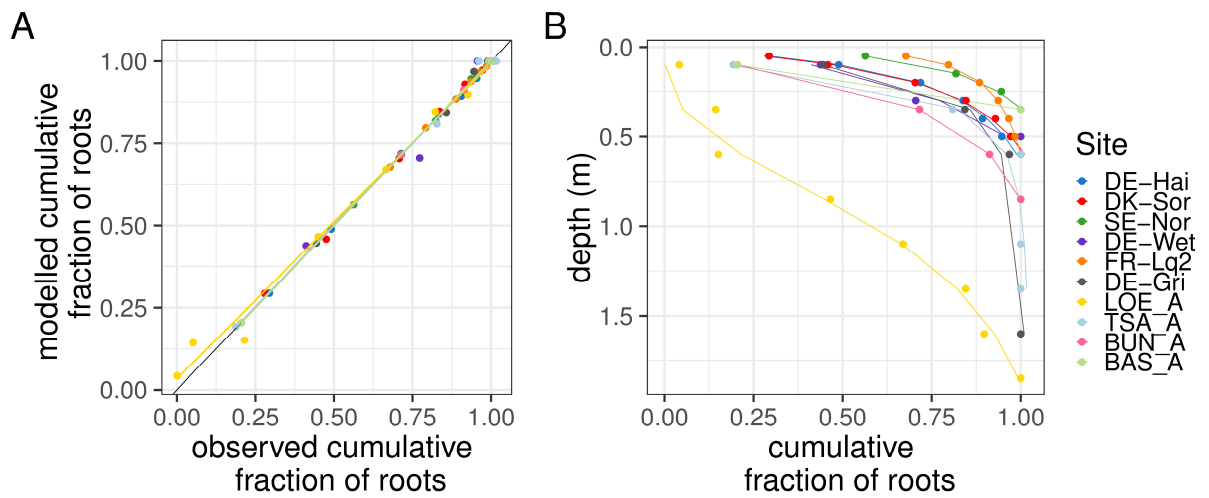
Supplementary figure 1: Root distributions at the ten calibration sites and performance of the logistic dose-response curve of Schenk and Jackson (2002) to represent them. (A) Modelled compared to observed cumulative fraction of roots. Lines are the regression lines of modelled vs observed cumulative fraction of roots at the respective sites. (B) Depth profiles of modelled and observed cumulative fractions.
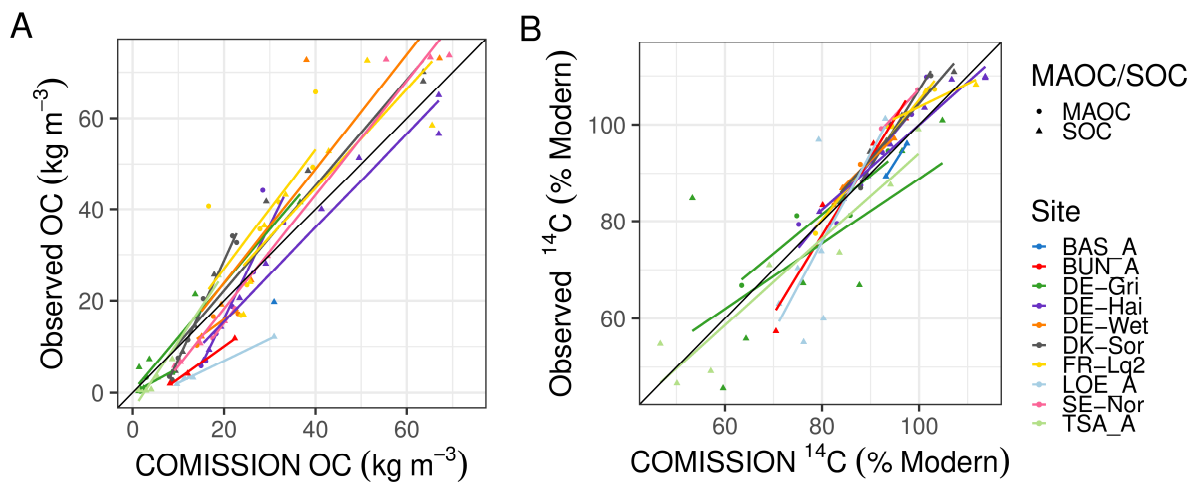
Supplementary figure 2: Scatterplots of observed vs. modeled volumetric SOC and MAOC concentrations (A) and ^{14}C of SOC and MAOC (B). Lines are the regression lines of modelled vs observed volumetric SOC and MAOC concentrations and ^{14}C at the respective sites.

A

B
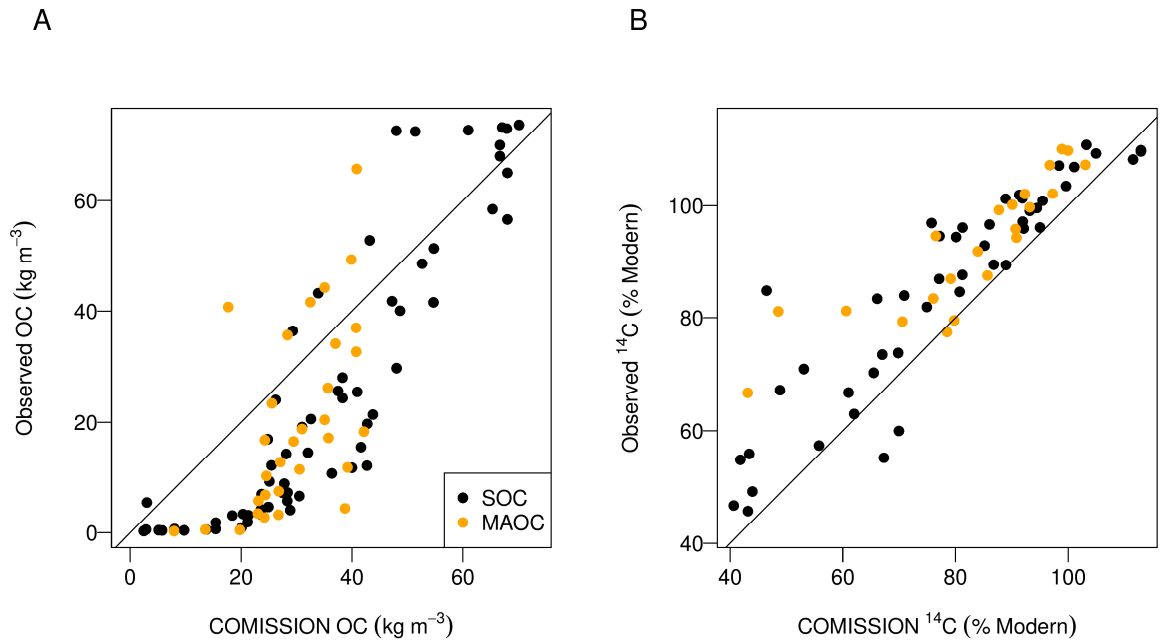
Supplementary figure 3: Test of COMISSION with a maximum Q_{max}^m of 108 g (kg mineral soil)$^{-1}$ for all sites: Scatterplots of observed vs. modeled volumetric OC concentration (A) and ^{14}C (B).

A

B
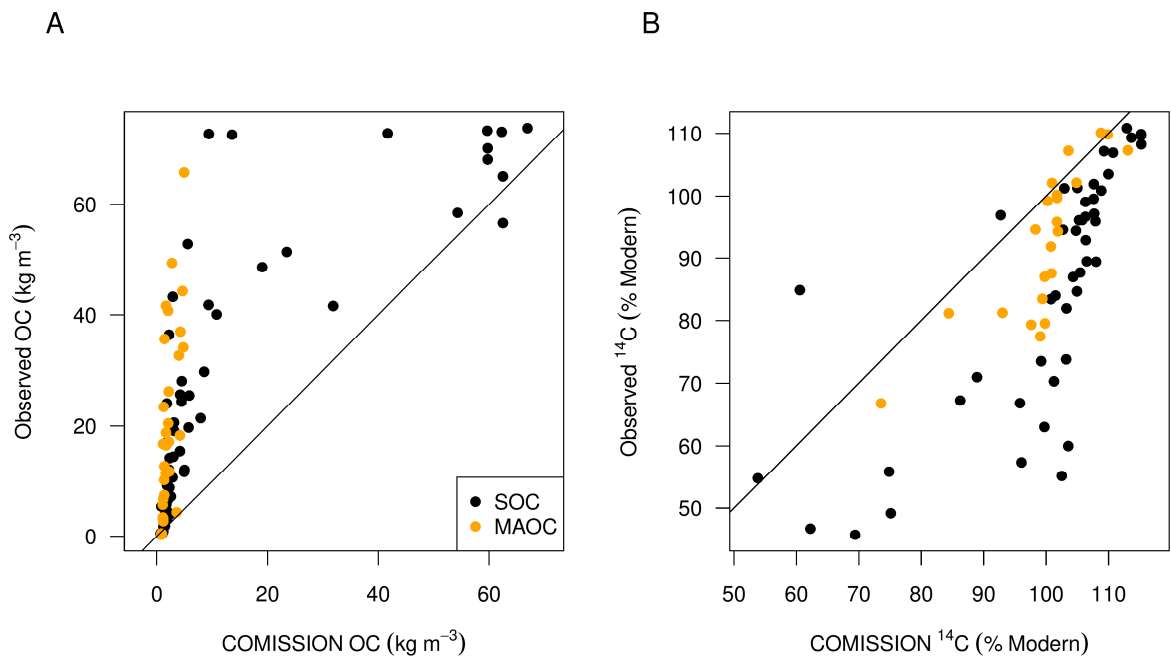
Supplementary figure 4: Test of COMISSION v2.0 with maximum Q_{max}^m of 4.68 g (kg mineral soil)$^{-1}$ for all sites: Scatterplots of observed vs. modeled volumetric OC concentration (A) and ^{14}C (B).

$$(\text{Depoly On}) - (\text{Depoly Off})$$
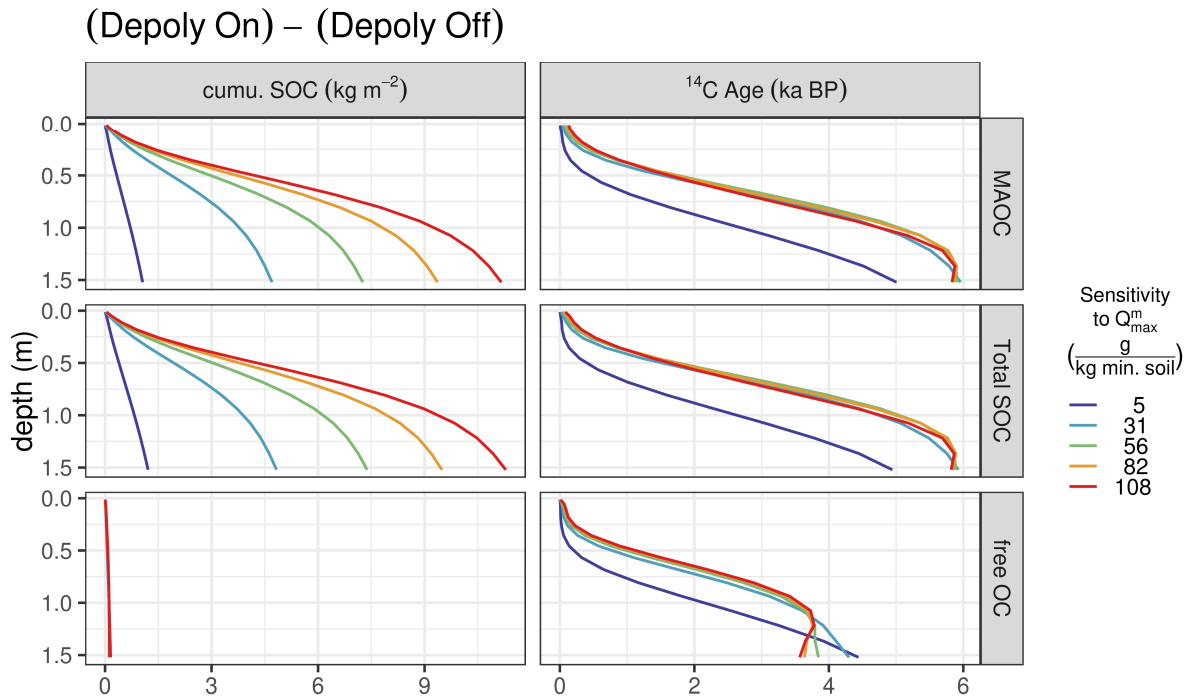
Supplementary figure 5: Difference in soil organic carbon (SOC) stocks and ^{14}C ages for the two scenarios with microbial depolymerization limitation on (Depoly On) and off (Depoly Off). Colored lines represent simulations with varying Q^m_{max}.

$$\left(Q^m_{max} = 108\right) - \left(Q^m_{max} = 5\right)$$
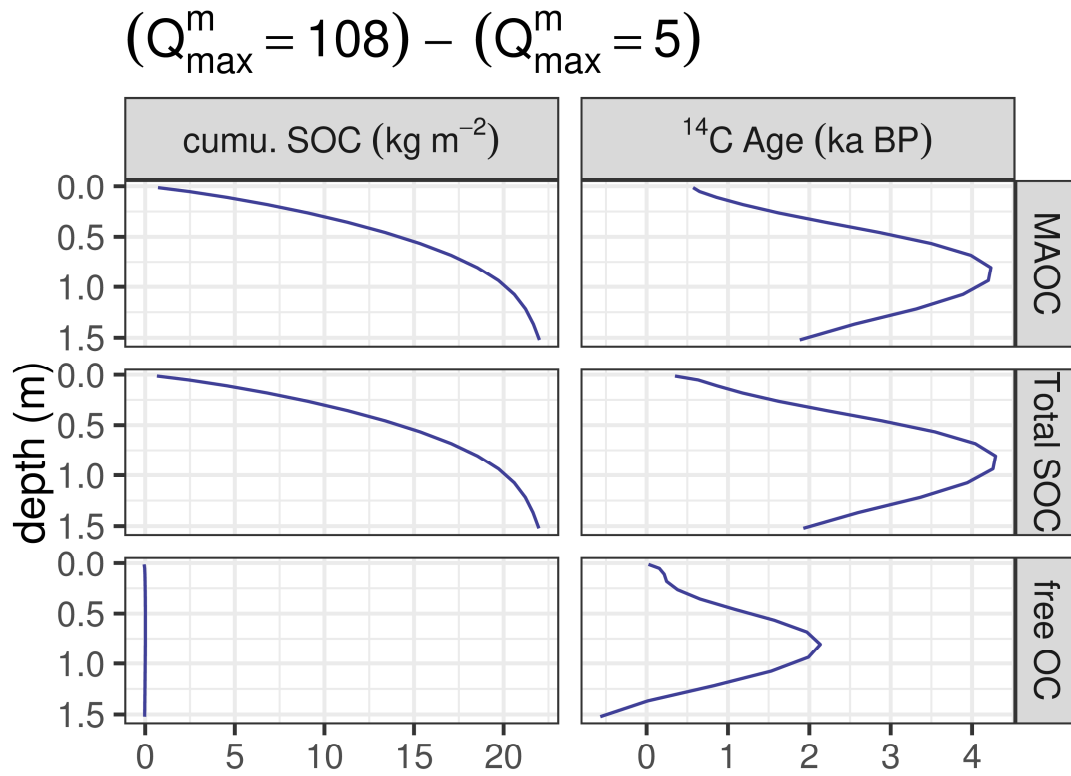
Supplementary figure 6: Difference in soil organic carbon (SOC) stocks and ^{14}C ages for Q_{max} = 108 g (kg mineral soil)[-1] and Q_{max} = 5 g (kg mineral soil)[-1].
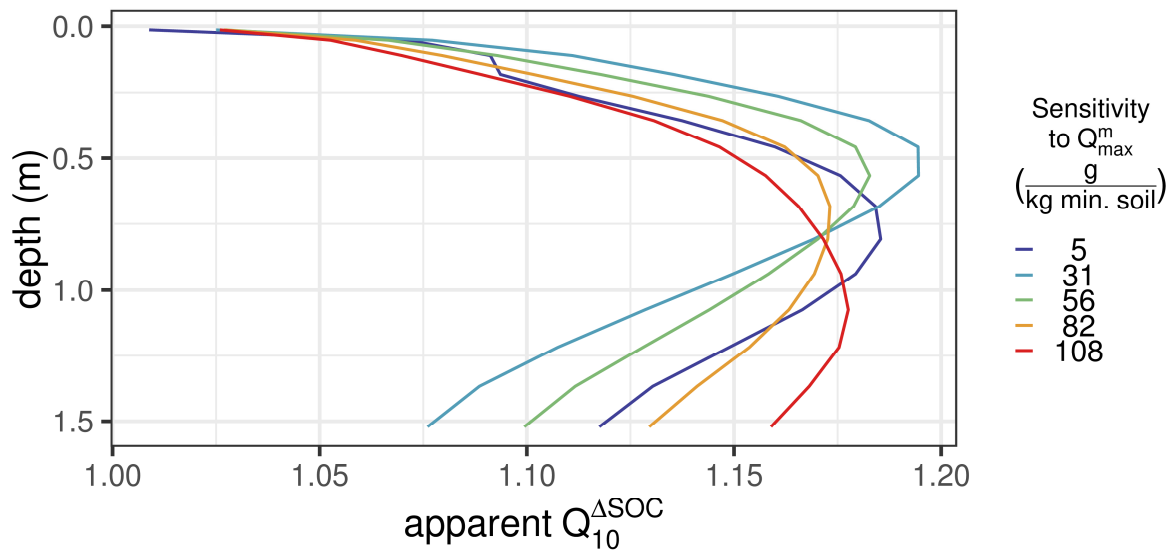
Supplementary figure 7: Model experiment MAAT–Q_{max} interaction with all activation energies from Table 5-1 set 0 kJ/mol except for adsorption and desorption: Effect of sorption capacity (Q_{max}^m) on apparent Q_{10} values in depth z calculated from SOC concentration differences between the 5.45 °C and 8.70 °C model experiment. Except for temperature and Q_{max}^m, simulations were performed using the forcing and parameters of TSA_A.

5.10.5 JSBACH simulations at CarboEurope sites and comparison with eddy covariance measurements

Supplementary Table 2: Comparison of JSBACH against eddy covariance measurements of gross primary productivity on monthly scale:

Site	Site years used in evaluation (eddy covariance)	NSE	Percent model bias
DE-Hai	2000 – 2006	0.95	-6.22
DK-Sor	1997 – 2006	0.89	-17.21
SE-Nor	1996 – 1997	0.65	7.48
DE-Wet	2002 – 2006	0.92	12.86
FR-Lq2	2004 – 2006	0.69	13.96

Supplementary Table 3: Comparison of JSBACH against eddy covariance measurements of evapotranspiration on monthly scale:

Site	Site years used in evaluation (eddy covariance)	NSE	Percent model bias
DE-Hai	2000 - 2006	0.42	-69.02%
DK-Sor	1997 - 2006	0.58	40.85
SE-Nor	1996 - 1997	0.85	20.90
DE-Wet	2002 - 2006	0.69	38.34
FR-Lq2	2004 - 2006	0.9	-0.52

Supplementary Table 4: Comparison of JSBACH against eddy covariance measurements of sensible heat flux on monthly scale:

Site	Site years used in evaluation (eddy covariance)	NSE	Percent model bias
DE-Hai	2000 - 2006	0.61	-40.97
DK-Sor	1997 - 2006	0.53	156.00
SE-Nor	1996 - 1997	0.82	26.64
DE-Wet	2002 - 2006	0.82	16.12
FR-Lq2	2004 - 2006	-0.37	116.45

5.10.6 SI References

Allison, S.D., Wallenstein, M.D., Bradford, M.A., 2010. Soil-carbon response to warming dependent on microbial physiology. Nature Geosci 3, 336-340.

Hagerty, S.B., van Groenigen, K.J., Allison, S.D., Hungate, B.A., Schwartz, E., Koch, G.W., Kolka, R.K., Dijkstra, P., 2014. Accelerated microbial turnover but constant growth efficiency with warming in soil. Nature Climate Change 4, 903-906.

Jarvis, N.J., Taylor, A., Larsbo, M., Etana, A., Rosén, K., 2010. Modelling the effects of bioturbation on the re-distribution of 137Cs in an undisturbed grassland soil. European Journal of Soil Science 61, 24-34.

Parton, W.J., Scurlock, J.M.O., Ojima, D.S., Gilmanov, T.G., Scholes, R.J., Schimel, D.S., Kirchner, T., Menaut, J.C., Seastedt, T., Garcia Moya, E., Kamnalrut, A., Kinyamario, J.I., 1993. Observations and modeling of biomass and soil organic matter dynamics for the grassland biome worldwide. Global Biogeochem. Cycles 7, 785-809.

Schenk, H.J., Jackson, R.B., 2002. The global biogeography of roots. Ecological Monographs 72, 311-328.

Wang, G., Post, W.M., Mayes, M.A., 2013. Development of microbial-enzyme-mediated decomposition model parameters through steady-state and dynamic analyses. Ecological Applications 23, 255-272.

Wang, G., Post, W.M., Mayes, M.A., Frerichs, J.T., Sindhu, J., 2012. Parameter estimation for models of ligninolytic and cellulolytic enzyme kinetics. Soil Biology and Biochemistry 48, 28-38.

Wieder, W.R., Grandy, A.S., Kallenbach, C.M., Taylor, P.G., Bonan, G.B., 2015. Representing life in the Earth system with soil microbial functional traits in the MIMICS model. Geosci. Model Dev. 8, 1789-1808.

Yan, Z., Bond-Lamberty, B., Todd-Brown, K.E., Bailey, V.L., Li, S., Liu, C., Liu, C., 2018. A moisture function of soil heterotrophic respiration that incorporates microscale processes. Nature Communications 9, 2562.

6 Synthesis

This thesis and the contained studies have shown that (1) different techniques of measuring root turnover can be reconciled and that (2) radiocarbon and SOC measurements can be reconciled under a modeling framework that includes a mechanistic description of vertical transport, microbial interactions, and sorption to minerals.

In the following chapters, I will revisit the objectives of this thesis (chapter 1.6) and discuss the insights of the different studies in the light of newer literature and ideas published in the meanwhile.

6.1 Reconcilable differences in root turnover

6.1.1 Generalizing root turnover modeling with survival functions

Survival functions that describe roots' lifetimes were the key to developing one common framework to jointly estimate root turnover with the ^{14}C and minirhizotron technique (Study I and II). This thesis could show that various survival functions can be convolved with the atmospheric radiocarbon curve to model ^{14}C in fine-roots (Objective **Obj-Root1**). This makes it possible to use statistical survival functions such as the Weibull function or the log-normal function to estimate mean residence times of fine-roots from ^{14}C. These statistical survival functions have been commonly used to estimate mean residence times from minirhizotron data. In ecological models, however, one commonly deals with compartmental models described as a system of interacting pools. In serial or parallel setting, two–pool models have been best reconciling minirhizotron and fine-root ^{14}C data (Study II, Objective **Obj-Root3**). Progressive suberization of some roots can explain why the probability for a root to die decreases in the serial two-pool model. For the parallel two-pool model, ectomycorrhizal infection of some roots would cause two structurally different types of fine-roots - short ectomycorrhizal roots and suberized supportive roots. Both explanations are open to further study hypothesis testing.

The generic derivation of survival functions for compartmental systems by Metzler et al. (2018), would now make it possible to convolve the survival functions of any compartmental model with the atmospheric ^{14}C curve as described in study I and II. At the same time, the technique of assimilating

minirhizotron observations could be used as described in study II for survival functions from any compartmental system (extension of Objective **Obj-Root3**).

6.1.2 Storage carbon remains a major bias for estimating root turnover from ^{14}C

Study II was also addressing the biases of the two techniques. For minirhizotrons, apparent lifetimes of roots are overestimated because dead and live roots are hard to distinguish. The observed lifetime of a root might also include the time-to-decomposition. Storage pools might be used to construct new roots, thereby leading to 'pre-aged' roots regarding ^{14}C. I addressed both biases by incorporating the prior knowledge accumulated in the literature so far and updated this prior knowledge with what could be learned from the data (Objective **Obj-Root4**).

After the publication of study II, a study by Solly et al. (2018) further highlighted the problems of storage pools and introduced a new technique to estimate the age of a root by counting its year rings. Solly et al. (2018) confirmed previous findings that stored radiocarbon could contribute considerably to calibrated ^{14}C ages of fine roots. Compared to Sah et al. (2011), they found that also fine-roots smaller than 0.5 mm can be much older than the actual ages of these roots. Overall, these contradicting results call the use of ^{14}C as a constraint into question. Solly et al. (2018) found that calibrated ^{14}C ages of $0-0.5$ mm in one boreal forest are between 2.5 and 10 years older than the chronological ages. By contrast, Sah et al. (2011) found that ^{14}C contents of $0-0.5$ mm roots agree with ingrowth core maximum ages in three Scots pine forests. Gaudinski et al. (2009) found that the average age of ^{14}C in a newly grown fine-root is 0.4 years old. In study II, storage carbon would only pre-age carbon in roots up to an imposed cutoff at five years. The findings of Solly et al. (2018) indicate that this can be longer. Although the sample size for small fine roots in the $0-0.5$ mm range of the Solly et al. (2018) study is small (n=4), three out of four roots show a storage turnover time longer than five years. With the combined estimation of root turnover with minirhizotrons and ^{14}C contents in chapter 3, it can, however, be ruled out that storage turnover times play such a substantial role in study II. Except for the exponential model, all models show storage turnover times smaller than 0.9 years. This is well constrained due to the combined use of minirhizotron and ^{14}C fine-root data. Based on the results of Solly et al. (2018), however, it would be prudent for future applications of the survival function framework to not truncate the prior of the storage turnover time at five years (Objective **Obj-Root4**). The findings also indicate that a targeted determination of the storage turnover time may be warranted.

6.1.3 Using age distributions to constrain mean residence times?

In study I, I clarified the concepts of mean residence time and mean age to estimate fine-root turnover (Objective **Obj-Root2**). The mean age of a root is not a direct quantity of interest since it cannot be directly used to calculate the root litter input which is possible with the mean residence time (under the assumption of steady-state). Up to now, reported fine-root ages from ingrowth cores could only be regarded as anecdotal evidence for long lifetimes of fine roots or would be used to determine the storage turnover time of ^{14}C. The technique of counting year rings (Solly et al., 2018) or ages of individual roots from ingrowth cores or nets (Sah et al., 2011; Lukac, 2012) could, however, be used in addition to the ^{14}C measurements and minirhizotron data in the survival function framework presented in study II. Instead of fitting the survival function to minirhizotron observations, the ages of individual roots could be directly used to fit the age distribution function, $A(\tau)$. The survival function and the age distribution function share the same parameters and can be derived from each other (Manzoni et al., 2009; Metzler et al., 2018). Thereby the ages of individual roots would also contribute to constraining the long tail of root turnover. The definition of cost functions presented in study II for minirhizotron data can be analogously used for age distribution functions and root ring assimilation into ecosystem models (extension of objective **Obj-Root3**).

However, using the dendrochronological age of roots can also underestimate roots' actual age since dry conditions can also lead to missing rings (Krause and Eckstein, 1993). Coutts and Lewis (1983) also reported missing growth rings in small diameter roots. Long-term ingrowth bags could be used to ensure that small roots do not regularly have missing year rings. This is another problem that would need reconciliation since dry years probably lead to missing year rings, whereas they lead to the use of stored carbon to construct new roots. Hence, this would lead to underestimating fine-root ages from dendrochronology while it leads to overestimation with the radiocarbon technique (extension of objective **Obj-Root4**).

6.2 Reconcilable differences in SOC turnover

6.2.1 Emerging processes in SOC formation and turnover

Apparent radiocarbon ages of soil organic carbon that range up to millennia have been a puzzle for decades in soil organic matter research. A multitude of models have been proposed to accommodate

pools that would allow for apparently millennial ^{14}C ages (Jenkinson and Coleman, 2008; Koven et al., 2013; Braakhekke et al., 2014; Dwivedi et al., 2017; Woolf and Lehmann, 2019). Models need to be reconciled with the observation that organic compounds *per se* have turnover times on relatively short timescales while models following the chemical recalcitrance paradigm were employing turnover times on up to millennial timescales for individual pools throughout the soil profile (Jenkinson and Coleman, 2008; Parton et al., 2010). The COMISSION v2.0 model reproduced ^{14}C observations across ten sites by representing mechanisms such as mineral association and microbial energy limitation. Study III and IV demonstrated that a model of the new class of soil organic matter models that follows the paradigm of microbial and organo-mineral interactions can reconcile organic carbon with ^{14}C observations without resorting to passive (Parton et al., 1994; Parton et al., 2010) or inert pools (Coleman et al., 1997; Jenkinson and Coleman, 2008) that were motivated by the persistence due to chemical recalcitrance paradigm (Objective **Obj-SOC1**).

6.2.2 Defining and parameterizing sorption capacity

I have explored two different ways to represent the limited amount of mineral surfaces available to form organo-mineral associations. In study III, I have used the maximum sorption capacity q_{max} as derived from batch sorption experiments together with the already mineral-associated organic carbon to parameterize COMISSION v1.0. In this version, only DOC was able to form mineral associations. In study IV, I used the clay + silt (< 20 µm) content to parameterize the maximum sorption capacity, Q_{max}, which can be saturated by DOC and microbial residues in COMISSION v2.0 (Objective **Obj-SOC2**).

Abramoff et al. (2021) have compiled a methodologically consistent database of batch sorption experiments in forest soils that have been evaluated with Langmuir sorption isotherms. The measured $q_{max,batch}$ used in study III are based on measurements presented in Guggenberger and Kaiser (2003) and are part of the study of Abramoff et al. (2021). Both study III and Abramoff et al. (2021) use the additional sorption potential, i.e., the sorption capacity that can still be saturated in addition to what is already sorbed. I moved away from this definition of maximum sorption capacity in the development from COMISSION v1.0 (study III) to COMISSION v2.0 (study IV) since one has to work with assumptions about the size of the already sorbed organic carbon (Objective **Obj-SOC2**).

Although Abramoff et al. (2021) derive scalable relationships of the additional sorption potential, these cannot be employed in models since models require the absolute amount of q_{max} to model

adsorption rates. The approach of defining q_{max} as the sum of mineral-associated carbon and additional sorption potential as in study III confounds the sorption of dissolved organic carbon and the association of microbial necromass (Miltner et al., 2012) on mineral surfaces into one process. This is probably why the calibrated equilibrium constant ($K = k_{ads}/k_{des}$) in study III is orders of magnitude too high (9076 m^3/g C) – as Abramoff et al. (2021) correctly noted – compared to what is found in batch sorption experiments (10^{-4} to 10^{-2} m^3/g C). In COMISSION v2.0, the calibrated equilibrium constant (5.476 ×10^{-4} to 3.48 ×10^{-4} m^3/g C for temperatures between 0 °C and 20 °C) is within the range of what Abramoff et al. (2021) reported. This shows that the development from COMISSION v1.0 to COMISSION v2.0 represents the range of processes that contribute to the formation of mineral-associated organic carbon better (Objective **Obj-SOC2**). Both microbial residues and dissolved organic carbon can form organo-mineral associations in COMISSION v2.0, and the maximum sorption capacity is defined as a function of clay and silt (< 20 µm) content.

While Abramoff et al. (2021) provide upscaled estimates of an additional DOC sorption potential of 107 Pg C globally, it is not possible to use these estimates in modeling efforts since the total DOC sorption capacity remains unknown. A possible remedy would be to quantify the initial amount of sorbed DOC, for example, by abandoning the equilibrium assumption for batch sorption experiments. Instead, one could use dynamic Langmuir equations (Van de Weerd et al., 1999, 2002) in which also the initial amount of sorbed DOC is treated as an unknown parameter. Thereby, it can be tested if individual maximum sorption capacities for dissolved organic carbon and microbial necromass are warranted. In COMISSION v2.0, dissolved organic carbon and microbial necromass 'compete' for the same sorption sites.

6.2.3 Influence of mineralogy and soil-forming processes on ^{14}C profiles

The study of Abramoff et al. (2021) has shown that the additional sorption potential and the equilibrium constant vary with soil order. Soil orders encode information such as mineralogy or weathering (United States Department of Agriculture, 1999), which are relevant factors to describe sorption mechanistically. In study IV, using a maximum sorption capacity based on the clay + silt (< 20 µm) content (Feng et al., 2013; Beare et al., 2014), information of soil type and soil order was incorporated to influence sorption to some extent. From hereon, I refer to the clay + silt (< 20 µm) content simply as clay + silt content. For the clay + silt-based definition of sorption capacity, three different relationships for soils dominated by 2:1 and 1:1 minerals and andisols (soils on volcanic substrate) have been derived (Feng et al., 2013; Beare et al., 2014). In study IV, nine soils were soils

dominated by 2:1 mineral soils, and one soil was an andisol. To test the findings of Feng et al. (2013) that 1:1 mineral soils have a lower maximum sorption capacity given a certain clay + silt fraction compared to 2:1 mineral soils, global runs of COMISSION v2.0 with the parameter set retrieved in Study IV were performed with JSBACH forcing (~ 1.9° resolution; Knauer et al. (2015)). On grid-cell level, ^{14}C values were compared to the ^{14}C profiles collected in the International Soil Radiocarbon Database (ISRaD; Lawrence et al., 2020). Globally, soils were split into high activity clay soils, low activity clay soils, and andisols (IPCC, 2003) with different relationships to the clay + silt fraction (Feng et al., 2013; Beare et al., 2014).

Across all US Soil Taxonomy orders, COMISSION v2.0 and the ISRaD database (Lawrence et al., 2020) show a similar mean radiocarbon profile (Figure 6-1). The modeled mean ^{14}C age across all soil orders in 1 m depth are too old by 89 years (n = 425, 2559^{+215}_{-207} mean modeled apparent age and 2470^{+385}_{-338} observed apparent age). Mean modeled apparent ^{14}C ages for Oxisols, which are dominated by 1:1 clay minerals, are too young by 134 years in 1 m depth (n = 94, 722^{+162}_{-174} mean modeled apparent age and 856^{+443}_{-414} observed apparent age). Ultisols, which are also dominated by 1:1 clay minerals, are the soil order in which COMISSION v2.0 shows the most considerable discrepancies to ISRaD. In 1 m depth, COMISSION v2.0 is 2312 years too young compared to Ultisols in ISRaD (n = 35, 2085^{+798}_{-623} mean modeled apparent age and 4396^{+1555}_{-1098} observed apparent age). This might point to a problem with the relationship between clay + silt and the maximum sorption capacity derived by Feng et al. (2013) for soils dominated by 1:1 minerals. Based on soil order grouping (Figure 6-1), the maximum sorption capacity for 1:1 mineral soils seems to work relatively well for Oxisols but not for Ultisols. The fact that COMISSION v2.0 is much too old for Ultisols may point to higher sorption capacities (study IV) than prescribed by the Feng et al. (2013) study. Abramoff et al. (2021) also found higher additional sorption capacities for Ultisols than other soil orders, although they do not have Oxisols in their database. This shows that the distinction into 1:1 mineral soils, 2:1 mineral soils, and Andisols may not be enough to get a good global estimate of sorption capacity. Andisols in COMISSION v2.0 on grid-cell level are also much too young (Figure 6-1). Study IV, however, showed that COMISSION could model apparent ^{14}C ages in Andisols on site-scale level with the parametrization of the maximum sorption capacity according to Beare et al. (2014). Therefore, this mismatch instead points out that none of the grid cells are dominated by volcanic soils. For poorly weathered soils, such as Inceptisols and Entisols, COMISSION v2.0 is rather too old (Figure 6-1), which may point to an overestimation of sorption capacities by the clay + silt relationship (Feng et al., 2013; Beare et al., 2014) for these soils. Again, the findings by Abramoff et al. (2021) corroborate this since they found

the lowest additional DOC sorption capacities for these two soil orders. In histosols, COMISSION v2.0 does not capture the characteristic shape of the ^{14}C age depth-gradient in ISRaD (Figure 6-1). COMISSION possesses the theoretical ability to model the build-up of peat layers due to the continuous profile setup outlined in studies III and IV but seems to model the characteristic ^{14}C age-depth distribution of a mineral soil for these histosols. This points to room for improvement either in the forcing from JSBACH or in the process representation of COMISSION regarding the soil moisture rate modifier of decomposition. Insufficient inhibition of litter decomposition through the 'enzymic latch' of phenol-oxidase (Freeman et al., 2001) could be a candidate process that needs to explicitly incorporated in COMISSION.

This thesis has been focused on mineral-associated organic carbon. The dichotomy between mineral-associated organic carbon on the one hand and 'unprotected' organic carbon in peatlands, and organic layers on the other hand, should also be able to be addressed with COMISSION. To assess the strength of the soil organic carbon – climate warming feedback both mineral-associated organic carbon and 'unprotected' organic carbon have to be represented adequately.
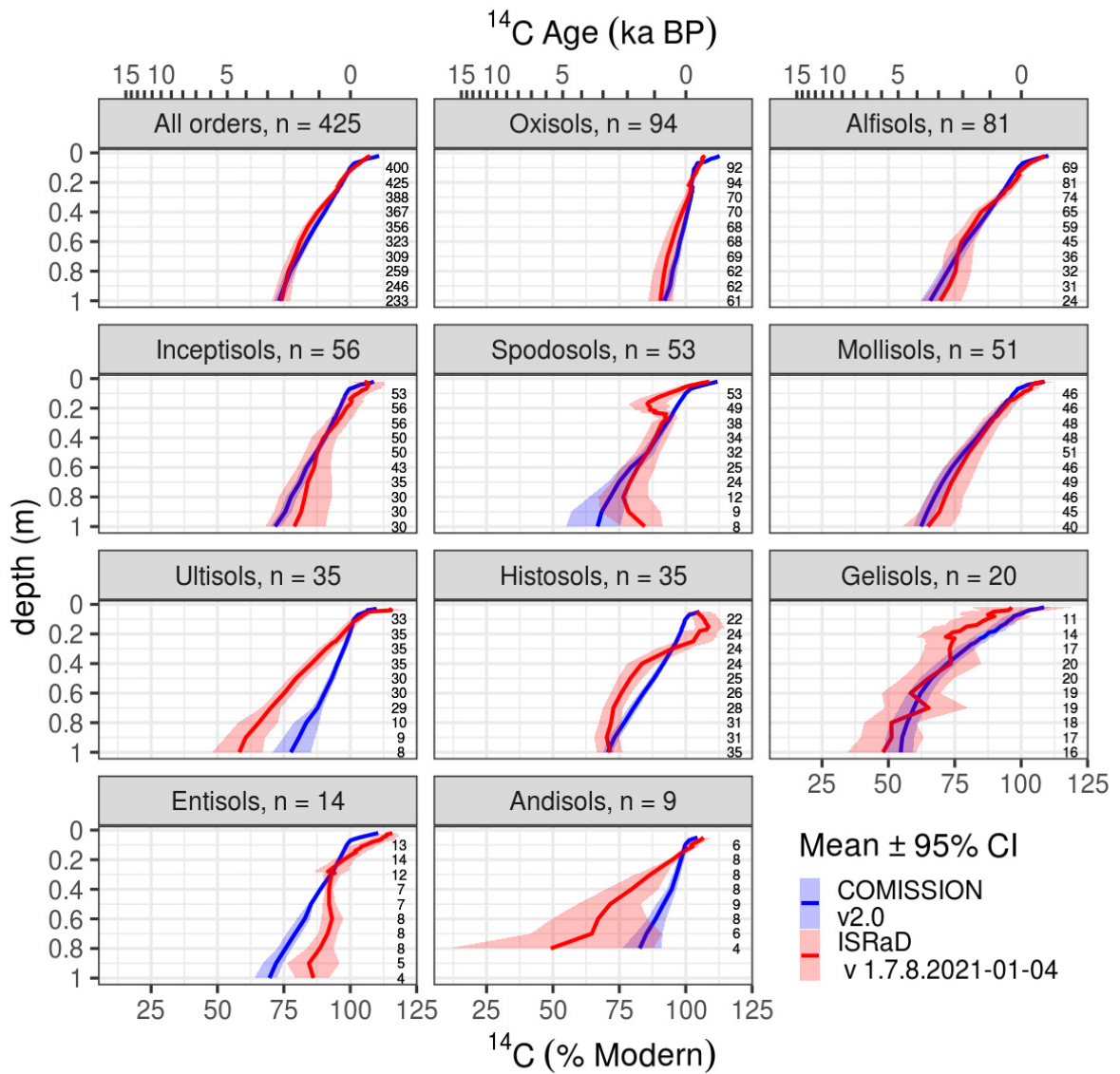
Figure 6-1: Mean ^{14}C contents at ISRaD profiles and at modeled COMISSION grid cells according to US Soil Taxonomy orders. Lines represent the bootstrapped mean and shaded areas the bootstrapped 95% confidence interval. The first panel comprises all soil orders. The total number of horizons (maximum n = 425) is smaller than the number of profiles in ISRaD due to the comparison on grid cell scale. Panels are ordered according to the maximum number of horizons of a soil order present in the database. The lower x-axis displays the ^{14}C content in percent Modern carbon. For illustration purposes, the upper x-axis shows the apparent conventional ^{14}C age with an arbitrary reference year of 1950. On the panels' right-hand side, the number of horizons that are present for this depth is displayed.

6.2.4   Understanding and using global patterns of radiocarbon for model evaluation

The growth of a global radiocarbon database (Mathieu et al., 2015; He et al., 2016; Lawrence et al., 2020) raises the question of how this database should be used to evaluate if SOC models can reconcile ^{14}C and SOC observations globally. I have showcased how a grid-cell-to-profile comparison could provide valuable insights in the previous paragraphs. Similarly, Chen et al. (2019) evaluated how well the ELM1.0 model can reproduce ^{14}C profiles on grid cells in which radiocarbon profiles have been measured. Their analysis showed that site-specific adjustments of root biomass profiles and depth-dependent decomposition rates are needed to match the observed profiles. The scale mismatch between grid-cells and individual measured profiles is an apparent issue. Shi et al. (2020) proposed to upscale the ^{14}C measurements in the ISRaD database using an ensemble of decision trees (Random forest) that was learned using the covariates depth, mean annual temperature, precipitation, land cover, clay content, and soil order according to the USDA classification. Although these authors achieve good explanatory power (R^2 = 0.69), it is not satisfying that depth is the most important variable with a variable importance of 60%. For the chosen method (Random forest) this poses the problem of extrapolation and interpolation mainly based on depth with still a rather sparse dataset. For radiocarbon, the extrapolation problem extends into two dimensions. Horizontally the number of profiles is sparse, but the number of profiles gets even sparser with soil depth. The number of horizons or layers decreases from 503 in 20 cm to 293 in 100 cm. The analogous global SOC product is based on more than 100,000 profiles. Hengl et al. (2018) noted that Random forests could fail in regions that have not been used for training.

Up to now, the two papers that use statistical learning from the radiocarbon databases had to rely on using measurement depth as a variable explicitly (Mathieu et al., 2015; Shi et al., 2020). While Mathieu et al. (2015), with a more limited database of 122 profiles, did not attempt to use their statistical model to upscale ^{14}C to the global scale, Shi et al. (2020) used the data-learned relationships with the aforementioned five explanatory variables and measurement depth to produce global maps of ^{14}C in soil organic carbon. They used this global gridded product to evaluate the global land models ELM1.0 and CLM5 regarding their ability to represent radiocarbon throughout the soil organic carbon profile. These two models could not produce apparent radiocarbon ages that were consistent with the upscaled global product. They concluded that soil organic carbon models must be depth-resolved as an indispensable and essential condition for explaining apparent millennial ^{14}C ages. Yet, the study is missing an analysis of the area of applicability (Meyer and

Pebesma, 2020) which should considerably shrink with depth as measurements are getting scarcer. Ploton et al. (2020) have further shown that if an inappropriate cross-validation is applied, global mapping products can show high apparent predictive capabilities when observations are clustered. While the increase in radiocarbon and SOC data holds strong potential for improving SOC process representation in Earth system models, upscaling products need to consider uncertainty and area of applicability, and model-data comparison needs to be performed with care.

Both in statistical models (Mathieu et al., 2015; Shi et al., 2020) and process-based models such as ELM1.0 and CLM5 (Chen et al., 2019; Shi et al., 2020) the explicit inclusion of a depth-dependence contradicts the new paradigm of persistence through multi-process interactions (Schmidt et al., 2011). The emergence of depth as the most important predictor in statistical models describing the global radiocarbon distribution may be a necessary side-effect of the lack of depth-resolved predictors. Nevertheless, until the extrapolation issue horizontally and with depth is not addressed, I recommend not implementing ad-hoc fixes for process-based models even if they concern only non-mechanistic aspects such as the imposed depth-dependence of decomposition rates.

A combination of process-based modeling and machine learning could remedy the issue of extrapolation to unseen conditions (Raissi et al., 2019; Reichstein et al., 2019; Rackauckas et al., 2020). Combining machine learning-based approaches with process-based approaches to universal differential equations (Rackauckas et al., 2020) or physics-informed neural networks (Raissi et al., 2019; Yazdani et al., 2020) could be highly beneficial for learning the drivers of ^{14}C globally. At the same time, knowledge can be encoded into the model by prescribing partial differential equations as additional constraints. Physics-informed neural networks seem more promising for global-scale applications since they are computationally efficient (Raissi et al., 2020) compared to parameter calibration of a numerically solved partial differential equation with embedded neural networks (Rackauckas et al., 2020). Specifically, one could prescribe the partial differential equations that make up the COMISSION model or any other mechanistic SOC profile into a neural network. Simultaneously, learning from the ISRaD database how environmental covariates influence the ^{14}C depth gradients (Raissi et al., 2020).

6.3   Reconciling root turnover observations and SOC turnover observations

6.3.1   Linking observations of root turnover and SOC turnover

One limitation of the studies presented in this thesis is the lack of combining root turnover measurements, such as time-to-disappearance data from minirhizotrons and ^{14}C content in fine-roots, with measurements of SOC formation and turnover in an integrated modeling exercise. While study I and study II showed the potential for modeling to reconcile minirhizotron data and ^{14}C in fine-roots to estimate turnover times in root models, I did not translate these turnover times into estimates of root litter production that could be the input for the COMISSION model. Instead, I used results from the JSBACH model whose fine-root litter inputs are of the same size as its aboveground inputs. This modeling scheme has not been informed by any measurement specific to root turnover.

The Radix model by Riley et al. (2009) has the capability to produce fine-root litter fluxes. However, this model had the shortcoming that a possibly biased mean minirhizotron root lifetime was used to directly parameterize the fast root pool's turnover time. The finding that two-pool models for root turnover can reconcile time-to-disappearance minirhizotron data with ^{14}C data shows how both data sources can be combined into an integrated root-SOC turnover model by explicitly modeling root pools. These root pools can then be additionally compared with root biomass and necromass measurements to get a better constraint on overall root litter production. The direct coupling to a ^{14}C enabled SOC turnover model would then make it possible to check the plausibility of the root litter inputs given SOC stocks and ^{14}C, or even litter pools such as the lignified litter pool in the COMISSION model.

6.3.2   Constraining root litter inputs with depth

The main issue for assimilating root and SOC turnover data into vertically explicit models is that depth-resolved measurements of fine-root ^{14}C and minirhizotrons are scarce. Especially for constraining root litter inputs with depth, ^{14}C measurements are valuable since minirhizotron measurements with depth are more challenging from a technical standpoint and because of the increasing scarcity of fine roots with depth. Gaul et al. (2009) conducted one of the few studies to report ^{14}C contents in fine roots over a depth gradient. These authors found that ^{14}C indicated increasing root ages with soil depth pointing to a higher proportion of suberized roots (Study II). Given the importance of the root litter input distribution to reproduce apparently millennial ^{14}C ages

(Study IV, Objective **Obj-SOC4**), such depth-resolved fine-root ^{14}C profiles would be valuable information sources. This thesis only used observed ^{14}C lags between atmosphere and roots to get the ^{14}C signature of the root litter inputs right but did not use ^{14}C measurements to constrain root litter inputs with depth.

The combination of modeling root-turnover and SOC formation, especially in a depth-resolved way, is a major research gap for understanding why SOC seems to be particularly persistent in the deep soil. Up to now, all modeling approaches either resort to prescribing typical root biomass distributions as root litter distributions (Riley et al., 2014; Dwivedi et al., 2017) or using measured root biomass distributions to prescribe root litter distributions (this thesis). The results of Gaul et al. (2009) show that the ^{14}C of fine roots may indicate increasing fine-root turnover times with depth and thereby lower root litter inputs with depth. If root turnover times were not changing with depth, it would be reasonable to use observed root biomass distributions to describe the depth distribution of root litter inputs. However, if observations and modeling point to a larger proportion of slowly cycling roots with depth, root litter input profiles would be shallower than root biomass profiles. Thereby, root litter inputs may have been overestimated by using root biomass profiles. An integrated modeling of depth-resolved root litter turnover and SOC formation and turnover is therefore paramount to advance the understanding of SOC persistence.

Modeling efforts on dynamically allocating roots with depth according to water and nutrient demands (Caldararu et al., 2020) have to be supported by large-scale observations of root biomass (Schenk and Jackson, 2002; Iversen et al., 2017; Huang et al., 2021). While the database used in study IV already provides a good starting point for further detailed studies on the connection of root turnover and SOC turnover, an effort similar to the International Soil Radiocarbon Database (ISRaD; Lawrence et al., 2020) would be ideal for supporting larger scale evidence for changes of root turnover with soil depth. The measurements of the ISRaD database and the large number of SOC profiles from the World Soil Information Service (WoSIS; Batjes et al., 2020), however, can also serve as a stand-in. The plausibility of modeled root biomass distributions can be evaluated by checking if the resulting root litter inputs would produce realistic ^{14}C and SOC profiles.

6.4 Coupling microbial processes with the nitrogen and phosphorus cycle

Model experiments with COMISSION have highlighted the importance of the continued microbial recycling of SOM (study III and IV). However, further developments of the COMISSION model to include stoichiometric controls on microbial carbon use efficiency and optimal investment of extracellular enzymes are on the way. They are crucial to elucidate the role of plant litter compared to microbial necromass. The COMISSION v2.0 model has been taken as the backbone for developing the Jena Soil Model (JSM). In a collaboration, the COMISSION model has already been coupled and integrated with the nitrogen and phosphorus cycle to form the JSM model (Yu et al., 2020a; Yu et al., 2020b). JSM will be eventually coupled with the vegetation component of the new terrestrial ecosystem model QUINCY (Thum et al., 2019). To elucidate the contribution of microbial necromass and as a further constraint for depth-dependent processes that affect soil organic matter formation and turnover, the δ^{13}C signature of mineral-associated organic matter, dissolved organic matter, and microbial biomass could be used. ^{13}C is fractionated during microbial transformation of soil organic matter can thereby be used as an additional carbon isotope affected by all the processes that affect ^{12}C (Poage and Feng, 2004; Wynn et al., 2005; Wynn, 2007). In conjunction with profiles of C:N and C:P ratios (Yu et al., 2020a), ^{13}C offers the potential to learn more about depth-dependent processes.

6.5 Understanding the stability of mineral associated organic carbon

The main bracket around this thesis was the quest to better understand apparent stability of mineral associated organic carbon. This apparent stability had been derived from apparently millennial ^{14}C ages which led amongst other factors to the inclusion of passive or inert pools in models (Jenkinson and Coleman, 2008; Parton et al., 2010). Since, however, these pools were difficult to justify mechanistically, it was also difficult to assign justifiable temperature sensitivities to these pools. Davidson and Janssens (2006) noted that most of these models assigned the same temperature sensitivity to these pools, although the so-called carbon-quality temperature theory would have dictated the highest temperature sensitivities if these pools were indeed composed of chemically recalcitrant compounds (Kleber, 2010; Lehmann and Kleber, 2015). The landmark review of Schmidt et al. (2011) highlighted that instead, the persistence of soil organic carbon is an 'ecosystem property'. This means the persistence of soil organic carbon is a function of its abiotic and biotic environment (Schmidt et al., 2011).

In this thesis, a focus has lain on the interactions of microbial energy limitation and sorption to mineral surfaces to produce apparently millennial ^{14}C ages in mineral soils. Several other mechanisms leading to long-term persitence of soil organic carbon obviously exist: In some ecosystems, permafrost is causing the persistence of soil organic carbon, while in other ecosystems water saturation is responsible for the accumulation of peat layers. A combination of the two acts in regularly freezing and thawing landscapes. While the persistence of soil organic carbon due to freezing, thawing, and anoxia depends on the inhibition of microbial decomposition, Bradford et al. (2016) noted that microbes are not only agents of soil organic carbon decomposition but also of its formation. This is also one of the main messages from this thesis. Only in combination with sorption to mineral surfaces, microbial decomposition can form substantial soil organic carbon stocks with apparently millennial ^{14}C ages as a byproduct of microbial death (study IV, objective **Obj-SOC3**).

Here, the interaction with roots comes into play – microbial limitation due to a decreasing supply of substrate with depth is further responsible for apparently millennial ^{14}C ages, especially in conjunction with a high available sorption capacity (study IV, objective **Obj-SOC4**). The aforementioned processes like permafrost or anoxia theoretically do not limit soil organic carbon accrual. The formation of mineral-associated organic carbon is limited, however, by the finite amount of mineral surfaces available (this thesis) but also by stoichiometric demands for the formation of microbial biomass (Yu et al., 2019; Spohn, 2020).

In study IV, I also tangentially touched upon the temperature sensitivity of the mineral-associated organic carbon stocks. In long-term equilibrium, soils with a higher sorption capacity exhibit a lower apparent temperature sensitivity (study IV, objective **Obj-SOC4**). This is due to the overall lower temperature sensitivity of mineral association (adsorption, desorption) compared to microbial processes (Bradford et al., 2016; Abramoff et al., 2019). Although the temperature sensitivity of organo-mineral association is not settled (Conant et al., 2011; Bradford et al., 2016; Abramoff et al., 2019; Abramoff et al., 2021), there seems to be a consensus that sorption is less temperature sensitive than microbial processes. Nevertheless, the vulnerability of mineral-associated organic carbon to global change is still under active research. Keiluweit et al. (2015) showed that root exudates of oxalic acid can release organic matter from mineral association. Thereby, plants can tap into the nutrient store of mineral-associated organic matter. Similarly, it is not clear to which extent microbes can attack mineral-associated organic carbon and thereby impose the higher temperature sensitivity of microbial processes on mineral-associated organic carbon. Mineral-associated organic

carbon is not inherently stable or insensitive to environmental changes. Thus, more insights on mechanisms that liberate organic matter from mineral surfaces have to be gathered and eventually implemented into models such as COMISSION.

7   Conclusion

The overall objective of this thesis was to make better use of radiocarbon measurements to improve our understanding of two important belowground processes – root turnover and SOC formation and turnover. In both fields, radiocarbon had contradicted the prevailing paradigm and led, together with the accumulation of other contradictory observations, to paradigm shifts. This thesis showed that the apparently contradictory insights from radiocarbon measurements can be reconciled with other observations and insights under the new paradigms.

For root turnover, the contradiction between mean residence times of roots estimated with radiocarbon and minirhizotrons could be resolved by abandoning the notion that the survival probability of a root is constant throughout its lifetime. Survival functions representing two fine-root pools in parallel or in series were best at reconciling radiocarbon and minirhizotron measurements. Compared to statistical survival functions, these two-pool models could be easily implemented into ecosystem models and can also be interpreted mechanistically as effects of suberization or ectomycorrhizal infection.

For the reconciliation of radiocarbon and minirhizotron observations of fine-roots, it was crucial to account for the inherent biases of the techniques: Minirhizotrons generally overestimate the lifetimes of roots since dead and live roots are hard to distinguish. Radiocarbon that has resided in storage pools can be used to grow new roots and thereby make the root 'look older' than it is. The combined use of minirhizotron and radiocarbon data makes it possible to constrain these biases. For future applications of the introduced framework, a larger flexibility for storage residence time biases should be allowed. Ideally, an attempt to quantify storage residence times should be made.

Apparent radiocarbon ages of soil organic carbon up to millennia have been used to justify the existence of 'slow' pools or humified pools with intrinsic decomposition rates on millennial time scales. Analytical evidence, however, accumulated that chemical recalcitrance is not the dominating factor that can explain the long-term persistence of soil organic carbon. The work presented shows that a new paradigm highlighting microbes and organo-mineral interactions as the drivers for long-term persistence of soil organic carbon can successfully be translated into a process-based model of soil organic carbon formation and turnover, COMISSION. The COMISSION model is vertically explicit,

treats microbes as the actors of SOC formation and decomposition, and represents organo-mineral associations with a finite sorption capacity.

Two possibilities to represent a finite sorption capacity were explored. In the first version of COMISSION, sorption capacity was defined as the amount of already mineral-associated organic carbon plus the extra dissolved organic carbon that could be sorbed in batch sorption experiments. The interaction of microbial processes and mineral association was found to be the main factor for apparently millennial ^{14}C ages in the subsoil of a Podzol. In the topsoil, organo-mineral associations were the dominant driver for high apparent ^{14}C ages.

In the second version of COMISSION, a scalable definition of a maximum sorption capacity was introduced that could be used to study the drivers of radiocarbon age gradients across multiple sites. Empirical relationships between clay + silt content and mineral-associated organic carbon were used to represent the finite amount of mineral surfaces that can form associations with dissolved organic carbon and microbial necromass. Differences in sorption capacity across sites in combination with microbial limitation, were responsible for differences in apparent ^{14}C ages of up to 4000 years in the subsoil. Root litter distributions were found to be vital in explaining between-site differences in radiocarbon ages due to the lift of microbial limitations when the point-of-entry of root litter is deeper. This highlights the importance of better understanding fine-root turnover, especially how it is changing with depth. In comparison, temperature differences between the sites were only responsible for 300 years difference in apparent radiocarbon age when the sorption capacity was low, underscoring the importance of the aforementioned processes for understanding apparent millennial ^{14}C ages in soils.

The lower temperature sensitivity of processes related to the mineral association of organic matter compared to microbial processes warrants further investigation. Are mineral-associated organic carbon stocks indeed less vulnerable to climate warming than organic carbon stocks that are not associated with mineral surfaces such as organic layers or peat? Is desorption a prerequisite for microbial decomposition, or are microbes able to decompose mineral-associated organic carbon while it is sorbed? Answers to these questions are crucial to be able to judge if mineral-associated organic carbon has the same likelihood to exacerbate climate warming as 'unprotected' soil organic carbon. Similarly, it is crucial to account for the nutrient demands of the formation of mineral-associated organic carbon. Most of the mineral-associated organic carbon is of microbial origin, and the sequestration of mineral-associated organic carbon would require meeting the stoichiometric

demands of microbes. Although rooting patterns and the amount of carbon might change under global change, it remains unclear if the large available sorption capacity in the subsoil can be further saturated given the nutrient demand for the formation of mineral-associated organic carbon.

Enhanced mechanistic understanding of belowground processes has in recent years greatly improved our understanding of soil organic matter formation, turnover and persistence. Important open questions remain about describing these processes across different soil orders, their temperature sensitivities, as well as the interplay of microbially mediated SOC decomposition and formation with other processes such as the nitrogen and phosphorus cycle. These are also important steps to be made for upscaling SOC and ^{14}C profiles in a mechanistically informed way and integrating the new generation of soil organic matter models into Earth system models. Physics-informed machine learning and hybrid modeling techniques hold potential for addressing current unknowns in drivers of SOC turnover and ^{14}C depth-gradients without getting entrenched on the machine learning or mechanistic modeling side. Given the importance of belowground carbon stored and cycled in terrestrial ecosystems for the global carbon cycle and atmospheric CO_2 concentrations, progress in the field matters beyond mere scientific curiosity: It is both timely and necessary to constrain the uncertain future of terrestrial carbon cycling under the influence of climate change.

8 References Chapter 6 and 7

Abramoff, R.Z., Georgiou, K., Guenet, B., Torn, M.S., Huang, Y., Zhang, H., Feng, W., Jagadamma, S., Kaiser, K., Kothawala, D., Mayes, M.A., Ciais, P., 2021. How much carbon can be added to soil by sorption? Biogeochemistry 152, 127-142.

Abramoff, R.Z., Torn, M.S., Georgiou, K., Tang, J.Y., Riley, W.J., 2019. Soil Organic Matter Temperature Sensitivity Cannot be Directly Inferred From Spatial Gradients. Global Biogeochemical Cycles 33, 761-776.

Batjes, N.H., Ribeiro, E., Van Oostrum, A., 2020. Standardised soil profile data to support global mapping and modelling (WoSIS snapshot 2019). Earth System Science Data 12, 299-320.

Beare, M.H., McNeill, S.J., Curtin, D., Parfitt, R.L., Jones, H.S., Dodd, M.B., Sharp, J., 2014. Estimating the organic carbon stabilisation capacity and saturation deficit of soils: a New Zealand case study. Biogeochemistry, 1-17.

Braakhekke, M.C., Beer, C., Schrumpf, M., Ekici, A., Ahrens, B., Hoosbeek, M.R., Kruijt, B., Kabat, P., Reichstein, M., 2014. The use of radiocarbon to constrain current and future soil organic matter turnover and transport in a temperate forest. Journal of Geophysical Research: Biogeosciences, 2013JG002420.

Bradford, M.A., Wieder, W.R., Bonan, G.B., Fierer, N., Raymond, P.A., Crowther, T.W., 2016. Managing uncertainty in soil carbon feedbacks to climate change. Nature Clim. Change 6, 751-758.

Caldararu, S., Thum, T., Yu, L., Zaehle, S., 2020. Whole‐plant optimality predicts changes in leaf nitrogen under variable CO_2 and nutrient availability. New Phytologist 225, 2331-2346.

Chen, J., Zhu, Q., Riley, W.J., He, Y., Randerson, J.T., Trumbore, S., 2019. Comparison With Global Soil Radiocarbon Observations Indicates Needed Carbon Cycle Improvements in the E3SM Land Model. Journal of Geophysical Research: Biogeosciences 124, 1098-1114.

Coleman, K., Jenkinson, D.S., Crocker, G.J., Grace, P.R., Klír, J., Körschens, M., Poulton, P.R., Richter, D.D., 1997. Simulating trends in soil organic carbon in long-term experiments using RothC-26.3. Geoderma 81, 29-44.

Conant, R.T., Ryan, M.G., Ågren, G.I., Birge, H.E., Davidson, E.A., Eliasson, P.E., Evans, S.E., Frey, S.D., Giardina, C.P., Hopkins, F.M., Hyvönen, R., Kirschbaum, M.U.F., Lavallee, J.M., Leifeld, J., Parton, W.J., Megan Steinweg, J., Wallenstein, M.D., Martin Wetterstedt, J.Å., Bradford, M.A., 2011. Temperature and soil organic matter decomposition rates – synthesis of current knowledge and a way forward. Global Change Biology 17, 3392-3404.

Coutts, M.P., Lewis, G.J., 1983. When is the structural root system determined in Sitka spruce? 71, 155-160.

Davidson, E.A., Janssens, I.A., 2006. Temperature sensitivity of soil carbon decomposition and feedbacks to climate change. Nature 440, 165-173.

Dwivedi, D., Riley, W.J., Torn, M.S., Spycher, N., Maggi, F., Tang, J.Y., 2017. Mineral properties, microbes, transport, and plant-input profiles control vertical distribution and age of soil carbon stocks. Soil Biology and Biochemistry 107, 244-259.

Feng, W., Plante, A.F., Six, J., 2013. Improving estimates of maximal organic carbon stabilization by fine soil particles. Biogeochemistry 112, 81-93.

Freeman, C., Ostle, N., Kang, H., 2001. An enzymic'latch'on a global carbon store. Nature 409, 149-149.

Gaudinski, J.B., Torn, M.S., Riley, W.J., Swanston, C., Trumbore, S.E., Joslin, J.D., Majdi, H., Dawson, T.E., Hanson, P.J., 2009. Use of stored carbon reserves in growth of temperate tree roots and leaf buds: analyses using radiocarbon measurements and modeling. Global Change Biology 15, 992-1014.

Gaul, D., Hertel, D., Leuschner, C., 2009. Estimating fine root longevity in a temperate Norway spruce forest using three independent methods. Functional Plant Biology 36, 11-19.

Guggenberger, G., Kaiser, K., 2003. Dissolved organic matter in soil: challenging the paradigm of sorptive preservation. Geoderma 113, 293-310.

He, Y., Trumbore, S.E., Torn, M.S., Harden, J.W., Vaughn, L.J., Allison, S.D., Randerson, J.T., 2016. Radiocarbon constraints imply reduced carbon uptake by soils during the 21st century. Science 353, 1419-1424.

Hengl, T., Nussbaum, M., Wright, M.N., Heuvelink, G.B.M., Gräler, B., 2018. Random forest as a generic framework for predictive modeling of spatial and spatio-temporal variables. PeerJ 6, e5518.

Huang, Y., Ciais, P., Santoro, M., Makowski, D., Chave, J., Schepaschenko, D., Abramoff, R.Z., Goll, D.S., Yang, H., Chen, Y., Wei, W., Piao, S., 2021. A global map of root biomass across the world's forests. Copernicus GmbH.

IPCC, 2003. Good practice guidance for land use, land-use change and forestry, In: Penman, J., Gytarsky, M., Hiraishi, T., Krug, T., Kruger, D., Pipatti, R., Buendia, L., Miwa, K., Ngara, T., Tanabe, K. (Eds.), Japan: IPCC/OECD/IEA/IGES.

Iversen, C.M., McCormack, M.L., Powell, A.S., Blackwood, C.B., Freschet, G.T., Kattge, J., Roumet, C., Stover, D.B., Soudzilovskaia, N.A., Valverde-Barrantes, O.J., van Bodegom, P.M., Violle, C., 2017. A global Fine-Root Ecology Database to address below-ground challenges in plant ecology. New Phytol 215, 15-26.

Jenkinson, D.S., Coleman, K., 2008. The turnover of organic carbon in subsoils. Part 2. Modelling carbon turnover. European Journal of Soil Science 59, 400-413.

Keiluweit, M., Bougoure, J.J., Nico, P.S., Pett-Ridge, J., Weber, P.K., Kleber, M., 2015. Mineral protection of soil carbon counteracted by root exudates. Nature Climate Change.

Kleber, M., 2010. What is recalcitrant soil organic matter? Environmental Chemistry 7, 320-332.

Knauer, J., Werner, C., Zaehle, S., 2015. Evaluating stomatal models and their atmospheric drought response in a land surface scheme: A multibiome analysis. Journal of Geophysical Research: Biogeosciences 120, 1-18.

Koven, C.D., Riley, W.J., Subin, Z.M., Tang, J.Y., Torn, M.S., Collins, W.D., Bonan, G.B., Lawrence, D.M., Swenson, S.C., 2013. The effect of vertically resolved soil biogeochemistry and alternate soil C and N models on C dynamics of CLM4. Biogeosciences 10, 7109-7131.

Krause, C., Eckstein, D., 1993. Dendrochronology of roots. Dendrochronologia 11, 9 - 23.

Lawrence, C.R., Beem-Miller, J., Hoyt, A.M., Monroe, G., Sierra, C.A., Stoner, S., Heckman, K., Blankinship, J.C., Crow, S.E., McNicol, G., Trumbore, S., Levine, P.A., Vindušková, O., Todd-Brown, K., Rasmussen, C., Hicks Pries, C.E., Schädel, C., McFarlane, K., Doetterl, S., Hatté, C., He, Y., Treat, C., Harden, J.W., Torn, M.S., Estop-Aragonés, C., Asefaw Berhe, A., Keiluweit, M., Della Rosa Kuhnen, Á., Marin-Spiotta, E., Plante, A.F., Thompson, A., Shi, Z., Schimel, J.P., Vaughn, L.J.S., Von Fromm, S.F., Wagai, R., 2020. An open-source database for the synthesis of soil radiocarbon data: International Soil Radiocarbon Database (ISRaD) version 1.0. Earth System Science Data 12, 61-76.

Lehmann, J., Kleber, M., 2015. The contentious nature of soil organic matter. Nature 528, 60-68.

Lukac, M., 2012. Fine Root Turnover, In: Mancuso, S. (Ed.), Measuring Roots. Springer Verlag, Berlin Heidelberg, pp. 363-373.

Manzoni, S., Katul, G.G., Porporato, A., 2009. Analysis of soil carbon transit times and age distributions using network theories. Journal of Geophysical Research 114, 1-14.

Mathieu, J.A., Hatte, C., Balesdent, J., Parent, E., 2015. Deep soil carbon dynamics are driven more by soil type than by climate: a worldwide meta-analysis of radiocarbon profiles. Glob Chang Biol 21, 4278-4292.

Metzler, H., Müller, M., Sierra, C.A., 2018. Transit-time and age distributions for nonlinear time-dependent compartmental systems. Proceedings of the National Academy of Sciences 115, 1150-1155.

Meyer, H., Pebesma, E., 2020. Predicting into unknown space? Estimating the area of applicability of spatial prediction models. arXiv preprint arXiv:2005.07939.

Miltner, A., Bombach, P., Schmidt-Brücken, B., Kästner, M., 2012. SOM genesis: microbial biomass as a significant source. Biogeochemistry 111, 41-55.

Parton, W.J., Hanson, P.J., Swanston, C., Torn, M., Trumbore, S.E., Riley, W., Kelly, R., 2010. ForCent model development and testing using the Enriched Background Isotope Study experiment. Journal of Geophysical Research: Biogeosciences 115, G04001.

Parton, W.J., Schimel, D., Ojima, D., Cole, C.V., Bryant, R., Arnold, R., 1994. A general model for soil organic matter dynamics: sensitivity to litter chemistry, texture and management, Quantitative modeling of soil forming processes: proceedings of a symposium sponsored by Divisions S-5 and S-9 of the Soil Science Society of America in Minneapolis, Minnesota, USA, 2 Nov. 1992. Soil Science Society of America Inc., pp. 147-167.

Ploton, P., Mortier, F., Réjou-Méchain, M., Barbier, N., Picard, N., Rossi, V., Dormann, C., Cornu, G., Viennois, G., Bayol, N., Lyapustin, A., Gourlet-Fleury, S., Pélissier, R., 2020. Spatial validation reveals poor predictive performance of large-scale ecological mapping models. Nature Communications 11.

Poage, M.A., Feng, X., 2004. A theoretical analysis of steady state delta13C profiles of soil organic matter. Global Biogeochem. Cycles 18, GB2016.

Rackauckas, C., Ma, Y., Martensen, J., Warner, C., Zubov, K., Supekar, R., Skinner, D., Ramadhan, A., 2020. Universal Differential Equations for Scientific Machine Learning.

Raissi, M., Perdikaris, P., Karniadakis, G.E., 2019. Physics-informed neural networks: A deep learning framework for solving forward and inverse problems involving nonlinear partial differential equations. Journal of Computational Physics 378, 686-707.

Raissi, M., Yazdani, A., Karniadakis, G.E., 2020. Hidden fluid mechanics: Learning velocity and pressure fields from flow visualizations. Science 367, 1026-1030.

Reichstein, M., Camps-Valls, G., Stevens, B., Jung, M., Denzler, J., Carvalhais, N., Prabhat, 2019. Deep learning and process understanding for data-driven Earth system science. Nature 566, 195-204.

Riley, W.J., Gaudinski, J.B., Torn, M.S., Joslin, J., Hanson, P.J., 2009. Fine‐root mortality rates in a temperate forest: Estimates using radiocarbon data and numerical modeling. New Phytologist 184, 387-398.

Riley, W.J., Maggi, F., Kleber, M., Torn, M.S., Tang, J.Y., Dwivedi, D., Guerry, N., 2014. Long residence times of rapidly decomposable soil organic matter: application of a multi-phase, multi-component, and vertically resolved model (BAMS1) to soil carbon dynamics. Geosci. Model Dev. 7, 1335-1355.

Sah, S., Jungner, H., Oinonen, M., Kukkola, M., Helmisaari, H.S., 2011. Does the age of fine root carbon indicate the age of fine roots in boreal forests? Biogeochemistry 104, 91-102.

Schenk, H.J., Jackson, R.B., 2002. The global biogeography of roots. Ecological Monographs 72, 311-328.

Schmidt, M.W.I., Torn, M.S., Abiven, S., Dittmar, T., Guggenberger, G., Janssens, I.A., Kleber, M., Kogel-Knabner, I., Lehmann, J., Manning, D.A.C., Nannipieri, P., Rasse, D.P., Weiner, S., Trumbore, S.E., 2011. Persistence of soil organic matter as an ecosystem property. Nature 478, 49-56.

Shi, Z., Allison, S.D., He, Y., Levine, P.A., Hoyt, A.M., Beem-Miller, J., Zhu, Q., Wieder, W.R., Trumbore, S., Randerson, J.T., 2020. The age distribution of global soil carbon inferred from radiocarbon measurements. Nature Geoscience.

Solly, E.F., Brunner, I., Helmisaari, H.-S., Herzog, C., Leppälammi-Kujansuu, J., Schöning, I., Schrumpf, M., Schweingruber, F.H., Trumbore, S.E., Hagedorn, F., 2018. Unravelling the age of fine roots of temperate and boreal forests. Nature Communications 9.

Spohn, M., 2020. Increasing the organic carbon stocks in mineral soils sequesters large amounts of phosphorus. Global Change Biology 26, 4169-4177.

Thum, T., Caldararu, S., Engel, J., Kern, M., Pallandt, M., Schnur, R., Yu, L., Zaehle, S., 2019. A new model of the coupled carbon, nitrogen, and phosphorus cycles in the terrestrial biosphere (QUINCY v1.0; revision 1996). Geoscientific Model Development 12, 4781-4802.

United States Department of Agriculture, 1999. Soil taxonomy: A basic system of soil classification for making and interpreting soil surveys, In: Staff, S.S. (Ed.), Agriculture Handbook, 2nd Edition ed. RE Krieger Pub. Co.

Van de Weerd, H., Van Riemsdijk, W., Leijnse, A., 1999. Modeling the dynamic adsorption/desorption of a NOM mixture: effects of physical and chemical heterogeneity. Environmental Science & Technology 33, 1675-1681.

Van de Weerd, H., Van Riemsdijk, W., Leijnse, A., 2002. Modeling transport of a mixture of natural organic molecules: Effects of dynamic competitive sorption from particle to aquifer scale. Water Resources Research 38, 1158.

Woolf, D., Lehmann, J., 2019. Microbial models with minimal mineral protection can explain long-term soil organic carbon persistence. Sci Rep 9, 6522.

Wynn, J.G., 2007. Carbon isotope fractionation during decomposition of organic matter in soils and paleosols: Implications for paleoecological interpretations of paleosols. Palaeogeography, Palaeoclimatology, Palaeoecology 251, 437-448.

Wynn, J.G., Bird, M.I., Wong, V.N.L., 2005. Rayleigh distillation and the depth profile of 13C/12C ratios of soil organic carbon from soils of disparate texture in Iron Range National Park, Far North Queensland, Australia. Geochimica et Cosmochimica Acta 69, 1961-1973.

Yazdani, A., Lu, L., Raissi, M., Karniadakis, G.E., 2020. Systems biology informed deep learning for inferring parameters and hidden dynamics. PLOS Computational Biology 16, e1007575.

Yu, L., Ahrens, B., Wutzler, T., Schrumpf, M., Zaehle, S., 2019. Jena Soil Model: a microbial soil organic carbon model integrated with nitrogen and phosphorus processes. Copernicus GmbH.

Yu, L., Ahrens, B., Wutzler, T., Schrumpf, M., Zaehle, S., 2020a. Jena Soil Model (JSM v1.0; revision 1934): a microbial soil organic carbon model integrated with nitrogen and phosphorus processes. Geoscientific Model Development 13, 783-803.

Yu, L., Ahrens, B., Wutzler, T., Zaehle, S., Schrumpf, M., 2020b. Modeling Soil Responses to Nitrogen and Phosphorus Fertilization Along a Soil Phosphorus Stock Gradient. Frontiers in Forests and Global Change 3.

9 Acknowledgements

Thank you, Tiana, for being my friend through good and hard times! Thank you, Jake, for being my friend and reconciling constantly between Tiana and me.

I want to thank my brother Johannes for always being there for me and discussing the lack of progress with me. Thank you, Johannes! Thanks also to Francesca Zappala and Marco Andrea Ahrens for reminding me that there is more than science – just being joyful in life.

I thank my parents, Margret and Wilfried Ahrens, for continuing to believe in me and support me throughout this journey. Danke dir, Mama, dass du mir so oft zugehört hast. Danke! Danke dir, Papa, dass du mir Verständnis gezeigt hast.

Curriculum vitae

Personal Information

Citizenship: German

Date of Birth: 04 August 1984, Herford (Germany)

Education

Since 11/2013   Ph.D. student, Max Planck Institute for Biogeochemistry, Jena (Germany)

                       Thesis: *Reconciling turnover models of roots and soil organic carbon with radiocarbon measurements*

16/09/2011   Master of Science Global Change Ecology

10/2008 – 09/2011   Global Change Ecology (M.Sc.) within the Elite Network of Bavaria at the University of Bayreuth (Germany)

                       Thesis: *Constraining a simple soil organic carbon model with ^{14}C data*

29/09/2008   Bachelor of Science Geoecology

10/2005 – 09/2008   Geoecology (B.Sc.) at the University of Bayreuth (Germany)

                       Thesis: *Long-term trends in throughfall and soil solution in Bavarian forest ecosystems: Are there signs of recovery?*

09/1995 – 05/2004   High school, Platen-Gymnasium, Ansbach (Germany)

Professional Experience

11/2013 – now   Ph.D. student: Department for Biogeochemical Integration, Max Planck Institute for Biogochemistry, Jena (Germany)

10/2011 – 10/2013   Research Assistant: Biogeochemical Model-Data Integration Group, Max-Planck-Institute for Biogeochemistry, Jena (Germany)

                       Vertical reaction-transport modeling of soil organic carbon with ^{14}C data

03/2010 – 05/2010   Internship: Biogeochemical Model-Data Integration Group, Max-Planck-Institute for Biogeochemistry, Jena (Germany)

                       Inverse modelling of soil carbon balances with ^{14}C data

03/2009 – 04/2009   Internship: LWF, Bavarian Forest Institute, (Freising, Germany), Department for Climate and Water Protection

                       Long-term trend of dissolved organic carbon in throughfall and soil solution of 22 Bavarian forests

03/2008 – 04/2008	Internship: Tauw Lubag Würzburg, consultant's office for environment, technology and construction
	Site investigations with Dynamic Probing Heavy (DPH)
09/2004 – 08/2005	Civilian service at the Bavarian Society for the Protection of Birds (LBV)
	Conservation and public relations

Distinctions

10/2005 – 09/2011	Full scholarship of the Bavarian State (Bavarian Law for Promotion of Talented)

Publications

Ahrens, B., Braakhekke, M.C., Guggenberger, G., Schrumpf, M., Reichstein, M., 2015. Contribution of sorption, DOC transport and microbial interactions to the 14C age of a soil organic carbon profile: Insights from a calibrated process model. Soil Biology and Biochemistry 88, 390-402.

Ahrens, B., Guggenberger, G., Rethemeyer, J., John, S., Marschner, B., Heinze, S., Angst, G., Mueller, C.W., Kögel-Knabner, I., Leuschner, C., Hertel, D., Bachmann, J., Reichstein, M., Schrumpf, M., in revision. Combination of energy limitation and sorption capacity explains 14C depth gradients. Submitted to Soil Biology & Biochemistry.

Ahrens, B., Hansson, K., Solly, E.F., Schrumpf, M., 2014. Reconcilable differences: a joint calibration of fine-root turnover times with radiocarbon and minirhizotrons. New Phytol 204, 932-942.

Ahrens, B., Reichstein, M., 2014. Reconciling ^{14}C and minirhizotron-based estimates of fine-root turnover with survival functions. Journal of Plant Nutrition and Soil Science 177, 287-296.

Ahrens, B., Reichstein, M., 2017. Soil carbon: Depth of understanding. Nature Clim. Change 7, 762-763.

Ahrens, B., Reichstein, M., Borken, W., Muhr, J., Trumbore, S.E., Wutzler, T., 2013. Bayesian calibration of a soil organic carbon model using Δ^{14}C measurements of soil organic carbon and heterotrophic respiration as joint constraints. Biogeosciences Discuss. 10, 13803-13854.

Ahrens, B., Reichstein, M., Borken, W., Muhr, J., Trumbore, S.E., Wutzler, T., 2014. Bayesian calibration of a soil organic carbon model using Δ14C measurements of soil organic carbon and heterotrophic respiration as joint constraints. Biogeosciences 11, 2147-2168.

Braakhekke, M., Wutzler, T., Beer, C., Kattge, J., Schrumpf, M., **Ahrens, B.**, Schöning, I., Hoosbeek, M., Kruijt, B., Kabat, P., 2013. Modeling the vertical soil organic matter profile using Bayesian parameter estimation. Biogeosciences 10, 399-420.

Braakhekke, M.C., Beer, C., Schrumpf, M., Ekici, A., **Ahrens, B.**, Hoosbeek, M.R., Kruijt, B., Kabat, P., Reichstein, M., 2014. The use of radiocarbon to constrain current and future soil organic matter

turnover and transport in a temperate forest. Journal of Geophysical Research: Biogeosciences, 2013JG002420.

Camino-Serrano, M., Gielen, B., Luyssaert, S., Ciais, P., Vicca, S., Guenet, B., Vos, B.D., Cools, N., **Ahrens, B.**, Altaf Arain, M., Borken, W., Clarke, N., Clarkson, B., Cummins, T., Don, A., Pannatier, E.G., Laudon, H., Moore, T., Nieminen, T.M., Nilsson, M.B., Peichl, M., Schwendenmann, L., Siemens, J., Janssens, I., 2014. Linking variability in soil solution dissolved organic carbon to climate, soil type, and vegetation type. Global Biogeochemical Cycles, 2013GB004726.

Carvalhais, N., Forkel, M., Khomik, M., Bellarby, J., Jung, M., Migliavacca, M., Mu, M., Saatchi, S., Santoro, M., Thurner, M., Weber, U., **Ahrens, B.**, Beer, C., Cescatti, A., Randerson, J.T., Reichstein, M., 2014. Global covariation of carbon turnover times with climate in terrestrial ecosystems. Nature 514, 213-217.

Fan, N., Koirala, S., Reichstein, M., Thurner, M., Avitabile, V., Santoro, M., **Ahrens, B.**, Weber, U., Carvalhais, N., 2020. Apparent ecosystem carbon turnover time: uncertainties and robust features. Earth System Science Data 12, 2517-2536.

Jenny, J.-P., Koirala, S., Gregory-Eaves, I., Francus, P., Niemann, C., **Ahrens, B.**, Brovkin, V., Baud, A., Ojala, A.E., Normandeau, A., 2019. Human and climate global-scale imprint on sediment transfer during the Holocene. Proceedings of the National Academy of Sciences, 201908179.

Jenny, J.-P., Koirala, S., Gregory-Eaves, I., Francus, P., **Ahrens, B.**, Brovkin, V., Ojala, A.E.K., Zolitschka, B., Bader, J., Carvalhais, N., 2020. Reply to Li et al.: Human societies began to play a significant role in global sediment transfer 4,000 years ago. Proceedings of the National Academy of Sciences 117, 5571-5572.

Luo, Y., El-Madany, T., Filippa, G., Ma, X., **Ahrens, B.**, Carrara, A., Gonzalez-Cascon, R., Cremonese, E., Galvagno, M., Hammer, T., 2018. Using near-infrared-enabled digital repeat photography to track structural and physiological phenology in mediterranean tree–grass ecosystems. Remote Sensing 10, 1293.

Thurner, M., Beer, C., Santoro, M., Carvalhais, N., Wutzler, T., Schepaschenko, D., Shvidenko, A., Kompter, E., **Ahrens, B.**, Levick, S.R., Schmullius, C., 2014. Carbon stock and density of northern boreal and temperate forests. Global Ecology and Biogeography 23, 297-310.

Wutzler, T., Zaehle, S., Schrumpf, M., **Ahrens, B.**, Reichstein, M., 2017. Adaptation of microbial resource allocation affects modelled long term soil organic matter and nutrient cycling. Soil Biology and Biochemistry 115, 322-336.

Yu, L., **Ahrens, B.**, Wutzler, T., Schrumpf, M., Zaehle, S., 2020. Jena Soil Model (JSM v1.0; revision 1934): a microbial soil organic carbon model integrated with nitrogen and phosphorus processes. Geoscientific Model Development 13, 783-803.

Yu, L., **Ahrens, B.**, Wutzler, T., Zaehle, S., Schrumpf, M., 2020. Modeling Soil Responses to Nitrogen and Phosphorus Fertilization Along a Soil Phosphorus Stock Gradient. Frontiers in Forests and Global Change 3.